A Geochemical Characterization of a Cold-Water Acid Rock Drainage Stream Emanating From the Zn-Pb XY-Deposit, Howard's Pass, Yukon Territory, Canada

M.Sc. Earth Sciences thesis

Kristen B. Feige (M.Sc. Candidate)[1],

Dr. Paul Gammon[2] & Dr. Danielle Fortin[1]

[1]Department of Earth Sciences, Marion Hall, University of Ottawa, Ottawa Ontario

[2]Geological Survey of Canada, 601 Booth St, Ottawa Ontario

Submitted to: Department of Graduate Studies, Faculty of Science

Wednesday, September 22, 2010

Abstract

An acid rock drainage (ARD) stream emanating from the Zn-Pb XY-deposit in the Yukon Territory was examined in order to evaluate the physico-chemical and geochemical processes governing the distribution of dissolved elements from the creek. The creek showed very high concentrations of metals (300 mg/L Fe, 500 mg/L Zn, 15 000 µg/L Ni, 1300 µg/L Cu and 4500 µg/L Cd), low water temperatures (1 – 12°C) and was acidic to moderately acidic (pH 3.1 – 5.0). It was found that this stream experienced a strong seasonal evolution, with increased sulphate and metal concentrations and decreased pH over the course of the summer. The mineral precipitates that formed under low pH conditions were a mixture of schwertmannite, goethite, jarosite and barite, while those that formed under moderately acidic conditions were a mixture of jurbanite, hydrobasaluminite, gibbsite and an X-ray amorphous Al-sulphate phase. Most of the mineral precipitates were of inorganic origin, although microbes may have played a role in mineral formation and trace metal sequestration in some of the precipitates. All of the mineral precipitates contained anomalous concentrations of trace elements (up to 1.5 % wt Zn) and showed a seasonal evolution in their mineralogy, both of which were determined to be a function of the pH and prevailing geochemical conditions.

The geochemistry of the ARD creek draining the XY-deposit was compared to another ARD creek in the area that was likely draining shales. The two creeks were compared in order to determine if ARD geochemical characteristics can be used as a tool for the mineral exploration industry.

Résumé

Le drainage rocheux acide (DRA) émanant du site Zn-Pb-XY au Yukon a été étudié afin de déterminer les conditions physico-chimiques, ainsi que les processus géochimiques contrôlant la distribution des éléments dissouts dans l'eau du ruisseau. Ce ruisseau relativement acide (pH 3.1 – 5.0) présente des concentrations élevées de métaux (300 mg/L de Fe, 500 mg/L de Zn, 15 000 µg/L de Ni et 4500 µg/L de Cd) et des températures très froides (1- 12°C). Nos résultats ont démontré que la composition chimique de l'eau du ruisseau évolue en fonction des saisons, les concentrations de sulfate et de métaux étant plus élevées pendant l'été, alors que le pH baisse. Les précipités de minéraux se formant à bas pH sont un mélange de schwertmannite, goethite, jarosite et barite, alors ceux précipitant à un pH légèrement plus élevé sont composés de jurbanite, hydrobasaluminite, gibbsite et d'un minéral amorphe riche en sulfate et en aluminium. Tous les minéraux se formant dans le ruisseau sont d'origine inorganique car les bactéries semblaient peu abondantes. De plus, les minéraux démontrent des concentrations anormales de métaux traces (jusqu'à 1.5 % de Zn en poids) et évoluent minéralogiquement dans le temps en réponse aux fluctuations de pH et des conditions géochimiques du site.

La géochimie du DRA dans le ruisseau du site XY sont toutefois comparables aux conditions existant dans un ruisseau de DRA adjacent, lequel draine des boues et des shales carbonatés. Les deux ruisseaux ont été comparés afin de déterminer si les caractéristiques géochimiques du DRA peut être utilisées dans l'exploration minière.

Table of Contents

Figures

Tables

Appendices

1. Introduction

1.1. The generation of acid rock drainage and acid mine drainage

Acid rock drainage (ARD) and acid mine drainage (AMD) are acidic, metal-rich effluents produced by the oxidation of metal-sulphide minerals, such as pyrite (FeS_2), chalcopyrite ($CuFeS_2$), pyrrhotite ($Fe_{(1-x)}S_x$) (x = 0 – 0.2), sphalerite (ZnS) and galena (PbS). The production of ARD occurs naturally during the weathering of metal-sulphide ore deposits, while AMD is produced by mining and mineral processing. When metal-sulphides (e.g. FeS_2) are exposed to water and oxygen they are oxidized, releasing acid, ferrous iron, and other metals associated with the mineral [eq. 1]. Under low pH conditions, the chemical oxidation of FeS_2 by O_2 is very slow (Singer and Stumm, 1970) and ferrous iron oxidation is catalyzed through bio-oxidation [eq. 2]. The acidic conditions generated by the initial FeS_2 oxidation by O_2 have selected for microorganisms that are acidophilic (optimal growth at pH < 3) or acidotolerant (tolerate acidic conditions, but optimal growth is at pH > 3 – 5) and capable of withstanding high concentrations of heavy metals (Johnson and Hallberg, 2003). Bio-oxidation of ferrous iron generates ferric iron (Johnson and Hallberg, 2003), which can further oxidize FeS_2, at rates that are 10 – 100 fold faster than oxygen under acidic conditions (pH < 3) (Ritchie, 1994). The oxidation of FeS_2 by Fe^{3+} regenerates Fe^{2+} and more acid, driving the pH down further [eq. 3]. Ferrous iron is subject to bio-oxidation, creating a positive feedback loop between [eq. 2] and [eq. 3].

$$4\ FeS_2 + 14\ O_2 + 4\ H_2O \leftrightarrow 4\ Fe^{2+} + 8\ SO_4^{2-} + 8\ H^+ \quad [1]$$

$$2Fe^{2+} + \tfrac{1}{2}\ O_2 + 2\ H^+ \leftrightarrow 2\ Fe^{3+} + H_2O \text{ (microbially-catalyzed)} \quad [2]$$

$$FeS_2 + 14\ Fe^{3+} + 8\ H_2O \leftrightarrow 15\ Fe^{2+} + 2\ SO_4^{2-} + 16\ H^+ \quad [3]$$

Other rock-forming elements, including Al, Si and Ca are often present at very high concentrations in ARD/AMD, due to the dissolution of feldspars, micas, kaolinite, and carbonate rocks, all of which readily dissolve in acidic waters (Blowes and Pacek, 1994; Cravotta, 1994).

The weathering of sulphide-ore bodies in cold climates was initially thought to be limited due to the absence of Fe(II)-oxidizing microbes and liquid water in these environments. However, pyschrotolerant (capable of growth at near-zero temperatures) Fe(II)-oxidizing bacteria have been documented in ARD/AMD at many northern locations (Braddock et al., 1984; Ferroni et al., 1986; Ahonen et al., 1989; Ahonen et al., 1990, Ahonen et al., 1992; Berthelot et al., 1993; Leduc et al., 1993; Leduc et al., 1994; Langdahl and Ingvorsen, 1997; Elberling et al., 2000, Johnson et al., 2001; Dopson et al., 2007; Kupka et al., 2007). *Acidothiobacillus ferrooxidans* and *Leptospirillium ferrooxidans* are two Fe(II)-oxidizing bacteria ubiquitous to most AMD/ARD environments (Johnson and Hallberg, 2003), although *L. ferrooxidans* is not detected in cold-water AMD/ARD because it is highly sensitive to low temperature conditions relative to *A. ferrooxidans* (Hallmann et al., 1992). Algae and fungi have also been detected in low temperature AMD/ARD waters (Brake et al., 2001a,b, 2004; Lawrence et al., 1998). It has been concluded that low temperature limits the bio-oxidation process indirectly, due to limited cell growth (Langdahl and Ingvorsen, 1997) at near-zero temperatures and slow rates of Fe^{2+} regeneration through the oxidation of FeS_2 by Fe^{3+} [eq. 3] (Okereke and Stevens, 1991). Liquid water is often present in sulphide-ore bodies and tailings impoundments in northern climates since these waters are hyper-concentrated with dissolved ions, suppressing their freezing

point to below zero-temperatures (Meldrum et al., 2002). Furthermore, pyrite oxidation is an exothermic process and generates heat, which aids in the maintenance of liquid water in these environments. The heat generated by pyrite oxidation may also help to maintain temperature conditions that promote microbial growth and Fe-oxidation.

1.2. Self-mitigation processes: hydrolysis and neutralization reactions

As the acidic effluent enters the surface environment, Fe^{3+} generated by bio-oxidation (in the subsurface and at the surface) hydrolyzes and precipitates as ferric-hydroxysulphates and ferric-oxides, which generates acidity [eqs. 4, 5]. Low temperatures enhance the solubility of ferric iron, which makes the precipitation of Fe(III)-minerals and the generation of acid a very slow process (Leduc et al., 1993; Dopson et al., 2007). The precipitation of these minerals also occurs due to oxygenation of these waters by oxygen as they equilibrate with the atmosphere (although oxidation by oxygen is slow due to low pH conditions). Acid rock drainage is naturally self-mitigating, and concentrations of deleterious elements are often observed to be almost fully removed from these waters by natural processes (Sanchez-Espana et al., 2006), including hydrolysis reactions, dilution by near-neutral surface waters and neutralization by carbonate strata.

Fe(III)-hydroxysulphate and –oxyhydroxide minerals

Schwertmannite ($Fe_8O_8(SO_4)(OH)_6$), jarosite ($(H_3O,K,Na)Fe_3(SO_4)_2(OH)_6$) and goethite (α-FeOOH) are the most common Fe-hydroxysulphate and Fe-oxide minerals associated with AMD/ARD, although goethite rarely directly precipitates from these waters due to high concentrations of sulphate (Bigham et al., 1996b, Yu et al., 1999). Schwertmannite [eq. 4] is favoured to precipitate under acidic conditions (pH 2.8 – 3.2)

(Bigham et al., 1996b), high sulphate concentrations (1000 – 3000 mg/L) (Bigham et al., 1994), and in the presence of Fe-oxidizing bacteria (Bigham et al., 1990). Jarosite will precipitate [eq. 5] if the pH is lower (pH 1.9 – 2.1) and if jarosite-directing monovalent cations, such as K^+, NH_4^+, Na^+, and H_3O^+, are present at high concentrations (Barham, 1997; Wang et al., 2006).

$$8\ Fe^{3+} + SO_4^{2-} + 14H_2O \leftrightarrow Fe_8O_8(OH)_6(SO_4) + 22\ H^+ \quad [4]$$

$$3\ Fe^{3+} + 2\ SO_4^{2-} + 7\ H_2O \leftrightarrow (H_3O)Fe_3(SO_4)_2(OH)_6 + 5\ H^+ \quad [5]$$

Schwertmannite is highly metastable and recrystallizes as jarosite [eq. 6] and goethite [eq. 7], both of which may be present as subdominant phases depending on the prevailing geochemical conditions (Bigham et al., 1996a,b; Kumpulainen et al., 2008). As the pH exceeds 3.0, goethite constitutes a greater proportion of the mineral precipitates, while a pH less than 3.0 favours the formation of jarosite (Bigham et al., 1996a). The formation of jarosite may be limited under cold temperatures due to the enhanced solubility of Fe^{3+}, which slows the rate of Fe(III)-hydrolysis and keeps the pH within the range required for schwertmannite precipitation (Leduc et al., 1993). Seasonal changes in hydrological conditions, such as those that are encountered in northern environments, have been observed to result in the conversion of schwertmannite to goethite (Schroth and Parnell, 2005; Kumpulainen et al., 2007). However, it has been shown that low temperatures enhance the stability of schwertmannite (Jonsson et al., 2005), and thus the recrystallization of schwertmannite to goethite in northern AMD/ARD might be limited due to cold temperatures.

$$Fe_8O_8(OH)_6(SO_4) + H_2O + SO_4^{2-} + 17\ H^+ \leftrightarrow$$

$$(H_3O)Fe_3(SO_4)_2(OH)_6 + 5\ Fe^{3+} + 8\ H_2O \quad [6]$$

$$Fe_8O_8(OH)_6(SO_4) + 2\ H_2O_{(l)} \leftrightarrow 8\ FeOOH_{(s)} + 2\ H^+ + SO_4^{2-} \quad [7]$$

Although Fe(II)-oxidizing microbes such as *A. ferrooxidans* are often observed to be in association with Fe(III)-hydroxysulphates from ARD/AMD environments, they do not have a direct effect on the formation of these minerals (Gramp et al., 2009, Bigham and Nordstrom, 2000). Since AMD/ARD waters are usually oversaturated with respect to Fe(III)-hydroxysulphates, microbes provide a convenient template onto which minerals can nucleate. Concurrently, the mineralization of cells will occur despite their morphology and physiological condition (Ferris et al., 1989), providing further evidence that they do not directly control the precipitation of these minerals.

Al(III)-hydroxysulphate minerals

As the ARD/AMD is diluted by near-neutral surface waters or neutralized by the dissolution carbonate rocks, the pH increases and the oxidation of Fe^{2+} by oxygen becomes increasingly favourable. At pH > 4 Fe^{2+} oxidation by O_2 is very fast and the precipitation of Fe(III)-minerals occurs rapidly (Singer and Stumm, 1970). This causes the Fe to be almost entirely removed (by oxidation, hydrolysis and precipitation) from the waters as they reach pH 4 (Kim et al., 2002). Aluminum is conservative below pH 4.5, and as the pH approaches this value Al-hydroxysulphate minerals begin to form (Nordstrom and Ball, 1986), including hydrobasaluminite ($Al_4SO_4(OH)_{10}$-$4H_2O$), jurbanite ($AlOHSO_4$), alunite ($KAl_3(SO_4)_2(OH)_6$) and amorphous gibbsite ($Al(OH)_3$). It is these differences in Fe

and Al solubility that results in the general spatial separation between Fe-rich and Al-rich precipitates in AMD/ARD systems as they are neutralized (Sanchez-Espana et al., 2006).

Hydrobasaluminite is metastable and favoured to precipitate at pH > 5 [eq. 9], and is converted to basaluminite as it dehydrates over time (Nordstrom, 1982). Jurbanite precipitation is favoured at pH < 4.6 [eq. 8], while amorphous gibbsite [eq. 11] will precipitate as the pH approaches 5.7 (Nordstrom, 1982; Nordstrom and Alpers, 1999), due to the desorption of sulphate from the mineral precipitates as the pH increases (Munk et al., 2002). Gibbsite can also form via equilibration with basaluminite ($Al_4(SO_4)(OH)_{10}$) [eq. 12]. However, both hydrobasaluminite and basaluminite have been shown to be relatively stable under low temperature conditions (Nordstrom, 1982), so it is not clear if it will reach equilibrium with gibbsite in cold-water AMD/ARD. Although alunite [eq. 10] has been found in some AMD/ARD environments, it does not form at low temperatures (Theobald et al., 1963; Nordstrom, 1982) and thus is not found in ARD/AMD in cold climates. All of the Al-rich precipitates forming in these waters are invariably highly amorphous (Bigham and Nordstrom, 2000) and flocculent (Furrer et al., 2002).

$$Al^{3+} + SO_4^{2-} + H_2O \leftrightarrow Al(OH)SO_4 + H^+ \quad [8]$$

$$4\ Al^{3+} + SO_4^{2-} + 14\ H_2O \leftrightarrow Al_4(SO_4)(OH)_{10}\text{-}4H_2O + 10\ H^+ \quad [9]$$

$$3\ Al^{3+} + K^+ + 2\ SO_4^{2-} + 6\ H_2O \leftrightarrow KAl_3(SO_4)_2(OH)_6 + 6\ H^+ \quad [10]$$

$$Al^{3+} + H_2O \leftrightarrow Al(OH)_3 + 3\ H^+ \quad [11]$$

$$Al_4(SO_4)(OH)_{10} + 2\ H_2O \leftrightarrow 4\ Al(OH)_3 + 2\ H^+ + SO_4^{2-} \quad [12]$$

Generally, a hydrobasaluminite-basaluminite mixture is the most common Al-mineral to form in ARD/AMD waters at pH ~ 5 (Chapman et al., 1983; Sanchez-Espana et al., 2006; Bigham and Nordstrom, 2000). Microbes are seldom observed to be in association with these precipitates (Kim et al., 2002; Brake et al., 2001a), and any Al-adsorption that does occur onto microbial material has been found to be a passive process (Hard et al., 1999).

Local climatic conditions result in variations in AMD/ARD stream geochemistry over time (e.g. Kim et al., 2002; Canovas et al., 2007; Kumpulainen et al., 2007; Stillings et al., 2008) due to seasonal fluctuations in hydrology (waning recharge waters, inputs of near-neutral surface waters), which can result in spatio-temporal changes in mineral precipitation (e.g. Kim et al., 2002, 2003; Kim and Kim, 2004; Bambic et al., 2006; Murad and Rojik, 2005; Graham and Kelley, 2009; Butler et al., 2009) and thus may also influence trace element sequestration. Given the seasonal extremes observed in northern climates, seasonal climatic variations may result in similar observations.

1.3. Sequestration of trace elements

As a result of the progressive neutralization of AMD/ARD, the precipitation of Fe(III)- and Al(III)-minerals results in the natural attenuation of trace metals, including Pb, Zn, Ni, Cu, Cd, As, V, and U. Due to the large and highly reactive surfaces of these minerals, they are able to scavenge trace metals from the water column by way of adsorption or coprecipitation**.** Coprecipitation involves the incorporation of trace elements into mineral lattice during mineral precipitation, while adsorption is the process by which elements coordinate at the solid-water interface of a mineral precipitate, often as surface complexes due to the presence of functional groups (e.g. SO_4, OH, etc.) (Stumm and

Morgan, 1995). Usually, coordination of metals occurs so that the metal is bound to either one (monodentate complex) or two (bidentate complex) oxygen atoms at the surface of the mineral. However, the coordination sphere of a metal is often only partially occupied by surface oxygen groups, permitting other ligands, such as SO_4, to occupy the coordination sphere, forming a ternary complex (Schindler, 1990). Coordination mechanisms vary depending on the pH and the prevailing geochemical conditions, the mineral to which the metals are adsorbing, and the identity of the metals (Stumm and Morgan, 1995). Seasonal changes in hydrology or geochemistry can cause mineral precipitates to recrystallize to more stable phases and the adsorbed elements will be redistributed between the newly formed phases or released into the water column.

At low pH the surfaces of most mineral precipitates carry a net positive charge (Stumm and Morgan, 1995) and are not effective adsorbents for cations, such as Al^{3+}, Zn^{2+}, Cd^{2+} which behave conservatively under these conditions. With increasing pH, fewer binding sites are protonated on the surface of the mineral precipitate, and thus there are fewer positively charged sites available for adsorption (Stumm and Morgan, 1995), resulting in the adsorption of metal cations becoming more prevalent. When sulphate concentrations are very high (>1000 mg/L) extensive metal adsorption can occur at low pH due to the formation of metal-sulfate anions (e.g. $Zn(SO_4)_2^{2-}$, $Cd(SO_4)_2^{2-}$, etc) (Sanchez-Espana et al., 2006). Other negatively charged species, such as oxyanions of As and V (AsO_4^{3-} and VO_4^{3-}), are almost completely attenuated by schwertmannite at low pH (Acero et al., 2006). The general sequence for metal adsorption onto Fe(III)-hydroxysulphates and -oxyhydroxides is As > V > Pb > Cu,U > Zn > Cd > Ni (Dzombak and Morel, 1990; Lee et al., 2002; Sanchez-Espana et al., 2006), while the sequence for Al-

hydroxysulphates is very similar (Munk et al., 2002; Lee et al 2002; Kinniburgh et al., 1976). Accordingly, As, V, and Pb show strong adsorption at low pH, followed by Cu, Zn, Cd, and Ni, with adsorption edges (pH at which 50% of the trace metal has been adsorbed) occurring at increasing pH, respectively. However, the exact pH at which adsorption occurs and the extent of adsorption is subject to variation depending on the pH, prevailing geochemical conditions (Lee et al., 2002) and temperature (Parker et al., 2007). For example, high metal concentrations have been shown to shift adsorption edges for these metals to lower pH (Webster et al., 1998), due to the formation of ternary complexes (Webster et al., 1998; Swedlund et al., 2003; Swedlund et al., 2009; Weesner and Bleam, 1998) or by modifying the surface electrostratic charge (Penilla et al., 2005), although the former is likely more important with increasing pH (Elzinga et al., 2001).

Trace element sequestration by Fe(III)-minerals

Fe(III)-hydroxysulphates and –oxyhydroxides are capable of accumulating high concentrations of trace elements, aiding in the natural attenuation of AMD/ARD. The ways in which these metals adsorb to the surface or substitute into these mineral precipitates has been subject to much investigation in the literature; for example, the formation of Pb-SO_4 and Cd-SO_4 ternary complexes on the surface of goethite has been observed to enhance adsorption of Pb and Cd at low pH (Acero et al., 2006; Penilla et al., 2005; Webster et al., 1998; Ostergren et al., 2000; Weesner and Bleam, 1989), while the influence of SO_4 on Cu adsorption to goethite is less clear (Penilla et al., 2005, Webster et al., 1998). Schwertmannite has been observed to sequester high concentrations of oxyanions, such as AsO_4^{3-} and VO_4^{3-}, through the formation of ternary complexes on the mineral surface (Acero et al., 2006). Furthermore, the presence of microbes in these

precipitates enhances adsorption, by providing an additional surface for adsorption or by changing the way in which precipitation occurs (Webster et al., 1998). Substitution reactions (coprecipitation) can also account for the removal of trace elements from AMD/ARD. For example, the attenuation of Pb is known to occur via substitution for monovalent cations in the jarosite structure, forming the mineral plumbojarosite ($PbFe_6(SO_4)_4(OH)_{12}$) (Chapman et al., 1983, Hochella et al., 1999, Dutrizac and Jamor, 2000). Jarosite may also participate in the attenuation of Al, as it is known to replace Fe(III) in the jarosite structure (Dutrizac and Jambor, 2000), forming a solid solution between jarosite and alunite. Aluminum can also be removed from these waters by substitution for Fe(III) in the goethite structure, as goethite is isostructural to diaspore (α-AlOOH) (Herbert, 1996). The removal of oxyanions, such as $AsSO_4^{2-}$ and VSO_4^{2-} occur by substitution for SO_4^{2-} in the schwertmannite structure, and are generally very stable once in this configuration (Regenspurg and Peiffer, 2005).

Trace element sequestration by Al(III)-minerals

Similar to the Fe(III)-minerals forming in ARD/AMD environments, Al(III)-minerals are capable of accumulating high concentrations of trace elements. Zinc, Ni, Cd, and U often show a high level of enrichment in Al-hydroxysulphate precipitates (Sanchez-Espana et al, 2006; Munk et al., 2002; Lee et al., 2002), as the adsorption edges for these metals occur under the pH conditions that favour the precipitation of these minerals. Uranium has been shown to have a high affinity for Al-hydroxysulphate minerals (Luo et al., 2009), and likely forms a complex with the UO_2^{2+} species and the mineral surface (Gu et al., 2003). Silicon is often associated with Al-hydroxysulphates, as Si has a very high affinity for Al and SO_4 (Bigham and Nordstrom, 2000). The specific ways in which trace elements

accumulate in Al(III)-hydroxysulphates (i.e. adsorption and coprecipitation mechanisms) are largely undocumented in the literature relative to the number of studies focusing on the adsorption and coprecipitation of metals with Fe(III)-hydroxysulphates.

1.4. Mineral exploration applications of ARD geochemistry

Since the production of ARD involves the interaction between waters and metal-sulphide minerals, understanding the factors governing the mobility and dispersion of elements in acidic surface environments is of importance for vectoring toward buried mineral deposits. The geo-environmental setting of a particular deposit is highly influential on the migration of elements from the deposit into the surrounding environment (Seal et al., 2002; Hammarstrom and Seal, 2003; Desbarats and Dirom, 2007). For example, some metal-sulphide deposits are hosted by lithologies with little neutralization capacity (e.g. silicates), which may result in a greater extent of elemental distribution by acidic waters. Alternatively, some deposits are hosted by carbonate lithologies, which impart a high degree of neutralization capacity to these waters and can limit the dispersion of some elements from the deposit. The extent to which an element is distributed from an ore deposit into the surrounding environment is highly influenced by its geochemical properties, as some elements behave conservatively or non-conservatively under different geochemical conditions. Furthermore, the influence of climate is highly important, as the supply of water and prevailing temperature conditions are paramount to the production of ARD. Understanding the processes governing the dispersion and mobility of elements associated with metal-sulphides in ARD streams may be applicable to the mineral exploration industry, as the distribution of these metals in the surface environment can aid

in vectoring toward buried mineral deposits. However, the use of ARD geochemistry as a tool for mineral exploration remains to be evaluated.

1.5. Thesis objectives

Primarily, this thesis aims to investigate the seasonal dynamics of ARD geochemistry at the XY-deposit, to determine the factors controlling mineral precipitate formation and mineralogy, and to understand the processes controlling trace metal attenuation in these precipitates. As a secondary objective, this thesis will evaluate the potential of ARD geochemistry to be used as a tool for mineral exploration.

2. Site description

2.1. Site location and access

The ARD stream chosen for this study is located at the "XY" Zn-Pb sedimentary exhalative (SEDEX) deposit (62.27 N 129.11 W), located at Howard's Pass, in the Selwyn Basin, southeastern Yukon Territory (Figure 1). Given the remote location of Howard's Pass, site access was by helicopter or a twin-engine airplane. "Base-camp" was set up at an inactive exploration camp at the XY-deposit, belonging to Selwyn Resources.

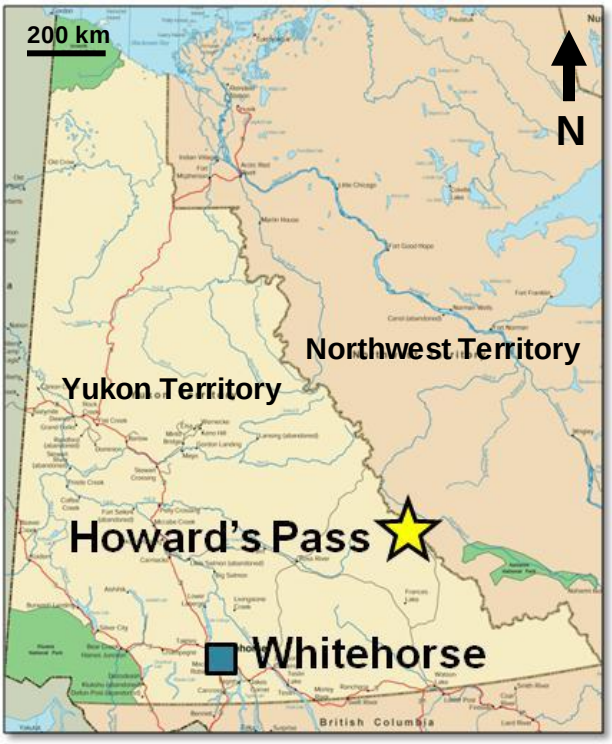

Figure 1: Map of the Yukon Territory showing the location of Howard's Pass relative to Whitehorse (modified from www.canada-maps.org/yukon).

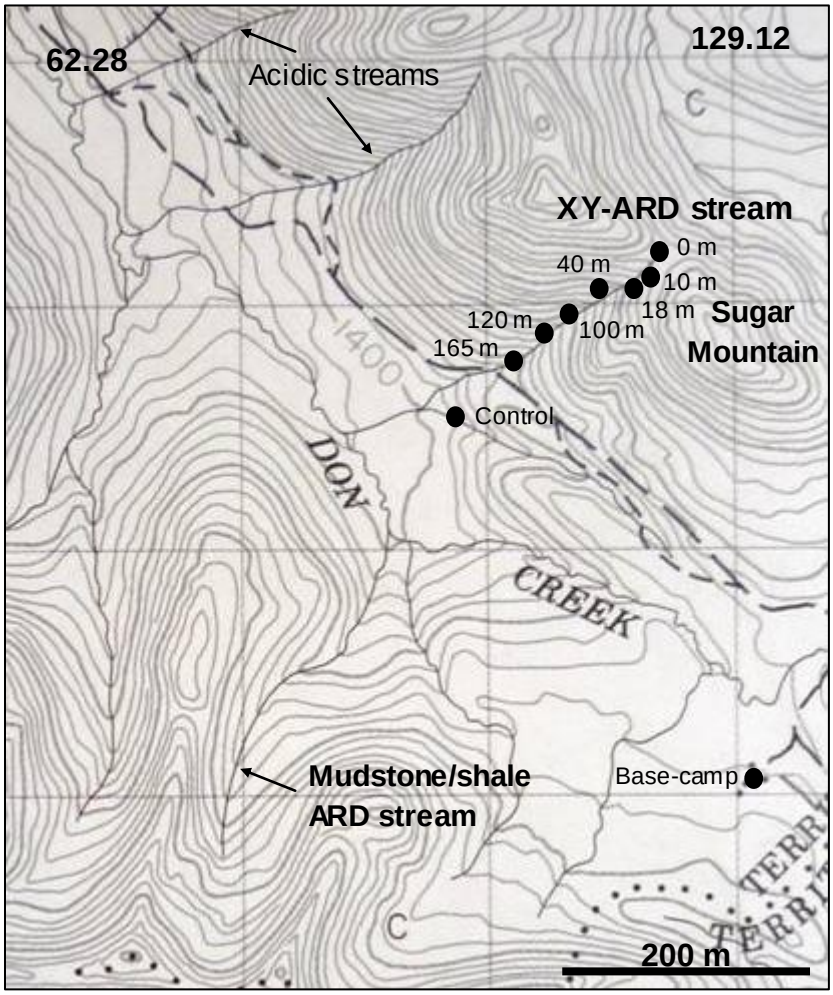

Figure 2: Topographical map (Map number 105-I/6) showing the location of the ARD creek at Howard's Pass that is draining the XY-deposit. Sampling sites are indicated. Another ARD stream likely to be draining shales is shown, as well as the location of two other acidic streams draining the XY-deposit. Trails are indicated by dashed lines.

2.2. Regional Geology

The Selwyn Basin is a Paleozoic marine basin that extends from Alaska, through the Yukon and British Columbia, and into the continental United States. Regionally, the area is stratigraphically defined by a basal sequence, the Windermere supergroup (pre-Cambrian - Cambrian), capped by basinal carbonates of the Rabittkettle formation

(Cambrian). These facies are overlain by the black shale, chert and mudstone of the Road River Group (Ordivician-Silurian), which is overlain by chert and clastics of the Earn Group (Devonian-Mississippian) (Figure 3).

The Howard's Pass district straddles the border between the Yukon and Northwest Territories (Figure 1), and there are several Zn-Pb SEDEX deposits located in this area, including XY, Anniv, OP, Pelly North, Brodel, and Don (Figure 3). The indicated and inferred tonnage and grade of the Zn-Pb ore suggests that these deposits can be classified as world-class. The Zn-Pb mineralization at Howard's Pass is found in a stratigraphic unit known as the Active Member, comprising what has been termed the "zinc-corridor".

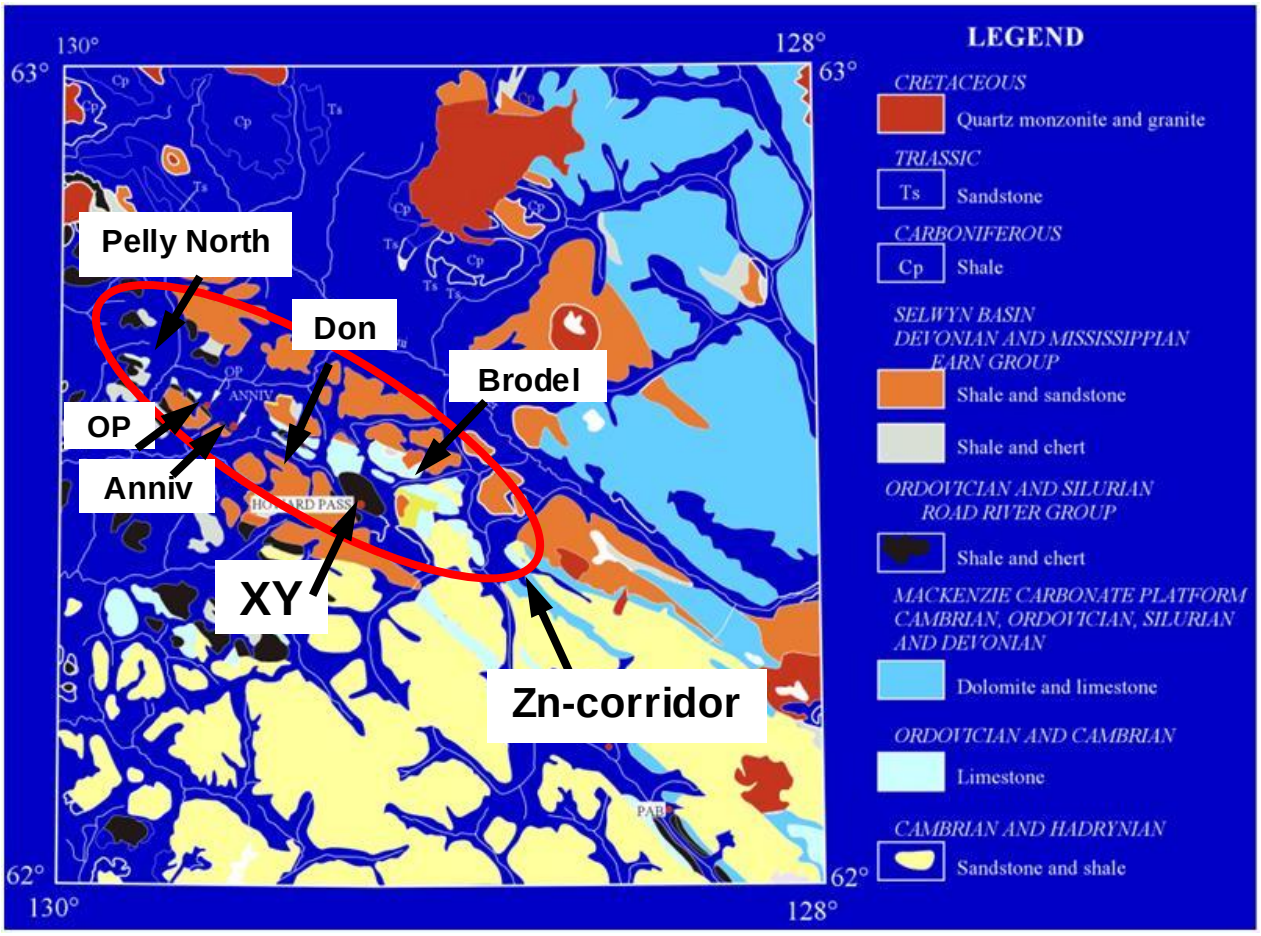

Figure 3: Geology of the Nahinni map-area, Selwyn Basin, Yukon Territory (modified from Gordey, 1981) showing the location of Howard's Pass and the "zinc corridor".

2.3. Local geology

Surface geology

The ARD creek chosen for this study is situated over a fault that lies directly above the central XY-deposit. The creek first emerges as a series of disseminated, acidic groundwater seeps (0, 10 m; Figure 4) at the summit of Sugar Mountain and flows over surficial Devonian shale (Figure 4). Further downstream, Devonian shale and chert are exposed at the surface (Figure 4) and due to their carbonate content, these units act to buffer the pH of the ARD waters, altering the stream geochemistry. In the lowermost

reaches of the creek, the surface waters flow over Silurian cherty mudstones before encountering Cambrian limestone (Figure 4), which acts to further neutralize these acidic waters.

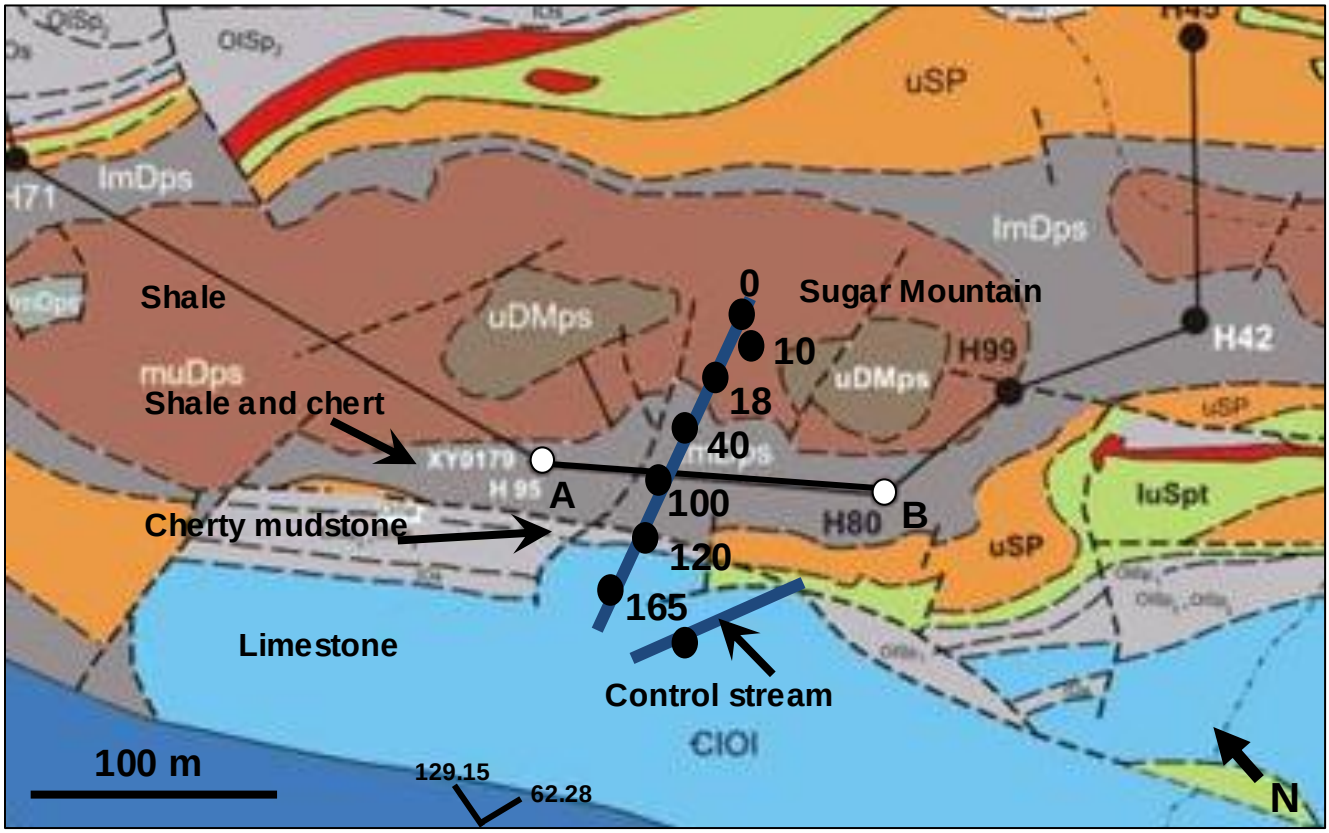

Figure 4: Map showing surficial geology in the vicinity of the ARD creek emanating at Sugar Mountain. Surficial geological units over which the stream flows are labelled and sampling locations are shown. Surface projection of the creek is shown as a blue line. Faults are shown as dashed lines. Modified from Goodfellow et al., 1983a.

Subsurface geology

The basal unit at the XY-deposit is Cambrian limestone (Rabbitkettle Formation), capped by a series of Ordovician to Lower Silurian mudstones, comprising the footwall sequence to the XY-deposit (Goodfellow et al., 1983a) (Figure 5). The lowermost unit in the footwall sequence is a pyritic mudstone, followed by calcareous and cherty mudstone

strata (Figure 5).

The Active Member, formed during the Lower Silurian, contains sphalerite and galena interbedded with argillaceous cherty limestone and carbonaceous cherty mudstone. Sphalerite, galena, and minor amounts of pyrite and chalcopyrite represent the only known sulphides in the Active Member (Goodfellow et al., 1983a). The Ordovician to Lower Silurian mudstones and the Active Member lie in a synclinal structure; however, the continuity of these units has been highly disrupted by extensive faulting.

The hanging wall is comprised of an Upper Silurian phosphatic chert and cherty mudstone unit, capped by an Upper Silurian orange-weathering dolomitic mudstone (Figure 5). The orange-weathering dolomitic mudstone is overlain by Lower to Mid Devonian shale and chert (Figure 5). These units are capped by Mid to Upper Devonian shale, overlain by Upper Devonian to Lower Mississippian brown-weathering mudstone, siltstone, and sandstone (not shown in stratigraphical column).

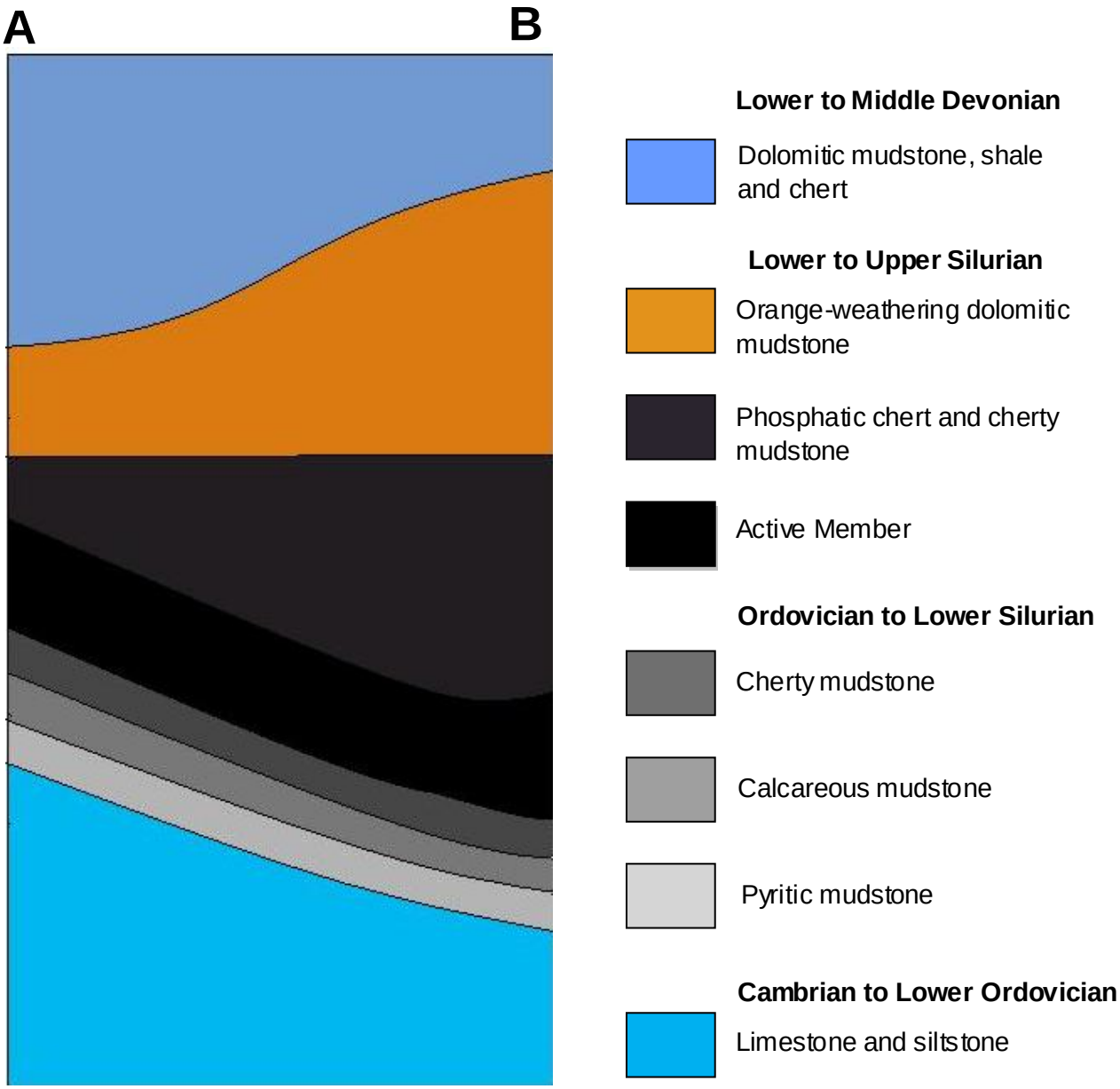

Figure 5: Geological cross-section of A-B in Figure 3. Modified from Goodfellow et al., 1983a. Vertical exaggeration is not to scale.

2.4. Local hydrology

The Howard's Pass area is characterized by discontinuous permafrost and is subject to heavy snowfall for 7 – 8 months of the year. The average field season temperature is 10 – 15 °C, while the average temperature from October – May is -15°C

(Morganti, 1979). Most of the streams in this area are second-order, and pervasive fracturing of the bedrock provides conduits for surface water-groundwater connectivity. Although aquifers in the area are recharged by melting snow and meteoric precipitation during the spring snowmelt, springs are fed mainly by groundwater in the later summer months (Jonasson et al., 1989). Perennial springs are common, and groundwater lenses have been observed at their vents during the winter months (Jonasson et al., 1989).

Since the hydrology is locally controlled, it can be inferred that the chemistry of these springs reflects the underlying geology (Jonasson et al., 1989). Most of the springs in the vicinity of Howard's Pass are alkaline due to the prevalence of limestone bedrock (Goodfellow et al., 1983b, Jonasson et al., 1989), although many acidic springs have also been observed. Numerous ARD streams emanate from the XY-deposit, flowing down avalanche chutes into Don Creek (Figure 2). Intensive local fracturing through the central XY-deposit provides conduits through which waters can interact with the Zn-Pb mineralization (Jonasson et al., 1989) and produce acidic drainage. Furthermore, springs were observed to emanate along almost all of the fault lines in the vicinity of the ARD stream (Figure 4).

3. Methods

3.1. Sample collection and preparation

3.1.1. Waters

In-situ measurements

Temperature (°C), pH, and ORP (mV) were measured at six locations along the streambed, various groundwater seeps, and one "control" (non-acidic) stream (Figure 4), during the summer (June – August) of 2008. Measurements were taken almost every day during the sampling campaign. Ferrous iron and sulphide were measured colorimetrically using phenanthroline and methlyene blue reagent sachets, respectively, on a field colorimeter (HACH). Samples above the upper limit of detection were diluted with filtered (0.45 µm) de-ionized water (DIW).

Due to logistical problems, pH and ORP measurements for the June sampling date could not be made (although samples for water and mineral precipitates were collected). Additionally, the upper reaches of the creek could not be sampled in June due to heavy snowpack and dangerous climbing conditions.

Water chemistry

A total of 130 water samples (10 % duplicates for quality assurance) were collected at six locations along the streambed, various groundwater seeps, and one "control" (non-acidic) stream (Figure 4), from June – August, 2008, for total elements and anions. Samples were syringe-filtered (0.45 µm) into HDPE bottles, and samples for total elemental analysis were acidified with ultrapure HNO_3 (1% v/v) upon returning to base-

camp. On one occasion (August 6, 2008) water samples were preserved with HCl (1% v/v) to determine the ferrous iron content upon returning to the laboratory.

All waters were sampled with a high degree of quality control: syringes were rinsed with stream water three times prior to filtering, and the first few drops of filtrate were discarded. HDPE bottles were rinsed with filtrate three times before the samples were dispensed into bottles. Travel blanks (acidified in the field) were prepared prior to departing for the field, and while in the field, acid blanks (unfiltered DIW transported from Ottawa + acid) and DIW blanks (filtered DIW + acid) were made on a daily basis when water samples (and travel blanks) were acidified. The reason for the series of blanks described here is to determine sources of systematic contamination to the samples; for example, travel blanks are used to determine if there was en-route contamination, while acid blanks are used to determine if the acid was contaminated, and DIW blanks are used to determine if the DIW was contaminated.

Samples were stored in the dark but could not be kept refrigerated due to the remote location of our sampling site and consequent lack of electricity. Samples were refrigerated promptly upon returning to the laboratory.

3.1.2. Mineral precipitates

Geochemistry and mineralogy

A total of 100 mineral precipitate samples (10 % duplicates for quality assurance) from six locations along the streambed and at various groundwater seeps around the XY-deposit (Figure 4) were collected using a clean spatula and Falcon tubes during the summer (June – August) of 2008. The pH, ORP (mV), and temperature (°C) of the water

flowing over the mineral precipitates were measured and syringe-filtered (0.45 µm) water samples were taken prior to sampling the mineral precipitates (see water sampling methods above). Some of the samples were laminated and the laminae were separated with a knife in order to analyze the geochemistry and mineralogy of the individual laminae. Pieces of talus and organic detritus cemented within the mineral precipitates were removed during sampling. All samples were stored in the dark prior to departure from the field and refrigerated promptly upon returning to the laboratory.

Precipitate preservation and embedding

A sub-set of the mineral precipitate samples were prepared for electron microscopy immediately upon returning to base-camp by fixing slurries and laminated samples with electron microscopy-grade glutaraldehyde to a final concentration of 2 % (v/v) for 30 minutes. Samples were washed five times with sterile-filtered (0.22 µm) stream water to remove the residual glutaraldehyde. A sub-set of these samples was stored wet in HDPE bottles for Environmental-scanning electron microscopy (E-SEM), while the remainder were put aside to be embedded (in the field) for thin sectioning (in the laboratory). The samples were dehydrated and infiltrated with Durcupan (Fluka) resin, which is miscible in water and precludes the need for sample dehydration with alcohol. Durcupan is comprised of four components, an embedding substance (component A), two hardeners (components B and C) and a plasticizer (component D). After samples were fixed and washed, they were dehydrated in a series of mixtures containing successively increasing concentrations of the embedding substance (Table 1).

Table 1: Mixtures used to dehydrate the mineral precipitate samples. The duration for which the sample was left in each mixture is indicated.

Solution number	Composition	Time
1	50 % component A 50 % DIW	30 minutes
2	70 % component A 30 % DIW	40 minutes
3	90 % component A 10 % DIW	40 minutes
4	100 % component A	90 minutes
5	100 % component A	90 minutes

The polymerization mixture was prepared with 5 mL of component A, 12 mL of component B, 1.2 mL of component C, and 0.4 mL of component D. The mixture was very viscous and left to penetrate the sample overnight. The following morning, gelatin capsules were filled with fresh polymerization mixture and charged with samples. These were cured in a camping oven at 40 °C for three days.

Upon returning to the laboratory and removing the gelatin capsules from the samples, it was apparent that the resin had not fully penetrated most of the samples and/or had not fully cured (some samples may have been too large and/or curing time/temperature may have been insufficient). Consequently, re-embedding was required prior to thin sectioning. Samples were re-infiltrated with a graded series of Durcupan and LR White (Table 2), which are miscible.

Table 2: Durcupan and LR white treatments for re-embedding the mineral precipitate samples.

Solution number	Composition	Time
1	50 % LR White 50 % Durcupan component A	30 minutes
2	70 % LR White 30 % Durcupan component A	30 minutes
3	90 % LR White 10 % Durcupan component A	30 minutes
4	100 % LR White	60 minutes
5	100 % LR White	60 minutes

Due to the very low viscosity of LR White, samples were left to infiltrate for an hour in each of the 100 % LR white treatments (Table 2). Gelatin capsules were filled with fresh LR White resin, charged with the samples, and cured at 60 °C for 24 hours. After treating the samples with LR white, they had been fully penetrated with the resin and had cured hard enough to be thin sectioned.

3.2. Laboratory methods

3.2.1. Water geochemistry

Water samples were analyzed at the GSC's Inorganic Geochemical Research Laboratory (IGRL) (Ottawa) by inductively-coupled plasma optical emission spectroscopy (ICP-OES) (Spectro Arcos EOP) for Al, Br, Ca, Cl, Fe, K, Mg, Mn, Na, Ni, P, S, Sc, Si, Y and Zn, and by inductively-coupled mass spectroscopy (ICP-MS) (Thermo-Electron X Series II) for Li, Be, B, Ti, V, Cr, Co, Cu, Ga, Ge, As, Se, Pb, Sr, Zr, Nb, Mo, Ag, Cd, In,

Sn, Sb, Te, Cs, Ba, La, Ce, Pr, Nd, Sm, Eu, Tb, Cd, Dy, Ho, Er, Tm Yb, Lu, Hf, Ta, W, Re, Tl, Pb, Bi, Th and U (Appendix 1). Rhodium and Ir were used as internal standards for the ICP-MS analyses. Ion chromatography (IC) (Dionex 600) was used to analyze Fe, Cl, SO_4, Br, NO_3 and PO_4 anions (Appendix 1). Analytical and field duplicates were always in close agreement with one another (Appendix 1). The molarity of sulphur determined by ICP-OES and IC were also in close agreement (Appendix 1). Accuracy and precision were verified against the following certified reference materials: ION-96.3, SLRS-4, and TMDA-51.3 for the ICP-OES, SLRS-4, TM-28.2, and TMDA-51.3 for the ICP-MS, and HAMILTON-20 and ION-96.2 for the IC. All analytes were in close agreement with the certified values (Appendix 1).

Prior to analyzing the anion samples, they were processed through on-Guard Na^+ columns to remove divalent and trivalent metals that can foul the IC column. This filtered the samples and removed any precipitates that had formed while samples were awaiting analysis.

Samples preserved with HCl in the field were analyzed colorimetrically by the Ferrozine method (Stookey et al., 1970) for their Fe(II) at the University of Ottawa (Ottawa) (Appendix 2). Total Fe (Fe(II) + Fe(III)) concentrations determined by the Ferrozine method were in agreement with those obtained by ICP-MS (Appendix 1).

3.2.2. Thermodynamic modeling

The geochemical program Phreeqc-*i* (version 2.15, Parkhurst and Appelo, 1999) was used to determine the aqueous speciation and saturation indices of mineral precipitates that could be expected when the ARD stream was at geochemical equilibrium. The solution composition (Al, Ba, Ca, Cd, Co, Cu, Fe (Fe^{2+}/Fe^{3+}), K, Mg, Mn, Na, Ni, Pb, S

(as S(VI)), Si, U, Zn), and solution parameters, including temperature, pH, Eh (derived from measured ORP values and adjusted for temperature (Appendix 3)) were input and simulations were performed for all of the sites sampled for two selected dates (July 17 and August 6, 2008). These dates were selected because the entire watercourse had been sampled on both of these dates. Simulations were run with the redox parameter specified as the pe or Fe^{2+}/Fe^{3+} redox couple (when Fe(II) values were known). The MINTEQ database, modified to include thermodynamic data for schwertmannite (Yu et al., 1999) and plumbojarosite (Hochella et al., 1999), was used to calculate the aqueous speciation and saturation indices for these waters.

3.2.3. Mineral precipitates

Geochemistry

Twenty-five mineral precipitate samples were selected for digestion and split into two aliquots; one aliquot was digested by Aqua-Regia (1:3 HNO_3:HCl) (Appendix 4) while the other was air dried at room temperature to calculate a wet-dry correction factor. Following the digest, elemental concentrations were determined by ICP-OES (Spectro Arcos EOP) (Al, Br, Ca, Cl, Fe, K, Mg, Mn, Na, Ni, P, S, Sc, Si, Y and Zn) and ICP-MS (Thermo-Electron X Series II) (Li, Be, B, Ti, V, Cr, Co, Cu, Ga, Ge, As, Se, Pb, Sr, Zr, Nb, Mo, Ag, Cd, In, Sn, Sb, Te, Cs, Ba, La, Ce, Pr, Nd, Sm, Eu, Tb, Cd, Dy, Ho, Er, Tm Yb, Lu, Hf, Ta, W, Re, Tl, Pb, Bi, Th and U) at the GSC's IGRL (Ottawa) (Appendix 5). Rhodium and Ir were used as internal standards for the ICP-MS analyses. Analytical and field duplicates were always in close agreement with one another (Appendix 5). Accuracy and precision of the ICP-MS were verified with the following certified reference materials:

Fe_2O_3, GXR-1, GXR-3, and Till-2. All analytes were in agreement with the certified values (Appendix 5).

Organic carbon content determination

The organic carbon content of the mineral precipitates was determined by loss on ignition (LOI), as described by Heiri et al. (2001). Mineral precipitate samples were weighed wet and successively baked at 105, 550 and 950 °C, for 24, 4 and 2 hours, respectively. The weight of the sample was measured when the sample had cooled after baking at each temperature, indicating the water content (loss at 105 °C), the organic carbon content (loss at 550 °C) and the carbonate carbon content (loss at 950 °C).

Mineralogy

The mineralogy of 20 mineral precipitate samples was determined by X-ray powder diffraction (XRD) (Bruker AXS) using copper Kα radiation and a LynxEye Position Sensitive detector at the GSC's Mineralogical Research Facility (Ottawa). Samples were prepared as pressed powders and scanned from 2 - 86° 2θ with a 0.02° step size and a step time of 10 s. Some of the scans were run with a knife-edge in order to determine if low angle peaks were real. The EVA software package and known X-ray spectra from the International Centre for Diffraction Data (ICDD) was used for fitting. For quality assurance, the major peaks for quartz that were naturally present in the samples were compared to standard reference spectra for quartz from the ICDD, and the XRD-determined mineralogy of the samples were cross-checked with the saturation indices generated from thermodynamic modeling.

Electron microscopy

Slurries of mineral precipitate that had been fixed in the field were prepared as whole mounts on carbon tape stubs for imaging by E-SEM at the GSC's Mineralogical Research Facility (Ottawa). Imaging and energy dispersive spectrometry (EDS) was performed using a Zeiss EVO 50 series scanning electron microscope operating at 20 kV, equipped with Everhart-Thronley backscattered, secondary, and variable pressure electron detectors, and an Oxford EDS system with an INCA X-series detector. Fitting of EDS spectra was completed with the INCA Energy 450 Microanalysis software.

Thin sections for transmission electron microscopy (TEM) were prepared at the University of Guelph. Imaging and EDS analysis were completed using a Phillips CM10 transmission electron microscope equipped with an EDAX Sapphire detector. The EDAX Genesis software program was used to fit the resulting spectra.

4. Results

4.1. Water Chemistry

4.1.1. Physico-chemical parameters

In the field, the creek was split into three areas defined by the appearance of their mineral precipitates, the groundwater seeps, the upper reaches, and the lower reaches. Subsequent locations were chosen for sampling in each of these three areas (Figure 4).

The groundwater seeps (locations 0 and 10 m) and upper reaches of the creek (locations 18 and 40 m) were acidic with pH ranges of 3.1 – 3.6 and pH 3.4 – 3.9, respectively (Figure 6). The lower reaches (locations 100 and 165 m) were moderately acidic, with a pH of 4.3 – 5.3 (Figure 6). All waters were highly oxidizing (pe 10 – 12)

(Figure 6) and very cold, with temperatures of 1 °C - 13 °C depending on the date and time of day (Appendix 6).

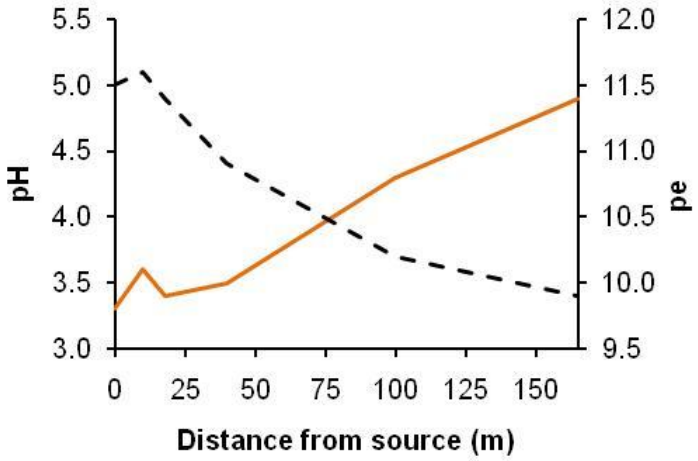

Figure 6: Change in pH (solid line) and pe (dashed line) with distance (m) from the ARD source (0 m). Data are representative of low-flow conditions (August 6, 2008).

4.1.2. Chemical characterization

Major elements

Overall, the elemental concentrations were highest at the groundwater seeps (0 and 10 m) and progressively decreased as the pH increased with distance downstream. Regardless of pH, sulphate (SO_4^{2-}) was the only major anion present in these ARD waters (Appendix 1). The groundwater seeps (0 and 10 m) were characterized by high concentrations of Fe (~300 mg/L), Al (~850 mg/L), SO_4 (~10 500 mg/L), and Si (~30 mg/L), in addition to extremely high concentrations of Zn for naturally acidic waters (maximum concentration was ~500 mg/L) (Table 3). These concentrations decreased with distance downstream, with Fe, Al, SO_4, Si, and Zn at concentrations of approximately 80, 200, 3000, 13, and 130 mg/L, respectively, under low-flow conditions (August 6) in the

upper reaches (18 and 40 m). Concentrations continued to decrease progressively into the lower reaches (100 and 165 m) of the creek as the pH increased, with Fe, Al, SO_4, Si, and Zn concentrations of approximately 25, 100, 2000, 10, and 80 mg/L, respectively, under base-flow conditions (Table 3).

Table 3: pH, sulphate and major elements (mg/L) in ARD waters for all sampling locations and a control stream. Data are representative of low-flow conditions (August 6). nd=not detected.

Distance (m)	pH	SO_4	Fe	Al	Zn	Si	Mg	Ca	Mn	K	Na
0	3.3	5064.1	158.2	353.6	411.4	13.2	371.2	285.5	41.4	1.6	1.3
10	3.6	10488.1	303.1	846.8	475.1	29.1	996.0	387.5	60.7	4.3	1.9
18	3.5	3271.5	84.4	187.4	134.4	13.1	314.3	264.7	19.0	2.2	1.4
40	3.5	2786.5	55.5	148.4	109.8	11.9	261.7	253.8	15.6	2.1	1.2
100	4.3	1998.1	25.5	103.0	76.8	9.6	194.3	228.8	10.8	1.9	1.0
165	4.9	1508.4	14.6	22.2	50.5	6.5	169.2	254.8	6.4	1.8	0.9
Control	8.3	277.8	nd	nd	0.3	2.7	40.1	114.3	nd	0.7	0.6

Trace elements

In general, the highest concentrations of trace elements (ug/L) were observed under low-flow conditions at the groundwater seeps (0 and 10 m) and the upper reaches (18 and 40 m) of the creek (Table 4). The groundwater seeps and upper reaches of the creek were characterized by high concentrations of Ni, Cd, Cu and Pb, with maximum concentrations of approximately 15 000, 4500, 1400, and 14 ug/L, respectively (Table 4). Nickel, Cu, and Cd concentrations were highest at one of the groundwater seeps (10 m,

pH 3.6), while Pb concentrations were highest at a more acidic groundwater seep (0 m, pH 3.3) (Table 4). Barium concentrations generally increased with distance and increasing pH (Table 4). Uranium concentrations were highest at the 10 m groundwater seep and decreased progressively with distance downstream and increased pH (Table 4).

Table 4: pH and select trace elements (ug/L) in ARD waters for all sampling locations and a control stream. Data are representative of low-flow conditions (August 6).

Distance (m)	pH	Ni	Cu	Cd	Pb	Ba	U
0	3.3	6866.4	246.0	1450.6	14.4	5.4	12.5
10	3.6	15251.8	1385.8	4560.5	10.7	6.7	605.7
18	3.5	4380.2	274.0	747.4	8.7	4.7	90.1
40	3.5	3676.4	209.0	620.2	7.5	5.8	75.4
100	4.3	2453.7	156.8	440.4	3.8	8.6	59.8
165	4.9	1759.3	84.4	259.3	1.5	16.2	47.5
Control	8.3	nd	0.2	1.1	0.3	81.0	7.6

4.1.3. Redox chemistry

Ferrous iron

The phenanthroline field analysis proved problematic for the determination of ferrous iron in the field as there was often precipitation within the sample holder. The ferrous iron concentrations determined by the phenanthroline method were invariably low (Table 5); given the highly acidic conditions of these waters, the proportion of Fe(II) comprising the total Fe pool should be much higher. When ferrous iron was measured by the Ferrozine method (for August 6 samples only), the results indicated that Fe(II)

comprised at least 65 – 75 % (molar abundance) of the total Fe pool for all of the sites that were sampled, despite the successively increasing pH (Table 5). These percent Fe(II) values, at least for the highly acidic waters (0, 10, 18 m), were much more typical of AMD/ARD compared to those determined by the phenanthroline method (Table 5). Therefore, the Ferrozine-determined Fe(II) concentrations were considered to be more reliable and were used for thermodynamic modeling when these data were available.

The Fe(II) concentrations determined by the phenanthroline method were convoluted because of chemical interferences from Ni, Cu, Zn, Mn, Al and Mg, as interferences have been noted for concentrations above 2.9, 4.4, 3.1, 4.5, 0.4, and 2.4 ug/L (Demirhan and Tuncel Elmali, 2003), respectively. Given the concentrations of these elements in the ARD waters at the XY-deposit (Table 3 and Table 4) it is clear that severe chemical interferences impeded the accurate determination of Fe(II) by this method. Although interferences with the Ferrozine method have been reported for Cu (Sarradin et al., 2005), the concentrations of Cu in our samples were not high enough to cause a problem with this anlaysis.

Table 5: Discrepancies between the percent molar abundance of ferrous iron determined by the Phenanthroline and Ferrozine methods for all sampling locations at two dates during the sampling campaign. pH and pe shown for reference.

Date	Site (m)	pH	pe	Percent molar abundance Fe(II)	
				Phenanthroline	*Ferrozine*
Jul-17	0	3.1	13.2	12	-
	10	3.5	11.9	15	-
	18	3.6	12.6	7	-
	40	3.9	12.2	6	-
	100	4.7	11.2	30	-
	165	5.3	10.6	2	-
Aug-06	0	3.3	11.5	16	-

	10	3.6	11.6	-	71
	18	3.5	11.4	24	60
	40	3.5	11.9	29	66
	100	4.3	10.2	3	68
	165	4.9	9.9	11	74

Sulphide

Sulphide (S^{2-}) concentrations were near-zero or non-detectable by field colorimetry. Given the highly oxidizing nature of these ARD waters (pe = 10 – 12), the absence of sulphide was not unexpected. Elemental S concentrations determined by ICP and sulphate concentrations determined by IC were in excellent agreement (Appendix 1), although, any reduced S species would have oxidized to sulphate prior to the samples being analyzed for sulphate in the laboratory.

4.2. Spatial evolution of water chemistry

4.2.1. Elemental attenuation with distance

All elemental concentrations showed a substantial decrease over the first 10 – 18 m of the creek despite relatively stable pH conditions (Figure 7), and continued to decline rapidly with increasing pH and distance (Figure 7).

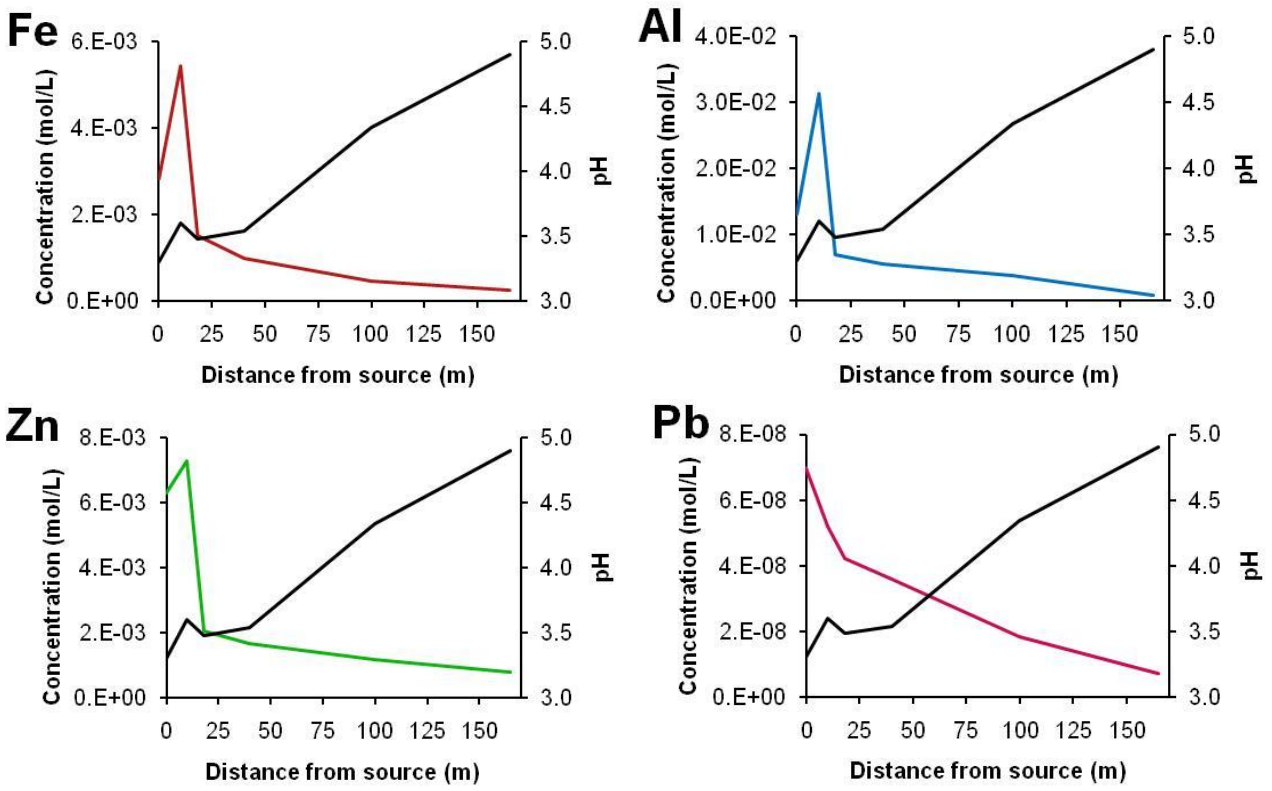

Figure 7: Attenuation for Fe, Al, Zn and Pb with pH and distance. Coloured lines represent concentrations (mol/L) and the black lines represent pH. Data is representative of low-flow conditions (August 6, 2008).

4.2.2. Dilution

To determine if dilution was the primary mechanism responsible for the attenuation of elements with increasing distance, the percent removal of certain elements was evaluated. Percent removal is defined here as the percent difference between the initial concentrations at the groundwater seeps relative to those in the lower reaches. Sodium is known to be conservative in natural waters and negligible concentrations of Na were detected in the mineral precipitates (Appendix 5) (i.e. natrojarosite ($NaFe_3(SO_4)_2(OH)_6$) is not a primary component of the mineral precipitates; this was confirmed by XRD), which suggested that it did indeed behave conservatively here. Thus, we expected the percent decrease in Na concentrations to be due to dilution. If dilution were the only process

responsible for the attenuation of other elements in the creek, we would expect them to show the same percent removal as Na. However, concentrations of Fe, Al, Cu Cd, S, Zn, Ni and Pb were over 80 % lower in the lower reaches of the creek relative to the groundwater seeps (Table 6), while concentrations of Na showed only a 50 % decrease (Table 6), indicating that over 30 % of the removal of Fe, Al, Cu, Cd, S, Zn, Ni and Pb were due to factors other than dilution. Calcium showed the least percent removal, at just over 30 % (Table 6), because Ca concentrations increased with distance downstream (Table 3). Although dilution will invariably play a role in the attenuation with elements downstream, it is not the only process responsible for the declining concentrations.

Table 6: Percent removal of selected elements from the stream waters. Percent removal is defined as the percent difference between the concentration of each element measured at the groundwater seeps and in the lower reaches of the creek.

Element	Percent removal
Fe	95
Al	97
S	86
Zn	89
Si	78
Ca	34
K	58
Na	53
Ni	88
Cu	94
Cd	94
Pb	86
Ba	48

4.3. Temporal evolution of water chemistry

4.3.1. Seasonal characterization

Generally, sulphate, major and trace element concentrations were the highest at all sampling sites under low-flow conditions (August 6) (Table 7 and Table 8). Although, on July 17, one of the groundwater seeps (0 m) had a low pH (3.1) with a higher load of dissolved metals when compared to August 6, with a pH of 3.3 (Table 7 and Table 8). For some of the sampling sites (40, 100, and 165 m) there was a decrease in pH over the course of the season, while for other sites (10 and 18 m) the pH was relatively constant with time (Table 7). The concentrations of some of the trace elements, including Ba, decreased from June to August (Table 8).

Table 7: pH, sulphate and major element concentrations (mg/L) for the sites sampled during the summer of 2008.

Date	pH	Fe	Al	SO_4	Zn	Si	Mg	Ca	Mn	K	Na
0 m											
Jul-17	3.1	190.2	470.0	6354.4	513.6	14.2	469.4	291.5	51.7	1.5	1.1
Aug-06	3.3	158.2	353.6	5064.1	411.4	13.2	371.2	285.5	41.4	1.6	1.3
10 m											
Jul-17	3.5	200.6	674.0	8268.1	337.8	29.0	719.7	368.4	45.3	3.7	1.6
Aug-06	3.6	303.1	846.8	10488.1	475.1	29.1	996.0	387.5	60.7	4.3	1.9
18 m											
Jul-17	3.5	58.2	140.0	2469.6	103.2	11.5	224.4	225.1	14.2	1.9	1.2
Aug-06	3.5	84.4	187.4	3271.5	134.4	13.1	314.3	264.7	19.0	2.2	1.4
40 m											
Jul-17	3.9	37.3	107.3	1997.2	78.9	10.2	179.5	211.6	10.9	1.8	0.9
Aug-06	3.5	55.5	148.4	2786.5	109.8	11.9	261.7	253.8	15.6	2.1	1.2
100 m											
Jul-17	4.7	13.7	50.2	1141.6	43.0	8.3	107.3	170.8	5.6	1.5	0.7
Aug-06	4.3	25.5	103.0	1998.1	76.8	9.6	194.3	228.8	10.8	1.9	1.0

165 m											
Jun-21	-	3.6	0.5	414.2	13.5	3.7	47.3	89.4	1.7	0.9	0.3
Jul-17	5.3	10.0	12.0	998.0	34.1	6.4	110.3	191.6	4.3	1.5	0.7
Aug-06	4.9	14.6	22.2	1508.4	50.5	6.5	169.2	254.8	6.4	1.8	0.9

Table 8: pH and trace elements (µg/L) for sites sampled during the summer of 2008.

Date	pH	Ni	Cu	Cd	Pb	Ba	U
0 m							
Jul-17	3.1	9086.5	321.0	1745.6	21.5	3.9	16.6
Aug-06	3.3	6866.4	246.0	1450.6	14.4	5.4	12.5
10 m							
Jul-17	3.5	11603.6	1044.9	2923.9	11.5	6.8	495.8
Aug-06	3.6	15251.8	1385.9	4560.5	10.7	6.7	605.8
18 m							
Jul-17	3.5	3354.2	210.0	571.0	6.6	4.7	66.4
Aug-06	3.5	4380.2	274.0	747.4	8.7	4.7	90.1
40 m							
Jul-17	3.9	2657.1	172.0	443.0	4.6	6.5	51.9
Aug-06	3.5	3677.2	209.0	620.2	7.5	5.8	75.4
100 m							
Jul-17	4.7	1482.2	115.2	253.1	1.8	10.5	34.6
Aug-06	4.3	2454.2	156.9	440.4	3.8	8.6	59.8
165 m							
Jun-21	-	0.5	36.7	62.8	0.3	35.6	0.7
Jul-17	5.3	1240.5	85.0	197.7	1.0	16.7	27.1
Aug-06	4.9	1759.7	84.4	259.3	1.5	16.2	47.5

4.3.2. Effect of rainfall on water chemistry

Meteoric precipitation influenced the water chemistry at all sites with the exception of the groundwater seep at 10 m (Figure 8). The metal concentrations in the first spring of acidic groundwater (0 m) were highest early in the season, decreased with increased meteoric precipitation, and increased again a few days after a large rainstorm (Figure 8 A). The concentrations measured at another groundwater seep (10 m) (Figure 8 B) increased over time, regardless of meteoric precipitation. The data for these two groundwater seeps (0 and 10 m) (Figure 8 A, B) (n=4) however, must be interpreted with caution as there were few samples relative to the other locations sampled (n=8) (Figure 8 C-F). The concentrations measured at locations 18, 40, 100, and 165 m fluctuated with rainfall and generally increased over time (Figure 8 C-F).

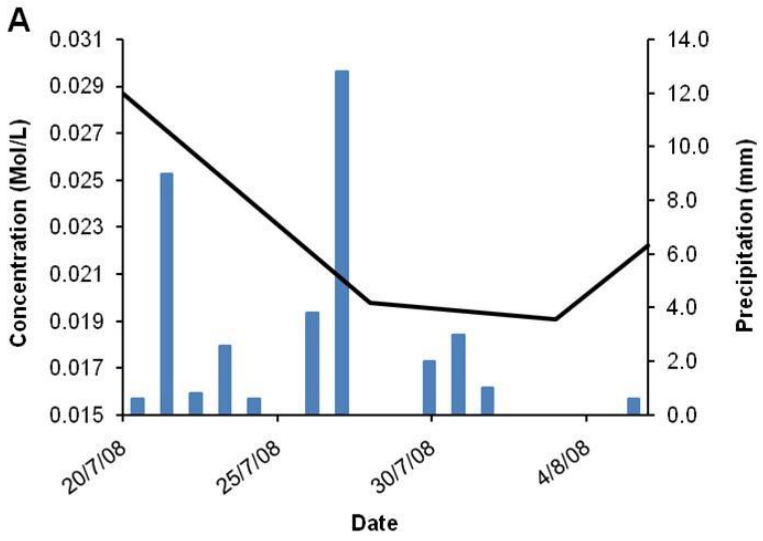

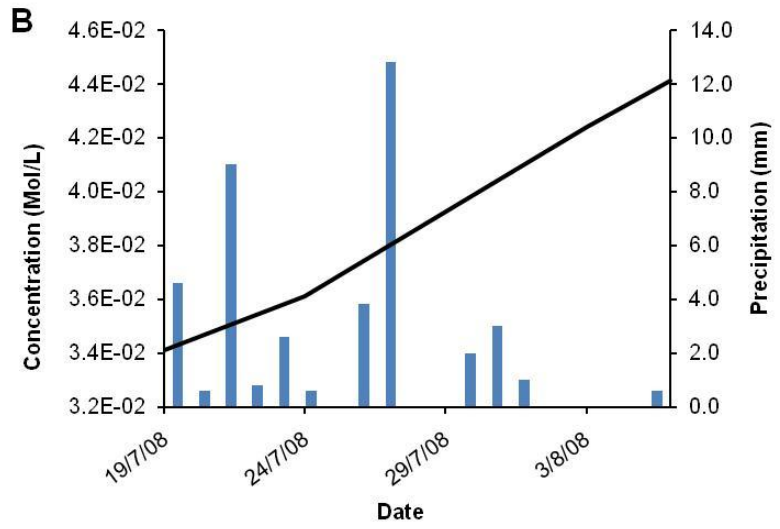
B
4.6E-02
4.4E-02
4.2E-02
4.0E-02
3.8E-02
3.6E-02
3.4E-02
3.2E-02
Concentration (Mol/L)
14.0
12.0
10.0
8.0
6.0
4.0
2.0
0.0
Precipitation (mm)
19/7/08
24/7/08
29/7/08
3/8/08
Date

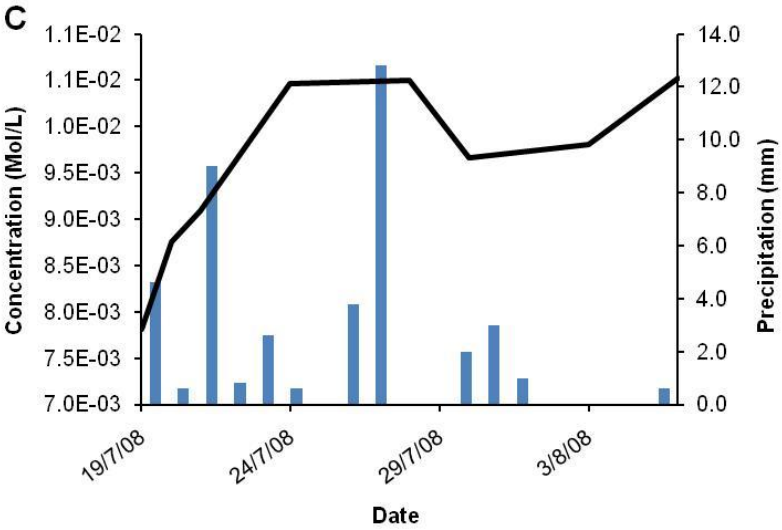
C
1.1E-02
1.1E-02
1.0E-02
9.5E-03
9.0E-03
8.5E-03
8.0E-03
7.5E-03
7.0E-03
Concentration (Mol/L)
14.0
12.0
10.0
8.0
6.0
4.0
2.0
0.0
Precipitation (mm)
19/7/08
24/7/08
29/7/08
3/8/08
Date

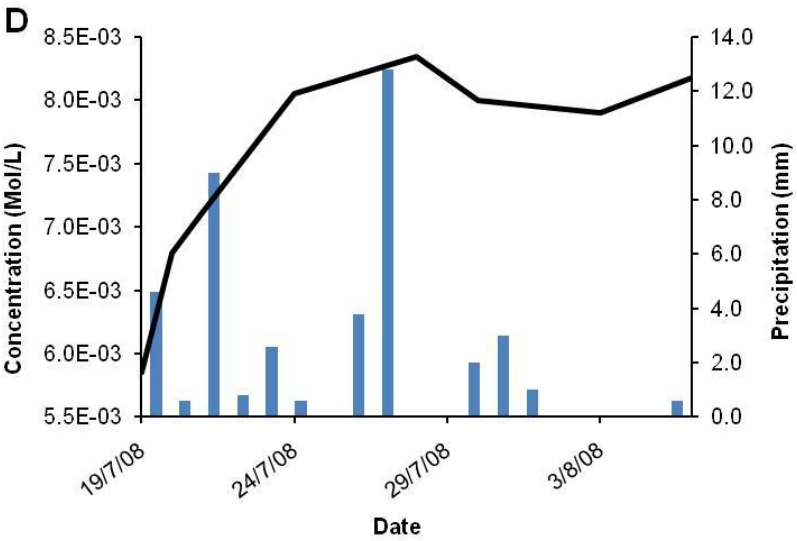
D
8.5E-03
8.0E-03
7.5E-03
7.0E-03
6.5E-03
6.0E-03
5.5E-03
Concentration (Mol/L)
14.0
12.0
10.0
8.0
6.0
4.0
2.0
0.0
Precipitation (mm)
19/7/08
24/7/08
29/7/08
3/8/08
Date

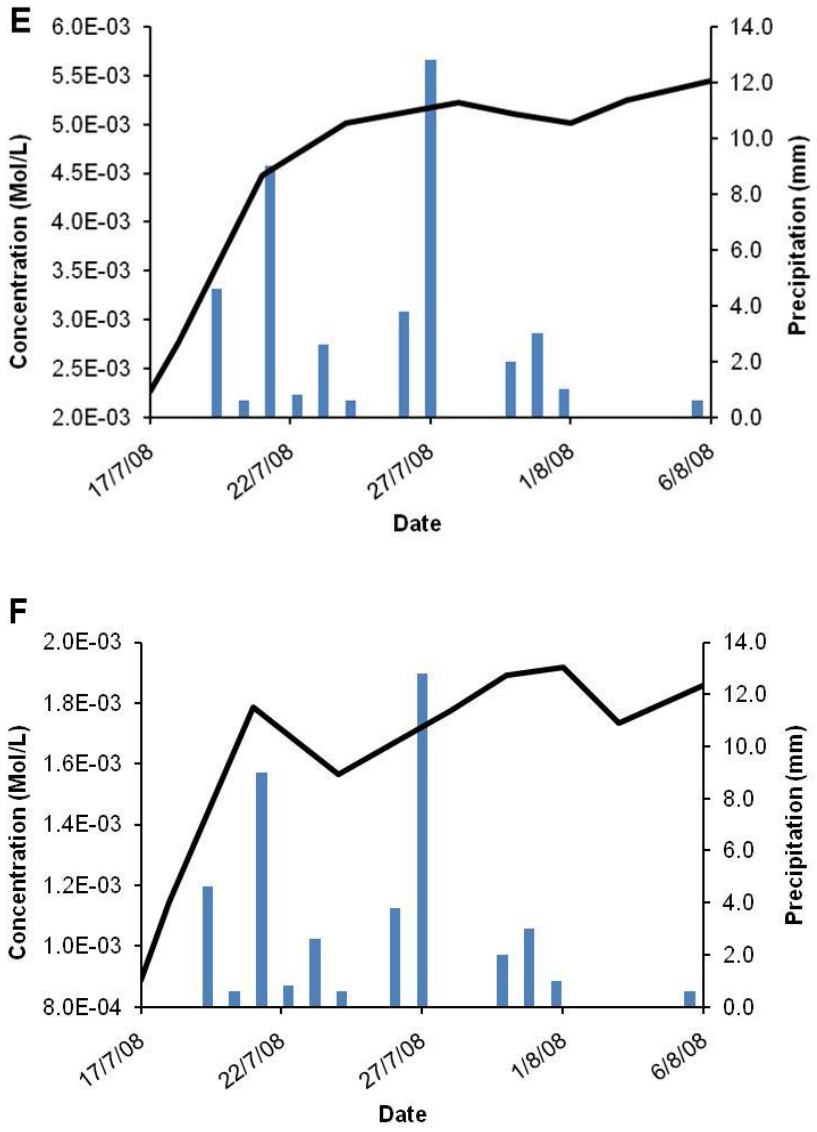

Figure 8: Meteoric precipitation (mm) and metal concentrations (Fe+Zn+Al) (mol/L) over the summer sampling season. The blue bars represent rainfall (m) and the black lines indicate the concentration of Fe+Zn+Al (mol/L). A, B, C, D, E and F correspond to sites 0, 10, 18, 40, 100 and 165 m, respectively.

4.4. Thermodynamic modeling

4.4.1. Ferrous iron

The modeled ferrous iron concentrations were generally in agreement with those determined by the Ferrozine assay, although they deviated with distance and increasing pH (Figure 9). Unexpectedly, the Ferrozine-determined percent Fe(II) values were close to

70 % in the lower reaches (100 and 165 m) (Table 9), despite the increase in pH (up to pH 4.9). Thermodynamic modeling indicated that Fe(II) should decline to near-zero values with increasing pH although this was not observed (Table 9).

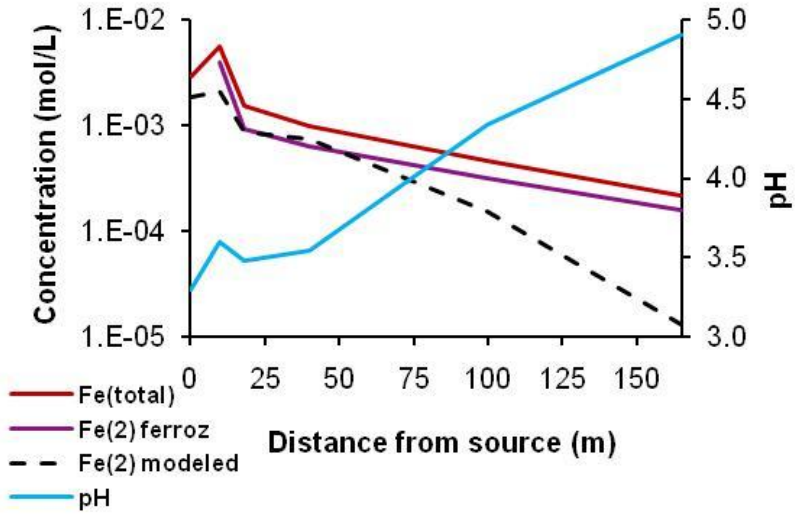

Figure 9: Concentration of ferrous iron determined by the Ferrozine method and by thermodynamic modeling. Total Fe was determined by ICP-MS. Data are representative of low-flow conditions (August 6, 2008).

Apart from the Fe(II)/Fe(III) speciation, the results of the thermodynamic modeling showed no significant differences ($p = 0.01$) in the species distribution patterns (or saturation indices) when the redox parameter was specified as the measured pe compared to when it was defined as the Ferrozine-determined Fe(II)/Fe(III) concentration. pe is known to be an accurate indicator for the Fe-redox chemistry in AMD/ARD, as Fe(II)/Fe(III) is often the dominant redox couple controlling the pe of these waters (Sanchez-Espana et al., 2005). Therefore, the speciation and saturation indices derived from the pe-defined simulations were considered valid.

Thermodynamic modeling showed that the ferrous iron pool was comprised of Fe^{2+} and $FeSO_4$, both of which remained at a constant 70 and 30 %, respectively, with distance downstream.

4.4.2. Ferric iron

For both the July and August thermodynamic calculations, $Fe(OH)_2^+$ was the dominant ferric iron species, making up nearly 100 % of the ferric iron pool as the pH approached 4 (Table 9). For July 17, $FeSO_4^+$ was found at the groundwater seeps (0 and 10 m) at 40 and 18 % $FeSO_4^+$, respectively (Table 9). For August 6 (low-flow conditions), $FeSO_4^+$ (30 – 15 %) was found at the 0, 10, 18 and 40 m sites (Table 9). $Fe(SO_4)_2^-$ was present at low abundances (~ 10 %) at the groundwater seeps (0 and 10 m) on the July 17, but was only found at the most acidic of these sites (0 m, pH 3.3) on August 6 simulations (Table 9). Fe^{3+} was present in low percent abundance levels (6 %) at the first groundwater seep (0 m), but only when the pH was very low (pH 3.1) on July 17 (Table 9). More complex ferric iron species, including $Fe_3(OH)_4^{5+}$ and $Fe_2(OH)_2^{4+}$, were present in low abundances (~ 5 – 10 %) at the 10 m site under low-flow conditions (Table 9). $Fe(OH)^{2+}$ was present in low abundances at 0, 18, and 40 m (~5%) during low-flow conditions only (Table 9).

Table 9: Distribution of ferric iron species (percent molar abundance) for the July 17 and August 6 thermodynamic modeling. Percent molar abundances < 5 % are not shown.

Site	pH	$Fe(OH)_2^+$	$FeSO_4^+$	$Fe(SO_4)_2^-$	Fe^{3+}	$Fe_2(OH)_2^{4+}$	$Fe_3(OH)_4^{5+}$	$FeOH^{2+}$
Jul-17								
0	3.1	30	40	13	6	-	-	-
10	3.5	57	18	7	-	-	-	-
18	3.5	86	8	-	-	-	-	-
40	3.9	97	-	-	-	-	-	-

100	4.7	100	-	-	-	-	-	-
165	5.3	100	-	-	-	-	-	-
Aug-6								
0	3.3	48	32	8	-	-	-	6
10	3.6	43	10	-	-	6	9	-
18	3.5	75	15	-	-	-	-	5
40	3.5	74	15	-	-	-	-	6
100	4.3	99	-	-	-	-	-	-
165	4.9	100	-	-	-	-	-	-

4.4.3. Sulphur

Sulphur was specified to be S(VI) for thermodynamic modeling, as reduced sulphur species were not detected and these waters were highly oxidizing. Sulphate (SO_4^{2-}) comprised the majority of the S-species (~ 60 – 70 %) in these waters, and progressively increased with distance and pH for both the July and August thermodynamic calculations (Figure 10 A and B). $AlSO_4^+$ followed in abundance, with approximately 20 % abundance in the upper reaches (18 and 40 m), but declined to near-zero levels with increasing pH and distance for both of the dates (Figure 10 A and B). $Al(SO4)_2^-$ was present at low abundances (5 %) at only one site under low-flow conditions (August 6) (Figure 10 B) and was the only other Al-sulfate species present in these waters. $MgSO_4$ abundance was approximately 10 %, regardless of the date, pH, or distance downstream (Figure 10 A and B). $CaSO_4$ showed a slight increase in abundance with increasing pH and distance, up to a maximum of approximately 13% for both dates (Figure 10 A and B).

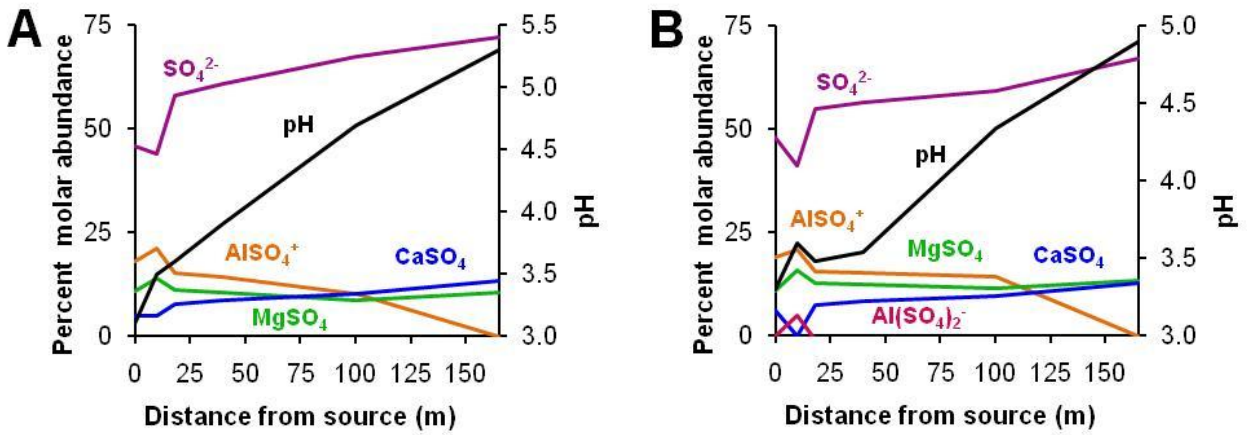

Figure 10: Distribution of S(VI) species with distance and pH for July 17 (A) and August 6 (B) thermodynamic calculations. Percent abundances < 5% were not shown.

4.4.4. Aluminum

$AlSO_4^+$ represented over 70 % of the total Al pool at almost every site that was sampled for both the July and August dates; however, slight decreases in $AlSO_4^+$ abundance were observed in the lower reaches of the creek (Figure 11 A and B). Al^{3+} represented a much smaller proportion of the total Al pool, with only 11 – 21 % abundance overall. In July, Al^{3+} increased with distance and pH, up to site 100 m, but had decreased (> 5 %) by site 165 m (Figure 11 A). Percent Al^{3+} abundances were generally lower and more stable with distance under low-flow conditions (August 6), and slightly increased with distance and pH (Figure 11 B). $Al(SO_4)_2^-$ abundance was greatest (15 %) at one of the groundwater seeps (10 m), and progressively decreased to zero with increasing pH and distance for the July calculations (Figure 11 A). Similar to Al^{3+}, the abundance of $Al(SO_4)_2^-$ was much more stable under low-flow conditions, and showed a slight decrease with increasing distance and pH (Figure 11 B). $Al(OH)_2^+$ was present (13 %) at the 165 m site in July (Figure 11), although this species was not present in the calculations for August.

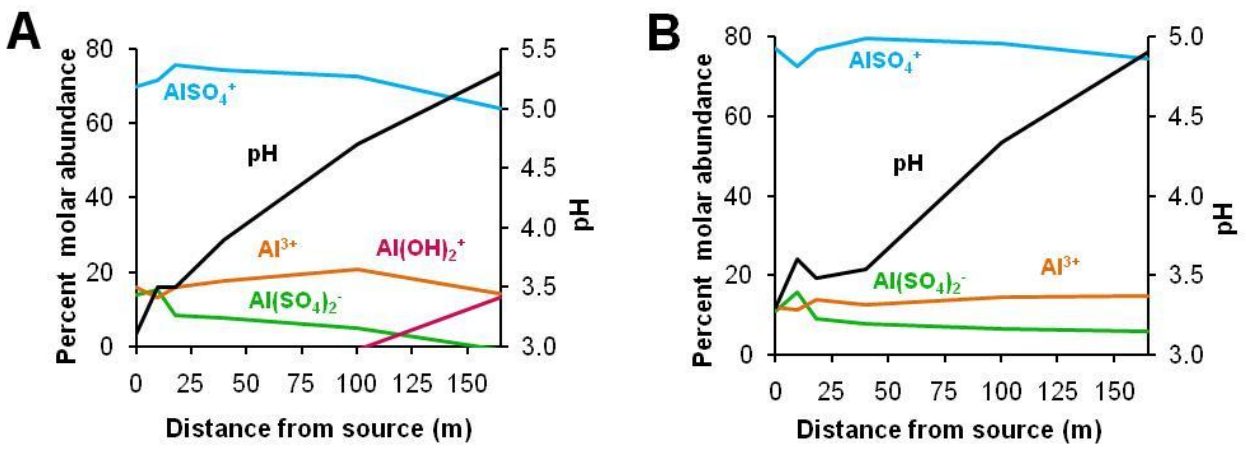

Figure 11: Distribution of Al species (percent molar abundance) with pH and distance for July 17 (A) and August 6 (B) thermodynamic calculations. Percent abundances < 5% were not shown.

4.4.5. Zinc and Cadmium

The dominant species of Zn and Cd were Zn^{2+} and Cd^{2+}, both of which had the lowest percent abundance at the 10 m groundwater seep (~ 35 and 28 % respectively). Zn^{2+} and Cd^{2+} progressively increased in abundance with distance and pH, up to 70 and 60 %, respectively, for both the July and August dates (Figure 12 A-D). Generally $ZnSO_4$ and $CdSO_4$ were the next most abundant species, with an abundance of approximately 30 % regardless of distance, pH or date (Figure 12). The least abundant Zn species was the Zn-bisulphate anion, $Zn(SO_4)_2^{2-}$. In July, the percent molar abundance of $Zn(SO_4)_2^{2-}$ was highest (~30 %) at one of the groundwater seeps (10 m) but declined to near-zero in the lower reaches (100 and 165 m) (Figure 12 A and B). However, in August, $Zn(SO_4)_2^{2-}$ was found to persist at low but up to the 100 m location (~5%) (Figure 12 B). $Cd(SO_4)_2^{2-}$ showed a similar distribution to $Zn(SO_4)_2^{2-}$, each with a maximum abundance of 47 and 35 %, respectively, under low-flow conditions (August 6). $Cd(SO_4)_2^{2-}$ was the dominant Cd species at one of the groundwater seeps (10 m) for the July and August dates (38 and 47 % respectively) (Figure 12 C and D), whereas $Zn(SO_4)_2^{2-}$ was never the dominant Zn

species for any of the locations or either of the dates. Similar to $Zn(SO_4)_2^{2-}$, $Cd(SO_4)_2^{2-}$ declined with distance and pH, and the maximum distance at which $Cd(SO_4)_2^{2-}$ was found in July was the 40 m site (Figure 12 A and C). However, unlike $Zn(SO_4)_2^{2-}$, $Cd(SO_4)_2^{2-}$ was found to be present (7 %) at the 165 m site in August (Figure 12 B and D).

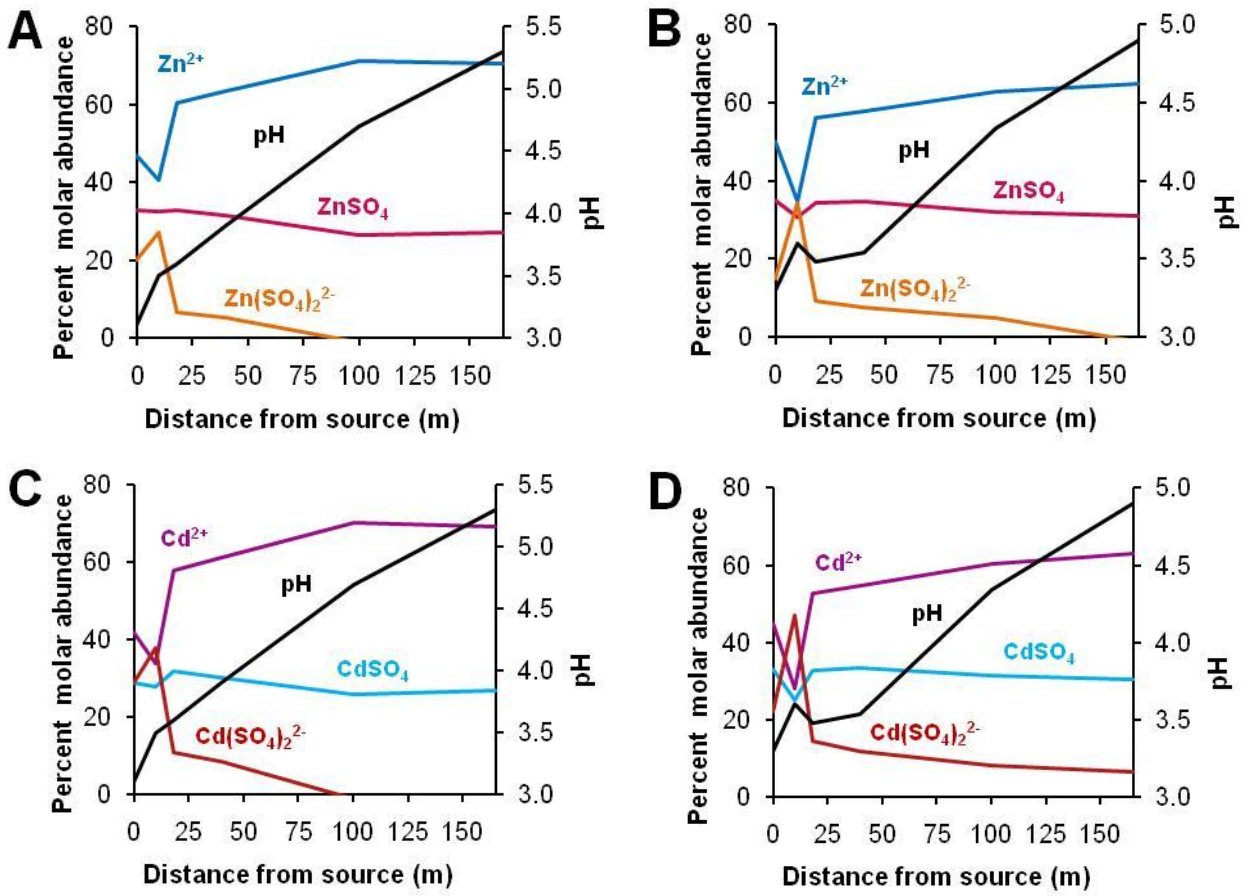

Figure 12: Distribution of Zn and Cd species (percent molar abundance) with pH and distance for July 17 (A and C) and August 6 (B and D) Phreeqc-i simulations. Percent abundances < 5% were not shown.

4.4.6. Nickel and Copper

For both the July and August thermodynamic calculations, Ni^{2+} and Cu^{2+} were the dominant Ni and Cu species, making up approximately 60 – 70 % of the total abundance

of each element at all but one of the sites that were sampled (Figure 13). $NiSO_4$ and $CuSO_4$ accounted for the remaining 30 – 40 % of Ni and Cu species (Figure 13), with maximum abundances at one of the groundwater seeps (10 m) (Figure 13). The distributions for the Ni and Cu species were very similar for July and August.

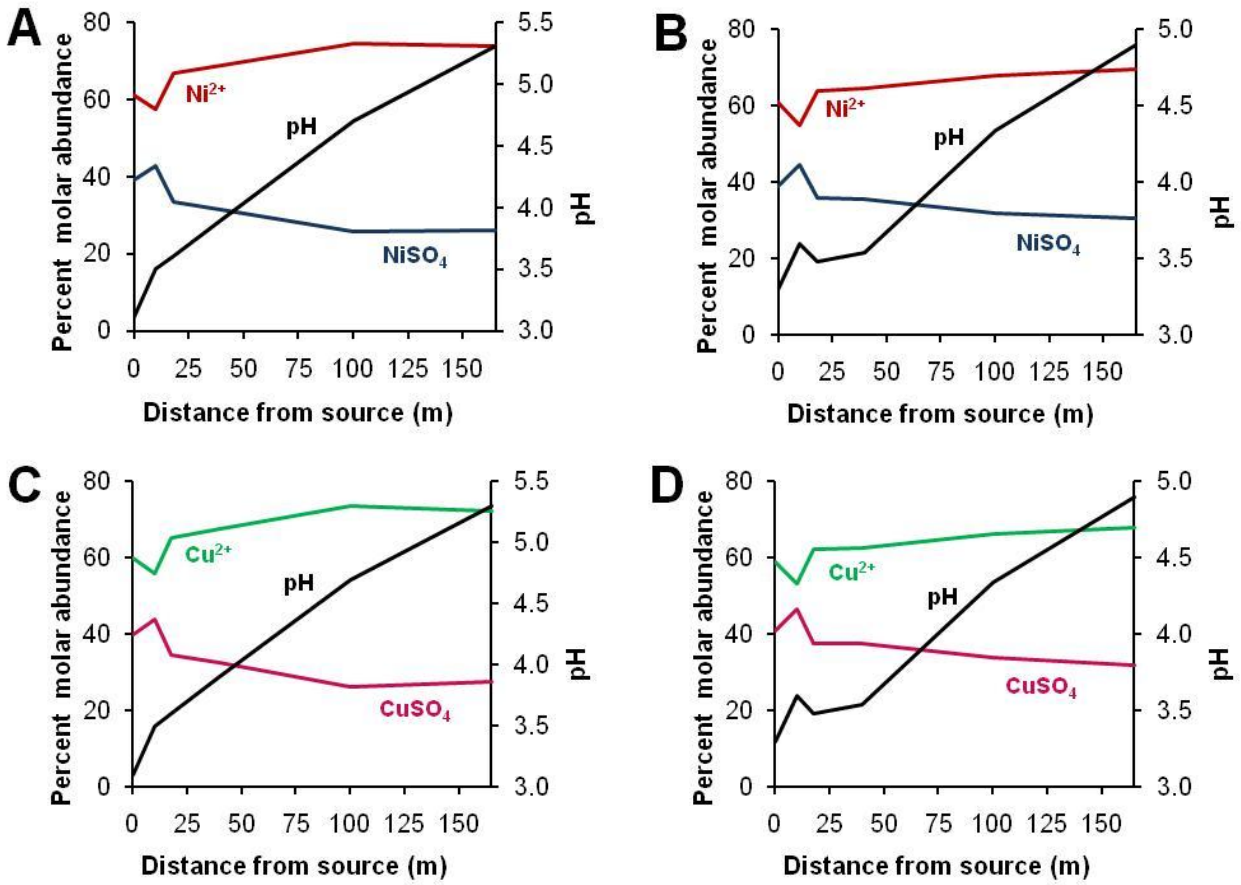

Figure 13: Distribution of Ni and Cu species (percent molar abundance) with pH and distance for July 17 (A and C) and August 6 (B and D) thermodynamic calculations. Percent abundances < 5% were not shown.

4.4.7. Lead

$PbSO_4$ comprised approximately 50 % of the total Pb pool in both July and August, and showed little fluctuation with increased distance and pH (Figure 14). Pb^{2+} followed in abundance, with the lowest Pb^{2+} percent abundances (25 %) found at the groundwater seeps (0 and 10 m) and higher percent abundances in the lower reaches (100 and 165 m)

of the creek (up to 50 %) (Figure 14). $Pb(SO_4)_2^{2-}$ was the least abundant Pb species, with a maximum abundance of approximately 30 % at one of the groundwater seeps (10 m) under low-flow conditions (August 6) (Figure 14B). In August, $Pb(SO_4)_2^{2-}$ was found to persist at low abundances (~5%) up to and at the 100 m site (Figure 14 B), whereas in July, the maximum distance at which $Pb(SO_4)_2^{2-}$ was found was 40 m (~5%) (Figure 14 A).

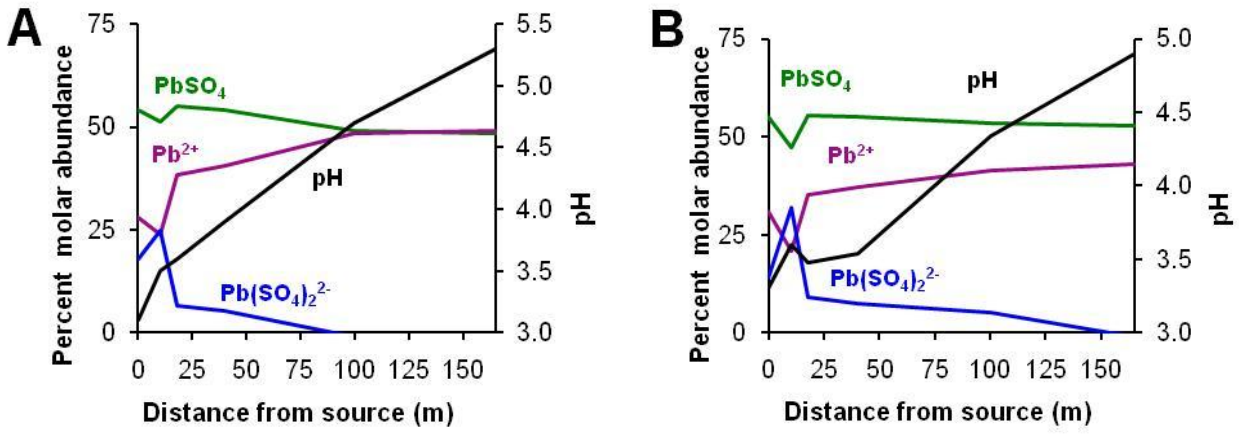

Figure 14: Distribution of Pb species (percent molar abundance) with pH and distance for July 17 (A) and August 6 (B) thermodynamic calculations. Percent abundances < 5% were not shown.

4.4.8. Uranium

UO_2SO_4 was the dominant U species, generally having 50 – 65 % abundance at all sampling locations (Figure 15). UO_2SO_4 abundance was lowest at one of the groundwater seeps (10 m), where $UO_2(SO_4)_2^{2-}$ abundance was maximum (45 %). $UO_2(SO_4)_2^{2-}$ abundances progressively decreased with increasing pH and distance; the maximum distance at which $UO_2(SO_4)_2^{2-}$ (~10%) was found in July was 40 m, while in August $UO_2(SO_4)_2^{2-}$ (~10%) was found at 165 m (Figure 15). $UO_2H_3SiO_4^+$ was present at low abundances (~5%) at 165 m in July, but was not present in August (Figure 15).

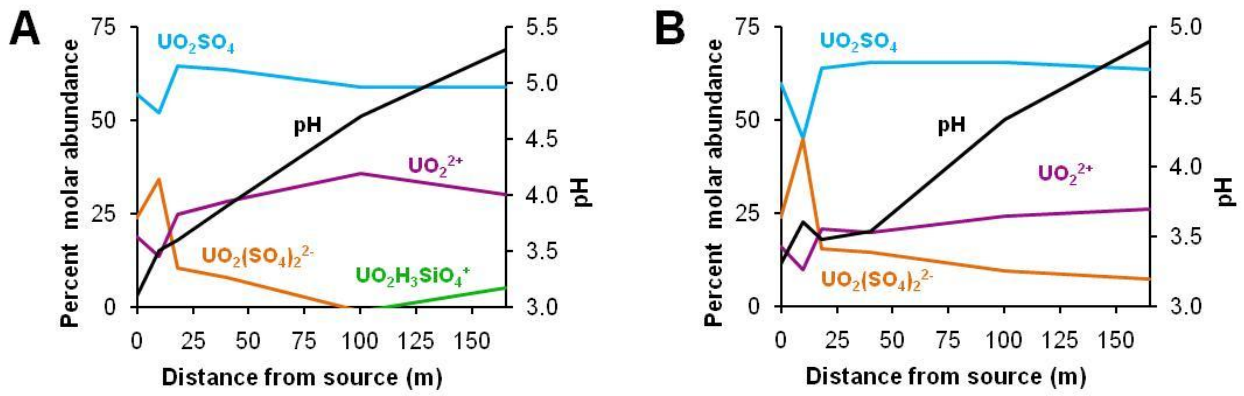

Figure 15: Distribution of U species (percent molar abundance) with pH and distance for July 17 (A) and August 6 (B) thermodynamic calculations. Percent abundances < 5% were not shown.

4.5. Mineral precipitates

4.5.1. In-situ description

Groundwater seeps

Mineral precipitates were very difficult to collect at one of the groundwater seeps (0 m) since they were only present as a thin coating on the streambed (Figure 16 A, B). The mineral precipitates at the second, larger groundwater seep (10 m) were in the form of a thick, maroon-coloured hardpan covering a talus slope (Figure 16 C, D).

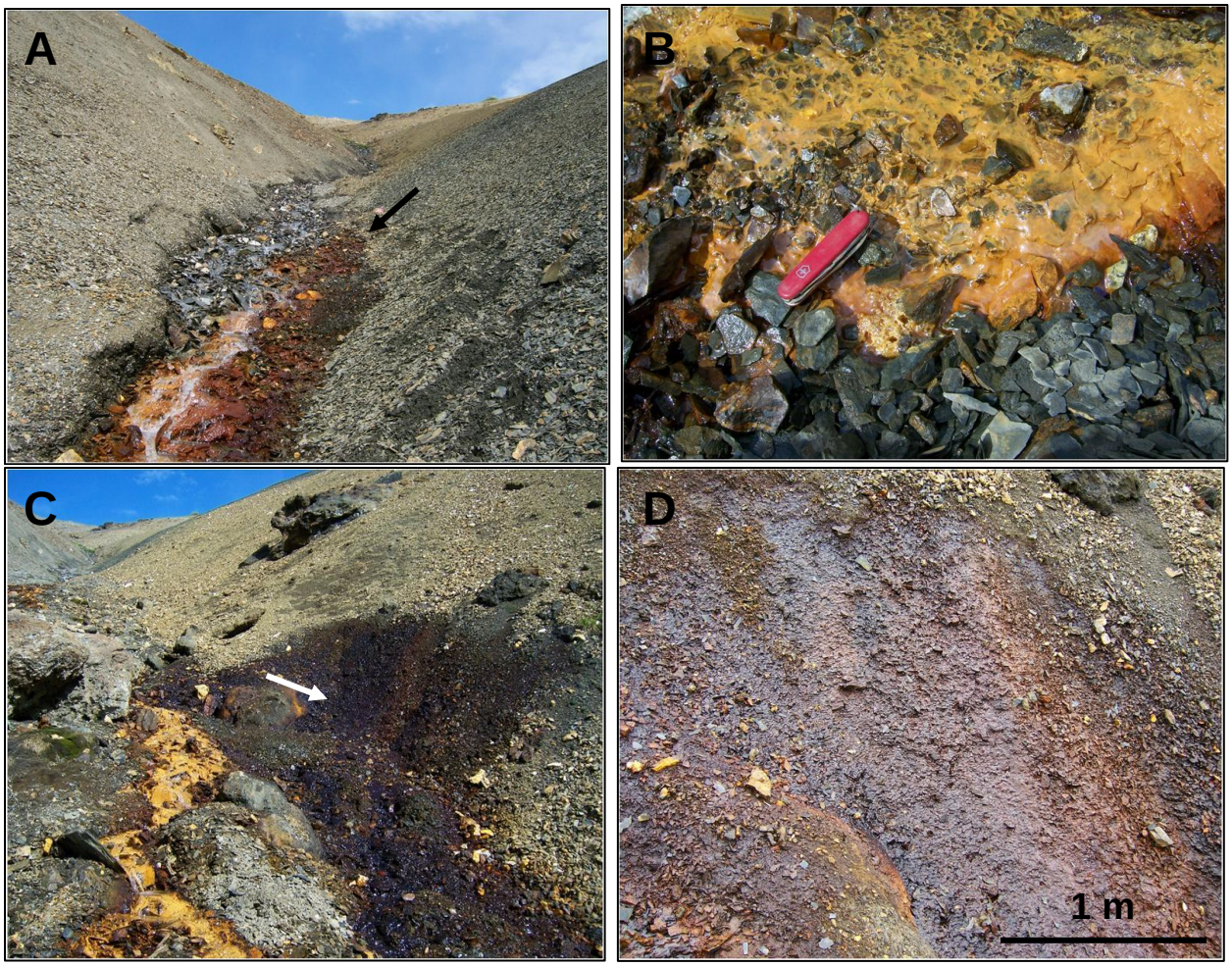

Figure 16: Mineral precipitates at the groundwater seeps. A) Mineral precipitates at the 0 m groundwater seep, arrow indicates location of (B). C) Mineral precipitates at the 10 m groundwater seep, arrow indicates location of the maroon-coloured hardpan precipitate (D).

Upper reaches

The mineral precipitates in the upper reaches (18 m) were identified as terraced iron formations (TIFs) (Figure 17 A-E) and consisted of alternating orange-coloured, soft laminae, with red-brown-coloured hard laminae (Figure 17). Terraced iron formations are defined by alternating pools and curved ridges that form perpendicular to the flow of water (Figure 17 E). Mounds of precipitates were often observed to coalesce in the pools and form incipient terrace rims (Figure 17 D).

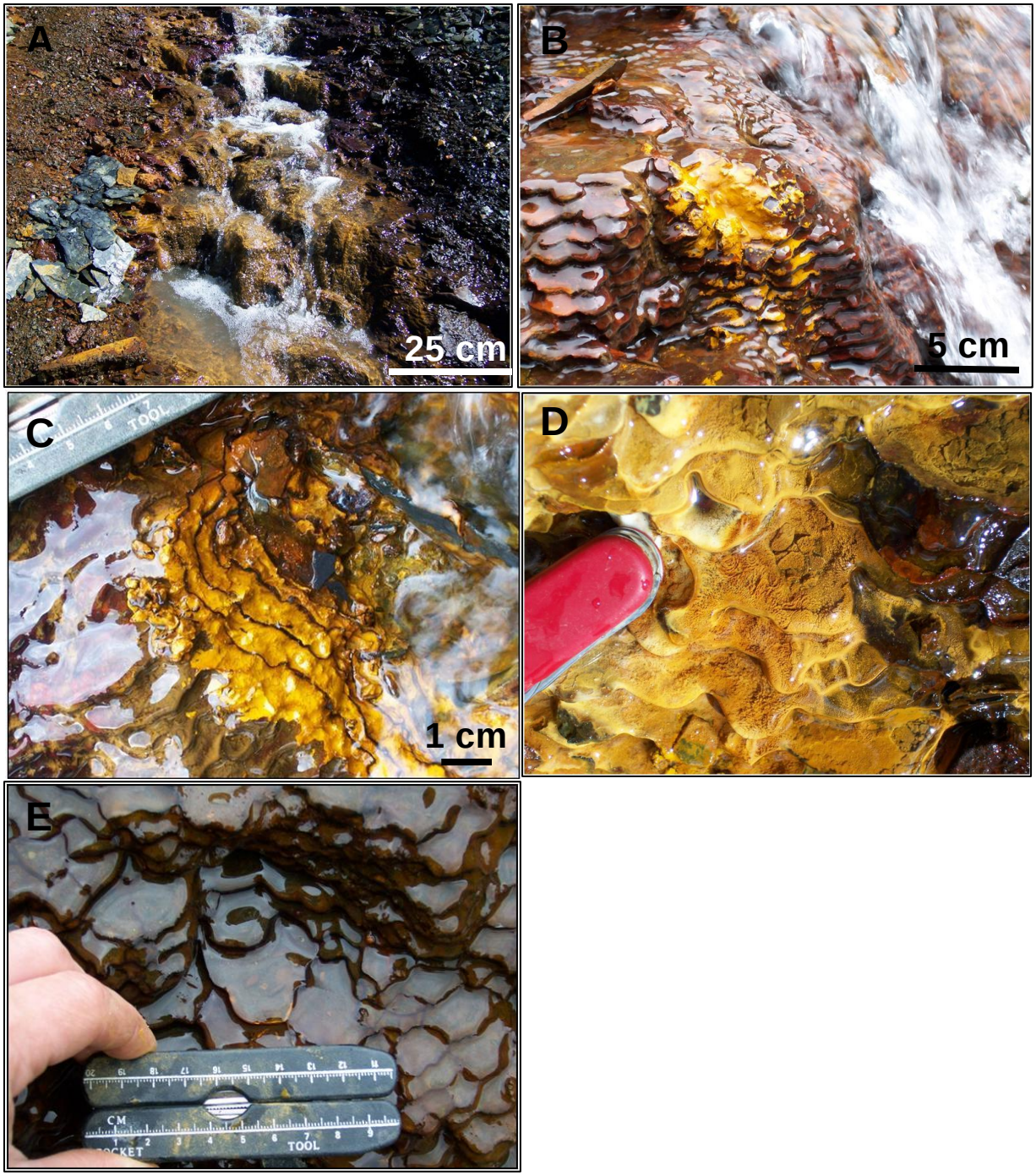

Figure 17: Terraced iron formations (TIFs) found at 18 m in the upper reaches. A) Terraced iron formations, B) TIFs with hard, brown-red-coloured surface removed exposing soft, orange-coloured precipitates, C) Cross-section of TIF, showing alternating thin red-brown-coloured ("red laminae") and thick orange-coloured laminae ("orange precipitate (b)"), D) mounds of loose orange-coloured precipitate coalescing in pools to form incipient rims ("orange precipitate (a)"), E) hard red-brown-coloured mineral precipitate forming alternating pools and incipient terrace rims.

The colour and texture of the mineral precipitates at the 18 m site changed over the duration of the sampling campaign. In July the surface of the TIFs were a red-brown colour and very hard (Figure 18 A and Figure 17 E), and as time progressed, soft, thick orange-coloured precipitates began to accumulate (Figure 18 B and Figure 17 D).

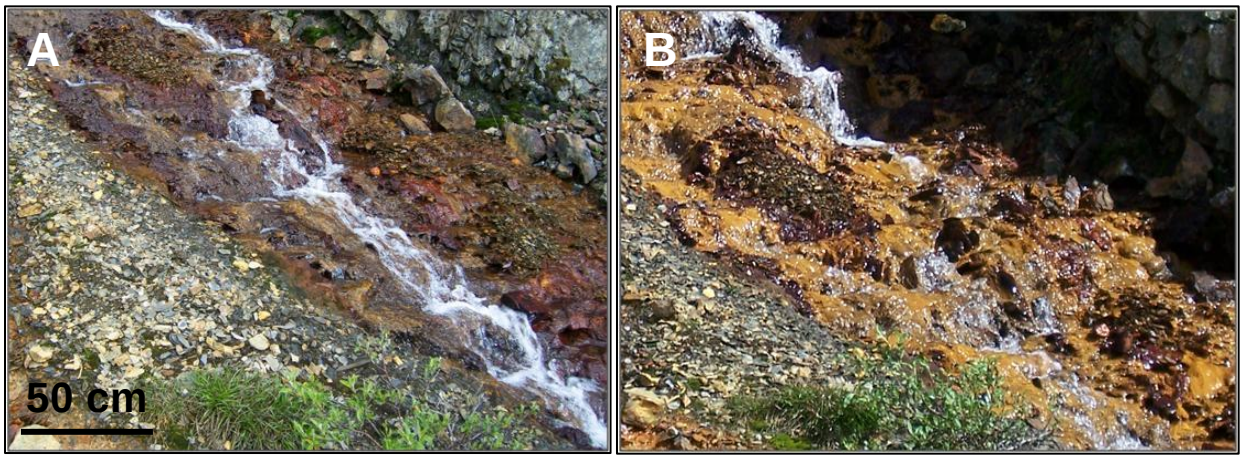

Figure 18: TIFs at 18 m in the upper reaches. A) red-brown-coloured mineral precipitates (July 24/08), B) orange-coloured mineral precipitates (August 8/08).

Although the orange-coloured mineral precipitates at the 40 m site were not TIFs, they did bear a similar structure, in that they had highly rippled surfaces (Figure 19 A) that looked similar to incipient terrace rims (Figure 17 D and E). These precipitates were not laminated (Figure 19 B) and showed no visually discernable colour change over the duration of the sampling campaign. The texture and cohesiveness of these precipitates were similar to the soft, orange-coloured laminae from the TIFs at 18 m.

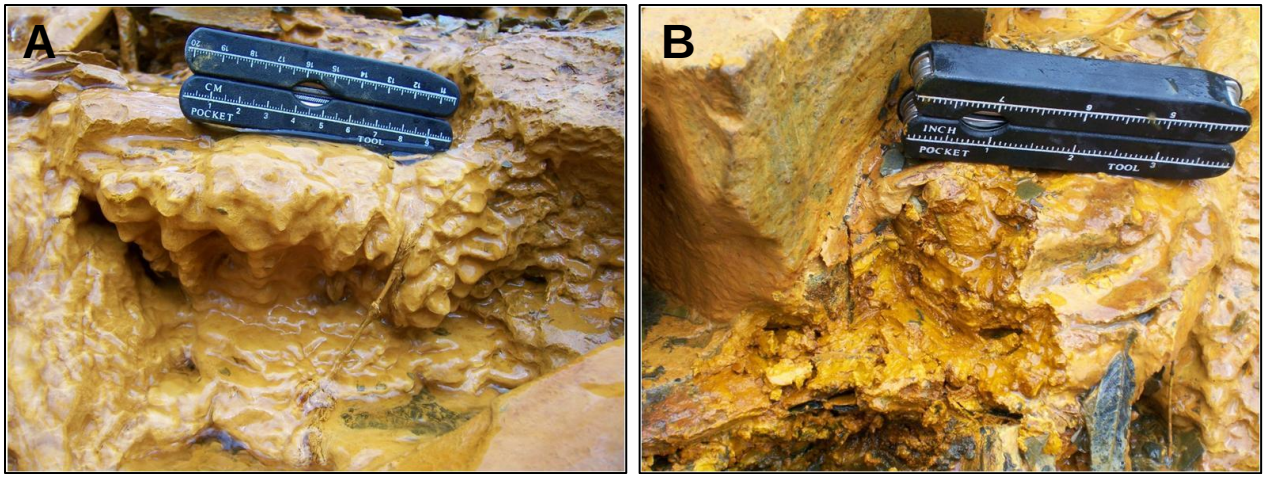

Figure 19: Orange-coloured mineral precipitates at 40 m in the upper reaches. A) Rippled surfaces are similar to incipient rims in TIFs, B) Cross-section of mineral precipitates, no laminations were observed in the mineral precipitates at this location.

Lower reaches

The light orange-coloured precipitates collected at 100 m had rippled surfaces similar to the TIFs (Figure 20) although they were not laminated. These precipitates were lighter in colour in July when compared to August, although the colour change was not as dramatic relative to the other sites.

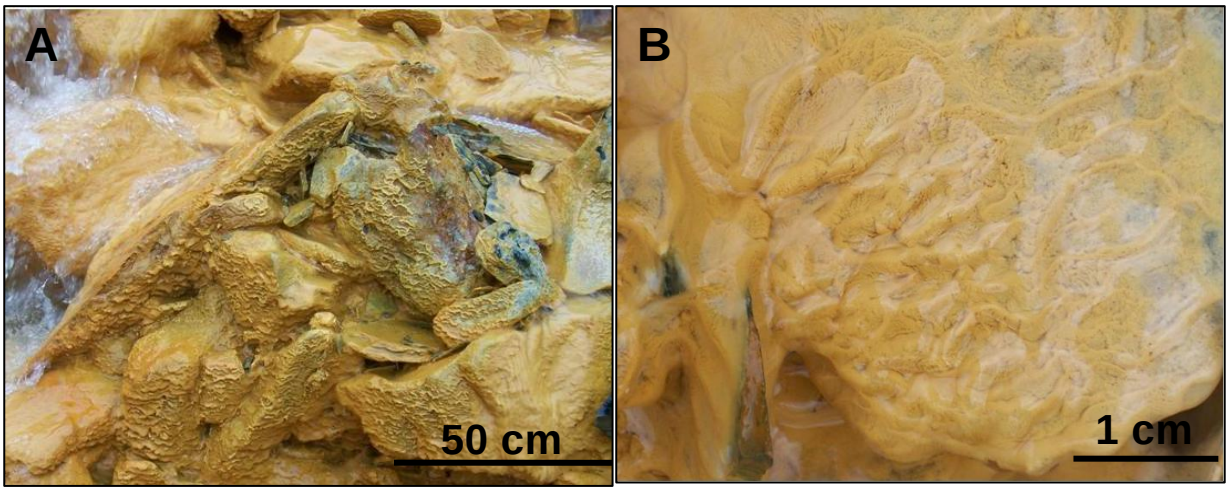

Figure 20: Light orange-coloured mineral precipitates from the 100 m site (A). Rippled surfaces similar to incipient rims were observed (B).

A waterfall (120 m) (Figure 21 A) between the two designated sites (100 and 165 m) in the lower reaches was sampled on a few occasions for mineral precipitates. The precipitates found here were white in colour and had rippled surfaces similar to TIFs (Figure 12 B). These precipitates were laminated, with alternating white, orange and red laminations (Figure 12 C). The white and orange-coloured laminae were much softer and thicker relative to the red-coloured laminae, which were thin and much harder.

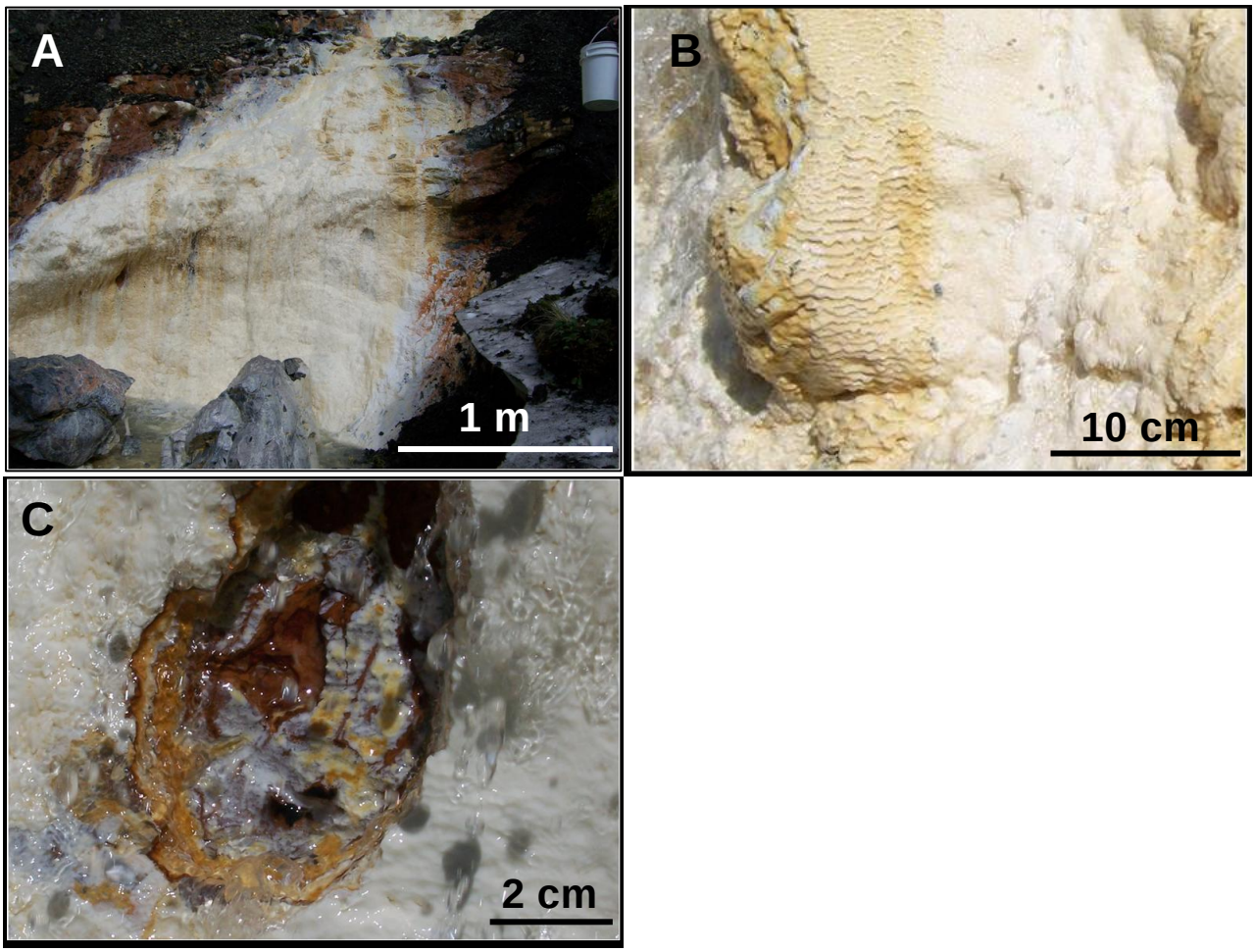

Figure 21: Mineral precipitates from the waterfall at 120 m. A) White-coloured precipitates forming at waterfall, red-coloured precipitates are visible along banks, B) rippled surfaces of white-coloured precipitates, C) cross-section of precipitates, white, orange, and red-coloured laminae are visible.

In June, the lower reaches (165 m, the only safely accessible site due to heavy snow pack) of the creek had orange-coloured mineral precipitates present as a thin layer along the stream banks (Figure 22 A). White-coloured precipitates began to deposit as a very thin layer in July and became progressively thicker and whiter in colour into August (Figure 22 B, C). Some of these precipitates also resembled terraces, in that they had rippled surfaces (Figure 22 D), although they were much less cohesive than any of the other precipitates sampled in the creek.

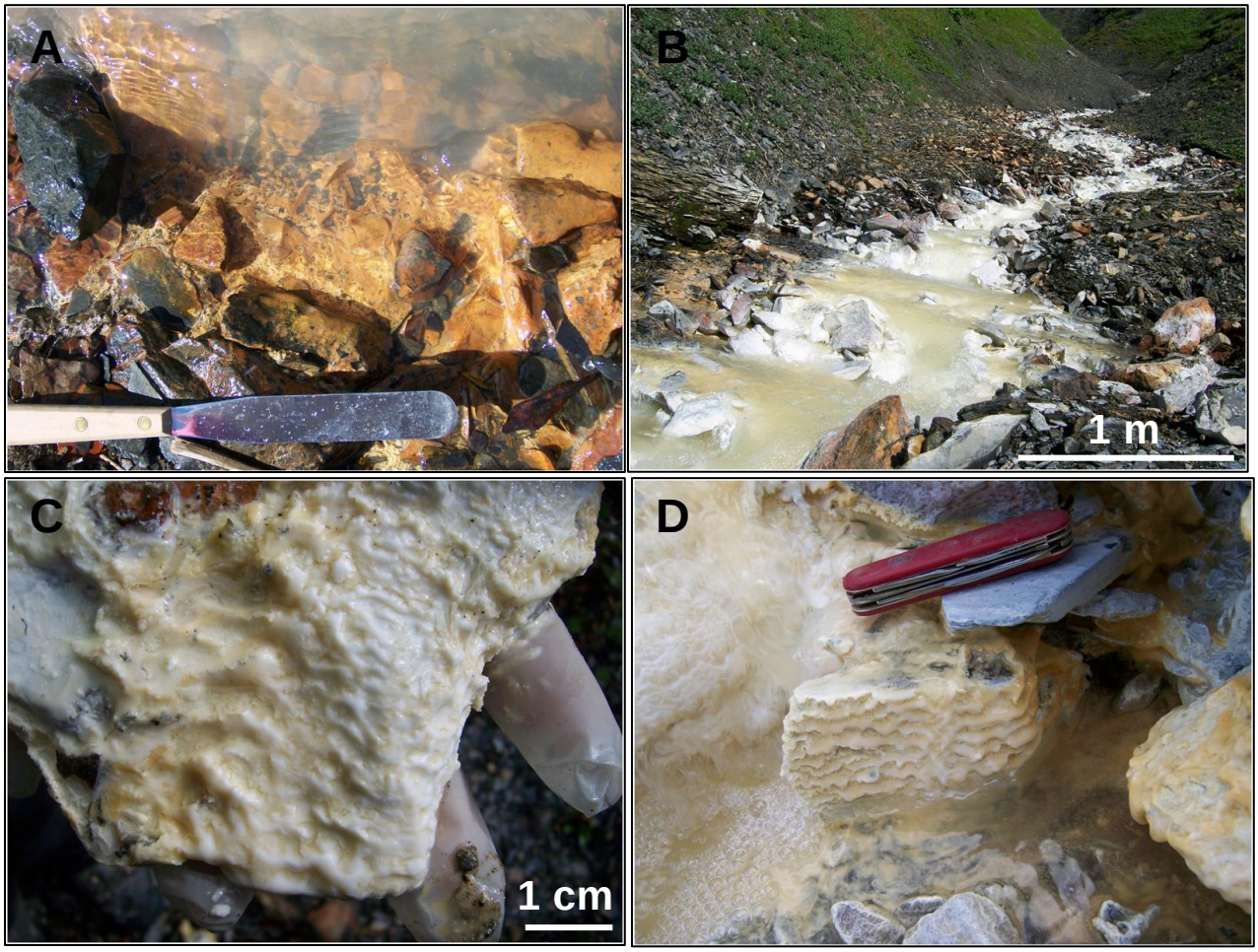

Figure 22: Mineral precipitates from 165 m in the lower reaches. A) Orange-coloured precipitates present in June/08, B and C) white-coloured mineral precipitates that formed in August/08, D) rippled, TIF-like surfaces of white-coloured precipitates.

Field evidence for microbial life

In August signs of microbial life in the ARD creek became apparent, although an abundance of microbial life was not observed in the field. Thin, sheeny films (Figure 23) were often observed in areas with low flowing or stagnant water, and may have been associated with Fe(II)-oxidizing bacteria (D. Fortin, personal comm.). Green organic material was observed to be sparsely coating rocks at the outflow of the 10 m groundwater seep (Figure 24), although it was not observed at other locations along the stream. Gas blisters forming under thin films of Fe-rich mineral precipitate were also observed (Figure 25 A) and the presence of sheeny films in association with these blisters (Figure 25 B) suggested that they may have been biogenic in origin.

Figure 23: Thin, sheeny films found in areas near the groundwater seeps and in the upper reaches of the creek near the end of the sampling campaign. Sheeny appearance may be due to the presence of waste products from Fe-oxidizing bacteria.

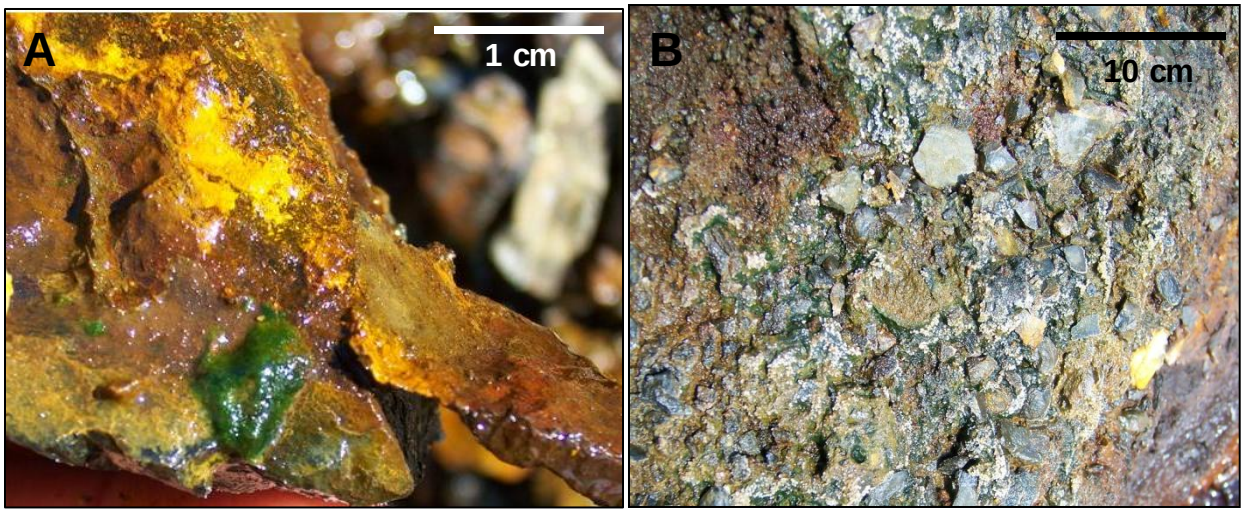

Figure 24: Green organic-like material found at the 10 m groundwater seep near the end of the sampling campaign. A) green organic material coating part of a rock from the streambed, and B) green organic material and evaporative salts near the outflow of the 10 m groundwater seep.

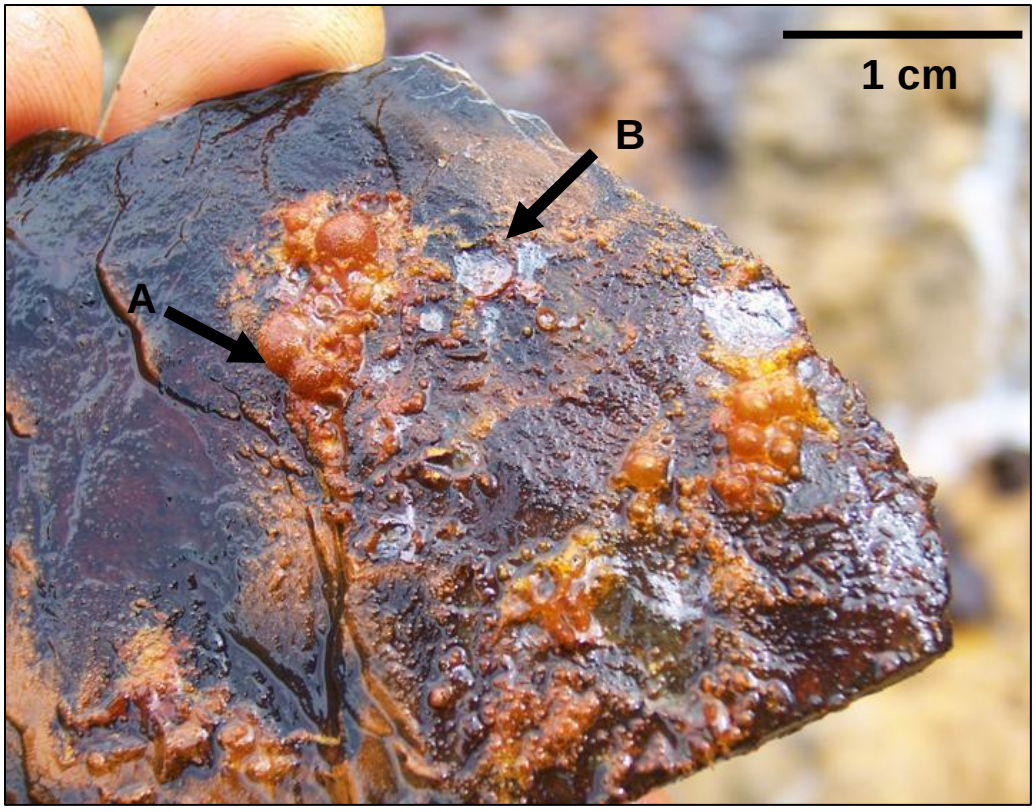

Figure 25: Biogenic gas blisters found on pieces of talus in the upper reaches of the creek near the end of the sampling campaign. A) Biogenic gas blisters comprised of thin films of Fe-rich precipitates, B) popped gas blister reveals sheeny substance that could be waste products from Fe-oxidizing bacteria.

4.5.2. Geochemistry

Fe:S and Al:S molar ratios

Fe:S and Al:S molar ratios of the mineral precipitates were examined to help identify Fe and Al minerals that may be comprising the mineral precipitate samples, as each Fe and Al-hydroxysulphate and -oxyhydroxide mineral forming in AMD/ARD waters has its own unique ratio (Table 11). The Fe:S molar ratios of the precipitates were generally much higher in the upper reaches of the creek relative to the lower reaches of the creek, while the opposite was true for the Al:S ratios (Table 10). The only groundwater seep for which mineral precipitates could be sampled (10 m) had an Fe:S ratio of approximately 12.8, which was similar to one of the samples taken at 18 m (Fe:S 11.3) (Table 10). Despite their similar Fe:S ratios, the Al:S ratios for these samples were dissimilar, with the groundwater seep (10 m) precipitates having a Al:S ratio of 0.2, while the 18 m precipitate (Fe:S 11.3) had an Al:S ratio that was slightly higher (1.0) (Table 10). The Fe:S molar ratios of the precipitates at 10 and 18 m suggested that they were a mixture of schwertmannite and goethite or ferrihydrite (Table 10 and 11). Given the very low Fe:S molar ratio for jarosite, it is unlikely that jarosite was a major component of these samples. Although ferrihydrite and goethite will both have a very high Fe:S ratio (since neither contain sulphur), it is unlikely that these precipitates contained ferrihydrite given its instability under low pH conditions (Bigham et al., 1996).

The laminae comprising the TIFs in the upper reaches (18 m) (with the exception of the precipitates described above) were characterized by Fe:S ratios of approximately 16.5, and Al:S ratios of 0.1 (Table 10), despite the difference in their appearance. The orange-coloured precipitates collected at the 40 m site showed almost identical Fe:S and Al:S

ratios to the TIFs at the 18 m site (Table 10). These molar ratios suggested that a schwertmannite-goethite mixture comprised these precipitates (Table 10 and 11). The Al:S molar ratios for the precipitates at the groundwater seeps and the upper reaches were very low due to the conservative nature of Al under low pH conditions.

Table 10: Description of mineral precipitate samples and their average Fe:S and Al:S molar ratios. pH was measured in the water flowing over the mineral precipitates prior to sampling.

Sample site	pH of water	Description	Number of samples	Fe:S	Al:S
10	3.5	Maroon hardpan	2	12.78 ± 0.067	0.19 ± 0.238
18	3.5	Orange ppt (a)[A]	1	11.27	0.96
18	3.5	Orange ppt (b)[A]	3	16.97 ± 0.032	0.09 ± 0.086
18	3.5	Red laminae[B]	2	16.03 ± 0.025	0.09 ± 0.129
40	3.9	Orange ppt	6	15.95 ± 0.032	0.11 ± 0.107
100	4.4	Light orange ppt	4	4.02 ± 0.23	1.81 ± 0.088
120[C]	4.7	White surface ppt[C]	1	1.36	6.83
120[C]	-	Orange laminae[C]	2	0.46 ± 0.004	3.25 ± 0.082
120[C]	-	Hard red laminae[C]	1	25.75	2.59
165	4.9	White surface ppt	3	1.32 ± 0.512	2.32 ± 0.249

[A]These precipitates were collected from the same site but have different geochemistry [B]Hard lamina from laminated TIF precipitates [C]Samples were a series of laminae at a waterfall (120 m) between sites 100 and 165 m. The pH of the waters from which the orange and red laminae (120 m) deposited is not known.

Table 11: Formulae and Fe:S and Al:S molar ratios for Fe- and Al-minerals that typically form in AMD/ARD environments.

Mineral name	Formula	Fe:S	Al:S
Schwertmannite	$Fe_8O_8(SO_4)(OH)_6$	4 – 8[A]	-
Jarosite	K,Na,H^+ $(Fe_3(SO_4)_2(OH)_6)$	1.5[B]	-
Goethite	α-FeOOH	Very high[C]	-
Ferrihydrite	$Fe(OH)_3$	Very high[C]	-
Hydrobasaluminite	$Al_4(OH)_{10}SO_4$-$4H_2O$	-	4[D]
Jurbanite	$AlOHSO_4$	-	1[E]
Gibbsite	$Al(OH)_3$	-	Very high[C]

[A,B] Bigham et al., 1996a

[C]These mineral do not contain sulphur giving rise to their Fe:S and Al:S molar ratios being much greater than those for Fe- and Al-hydroxysulphate minerals typically found in ARD

[D,E]Bigham and Nordstrom, 2000.

Mineral precipitates collected at the 100 m site had lower Fe:S (4.0) and higher Al:S (1.8) ratios than those from the upper reaches (Table 10). The Fe:S molar ratio strongly suggested the presence of schwertmannite, while the Al:S ratio may have indicated that there was a mixture of hydrobasaluminite and jurbanite. Alternatively, the Al:S molar ratio may reflect the presence of an amorphous Al-sulphate phase with a molar ratio intermediate of that for hydrobasaluminite and jurbanite. Samples were collected at a waterfall (120 m) between sites 100 and 165 m, and were found to be laminated (Figure 21). The white-coloured mineral precipitates that formed in the summer at the surface of the waterfall had a very high Al:S molar ratio (6.8) (Table 10), which suggested that they were a mixture of hydrobasaluminite and gibbsite (Table 11). The Al:S molar ratio of the orange laminae (Table 10) was very close to that of hydrobasaluminite, although it may have been slightly lower due to the presence of either jurbanite or an amorphous Al-sulphate phase with a low Al:S molar ratio. Although the Fe:S molar ratio in the white

surface laminae coincided very well with the ratio for jarosite (Fe:S = 1.5), the moderately acidic pH conditions found here would not be conducive to its precipitation (Dutrizac and Jambor, 2000), and thus the Fe:S ratio may have reflected adsorption of Fe onto the Al-rich precipitates. The thin and hard red-coloured laminae had the highest Fe:S ratio found along the entire creek, at approximately 25.8 (Table 10), possibly indicative of the presence of goethite or ferrihydrite (Table 11). Although ferrihydrite is known to form under neutral to high pH conditions, its presence cannot be ruled out since the pH conditions under which these red precipitates formed were not known. The Al:S molar ratio of this sample (Al:S = 2.6) (Table 10) suggested a mixture of hydrobasaluminite and jurbanite, or an amorphous Al-sulphate phase with an Al:S molar ratio that was intermediate of these phases. Alternatively, the Al:S ratio could have reflected adsorption of Al to the mineral precipitate. Since the pH conditions under which precipitation occurred were unknown, it was difficult to draw further conclusions about the Al-mineralogy of this sample based solely upon its Al:S molar ratio.

Further into the lower reaches, at the 165 m site, the Fe:S ratio was 1.3, similar to the white-coloured precipitates collected from the surface of the waterfall at 120 m (Table 10). The Al:S ratio for the white precipitates at 165 m was lower than any of those from the 120 m site, at only 2.3 (Table 10). Similar to the other locations in the lower reaches, the Al:S molar ratio suggested a mixture of hydrobasaluminite and jurbanite, or an amorphous Al-sulphate phase with a similar Al:S molar ratio. The Fe:S molar ratio of this sample (Fe:S = 1.4) suggested the presence of jarosite (Table 11); however, it was likely that the Fe was adsorbed to the Al-hydroxysulphate, as the moderately acidic pH conditions of these waters do not favour the precipitation of jarosite (Dutrizac and Jambor, 2000).

Trace element distribution coefficients

The distribution coefficients (K_d) were calculated for the mineral precipitates, where K_d = concentration in mineral precipitates (mol kg^{-1}) / concentration in waters (mol kg^{-1}) It was assumed that 1 L of water was equivalent to 1 kg. Distribution coefficients were calculated for Fe, Al, Pb, Ni, Cu, Cd, Ba, U and Si for all of the mineral precipitate samples examined in the previous sections, with the exception of the orange and red-coloured laminae from the waterfall at 120 m since the aqueous geochemical conditions under which these precipitates formed were not known.

Fe and Al

Iron and Al distribution coefficients showed two distinct trends. The partitioning of Fe to the solid phase was highly variable with respect to pH and distance (Figure 26), and distance and pH did not significantly influence the partitioning of Fe to the mineral precipitates ($p = 0.7878$). Alternatively, Al partitioning to the solid phase (Figure 26) was strongly positively correlated to pH (Spearman $R = 0.8752$, $p = 0.0044$) and distance downstream (Spearman $R = 0.9271$, $p = 0.0009$).

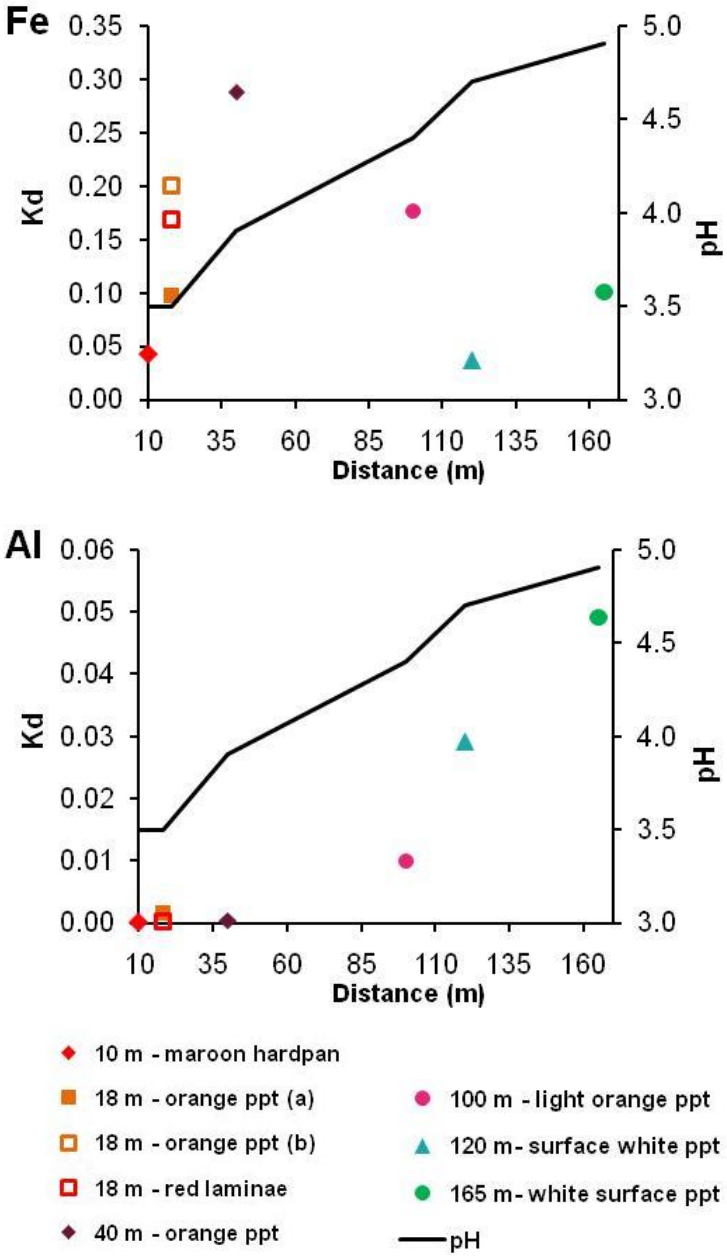

Figure 26: Iron and Al distribution coefficients (K_d) with distance downstream (m) and pH.

Zinc

Zinc distribution coefficients were highly positively correlated to both pH (Spearman R = 0.7864, p = 0.0206) and distance downstream (Spearman R = 0.8539, p = 0.0070). As this suggests, there was a general increase in Zn distribution coefficients with increasing

pH and distance downstream, however there was one anomalous K_d value for Zn in the white precipitates from the surface of the waterfall at 120 m (Figure 27).

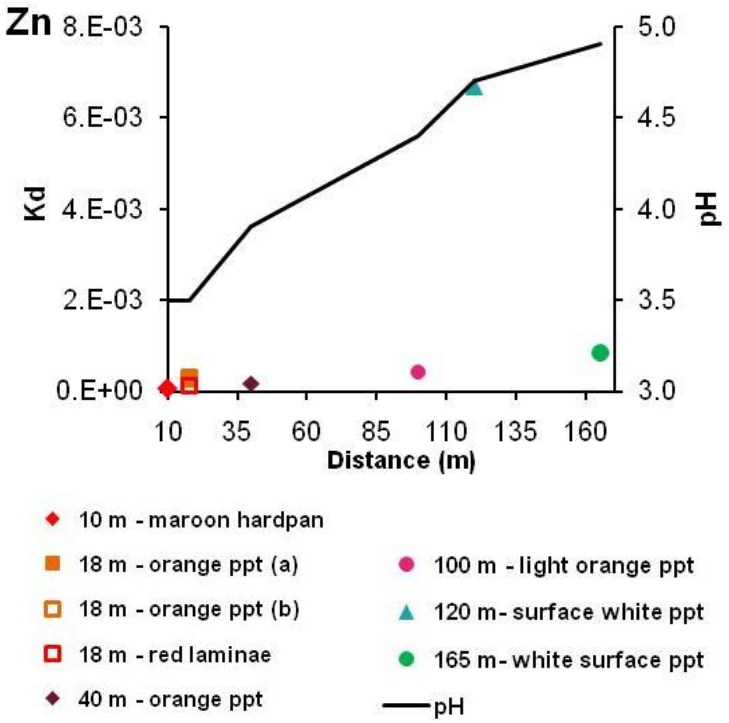

Figure 27: Zinc distribution coefficients (K_d) with distance downstream (m) and pH.

Lead

Lead showed highly variable distribution coefficients (Figure 28) that were generally much higher when compared to the distribution coefficients for any of the other elements examined. There was no significant correlation between Pb partitioning coefficients and pH ($p = 0.4635$) or distance downstream ($p = 0.5604$).

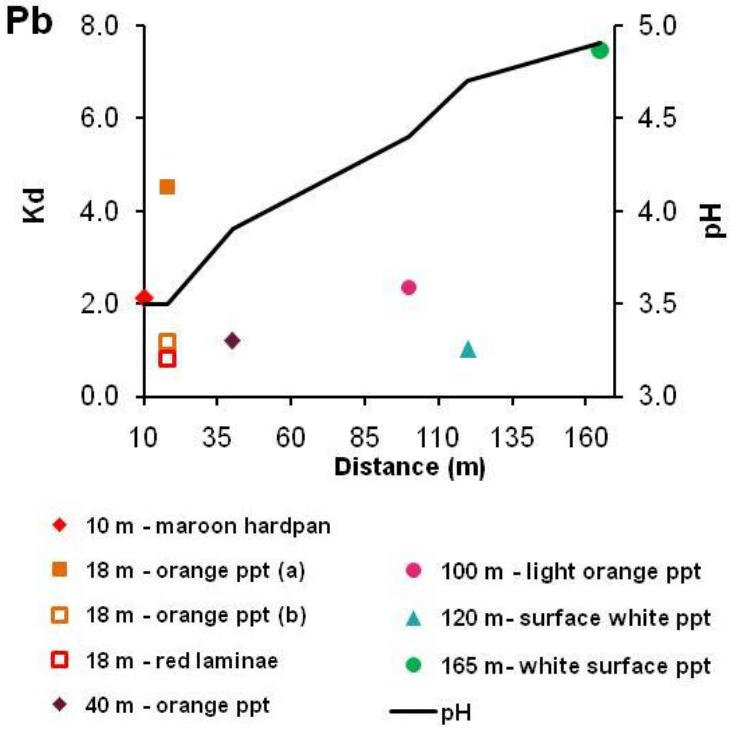

Figure 28: Lead distribution coefficients (K_d) with distance downstream (m) and pH.

Nickel and copper

The distribution coefficients for Ni and Cu generally increased with distance downstream and increasing pH (Figure 29). The partitioning of both elements showed strong positive correlations with pH (Spearman R = 0.7864, p = 0.0206 for Ni; Spearman R = 0.8498, p = 0.0075 for Cu) and distance downstream (Spearman R = 0.8051, p = 0.0159 for Ni; Spearman R = 0.9027, p = 0.0021 for Cu). Interestingly, the K_d values for both elements in the white-coloured mineral precipitates collected at the surface of the waterfall at 120 m were anomalously high relative to the distribution coefficients for the other mineral precipitate samples (Figure 29).

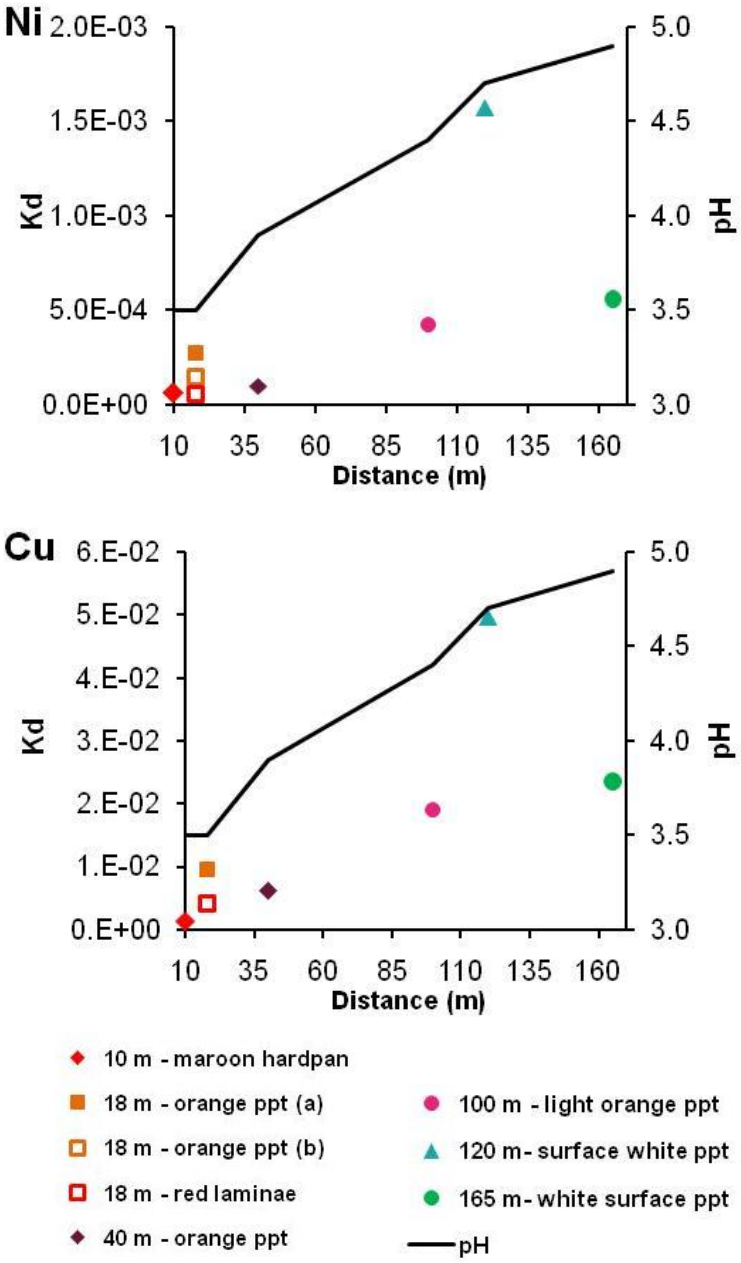

Figure 29: Nickel and Cu distribution coefficients (K_d) with distance downstream (m) and pH.

Cadmium

The partitioning of Cd to the mineral precipitates generally increased with increased pH and distance downstream (Figure 30). Cadmium was found to be highly positively correlated with pH (Spearman R = 0.8498, p = 0.0075) and distance downstream

(Spearman R = 0.9027, p = 0.0021). Similar to Zn (Figure 26), Ni and Cu (Figure 28), the white-coloured mineral precipitates from the surface of the waterfall at 120 m showed anomalous K_d values for Cd relative to all of the other mineral precipitate samples (Figure 30).

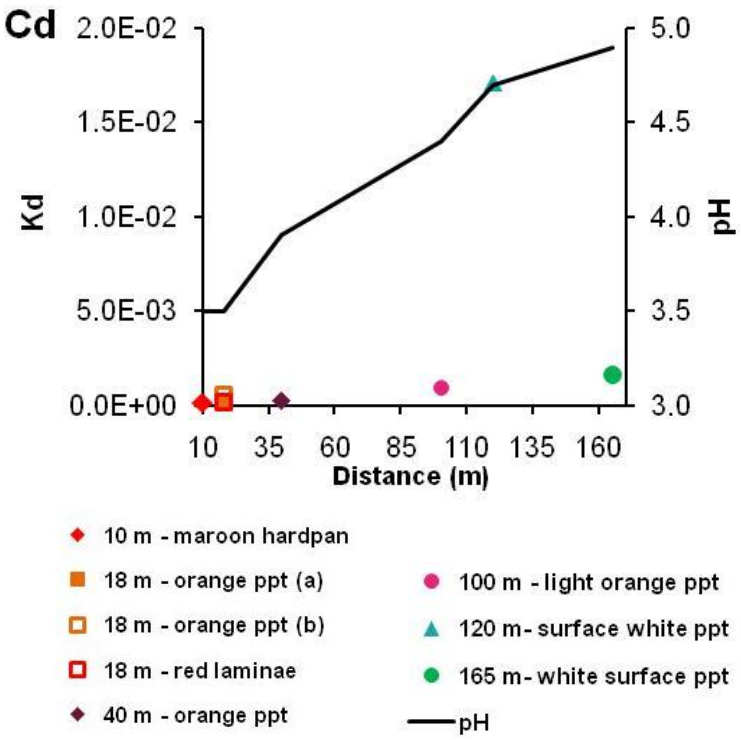

Figure 30: Cadmium distribution coefficients (K_d) with distance downstream (m) and pH.

Uranium

The partitioning of U to the mineral precipitates was strongly correlated with pH (Spearman R = 0.7230, p = 0.0427) and distance downstream (Spearman R = 0.8051, p = 0.0159). Similar to the K_d values for Zn (Figure 27), Ni, Cu (Figure 29) and Cd (Figure 30), the K_d for U was anomalously high in the white-coloured mineral precipitates collected at 120 m, relative to all of the other mineral precipitate samples (Figure 31).

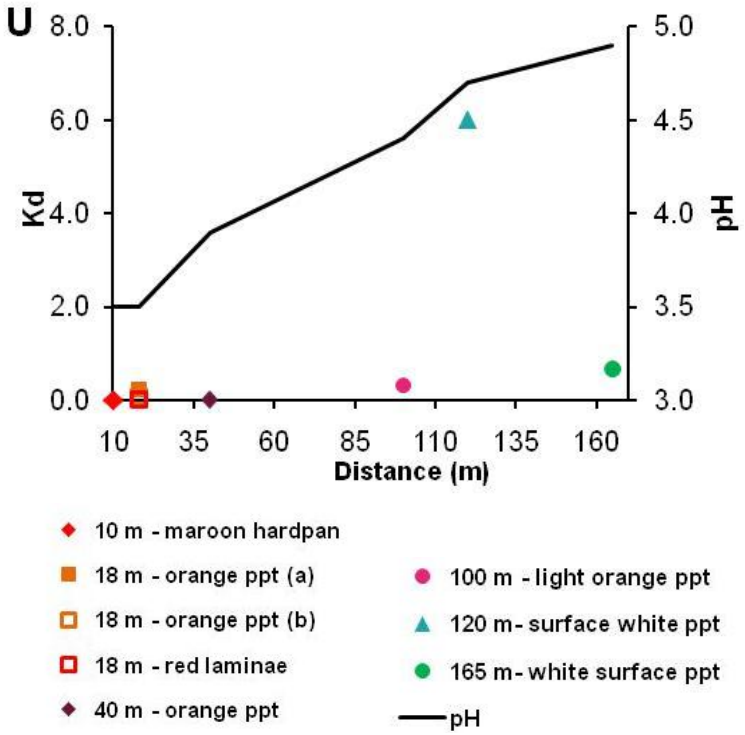

Figure 31: Uranium distribution coefficients (K_d) with distance downstream (m) and pH.

4.5.3. Influence of mineralogy on trace element geochemistry

Fe and Al

The concentrations of major and trace elements in the mineral precipitates were examined with respect to their Fe:S and Al:S molar ratios to help determine if mineralogy (defined by Fe:S and Al:S molar ratios) had an effect on the accumulation of elements in the precipitates.

The concentration of Al and Fe generally decreased with increasing Fe:S and Al:S molar ratios, respectively; however, the red-coloured lamina from the waterfall at 120 m showed anomalous Al and Fe concentrations when compared to samples with similar Fe:S and Al:S molar ratios (Figure 32). As suggested by the Fe:S and Al:S molar ratios, the mineral precipitates with the greatest Fe concentration were found at the groundwater

seep (10 m) and in the upper reaches of the creek (18 and 40 m), while those with the greatest Al concentrations were from the lower reaches of the creek (100, 120 and 165 m) (Figure 32).

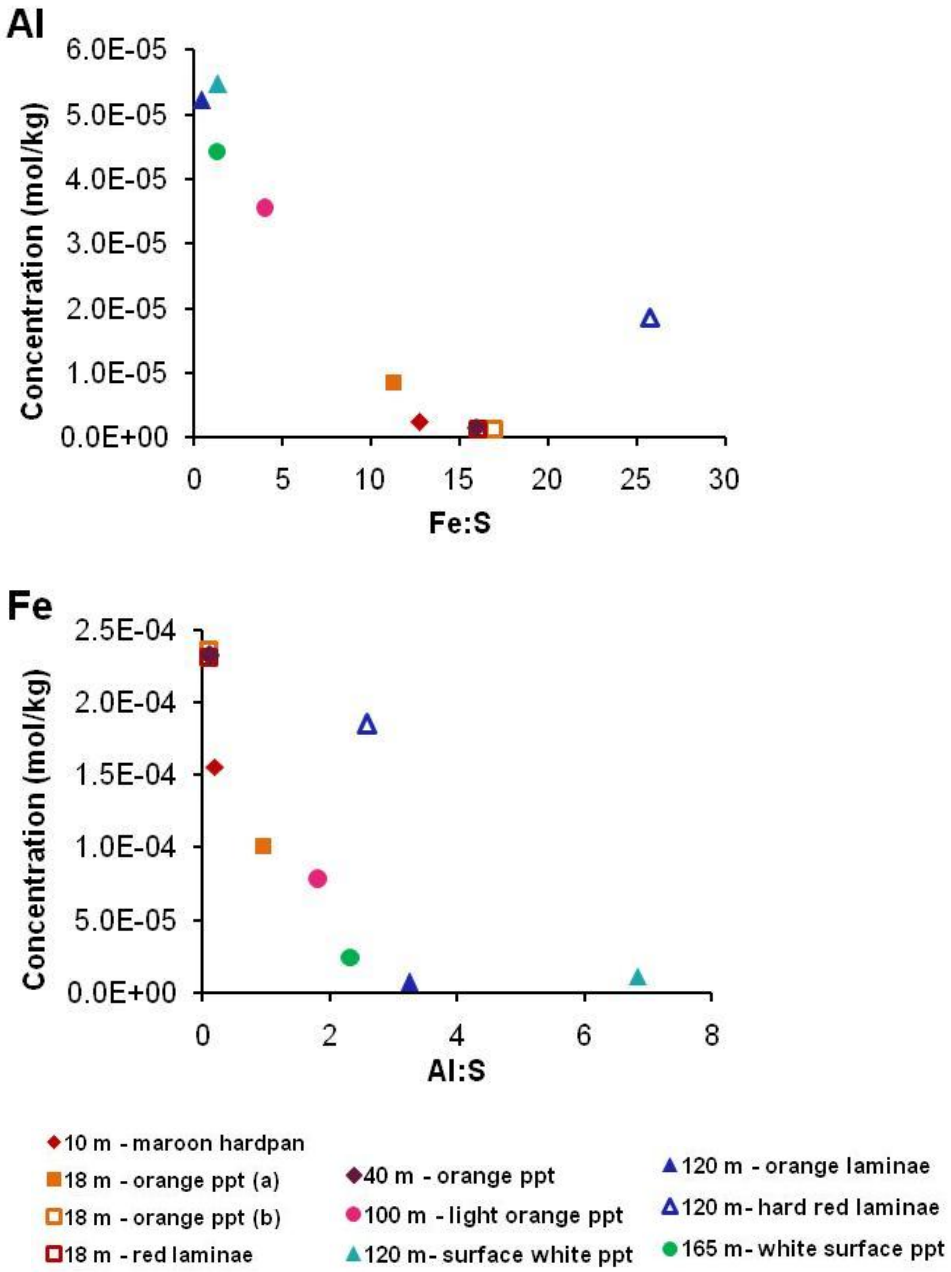

Figure 32: Fe and Al concentrations (mol/kg) in mineral precipitates defined by their Fe:S and Al:S molar ratios.

When all of the mineral precipitate samples were considered, the Fe:S molar ratio explained approximately 86 % of the total variability of the Al concentrations (Spearman R = -0.8630 and p=2.85E-08), and the Al:S molar ratio explained approximately 89 % of the total variability of the Fe concentrations (Spearman R = -0.8863, p=3.75E-09) in the mineral precipitates. Removing the red-coloured laminae with anomalous Fe and Al concentrations from the analyses improved the regression for both Fe:S and Al and Al:S and Fe, where the Fe:S and Al:S molar ratios explained approximately 94% (Spearman R = -0.9366) and 92% (Spearman R = -0.9171) of the total Al and Fe variability, respectively, with improved significance (p= 1.71E-11 and 2.98E-10, respectively).

Zinc

Zinc concentrations in the mineral precipitates generally increased with distance downstream and reached a maximum at the waterfall located at 120 m (Figure 33). The red-coloured laminae at this location contained anomalous concentrations of Zn, at approximately 1.5 % wt Zn (Appendix 5). The Zn concentrations further downstream, at the 165 m site, were comparable to those found in the mineral precipitates from the groundwater seeps and the upper reaches of the creek (Figure 33).

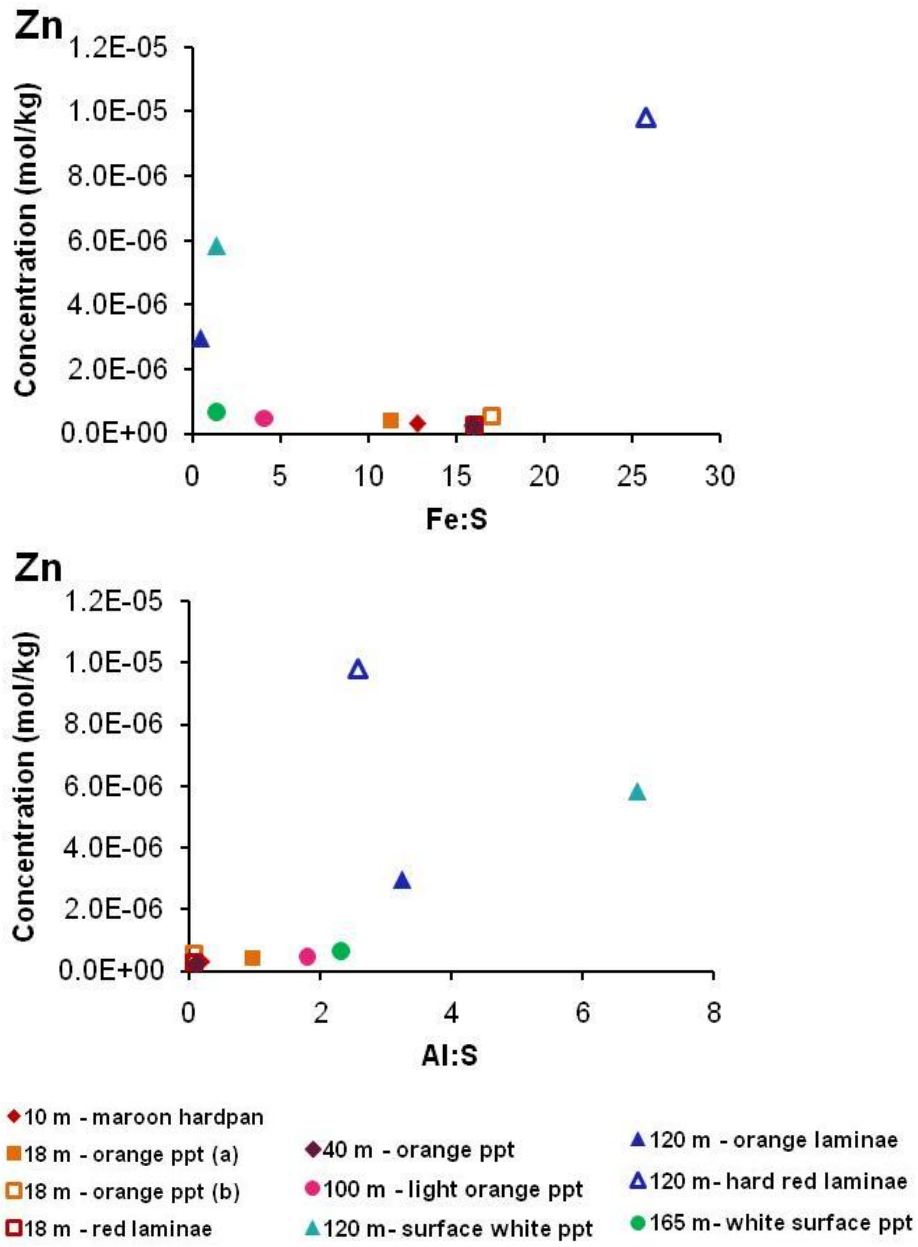

Figure 33: Zinc concentration (mol/kg) in the mineral precipitates defined by their Fe:S and Al:S molar ratios.

When all of the mineral precipitate samples were considered, the Fe:S molar ratio did not significantly explain the Zn variability ($p = 0.52$), although the Al:S molar ratio significantly explained approximately 53 % of Zn variability (Spearman $R = 0.5321$, $p = 6.20E\text{-}03$). When the data for the anomalous red-coloured laminae were removed from the regression analyses the regression for Fe:S and Zn improved but remained

insignificant. The correlation between Al:S and Zn decreased (Spearman R = 0.4797) when the red laminae were removed from the regression analyses, although the relationship was still significant (p=0.02).

Lead

The maroon-coloured hardpan from the 10 m groundwater seep and one sample ("orange precipitate (a)") from 18 m were enriched in Pb relative to all of the other samples (Figure 34). The Pb-content of the mineral precipitates generally decreased with distance downstream, but was slightly elevated at the 165 m site relative to other samples from the lower reaches of the creek (Figure 34). Lead variability could not be explained by the Fe:S (p=0.18) or Al:S (p=0.08) molar ratios. Removing the data for the anomalous red-coloured laminae at 120 m in the regression analyses only marginally improved the results for Fe:S and Pb (p=0.08), although it decreased the quality of the regression for Al:S and Pb (p=0.16).

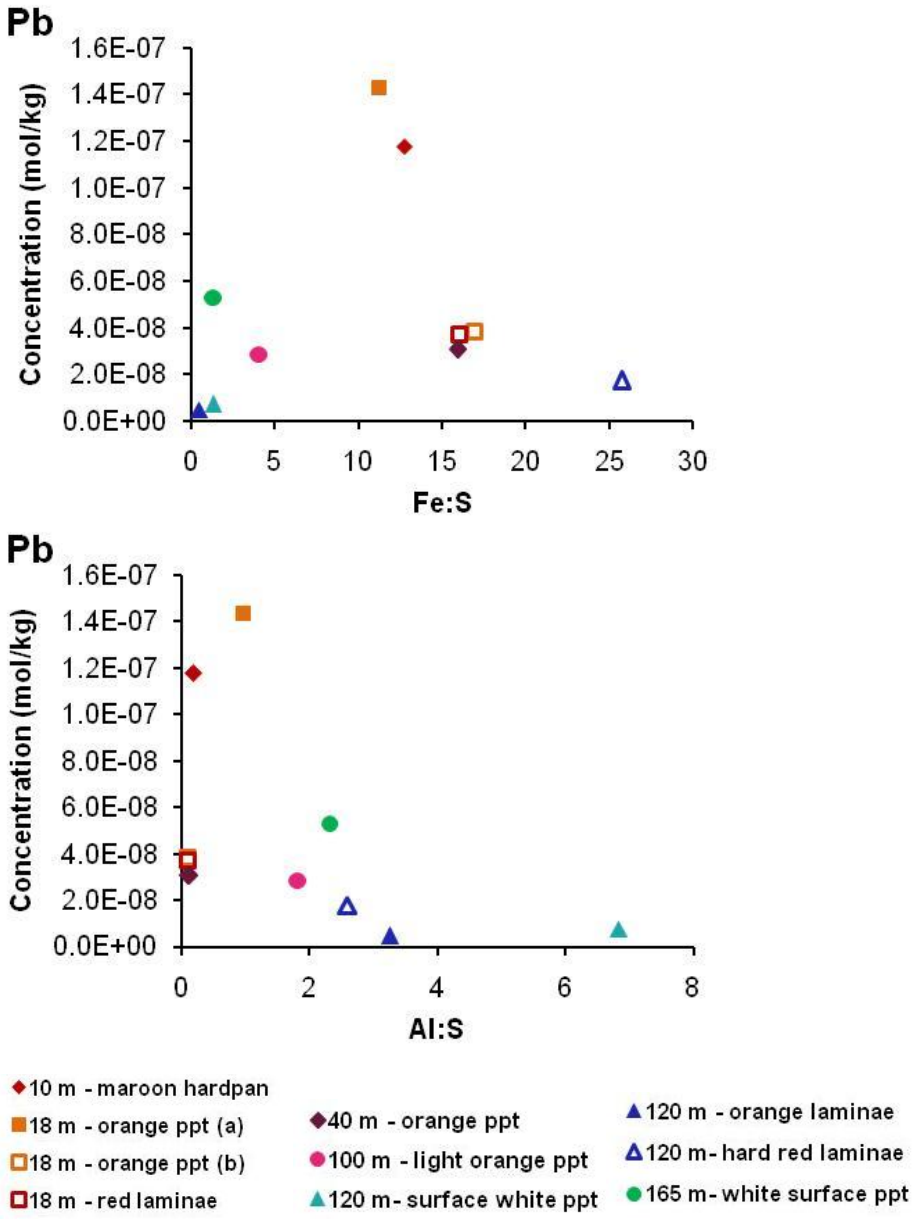

Figure 34: Lead concentrations (mol/kg) in the mineral precipitates, defined by their Fe:S and Al:S molar ratios.

Nickel and Cu

Nickel and Cu concentrations in the mineral precipitates generally increased with distance downstream and decreased with increasing Fe:S (Figure 35) and increased with increasing Al:S molar ratios (Figure 36). However, the red-coloured laminae from the

waterfall at 120 m (which have the highest Fe:S ratio) contained disproportionate levels of Ni and Cu relative to the other samples (Figure 35).

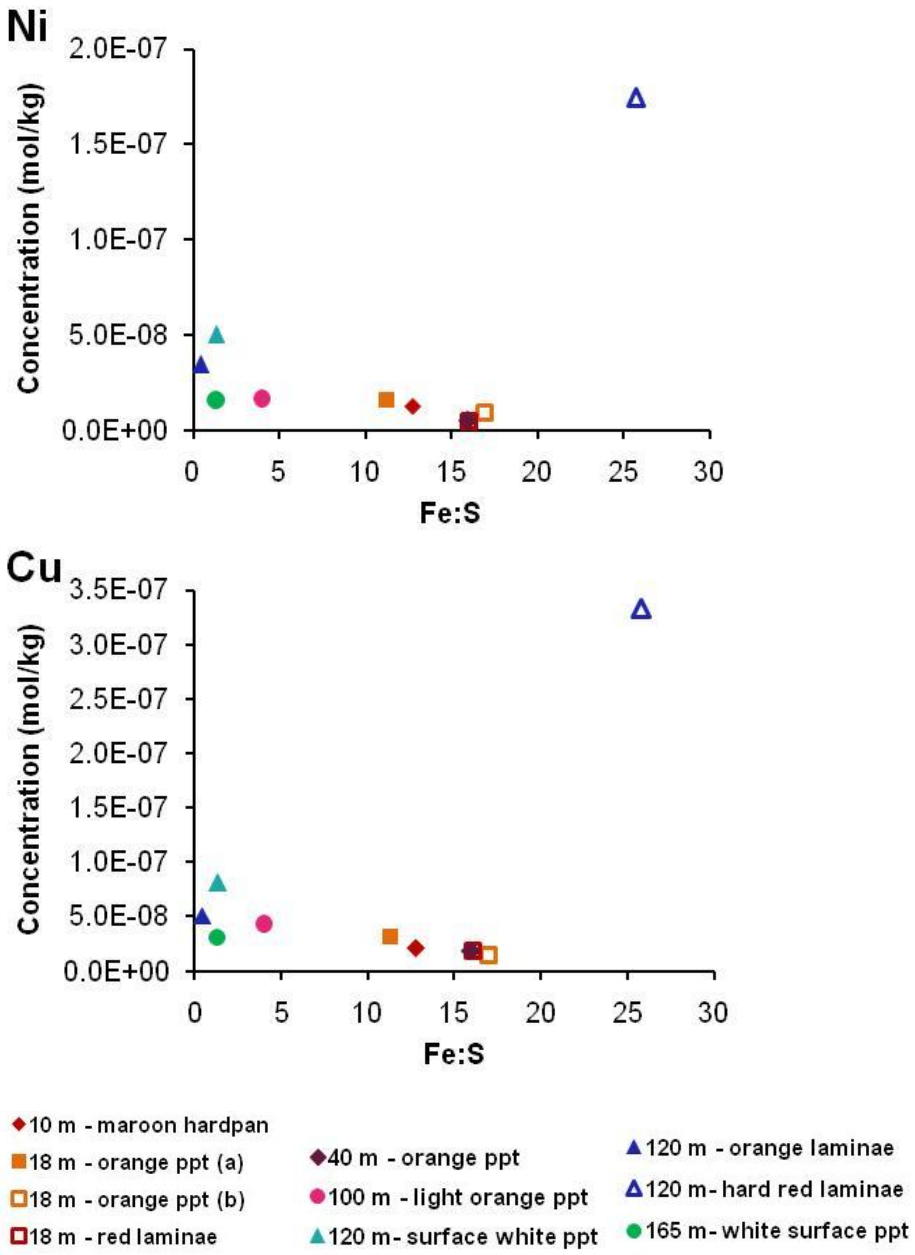

Figure 35: Nickel and Cu concentrations (mol/kg) in the mineral precipitates defined by their Fe:S molar ratios.

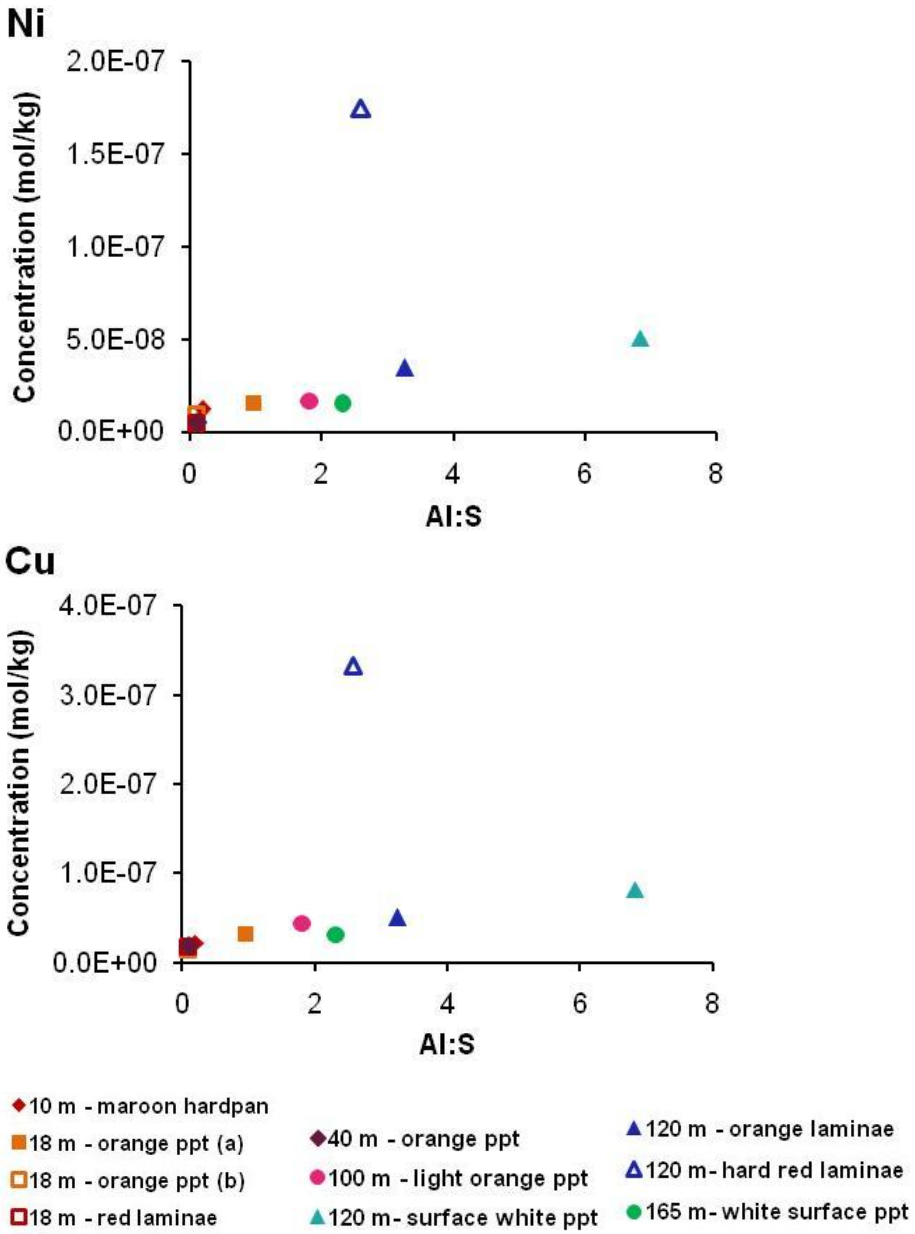

Figure 36: Nickel and Cu concentrations (mol/kg) in the mineral precipitates defined by their Al:S molar ratios.

When all of the mineral precipitate samples were considered, the Fe:S molar ratios explained approximately 42 % of the Ni (Spearman R = -0.419, p=0.04) and 41 % of the Cu variability (Spearman R = -0.4063, p=0.04), while the Al:S molar ratios explained approximately 77 % of both the Ni and Cu variability (Spearman R = 0.7729, p=5.94E-06). When the data for the anomalous red-coloured laminae were removed from the regression

analyses the Fe:S molar ratios explained approximately 60 % of both the Ni (Spearman R= -0.6042, p=1.80E-03) and Cu (Spearman R= -0.5900, p=2.40E-03) concentrations in the mineral precipitates, while the Al:S molar ratios explained approximately 75 % of the Ni (Spearman R = 0.7537, p=2.12E-05) and Cu (Spearman R = 0.7554, p =1.98E-05) variability.

Cadmium

Cadmium concentrations generally increased with increasing Al:S molar ratios and were the highest in the mineral precipitates from the waterfall at 120 m (Figure 37), while their relationship with Fe:S molar ratios was less clear (Figure 37). In particular, the red laminae contained a disproportionate amount of Cd relative to all of the other mineral precipitate samples (Figure 37). When all of the samples were considered, there was no significant relationship between Cd concentrations and Fe:S (p=0.10) molar ratios. The Al:S molar ratios, however, significantly explained approximately 65 % of the Cd variability (Spearman R = 0.6556, p=4.00E-04). When the anomalous red-coloured laminae was omitted from the regression analyses, the regression for Fe:S and Cd improved, with Fe:S explaining approximately 51 % of the Cd variability (Spearman R = -0.5104, p=0.01). The regression for Cd and Al:S did not improve when these data were removed (Spearman R = 0.6193, p=1.30E-03).

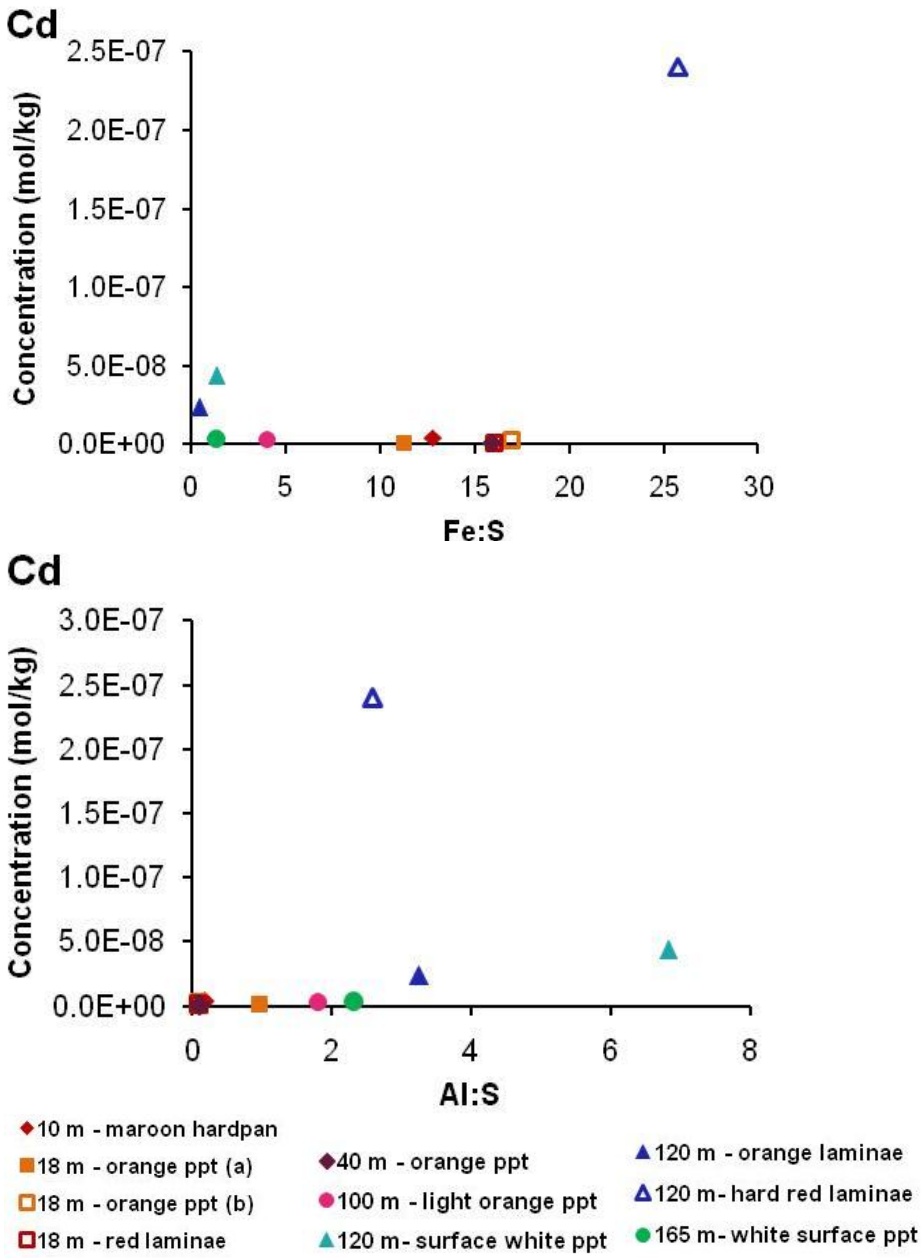

Figure 37: Cadmium concentrations (mol/kg) in the mineral precipitates, defined by their Fe:S and Al:S molar ratios.

Barium

Barium concentrations in the mineral precipitates were fairly constant with distance downstream, with the exception of one sample collected at 165 m (Figure 38). The variability in Ba concentrations was not governed by the Fe:S ($p=0.46$) or Al:S ($p=0.83$)

molar ratio of the mineral precipitates. One of the mineral precipitate samples from the lower reaches contained a disproportionate amount of Ba relative to all of the other mineral precipitate samples (Figure 38) so it was removed from the regression analyses. However, this did not improve the quality of the regression.

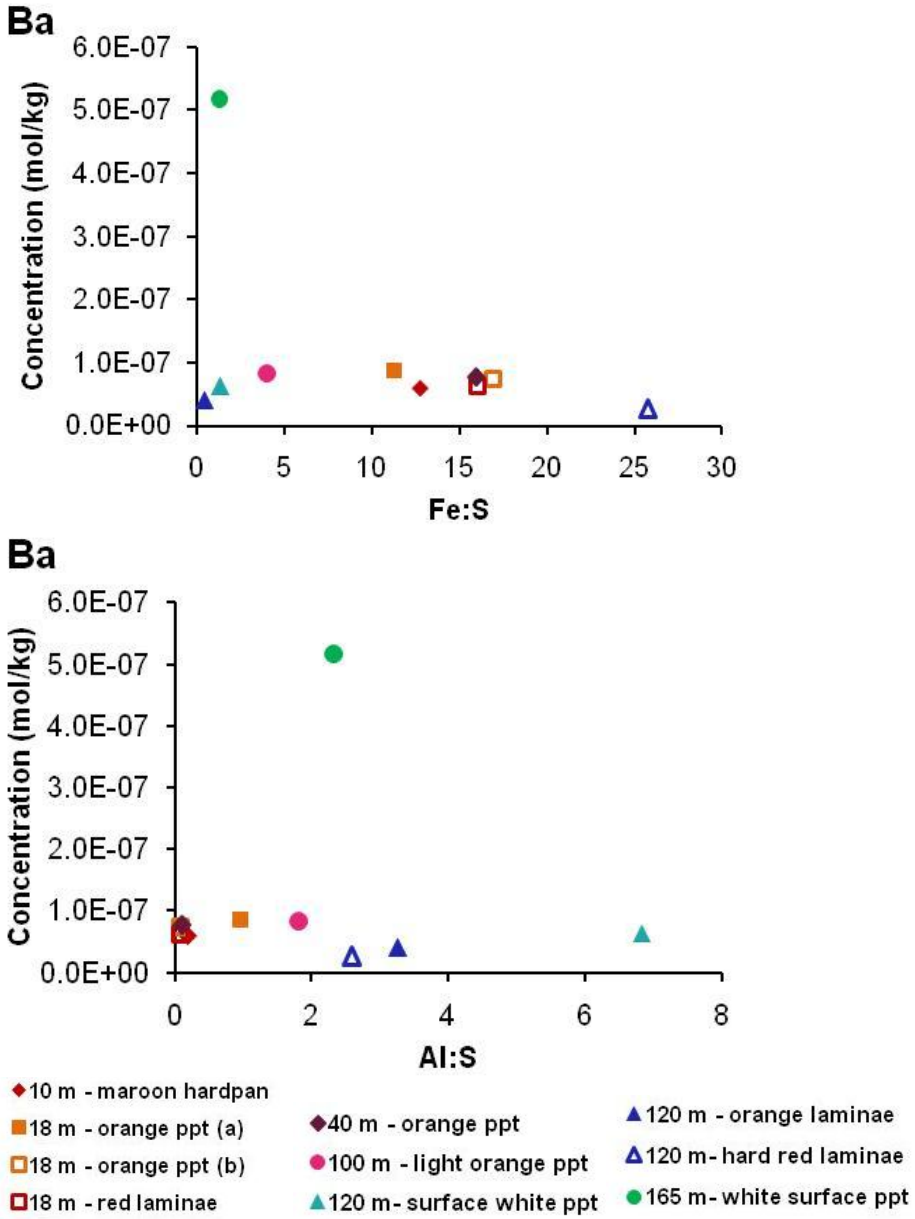

Figure 38: Barium concentrations (mol/kg) in the mineral precipitates, defined by their Fe:S and Al:S molar ratios.

Uranium

The concentration of U in the mineral precipitates increased with increasing Al:S molar ratios and reached a maximum at the 120 m waterfall (Figure 39), although the relationship between Fe:S molar ratios and the U concentrations was less clear (Figure 39). The U concentration in the precipitates at 165 m was slightly higher than the precipitates from the preceding sites, with the exception of the white-coloured precipitates from 120 m, which contained anomalous concentrations of U relative to the other mineral precipitate samples (Figure 39). The Fe:S molar ratio explained approximately 57% of the U variability (Spearman R = -0.5694, p=3.00E-03) while the Al:S molar ratio explained approximately 84 % of the U variability (Spearman R = 0.8364, p=1.97E-07) when all of the data were considered. When the data for the anomalous red-coloured laminae were omitted from the regression analyses, the results for the Fe:S and U regression improved, with Fe:S molar ratios explaining approximately 75 % of the U variability (Spearman R = -0.7467, p=2.78E-05). The Al:S and U regression did not improve when these data were removed.

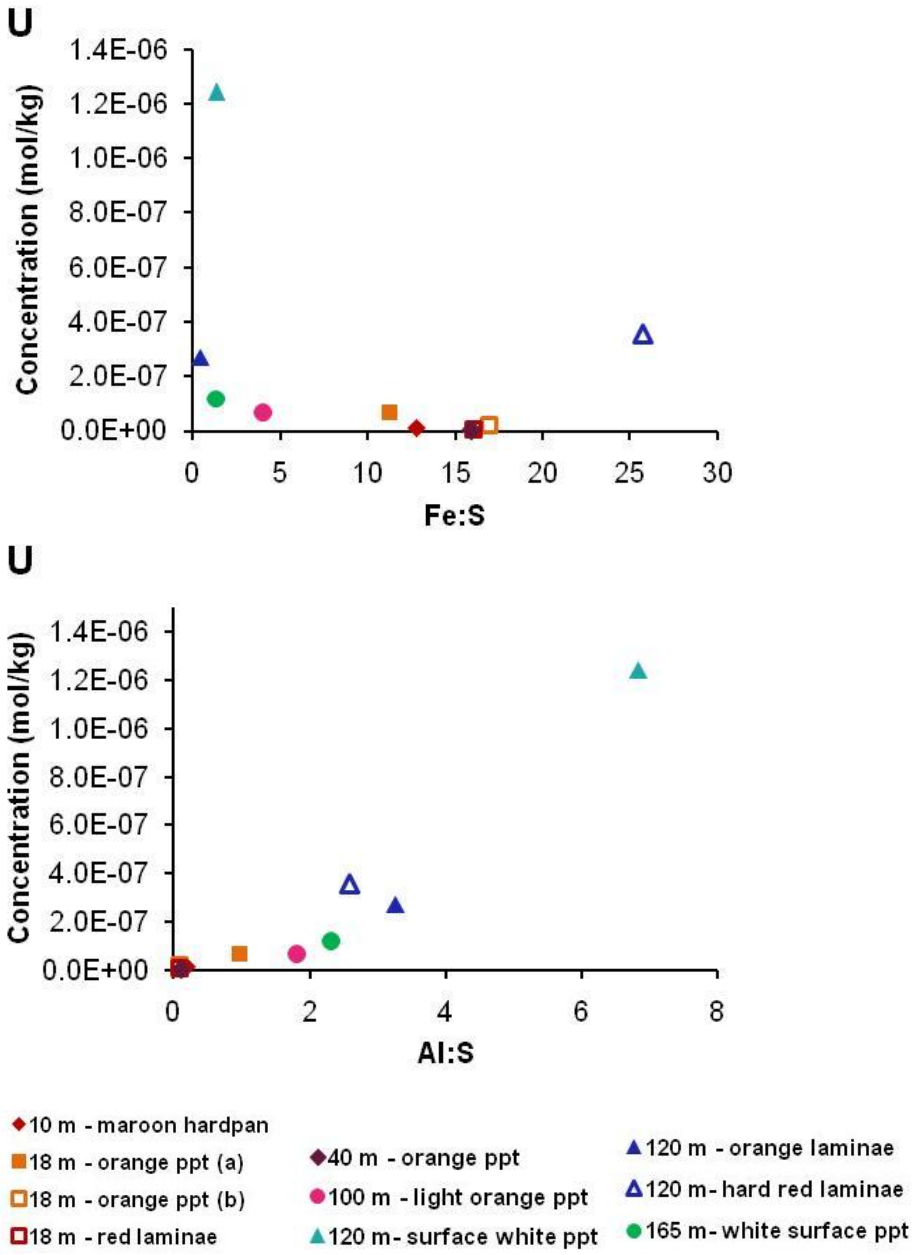

Figure 39: Uranium concentration (mol/kg) in the mineral precipitates, defined by their Fe:S and Al:S molar ratios.

Silicon

The Si concentration in the mineral precipitates generally increased with increasing Al:S and decreasing Fe:S molar ratios (Figure 40). The highest Si concentrations were found in the orange-coloured laminae at the waterfall at 120 m, while the lowest

concentrations of Si were found in the red-coloured laminae from the same location, followed by the precipitates from the upper reaches of the creek (Figure 40).

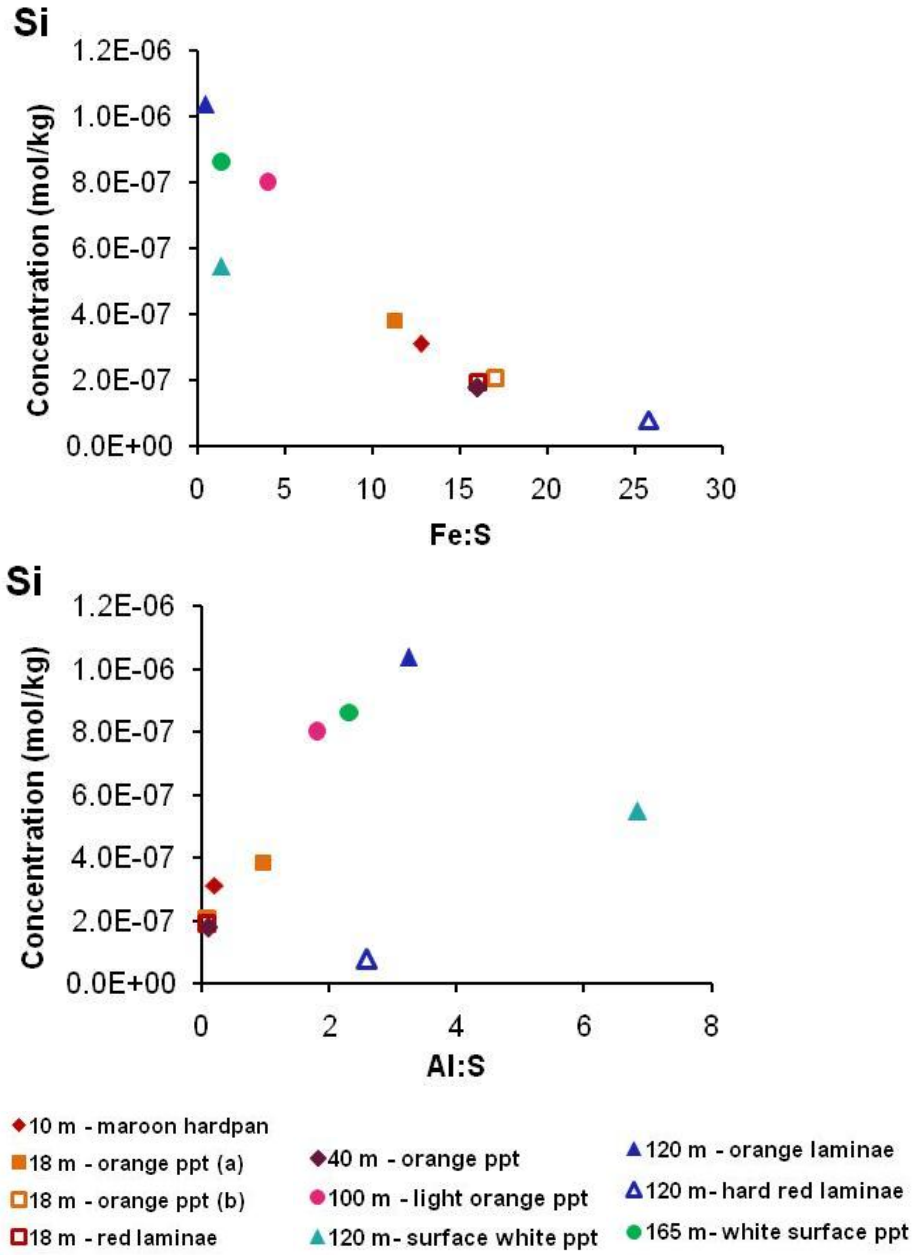

Figure 40: Silicon concentration (mol/kg) in the mineral precipitates, defined by their Fe:S and Al:S molar ratios.

When all of the data were considered, the Fe:S molar ratio explained approximately 75 % of the Si variability in the mineral precipitates (Spearman R= -0.7512, p=1.51E-05),

while the Al:S molar ratios explained 55% of the Si variability (Spearman R = 0.5535, p=0.0041). The red-coloured laminae (120 m) contained very little Si relative to the other data with a similar Al:S ratio, so these data were removed from the regression analyses for Al:S and Si. This improved the regression, with Al:S molar ratios explaining approximately 67 % of the Si variability (Spearman R = 0.6856, p=2.00E-04).

4.5.4. Rare earth elements

The distribution of rare earth elements (REE) in mineral precipitates was used to determine if the mineral precipitates were generated inorganically or if their precipitation was mediated by microbes. If microbially-mediated mineral precipitation had occurred, a weak peak around the middle REE (MREE) would be observed, followed by a sharp increase in the heavy REE (HREE) (Figure 41) due to the preferential adsorption of REE to bacterial cells (Takahashi et al., 2007).

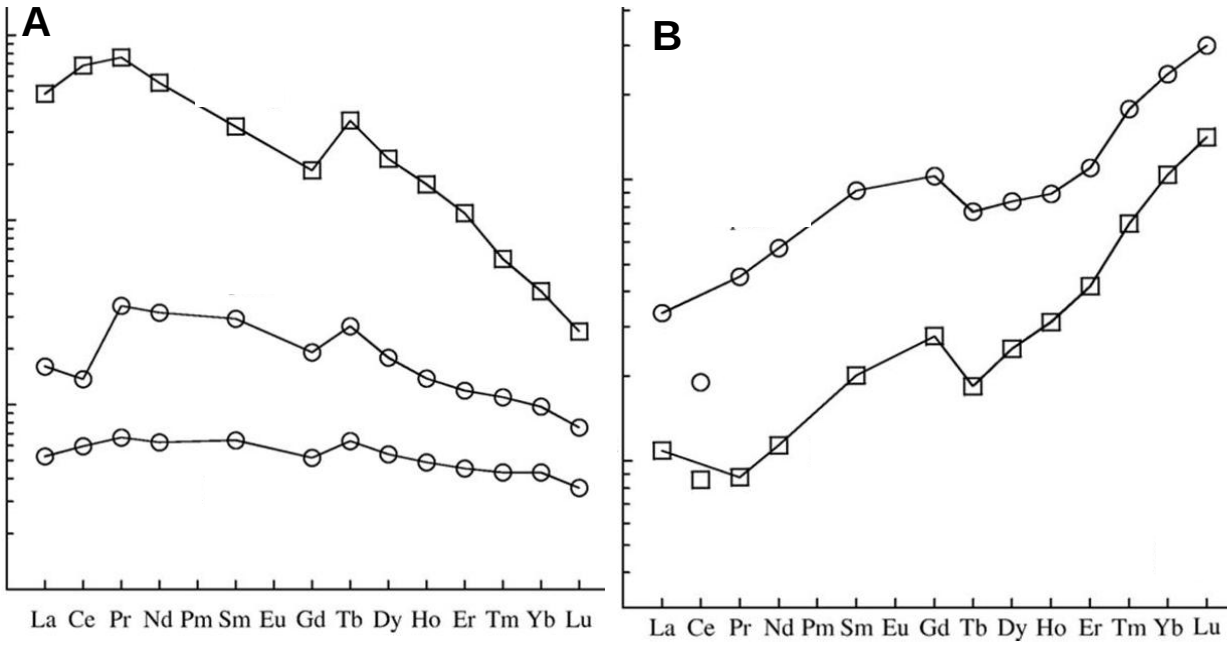

Figure 41: K_d distributions for rare earth elements in mineral precipitates that formed inorganically (A) and those formed in association with microbes (B). Modified from Takahashi et al., 2007.

The distribution of REE in the mineral precipitates collected in the upper reaches of the creek suggested that their formation was not microbially-mediated, as the REE K_d distributions generally showed a sharp peak in the MREE, followed by a weak peak in the HREE (Figure 42 A - D). The mineral precipitates collected in the lower reaches of the creek (Figure 42 E, F), however, conformed to the REE K_d distribution for microbially-mediated precipitation, showing a weak peak in the MREE and a sharp peak in the HREE (Figure 42 E, F). The sharp La peak in the mineral precipitates collected at 120 m (Figure 42 E) suggested that inorganically- and microbially-mediated precipitation may have occurred concomitantly. Promethium concentrations were not determined as it is not naturally occurring and consequently is unlikely to be present in these natural samples.

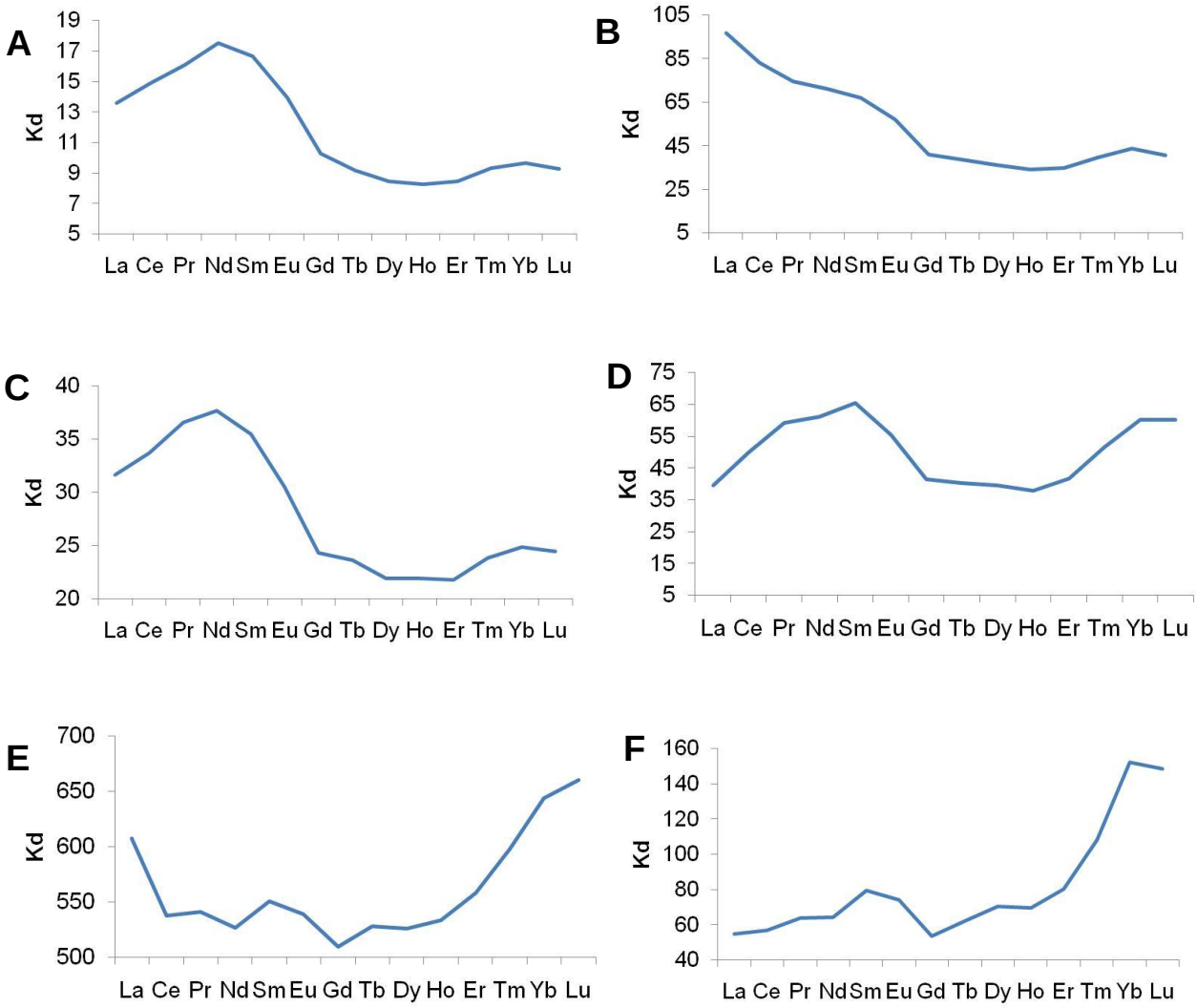

Figure 42: REE distribution patterns (K_d) for mineral precipitates collected at A) 10 m, B) 18 m, C) 40 m, D) 100 m, E) 120 m and F) 165 m.

4.5.5. Organic and inorganic carbon content

The organic and inorganic carbon content of the mineral precipitates was determined to be insignificant (< 5%) (Appendix 7).

4.5.6. Mineralogy by X-ray diffraction

Groundwater seeps

The maroon-coloured hardpan precipitate collected at the 10 m groundwater seep was identified by X-ray diffraction (XRD) as a mixture of barite ($BaSO_4$), jarosite ($KFe_3(SO_4)_2(OH)_6$), schwertmannite ($Fe_8O_8(SO_4)(OH)_6$) and goethite (α-FeOOH) (Figure 43). It was not possible to collect precipitates from the initial groundwater spring located at 0 m as these precipitates were very thin.

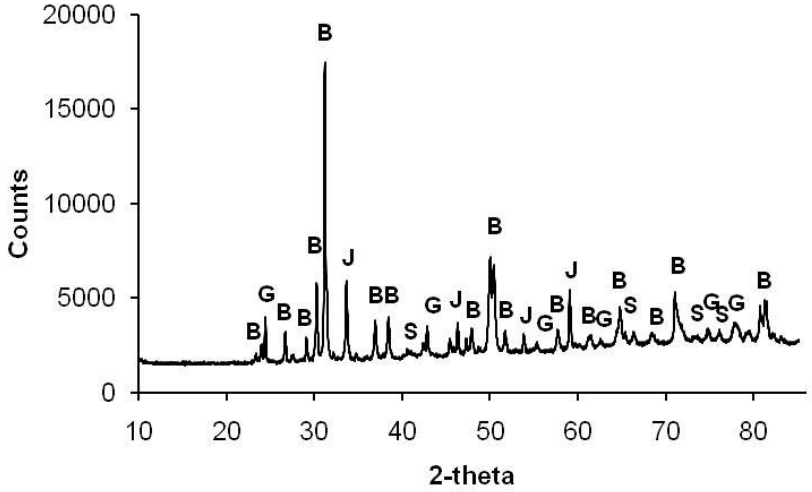

Figure 43: XRD spectrum for the maroon-coloured hardpan found at the 10 m groundwater seep. B = barite, J = jarosite, S = schwertmannite, G = goethite.

Upper reaches

The TIFs found in the upper reaches of the creek (18 m) showed slightly different mineralogy for the different laminae. For example, the soft orange-coloured laminae were a mixture of schwertmannite and goethite (Figure 44 A), while the hard red-brown-coloured laminae contained schwertmannite, goethite, and barite (Figure 44 B). The precipitates (non-laminated) collected at 40 m were composed of schwertmannite and goethite (Figure 45).

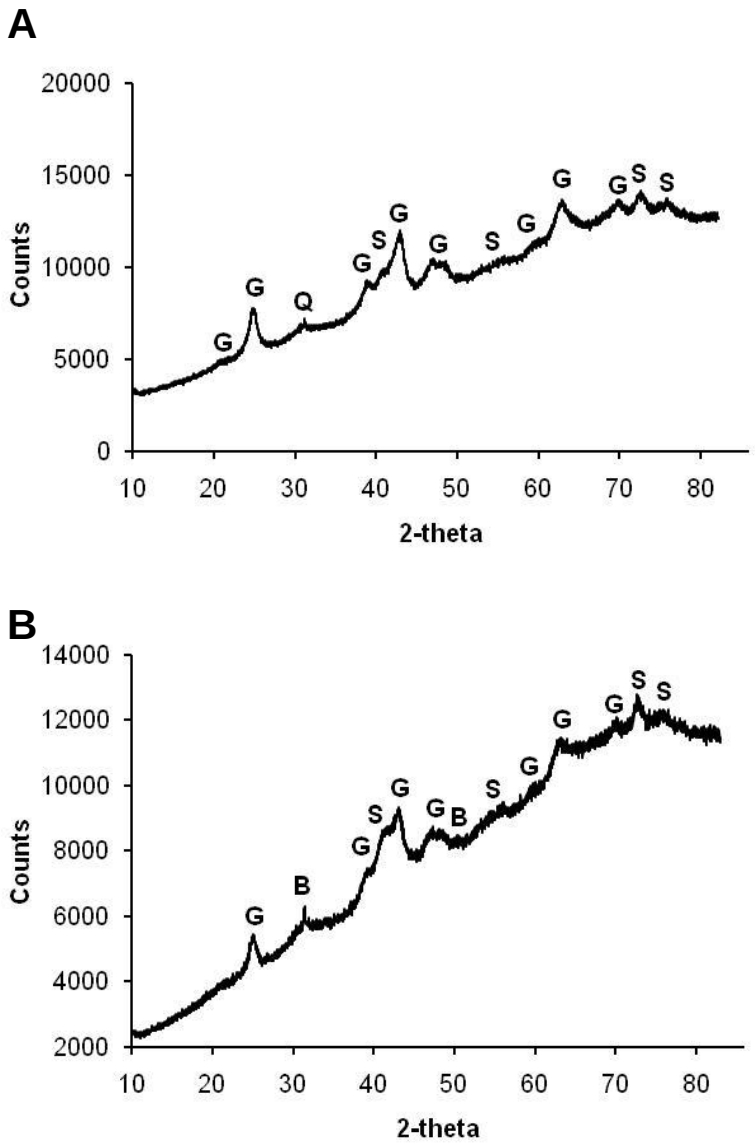

Figure 44: XRD spectra for the TIFs found at the 18 m site, comprised of soft orange laminae (A), and hard red-brown laminae (B). G = goethite, S= schwertmannite, B = barite and Q = quartz.

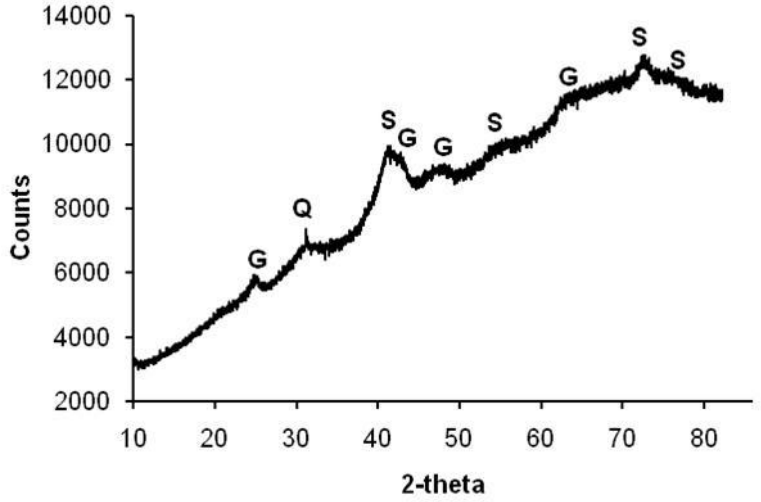

Figure 45: XRD spectrum for the non-laminated orange precipitates collected at 40 m. G = goethite, S = schwertmannite and Q = quartz.

Lower reaches

Schwertmannite and goethite were identified in the mineral precipitates collected at 100 m (Figure 46), although barite was occasionally present (Appendix 8).

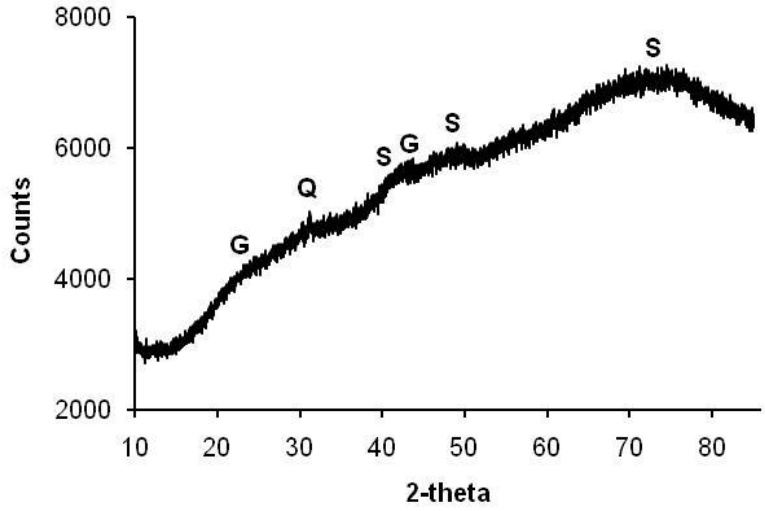

Figure 46: XRD spectrum for the non-laminated mineral precipitates collected at 100 m.

The laminated mineral precipitates at the waterfall (120 m) in the lower reaches of the creek showed distinctly different mineralogy for the white and red-coloured laminae.

The white laminae were composed of jurbanite ($AlOHSO_4$) (Figure 47 A), while the red-coloured laminae contained schwertmannite (Figure 47 B). The mineralogy of the orange-coloured laminae was not defined by XRD, as they became contaminated with pieces of the white and red laminae when they were separated.

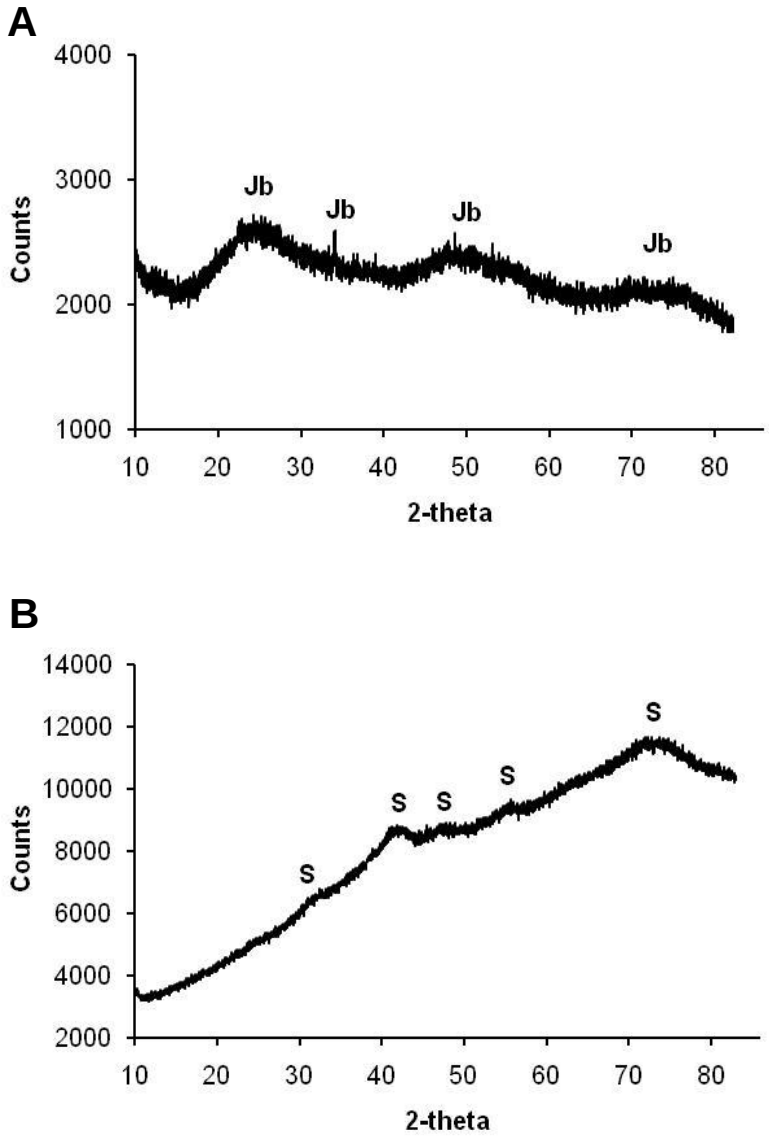

Figure 47: XRD spectrum for the white (A) and red-coloured (B) laminae from the waterfall at 120 m. Jb = jurbanite and S = schwertmannite.

The white-coloured mineral precipitates at 165 m were also identified as jurbanite (Figure 48 A), while the orange-coloured precipitates found here in June were a mixture of schwertmannite, goethite, jarosite, and barite (Figure 48 B).

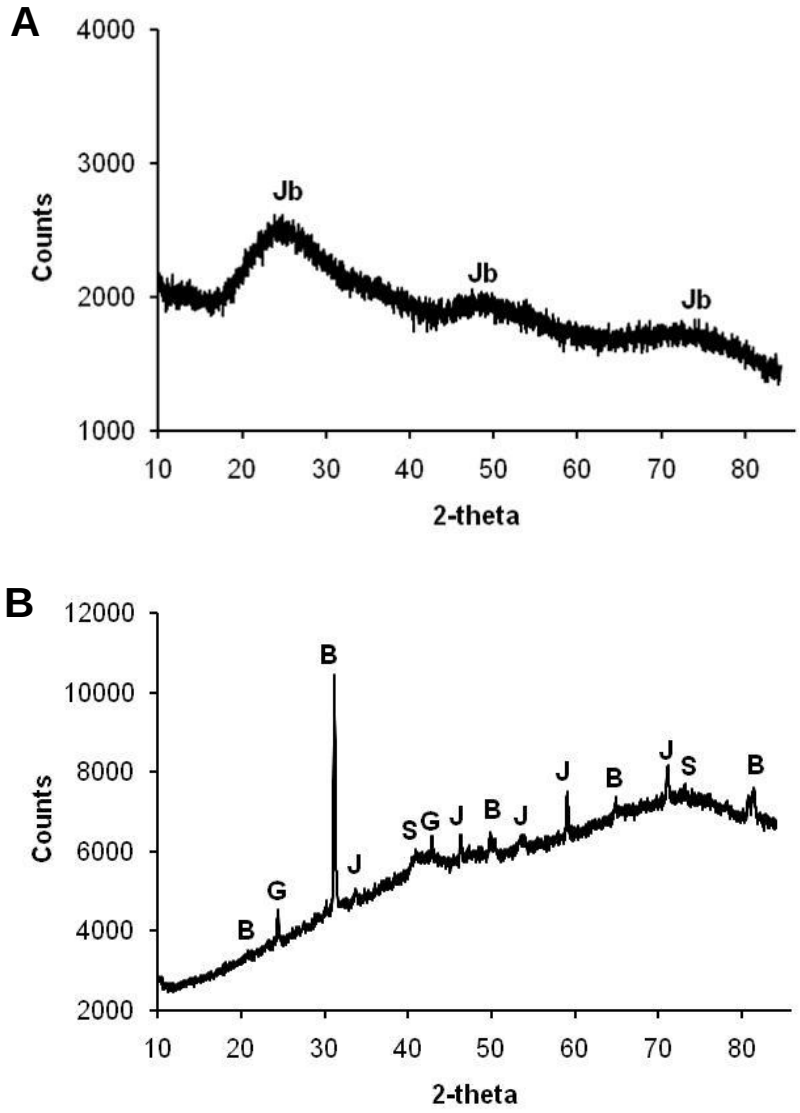

Figure 48: XRD spectra for the white-coloured mineral precipitates at 165 m collected in August (A), and orange-coloured mineral precipitates collected from the same location in June (B). Jb = jurbanite, B = barite, G = goethite, J = jarosite and S = schwertmannite.

4.5.7. Saturation indices

Iron minerals

Multiple minerals were supersaturated or at equilibrium in the creek, including schwertmannite, plumbojarosite, potassium jarosite, hydronium jarosite, goethite, and ferrihydrite (Figure 49 A, B). Natrojarosite also exceeded saturation, but due to the negligible concentrations of Na in the mineral precipitates (Appendix 5), it was omitted from the results. Thermodynamic modeling for July showed that the saturation indices for schwertmannite, goethite, and ferrihydrite generally increased with increasing pH and distance, while those for the jarosite-group minerals decreased with increasing pH and distance (Figure 49 A). Schwertmannite saturation was greater than goethite, which was in turn greater than ferrihydrite for all reaches of the creek (Figure 49 A). At the groundwater seeps and in the upper reaches of the creek, the SI values followed this order: plumbojarosite > potassium jarosite > hydronium jarosite, whereas in the lower reaches, potassium jarosite > plumbojarosite > hydronium jarosite (Figure 49 A).

The thermodynamic modeling for August showed a similar trend for all of the Fe-minerals, although all of the saturation indices were slightly higher (Figure 49 B). The distribution of the jarosite minerals was fairly consistent with the saturation indices calculated for July, except that in the August simulations, the saturation indices for potassium jarosite exceeded that of plumbojarosite, which was in turn greater than hydronium jarosite in the upper reaches (Figure 49 B).

The saturation indices determined by thermodynamic modeling were in agreement with the mineralogy determined by XRD.

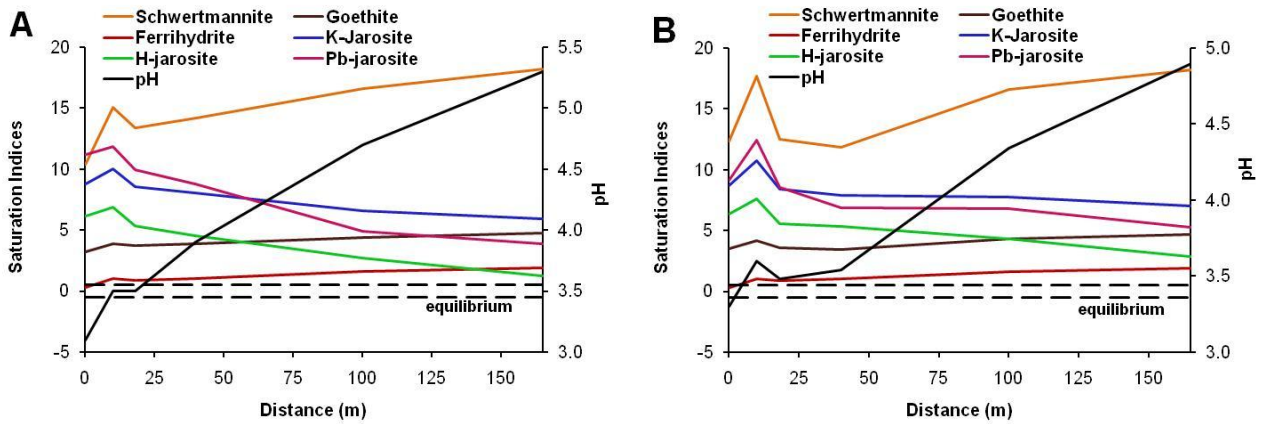

Figure 49: Saturation indices of selected Fe-minerals with pH and distance (m) for July (A) and August (B) thermodynamic modeling.

Aluminum minerals

Similar to the Fe-minerals, a variety of Al-minerals were predicted to be supersaturated or at equilibrium, including basaluminite, jurbanite, and gibbsite (Figure 50 A, B). The solubility constants for hydrobasaluminite are poorly defined, and basaluminite was used to represent hydrobasaluminite for thermodynamic modeling. Other Al-rich minerals including alunite were determined to be oversaturated (Appendix 9); however, the formation of alunite requires higher temperatures than what were observed here, so it was omitted from these results.

At the groundwater seeps and in the upper reaches of the creek, basaluminite and gibbsite were undersaturated for the July and August thermodynamic calculations (Figure 50 A, B). Basaluminite exceeded saturation in the lower reaches of the creek, and gibbsite was either at equilbirum or slightly oversaturated (Figure 50 A, B). Jurbanite was just above equilibrium for all locations in the creek (Figure 50 A, B). The distribution of the saturation indices for the Al-minerals did not change appreciably between the July and August thermodynamic calculations, although the distance at which basaluminite

exceeded saturation was further downstream in August when compared to July (Figure 50 A, B).

The saturation indices determined by thermodynamic modeling were in agreement with the mineralogy determined by XRD.

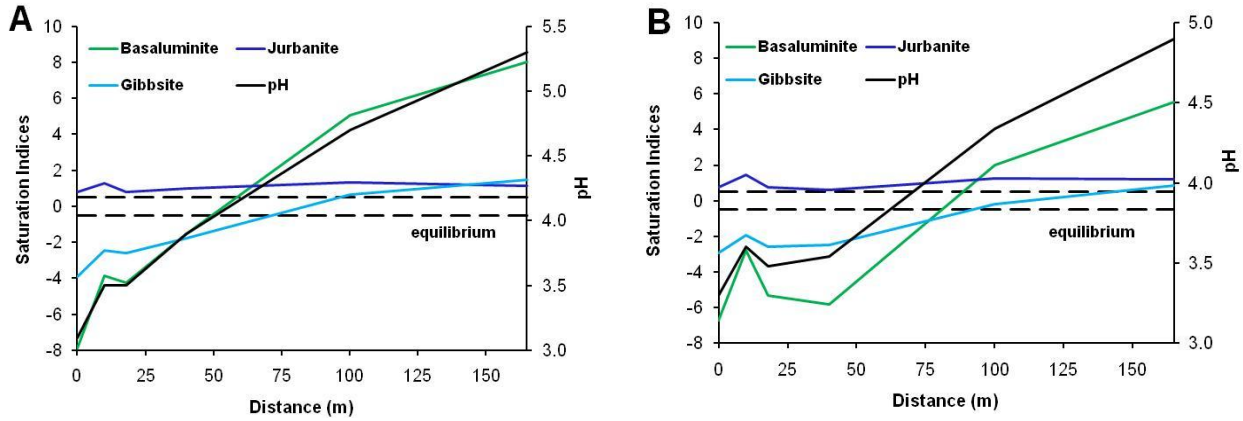

Figure 50: Saturation indices of selected Al-minerals with pH and distance (m) for July (A) and August (B) thermodynamic modeling.

Other minerals of interest

All of the Zn-sulfate and Zn-oxide mineral phases in the MINTEQ database were highly undersaturated over the length of the creek (Appendix 9). Anglesite ($PbSO_4$) was undersaturated for all of the waters sampled, while gypsum ($CaSO_4$-$2H_2O$) and barite ($BaSO_4$) were at equilibrium over all reaches of the creek (Appendix 9). Cadmium, Cu, Ni, and U minerals were determined to be undersaturated in all of the waters sampled (Appendix 9).

4.5.8. Electron microscopy

Terraced iron formations at 18 m

Transmission electron microscopy of the orange precipitates revealed a predominance of spherulitic crystals (and aggregates of crystals) that displayed a "hedgehog"-like morphology (Figure 51 A, B), often observed for schwertmannite

(Schwertmann et al., 1995). The crystals were very small, with a diameter ranging from 250 nm to almost 1 µm (Figure 51 A-D). The size of these schwertmannite crystals is in line with what has been observed in similar samples (Bigham et al., 1990; Bigham et al., 1996a,b; Wang et al., 2006). Occasionally cells were observed, and crystals were often seen growing on the outside of the cell (Figure 51 B). The cells had an average diameter of approximately 0.5 µm. Frequently, needle-like material was observed to be aggregating together (Figure 51 C), The red laminae from the TIFs had a planar morphology, with a much smoother texture compared to the orange precipitates (Figure 51 D, E). Needle-like precipitates were often observed to be growing off of this material (Figure 51 D).

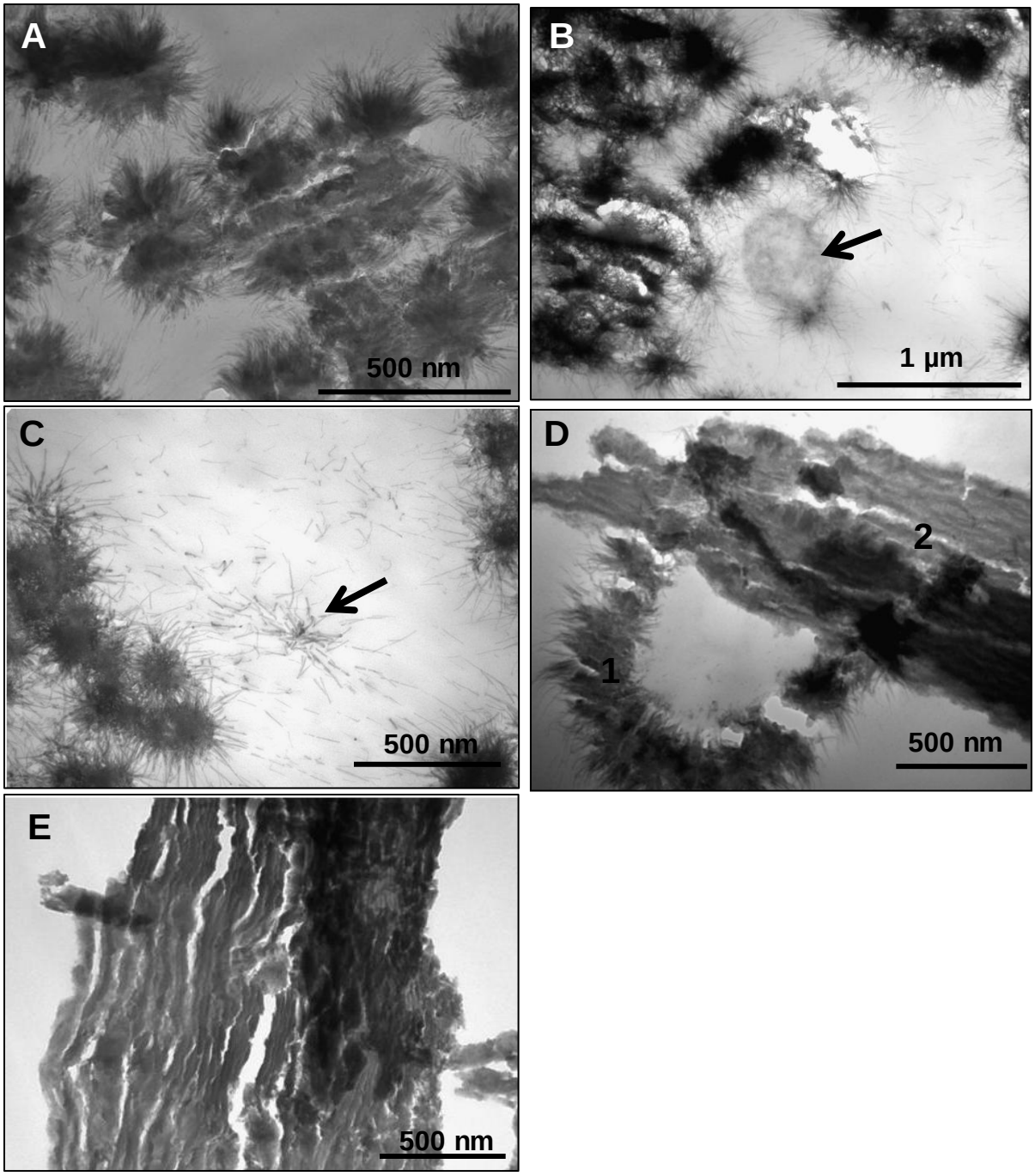

Figure 51: Transmission electron micrographs of TIF mineral precipitates collected at 18 m. A) crystals with a "hedge-hog" morphology similar to schwertmannite; B) cell in precipitate matrix, arrow indicates crystal forming on the exterior of the cell; C) arrow indicates needle-like crystals aggregating together; D) contrasting textures of the red (2) and orange-coloured (1) laminae in the TIFs; E) red-coloured lamina showing planar texture.

EDS analysis of the needle-like crystals (Figure 51 D1) indicated that these precipitates were rich in Fe, O, S and Zn (Figure 52). In terms of atomic percent, the crystal contained 93 % Fe, 4 % S, and 3 % Zn, which is consistent with schwertmannite (Schwertmann et al., 1995).

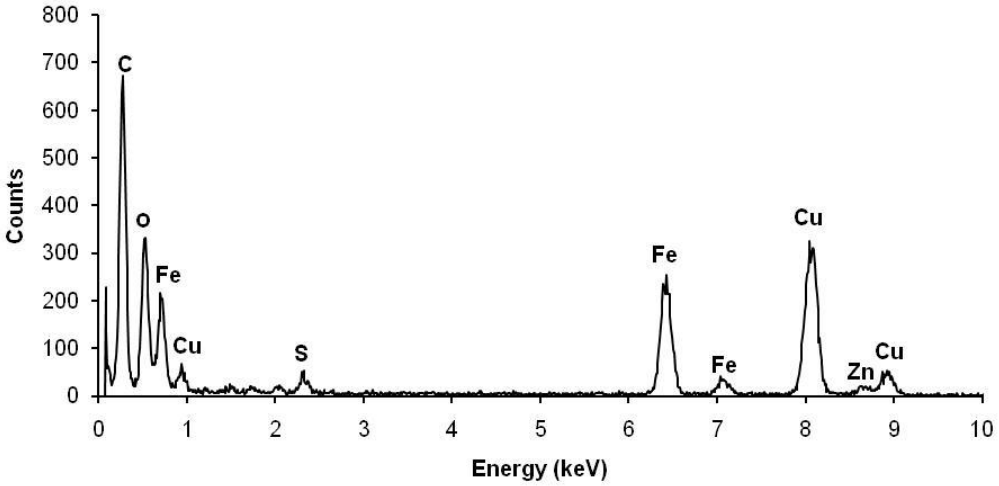

Figure 52: EDS spectra for crystal with schwertmannite-like morphology, seen in Figure 50 D1. Sample was prepared on a Cu grid.

Environmental SEM provided further evidence for the presence of schwertmannite, (Figure 53 C, D), although aggregates with a more crystalline texture were observed in some samples (Figure 53 A). The distinctly different morphology of the orange and red laminae was seen in some cases, whereby spherules were exposed (Figure 53 B1) from underneath flat, smooth material (Figure 53 B2). The spherules were highly aggregated together (Figure 53 B1), which has been observed in other studies where microbially-mediated preciptiation had occurred (Wang et al., 2007 GCA). EDS analysis of these spherules (Figure 54) indicated that this material was rich in Fe, S, and O, which suggested that these crystals were schwertmannite. The smooth, flat material (Figure 53

B2) was of similar elemental composition, but Al was also detected (Figure 55). Zinc was not detected by E-SEM (Figure 55).

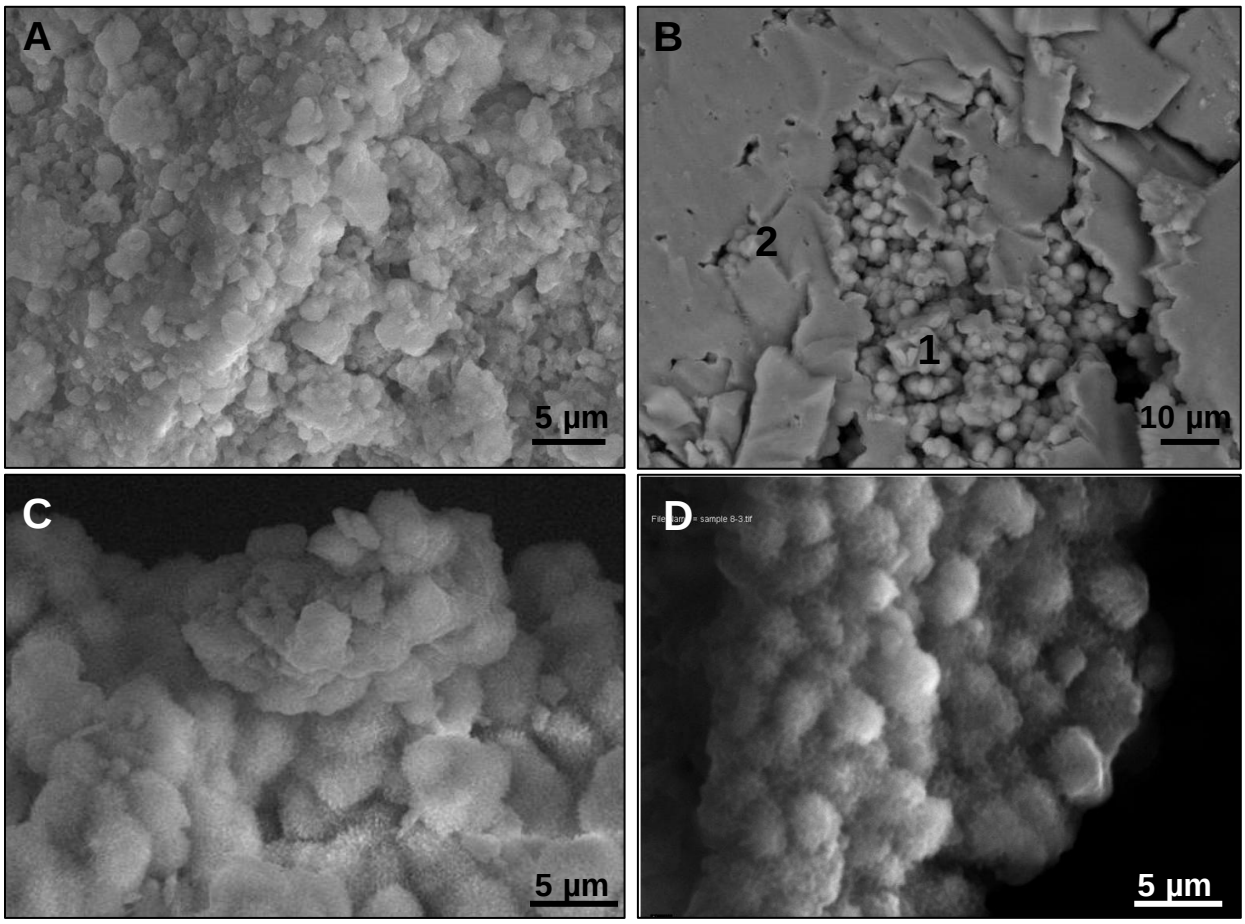

Figure 53: Scanning electron micrographs of orange mineral precipitates collected at 18 m. A) aggregates of precipitate with a crystalline texture; B) orange (1) and red lamina (2), spherules are exposed from underneath planar surface; C) spherulitic precipitates mixed with more crystalline precipitates; D) spherulitic precipitates.

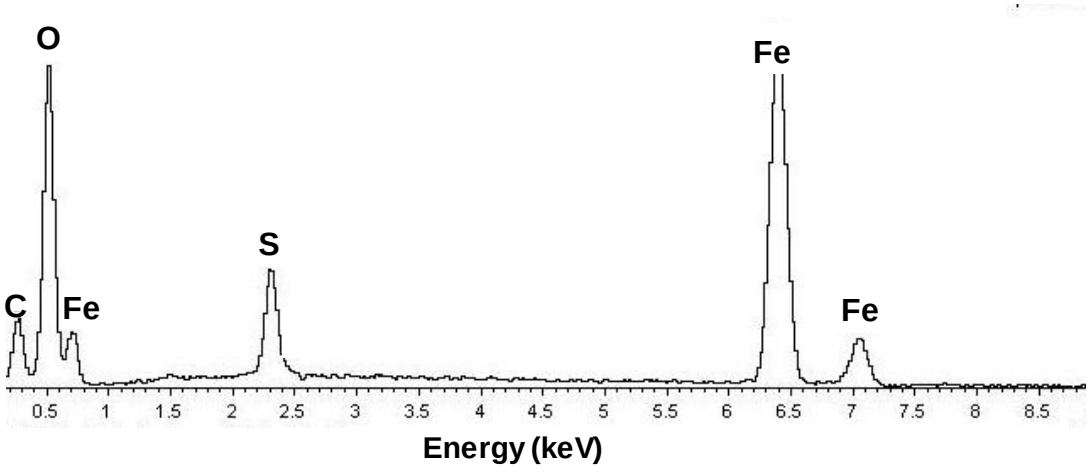

Figure 54: EDS spectrum for Figure 53 B1 (orange lamina in TIFs from upper reaches of the creek). Full scale is 2204 counts.

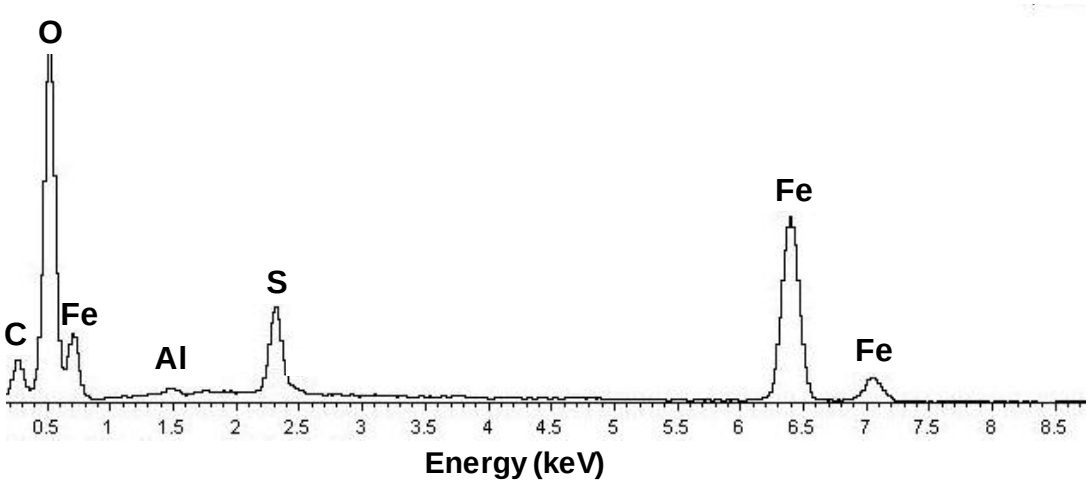

Figure 55: EDS spectrum for Figure 53 B2 (red lamina in TIFs from upper reaches of the creek). Full scale is 4320 counts.

Orange mineral precipitates at 40 m

The non-laminated orange mineral precipitates collected at 40 m contained spherulitic material, however the "hedgehog" texture typical of schwertmannite (Schwertmann et al., 1995) was only observed by TEM in a few samples (Figure 56 E). The average size of these spherulitic aggregates was approximately 0.5 µm in diameter. Internal and external mineralization of cells was occasionally observed (Figure 56 B1, B2);

however, external mineralization was observed more frequently (Figure 56 C1, D1). The cells had an average diameter of 0.5 µm (Figure 56 B, D), although some were slightly smaller (Figure 56 C). Very small spherules (less than 100 nm in diameter) and thin filaments were associated with larger aggregates of mineral precipitates in some samples (Figure 56 C2), while they were absent in others.

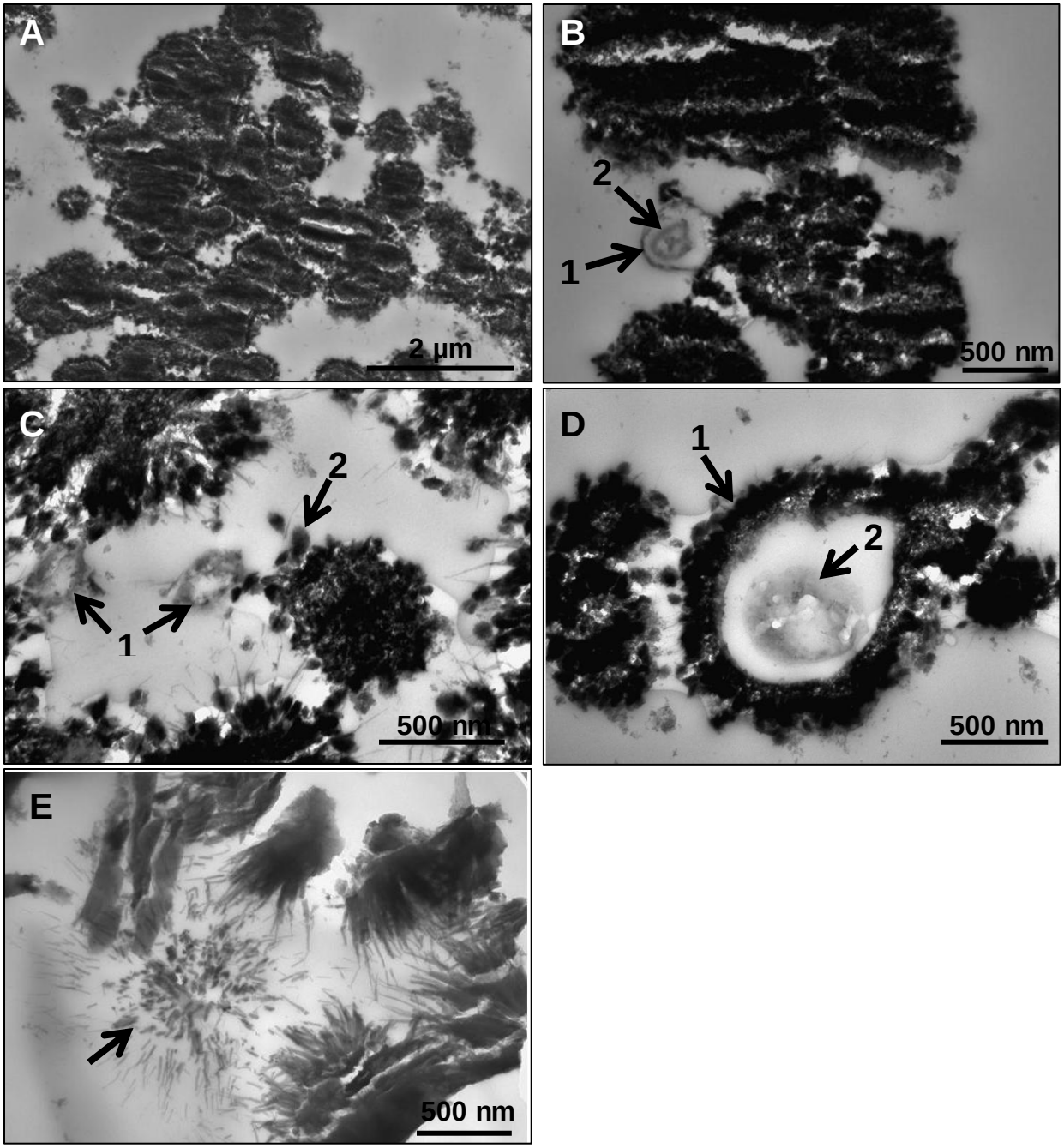

Figure 56: Transmission electron micrographs of orange-coloured mineral precipitates collected at 40 m. A) spherulitic material; B) cell associated with spherulitic material, external (1) and internal (2) mineralization were apparent; C) small cells (1) and associated small spherules and filaments (2); D) cell (2) incased in mineral precipitate (1); E) needle-like crystals.

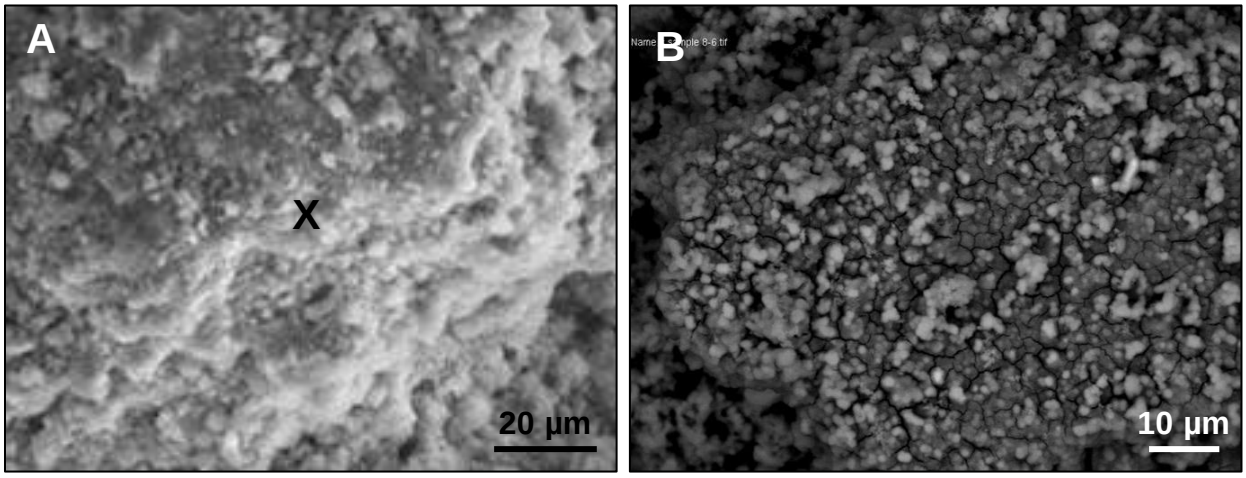

Figure 57: Scanning electron micrographs of orange mineral precipitates collected at 40 m. A) precipitates with a crystalline texture, X indicates location of EDS spot-analysis; B) aggregated spherulitic precipitates.

Environmental SEM revealed the presence of spherulitic crystals in some samples (Figure 57 B), while others were dominated by material that appeared to be more crystalline (Figure 57 A). EDS analysis indicated that this more crystalline material was rich in Fe, O, S, Al, Si, Ca, and Zn (Figure 58).

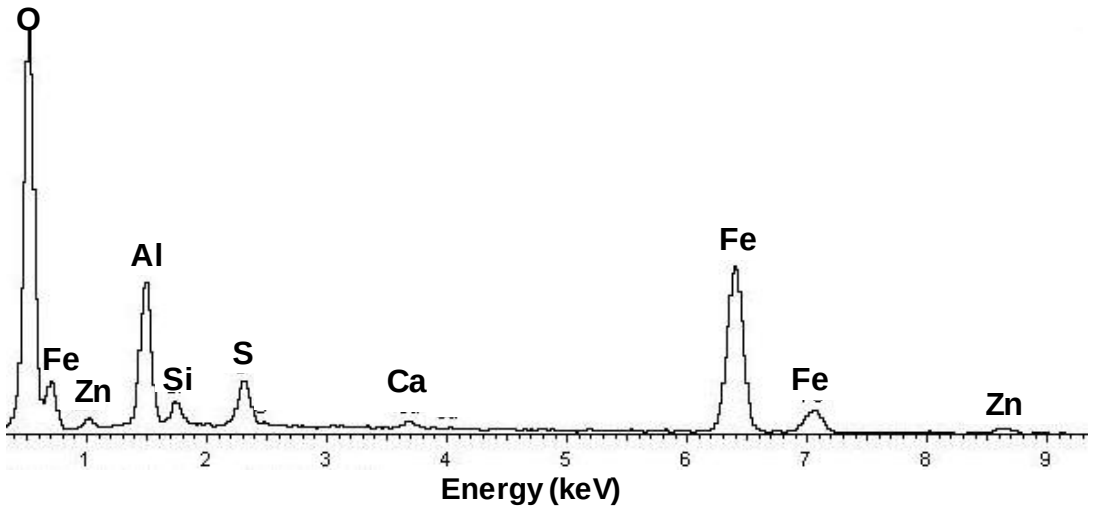

Figure 58: Spectrum for Figure 57A (orange-coloured mineral precipitates with a crystalline texture collected at 40 m). Full scale is 3860 counts.

Light orange mineral precipitates at 100 m

Transmission electron microscopy of the light orange mineral precipitates collected at 100 m revealed the presence of spherules (Figure 59 A2) that were less than 200 nm in diameter, and were occasionally associated with material that could possibly be cellular (Figure 59 A1). Further examination of the tiny spherules (Figure 59 B) revealed a dark centre (Figure 59 B1) surrounded by cross-hatched material (Figure 59 B2). Very small spherules similar to what was observed here have been reported for precipitates rich in Al(III)-hydroxysulphate minerals (Bigham and Nordstrom, 2000; Kim et al., 2002).

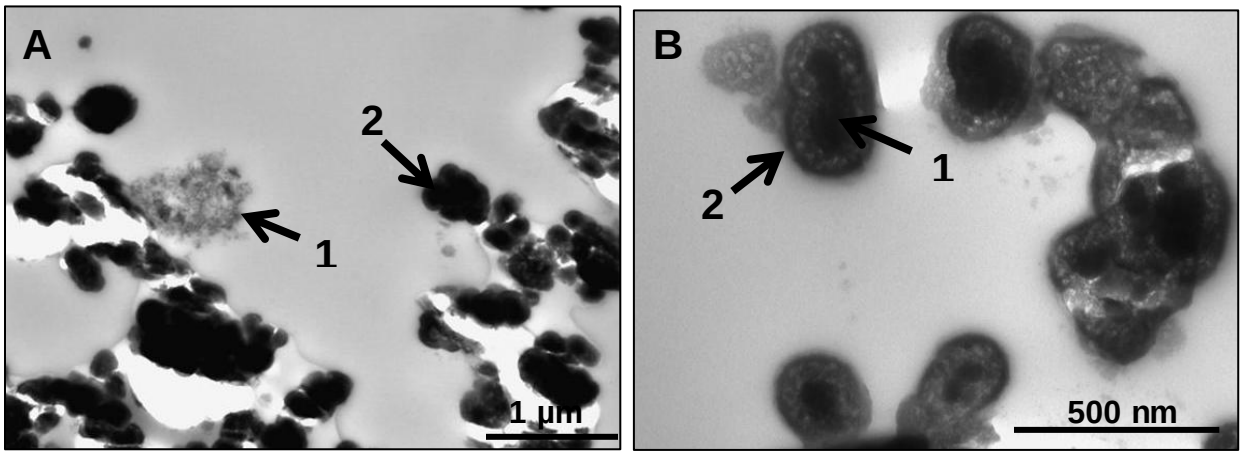

Figure 59: Transmission electron micrographs of light orange-coloured mineral precipitates collected at 100 m. A) organic-like material (1) associated with tiny spherules (2); B) close-up view of A2, showing that individual spheres (A2) are composed of an internal sphere (1) enveloped by material with a cross-hatched appearance (2).

White and red laminated mineral precipitates at 120 m

Transmission electron microscopy showed spherulitic material similar to the mineral precipitate samples collected at the 100 m site (Figure 60 A), but in this case they appeared to be surrounded by amorphous material (Figure 60 B, C). Close examination of these spherules showed that some of them contained an internal sphere (Figure 60 C1) surrounded by amorphous material (Figure 60 C2). Although the inner sphere is less than

200 nm in diameter, the overall diameter of whole structure is closer to 500 nm (Figure 60 C). Cells containing internal mineral precipitates were occasionally observed and had an average diameter of approximately 1 µm (Figure 60 D).

EDS analysis indicated that both the inner sphere (Figure 60 C1) and the outer amorphous material (Figure 60 C2) were of a very similar composition, and were rich in Al, O, Fe, Cu, Si, Zn and S (Figure 61). In terms of atomic percent, this material contained an approximately 53 % Al, 23 % Fe, 8 % Cu, 7 % Si, 5 % Zn and only 2 % S.

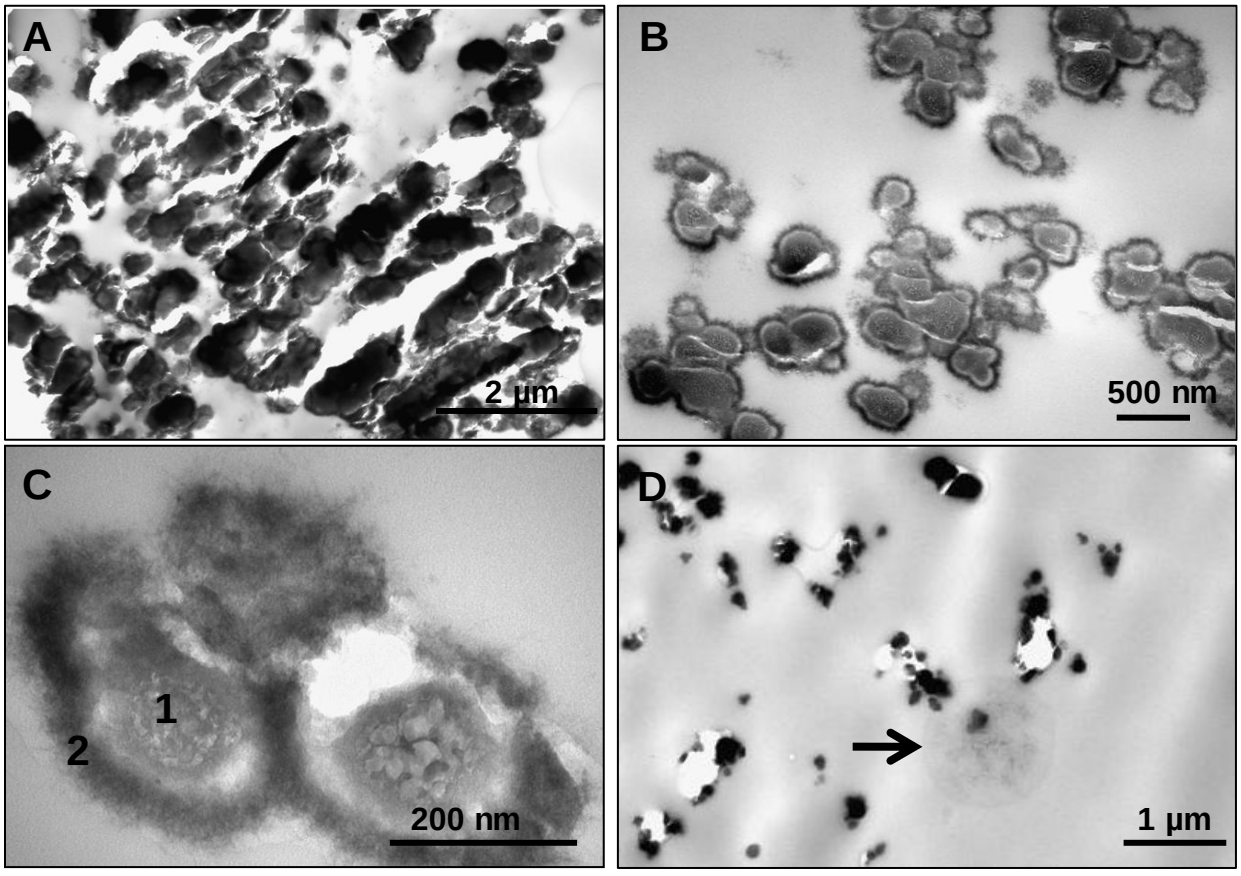

Figure 60: Transmission electron micrographs of white surface precipitate collected at the waterfall at 120 m. A) spherulitic precipitates; B) spherulitic precipitates surrounded by amorphous precipitates; C) close-up of B, showing internal (1) and external (2) mineralization that comprises these spherules, (1) is the spot for EDS-analysis; D) arrow indicates cell containing internal mineralization.

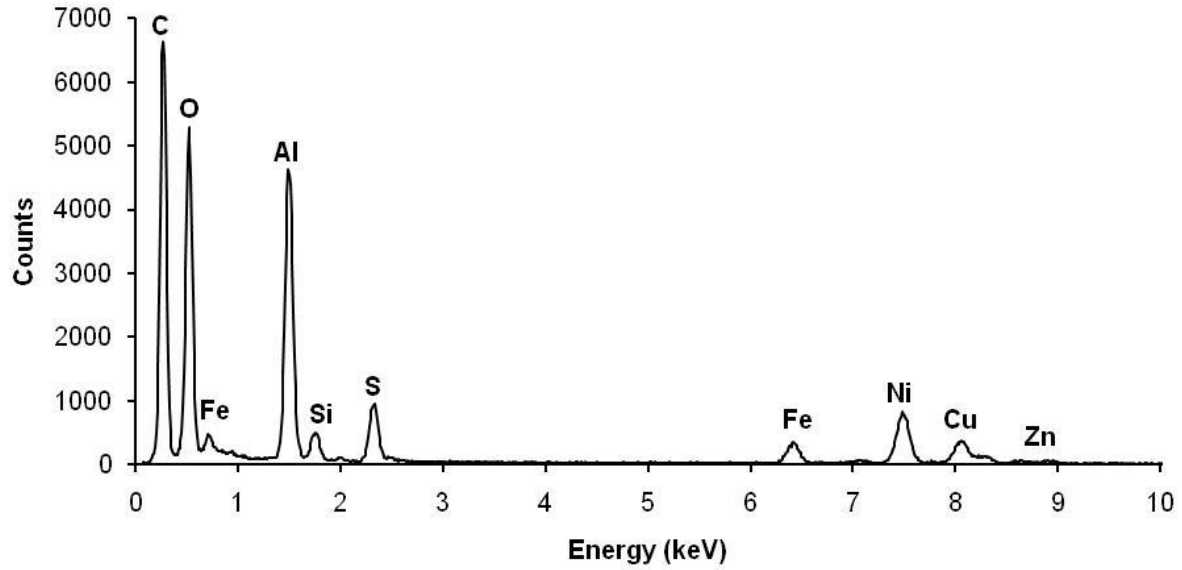

Figure 61: EDS spectrum for Figure 60 C1 (white-coloured mineral precipitates resembling mineralized cells, collected at 100 m). Sample was prepared on a Ni-grid.

Environmental SEM revealed the presence of a highly amorphous, spherulitic material comprising the white surface precipitates from the waterfall at 120 m downstream (Figure 62 A, B). These spherules were very small (diameter of less than 500 nm) and were similar in size to the Al-rich spherules observed at other locations in the stream (100 and 165 m). Similar spherulitic material with a very small diameter has been observed in samples rich in Al(III)-hydroxysulpahtes elsewhere (Bigham and Nordstrom, 2000). EDS analysis showed these spheres to be rich in Al, O, Fe, S, Si, Zn, and Ca (Figure 63).

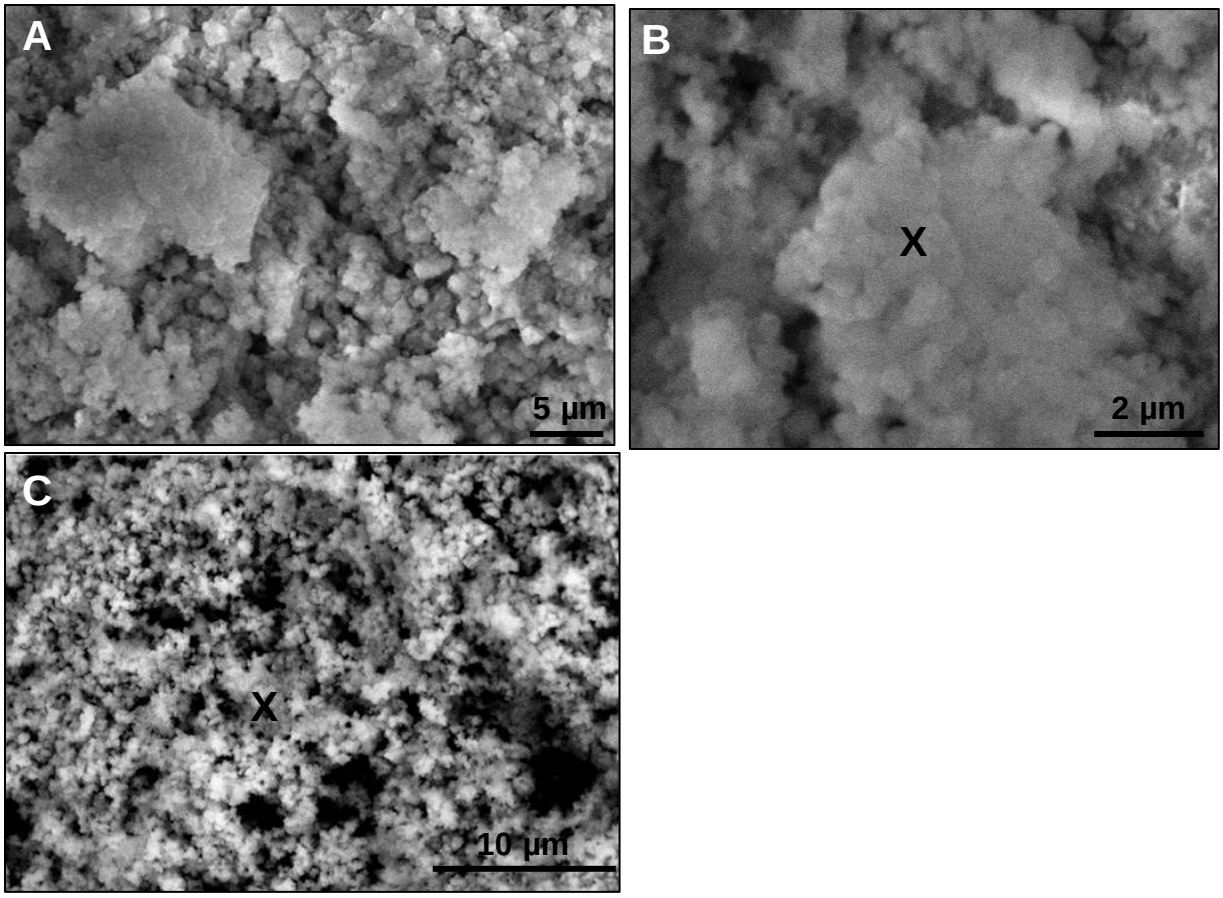

Figure 62: Scanning electron micrographs of white-coloured mineral precipitates collected at 120 m. A) white mineral precipitates with spherulitic texture; B) spherulitic white precipitates, X indicates location of EDS-spot analysis; C) red-coloured lamina, X indicates location of EDS-spot analysis.

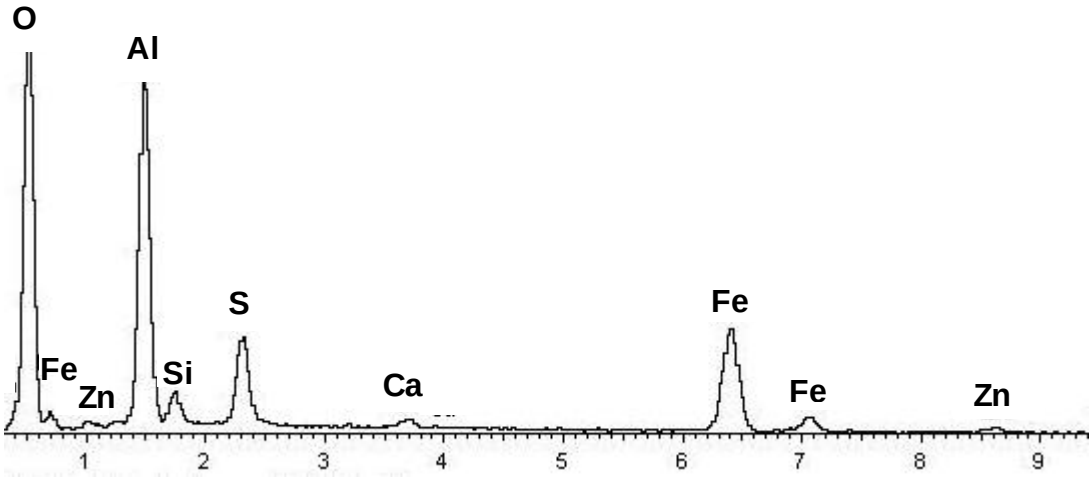

Figure 63: EDS spectrum for Figure 62 B (spherulitic white-coloured mineral precipitates collected at 120 m). Full scale is 3088 counts.

The red laminae from the waterfall at 120 m were composed of highly amorphous material; however, due to technical problems, it was not possible to obtain a micrograph at larger scale than shown (Figure 62 C). EDS analysis of this material indicated that it was rich in Fe, O, Al, S, Zn, Ca, and Si (Figure 64).

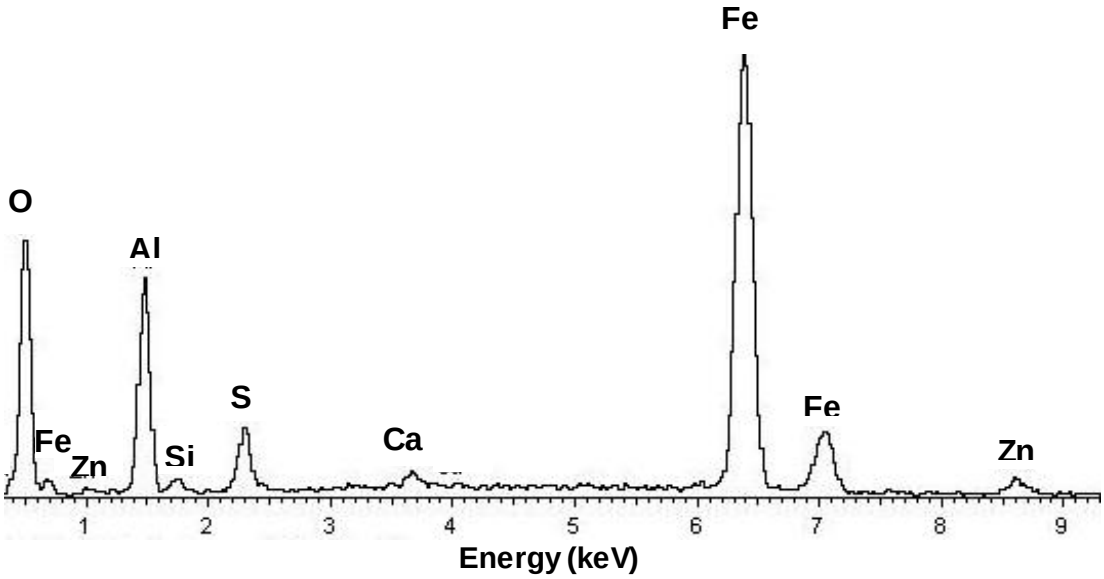

Figure 64: EDS spectrum for Figure 62 C (red-coloured laminae in mineral precipitates collected at 120 m). Full scale is 1361 counts.

White and orange mineral precipitates at 165 m

Transmission electron microscopy showed that the white surface precipitates collected (August 2008) at 165 m were composed of small spheres that were less than 500 nm in diameter (Figure 65 A, B). Similar to the spheres observed in the light orange precipitates at 100 m (Figure 59 B), these spheres contained an inner sphere (Figure 65 B1), surrounded by an envelope of material (Figure 65 B2). This material did not appear to be highly amorphous, and the cross-hatching observed in the precipitates at 100 m (Figure 59 B) was not prevalent here (Figure 65 B). EDS analysis revelaed that these spheres were rich in Al, O, S, Si, Fe, Cu and Zn (Figure 66).

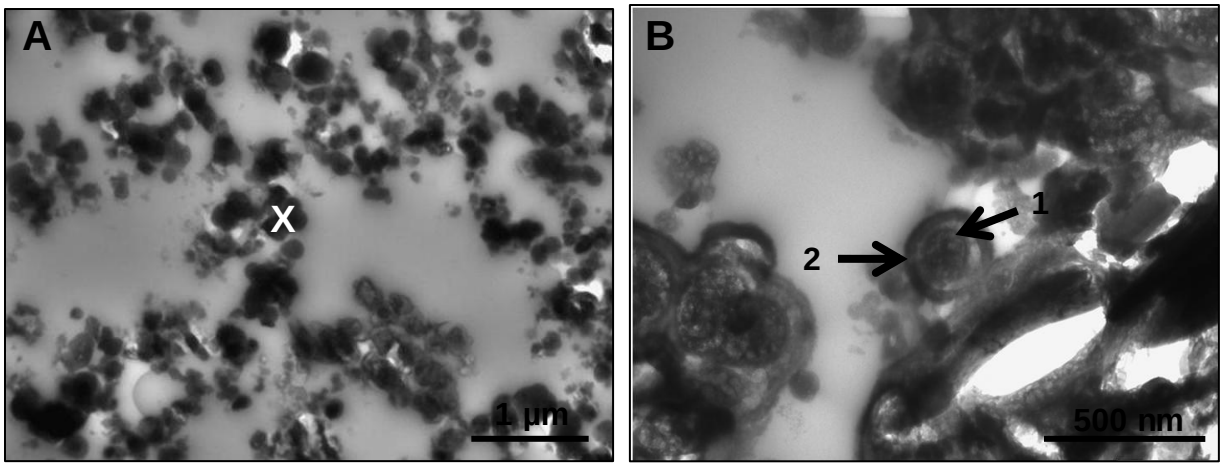

Figure 65: Transmission electron micrographs of white –coloured precipitates collected at 165 m. A) spherulitic mineral precipitates, X indicates location of EDS-spot analysis; B) close up of X in A, showing internal sphere (1) enveloped by external sphere (2).

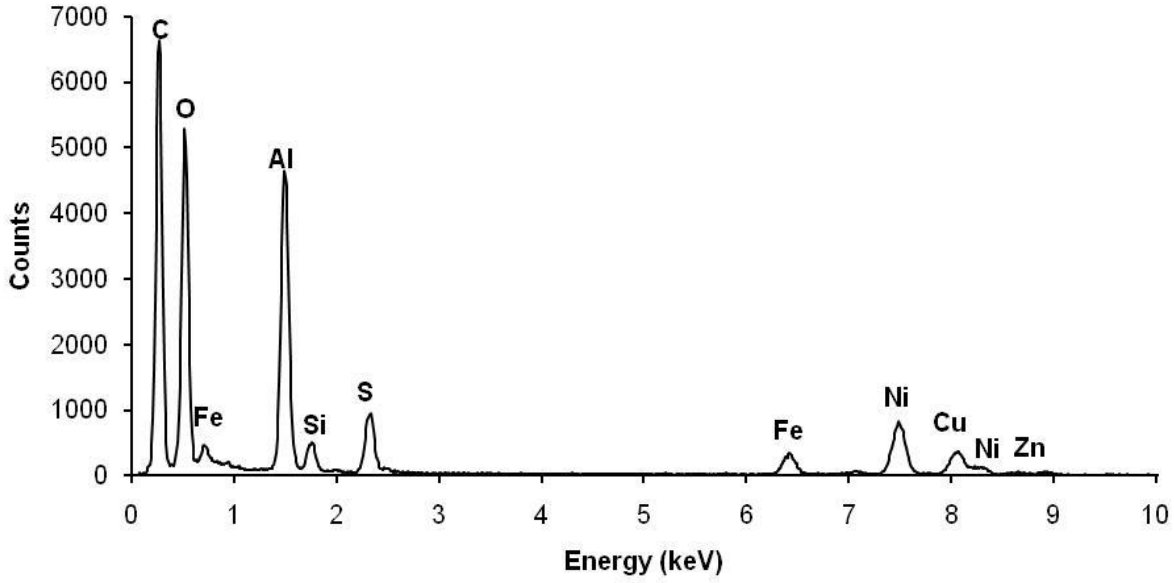

Figure 66: EDS spectrum for Figure 65 A (white-coloured precipitates collected at 165 m). Sample was prepared on a Ni grid.

The orange mineral precipitate collected at 165 m in June (2008) was examined by E-SEM and showed a highly amorphous texture (Figure 67 A). Certain areas in the sample had sphere-like material with a greater electron density around the periphery of the spheres (Figure 67 A). EDS spot analysis of this material indicated that it was rich in Al, O, Fe, Si and S (Figure 68). The white mineral precipitates had a very fluffy texture and

were very fine-grained (Figure 67 B). Potentially biological filamentous material that varied in width from 2 – 6 µm was frequently observed in these samples (Figure 67 C1, D, E1) and was surrounded or covered with fluffy material (Figure 67 C2, D, E2). Individual cells were rarely observed. EDS spot analysis showed that the fluffy material (Figure 67 B) contained Al, O, S, Si, Mg and Ca (Figure 69), and that the filaments covered in fluffy material (Figure 67 D) were rich in Al, O, S, Si and Fe (Figure 70). The compositions observed here are in line with what has been observed for Al-rich mineral precipitates forming in similar settings (Bigham and Nordstrom, 2000; Kim et al., 2002; Pu et al., 2010).

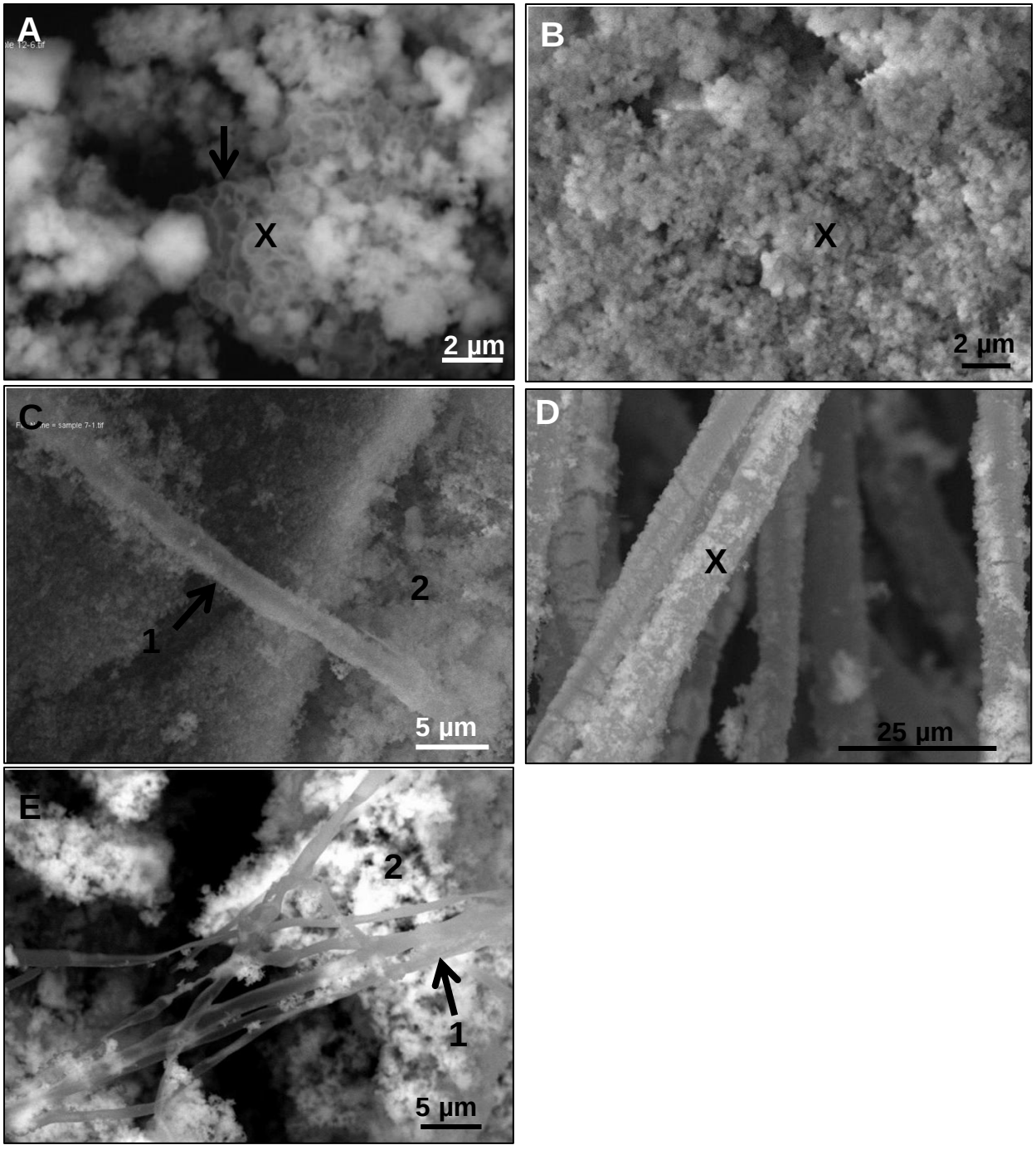

Figure 67: Scanning electron micrographs of the mineral precipitates collected at 165 m. A) orange-coloured mineral precipitates collected in June/08, arrow shows sphere-like material with greater electron density around the periphery of the spheres, X indicates location of EDS spot analysis; B) white-coloured precipitates collected in Aug/08, X indicates location of EDS spot analysis; C) white-coloured precipitates containing filamentous material (1) in a highly amorphous matrix (2); D) white-coloured precipitates containing filamentous material covered with fluffy precipitates, X indicates location of

EDS spot analysis; E) white-coloured precipitates containing filamentous material (1) in an amorphous matrix (2).

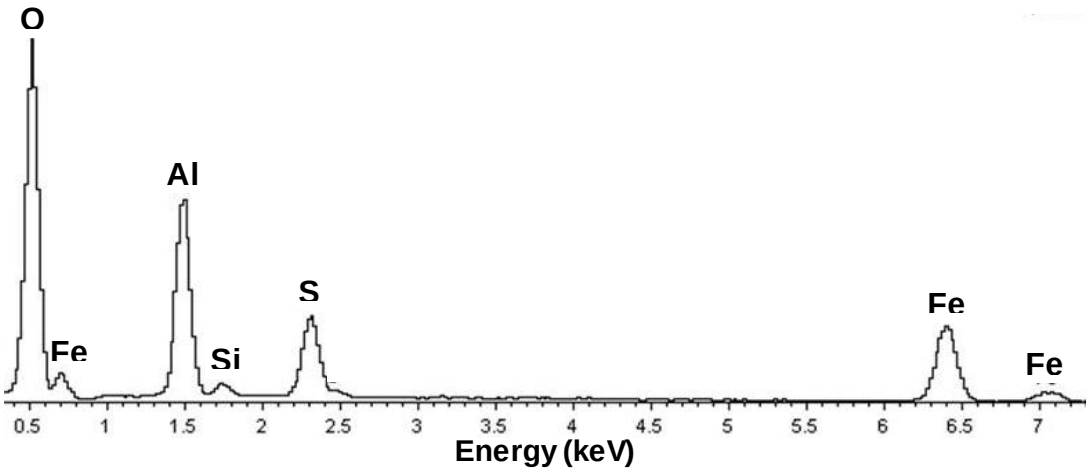

Figure 68: Spectrum for Figure 67 A (orange-coloured mineral precipitates collected in June at 165 m). Full scale is 4087 counts.

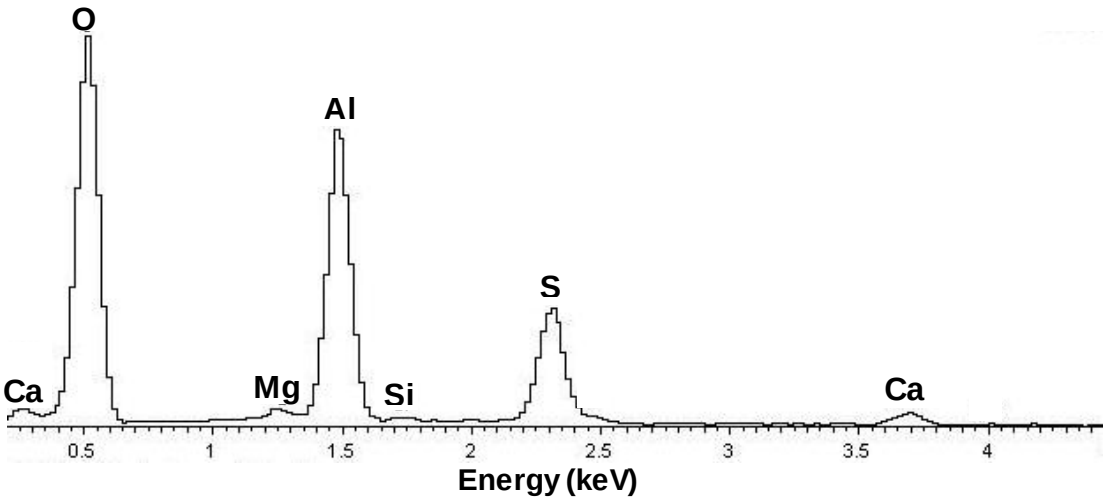

Figure 69: EDS spectrum for Figure 67 B (white-coloured mineral precipitates collected in August at 165 m). Full scale is 5056 counts.

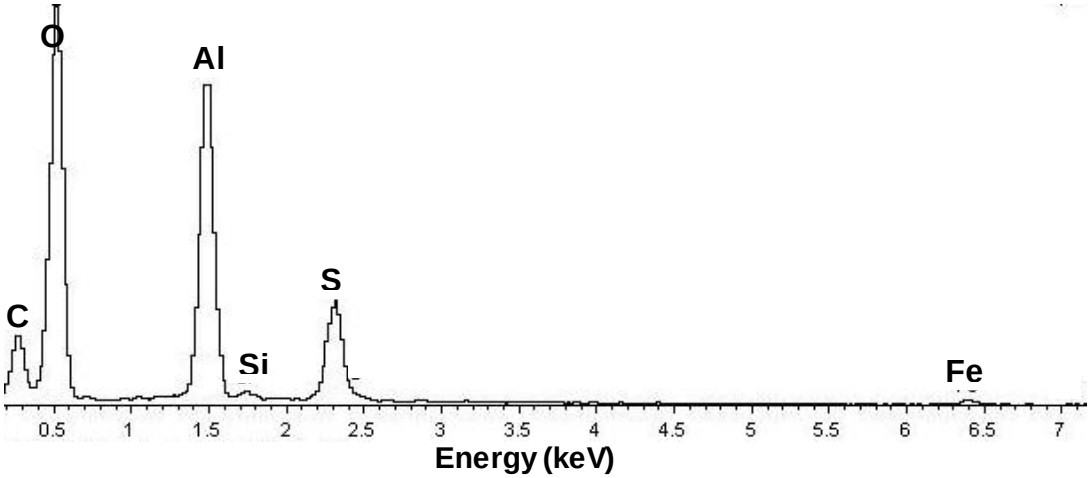

Figure 70: Spectrum for Figure 67 D (white-coloured mineral precipitates containing filamentous material from 165 m). Full scale is 4493 counts.

4.6. Mineral exploration applications

Cd/Zn and Pb/(Pb+Zn) molar ratios

Waters that have interacted with ore deposits are known to retain geochemical signatures of the ore body (Seal et al., 2002; Hammarstrom and Seal, 2003; Desbarats and Dirom, 2007), so the Cd/Zn and Pb/(Pb+Zn) ratios in the ARD waters and mineral precipitates were examined to determine if the signature of the Active Member was preserved in the surface environment. Cd/Zn molar ratios in the ARD waters generally conformed to those determined for the Active Member (Goodfellow et al., 1983b) (Table 12). The groundwater seeps (0 and 10 m) showed anomalous Cd/Zn ratios, with the 0 and 10 m sites having an average Cd/Zn ratio lower (2.01E-03) and higher (5.31E-03) than that of the Active Member (0.003) (Table 12), respectively. The Pb/(Pb+Zn) molar ratios for the waters were several orders of magnitude lower than the Pb/(Pb+Zn) ratios for the Active Member (Table 12). Non-parametric statistics showed that there was no significant correlation between pH and either the Cd/Zn ($p = 0.686$) and Pb/(Pb+Zn) ($p = 0.771$) ratios in these waters.

Table 12: Average Cd/Zn and Pb/(Pb+Zn) molar ratios for the waters draining the XY-deposit. The Cd/Zn ratio of the Active Member is 3.00E-03 while the Pb/Pb+Zn molar ratio ranges from 0.2 - 0.8 (Goodfellow et al., 1983b). Averages were based on the water chemistry in July and August.

Location downstream (m)	pH	Average Cd/Zn	Average Pb/(Pb+Zn)
0	3.3	2.01E-03	1.2E-05
10	3.6	5.31E-03	9.0E-06
18	3.5	3.23E-03	2.0E-05
40	3.5	3.28E-03	2.0E-05
100	4.4	3.38E-03	1.4E-05
165	4.9	3.18E-03	9.4E-06

The mineral precipitates showed highly variable Cd/Zn molar ratios, and Cd/Zn ratios that reflected the composition of the Active Member were found primarily in the mineral precipitates that formed at low pH (Table 13). Similarly, the Pb/(Pb+Zn) ratio of the Active Member was retained in the precipitates that formed at low pH, although the precipitates that formed at pH 4.7 also had a Pb/(Pb+Zn) ratio coinciding with the Active Member (Table 13). Non-parametric statistics indicated that there was no significant relationship between the pH at which the mineral precipitates formed and their Cd/Zn ($p = 0.690$) and Pb/(Pb+Zn) ratios ($p = 0.747$).

Table 13: Average Cd/Zn and Pb/(Pb+Zn) molar ratios for the mineral precipitates. The Cd/Zn ratio of the Active Member is 3.00E-03 while the Pb/(Pb+Zn) molar ratio is 0.2 - 0.8 (Goodfellow et al., 1983b). Averages were based on all of the mineral precipitate samples collected during the sampling campaign.

Location downstream (m)	Sample description	pH	Average Cd/Zn	Average Pb/(Pb+Zn)
10	maroon hardpan	3.6	0.013	**0.275**
18	orange ppt (a)	3.5	0.457	**0.512**
	orange ppt (b)	3.5	**0.006**	0.068
	red laminae	3.5	**0.004**	0.118
40	orange ppt	3.5	**0.004**	0.111
100	light orange ppt	4.4	**0.006**	0.075
120	surface white ppt	4.7	0.313	**0.462**

	orange laminae	-	0.008	0.002
	hard red laminae	-	0.024	0.002
165	white ppt	4.9	**0.006**	0.096

XY-drainage vs. shale drainage

On one occasion (July 24/08) the waters and mineral precipitates of an ARD stream draining an area that does not contain known Zn-Pb mineralization (located across the valley from the ARD creek draining the central XY-deposit, probably draining shales) (Figure 2) was sampled for comparative purposes with the waters that are likely draining the Active Member. In order to remove the seasonal effects (i.e. dilution by rainfall), these waters were compared to those collected on the same date from the ARD stream at the central XY-deposit.

The Cd/Zn molar ratios from the waters and mineral precipitates collected in the stream draining the shales (Table 14) were a few orders of magnitude higher than those from the XY-drainage (Table 12 and 13) and did not coincide with those for the Active Member. Moreover, the Cd/Zn molar ratios for the mineral precipitates in either drainage were not significantly different ($p = 0.5192$), while the Cd/Zn molar ratios in the waters were found to be significantly different ($p = 0.0016$). The Pb/(Pb+Zn) molar ratios for the waters draining the shales (Figure 14) were a few orders of magnitude higher than those found in the XY-drainage waters (Figure 12), and did not reflect the Pb/(Pb+Zn) molar ratio of the Active Member. Similarly, the Pb/(Pb+Zn) molar ratios in the mineral precipitates collected at the shale drainage were not within the range for the Active Member (Table 14), although they were similar to those calculated for the XY-drainage (Table 13). The Pb/(Pb+Zn) molar ratios in the mineral precipitates formed in either drainage were not

significantly different (p = 0.6674) although the Pb/(Pb+Zn) ratios in the waters were significantly different (p = 0.0084).

Table 14: Cd/Zn and Pb/(Pb+Zn) molar ratios for the waters and mineral precipitates collected at the acidic stream draining shales. The Cd/Zn ratio of the Active Member is 3.00E-03 while the Pb/(Pb+Zn) molar ratio is 0.2 - 0.8 (Goodfellow et al., 1983b).

	Cd/Zn	Pb/(Pb+Zn)
Waters	0.021	1.40 E-03
	0.021	1.12 E-03
	0.020	1.47 E-05
	0.020	8.66 E-04
	0.023	2.93 E-04
Mineral precipitates	0.011	0.145
	0.014	0.109

Further differences in the geochemistry of the waters and mineral precipitates from the XY-drainage and the shale drainage were evaluated using a Mann-Whitney U test (Table 15), in order to delineate water-rock interactions occurring in either stream.

Table 15: p-values for aqueous and mineral precipitate geochemistry of the ARD stream draining the XY-deposit compared to an ARD stream draining shales. p-values were determined by a Mann-Whitney U test. Significant p (< 0.05) are shown in bold.

Element	Waters	Mineral precipitates
Na	**0.015**	-
Mg	0.168	0.060
Al	0.168	**0.022**
Si	0.062	**0.022**
P	0.088	**0.022**
S	0.123	0.819
K	**0.005**	0.732
Ca	**0.005**	**0.022**
Sc	0.871	0.819
Cr	**0.005**	**0.022**
Mn	0.372	0.568
Fe	0.685	0.493
Co	0.291	0.530
Ni	0.088	0.110
Cu	0.168	1.000
Zn	**0.005**	**0.022**
Ga	0.570	**0.022**
As	-	**0.040**
Rb	**0.012**	0.392
Sr	**0.028**	**0.022**
Y	0.074	**0.022**
Mo	0.123	**0.022**
Ag	**0.042**	**0.040**
Cd	**0.005**	**0.022**
Sb	0.123	**0.040**
Ba	0.062	**0.022**
La	0.372	0.110
Ce	0.685	**0.022**
Pr	0.465	**0.022**
Nd	0.372	**0.022**
Sm	0.372	**0.022**
Eu	0.372	**0.022**
Tb	0.291	**0.022**
Gd	0.291	**0.022**
Dy	0.168	**0.022**
Ho	0.123	**0.022**
Er	0.088	**0.022**
Tm	0.088	**0.022**
Yb	0.123	**0.022**
Lu	0.088	**0.022**
Tl	**0.005**	**0.030**
Pb	0.088	**0.040**

Th	0.088	**0.022**
U	0.808	0.171

"-" Element was not detected in waters or mineral precipitates.

Significant differences (p-value < 0.05) in the aqueous geochemistry between the two ARD streams were detected for Na, K, Ca, Cr, Zn, Rb, Sr, Ag, Cd and Tl, while significant differences in the mineral precipitate geochemistry was found for Al, Si, P, Ca, Cr, Zn, Ga, As, Sr, Y, Mo, Ag, Cd, Sb, Ba, Ce, Pr, Nd, Sm, Eu, Tb, Gd, Dy, Ho, Er, Tm, Yb, Lu, Tl, Pb, and Th (Table 15). For the elements in the waters and the mineral precipitates that showed a significant difference between the two ARD streams, the U statistic was calculated to determine how these differences were distributed between the two streams (Table 16 and 17).

Table 16: U statistics for the elements that were significantly different in the waters between the two ARD streams. The U statistic indicates the number of times observations (concentrations) in one sample (XY ARD) precede those in the other sample (shale ARD) in the ranking used in the Mann-Whitney U test. The total number of observations (n_{TOT} = 35) is equal to the number of data points in one sample ($n_{XY\ ARD}$ = 7) multiplied by the number of data points in the other sample ($n_{shale\ ARD}$ = 5).

Elements (p< 0.05)	U (XY ARD)	U (shale ARD)
Na	**32.5**	2.5
K	**35**	0
Ca	**35**	0
Cr	0	**35**
Zn	**35**	0
Rb	**33**	2
Sr	**31**	4
Ag	5	**30**
Cd	**35**	0
Tl	**35**	0

Aqueous concentrations of Na, K, Ca, Zn, Rb, Sr, Cd, and Tl were greater in the ARD stream draining the XY-deposit, while Cr and Ag concentrations were greater in the ARD

stream draining the shales (Table 16). In the mineral precipitates, concentrations of Al, Si, Ca, Cr, Zn, Sr, Y, Cd, Ba, Ce, Pr, Nd, Sm, Eu, Tb, Gd, Dy, Ho, Er, Tm, Yb, Lu, Tl, and Pb were greater in the ARD stream at the XY-deposit, while concentrations of P, Ga, As, Mo, Ag, Sb and Th were greater in the mineral precipitates from the stream draining the shales (Table 17).

Table 17: U statistics for the elements that were significantly different in the mineral precipitates between the two ARD streams. The U statistic indicates the number of times observations (concentrations) in one sample (XY ARD) precede those in the other sample (mudstone/shale ARD) in the ranking used in the Mann-Whitney U test. The total number of observations (n_{TOT} = 40) is equal to the number of data points in one sample ($n_{XY\ ARD}$ = 20) multiplied by the number of data points in the other sample ($n_{shale\ ARD}$ = 2).

Elements (p<0.05)	U (XY ARD)	U (shale ARD)
Al	**40**	0
Si	**40**	0
P	0	**40**
Ca	**40**	0
Cr	**40**	0
Zn	**40**	0
Ga	0	40
As	2	**38**
Sr	**40**	0
Y	**40**	0
Mo	0	**40**
Ag	2	**38**
Cd	**40**	0
Sb	2	**38**
Ba	**40**	0
Ce	**40**	0
Pr	**40**	0
Nd	**40**	0
Sm	**40**	0
Eu	**40**	0
Tb	**40**	0
Gd	**40**	0
Dy	**40**	0
Ho	**40**	0
Er	**40**	0
Tm	**40**	0
Yb	**40**	0
Lu	**40**	0
Tl	**39**	1
Pb	**38**	2
Th	0	**40**

5. Discussion

5.1. Geochemistry of ARD waters

5.1.1. Subsurface reactions controlling pH and water composition

Acidic and metal-rich groundwaters emanate directly above the central XY-deposit, near the summit of Sugar Mountain (Figure 4), due to subsurface oxidation of the sphalerite (ZnS) [eq. 1], galena (PbS) [eq. 2], chalcopyrite ($CuFeS_2$) [eq. 3] and pyrite (FeS_2) [eq. 4] in the Active Member. Although the detailed hydrogeology of the XY-deposit remains undefined, the host rocks and the Active Member are highly fractured (Goodfellow et al., 1983a), which would provide ample conduits for groundwater-surface water connectivity. Given the topography and the fractured nature of the regolith, it is likely that the whole mountain is an unconfined aquifer, with substantial surface water infiltration (i.e. the infiltrating water is initially rich in oxygen). This general scenario suggests that at least some of the groundwater is actively intersecting and oxidizing sphalerite, galena, chalcopyrite and pyrite in the Active Member.

$$ZnS + 2\,O_2 \leftrightarrow Zn^{2+} + SO_4^{2-} \quad [1]$$

$$PbS + 2\,O_2 \leftrightarrow Pb^{2+} + SO_4^{2-} \quad [2]$$

$$CuFeS_2 + 4\,O_2 \leftrightarrow Fe^{2+} + Cu^{2+} + 2\,SO_4^{2-} \quad [3]$$

$$4\,FeS_2 + 14\,O_2 + 4\,H_2O \leftrightarrow 4\,Fe^{2+} + 8\,SO_4^{2-} + 8\,H^{+} \quad [4]$$

Although the oxidation of sphalerite, galena, and chalcopyrite by oxygen [eqs. 1, 2, 3] is non-acid generating, acid generation will occur from sphalerite (Hofmann and Schuwirth, 2008), galena, and chalcopyrite (Kimball et al., 2010) dissolution if these

reactions are mediated by ferric iron instead of oxygen [eqs. 6b, 7, 8] (Hofmann and Schuwirth, 2008). Ferric iron is derived from the microbial oxidation of ferrous iron [eq. 5] (Johnson and Hallberg, 2003), released during the dissolution of chalcopyrite [eq. 3] or pyrite [eq. 4] (Kimball et al., 2010). Ferrous iron may also be released during the dissolution of sphalerite, as Fe commonly substitutes for Zn in the sphalerite structure (Pring et al., 2008). Very little energy is produced by microbial ferrous iron oxidation under low pH conditions, and consequently microbes must oxidize large quantities of ferrous iron in order to meet their metabolic energy requirements (Lees et al.,1969).

$$2\ Fe^{2+} + \tfrac{1}{2}\ O_2 + 2\ H^+ \leftrightarrow 2\ Fe^{3+} + H_2O \text{ (microbially-catalyzed)} \quad [5]$$

Under the acidic conditions produced by pyrite oxidation [eq. 3], ferric iron is a much more potent oxidizing agent relative to oxygen (Rimstidt et al., 1994) and aggressively oxidizes the reduced sulphur moiety in sulphide minerals, producing acidity [eqs. 6, 7, 8] (Edwards et al., 1999). The oxidation of sulphide minerals by ferric iron regenerates ferrous iron [eqs. 6, 7, 8], which is then recycled by microbes and oxidized to ferric iron [eq. 5]. This ferric iron can then further oxidize sulphide minerals, releasing more ferrous iron and creating a positive feedback loop.

$$ZnS \text{ (or } PbS) + 2\ Fe^{3+} \leftrightarrow Zn^{2+} \text{ (or } Pb^{2+}) + S^0 + 2\ Fe^{2+} \quad [6a]$$

$$Zn^{2+} \text{ (or } Pb^{2+}) + S^0 + 4\ H_2O + 6\ Fe^{3+} \leftrightarrow Zn^{2+} \text{ (or } Pb^{2+}) + SO_4^{2-} + 6\ Fe^{2+} + 8\ H^+ \quad [6b]$$

$$CuFeS_2 + 16\ Fe^{3+} + 8\ H_2O \leftrightarrow Cu^{2+} + 17\ Fe^{2+} + 2\ SO_4^{2-} + 16H^+ \quad [7]$$

$$FeS_2 + 14\ Fe^{3+} + 8\ H_2O \leftrightarrow 15\ Fe^{2+} + 2\ SO_4^{2-} + 16\ H^+ \quad [8]$$

It has been suggested that low temperatures limit the biological activity of Fe(II)-oxidizing microbes in cold climates, precluding the microbial oxidation of ferrous iron (Kwong et al., 2009); thus ferric iron would not be generated and the oxidation (and acid generation) of sulphide minerals by ferric iron would be limited. Despite this idea, psychrophilic Fe(II)-oxidizing bacteria that are capable of Fe(II) oxidation under low temperature conditions ($T \leq 5°C$) have been reported from numerous mining-impacted and naturally acidic environments in cold climates (Ferroni et al., 1986; Ahonen et al., 1989; Ahonen et al., 1990, Ahonen et al., 1992; Berthelot et al., 1993; Leduc et al., 1993, 1994; Langdahl and Inversen, 1997; Elberling et al., 2000, Johnson et al., 2001; Dopson et al., 2007; Kupka et al., 2007). Furthermore, the oxidation of sulphide minerals is an exothermic reaction and may increase temperature to levels that permit Fe(II)-biooxidation. For example, temperatures on the order of a few hundred degrees have been observed at depth in sulphide deposits elsewhere (Ninteman, 1978; Nordstrom and Bigham, 2000). Thus it is possible that microbial ferrous iron oxidation is occurring in the subsurface environment around the Active Member, creating the positive feedback loop that is responsible for perpetuating the production of ARD.

5.1.2. Surface reactions controlling pH and water composition

Fe-hydrolysis reactions

The pH of the groundwater springs and stream waters in the upper reaches of the creek varied from approximately 3.1 – 3.6 over the entire sampling season (Table 7) and the precipitation of Fe-minerals, identified as a mixture of schwertmannite ($Fe_8O_8(OH)_6(SO_4)$), jarosite ($(K,H_3O)Fe_3(SO_4)_2(OH)_6$) and goethite (α-FeOOH), was

prolific. It was likely that schwertmannite [eq. 9] and jarosite [eq. 10] directly precipitated from these waters, although due to their metastability they recrystallized as goethite [eq. 11] over time (Bigham et al., 1996a,b; Schwertmann and Carlson, 2005).

$$8\ Fe^{3+} + SO_4^{2-} + 14H_2O \leftrightarrow Fe_8O_8(OH)_6(SO_4) + 22\ H^+ \quad [9]$$

$$3\ Fe^{3+} + 2\ SO_4^{2-} + 7\ H_2O \leftrightarrow (H_3O)Fe_3(SO_4)_2(OH)_6 + 5\ H^+ \quad [10]$$

$$Fe_8O_8(OH)_6(SO_4) + 2\ H_2O_{(l)} \leftrightarrow 8\ FeOOH_{(s)} + 2\ H^+ + SO_4^{2-} \quad [11]$$

The precipitation of such Fe minerals generates H^+ [eqs. 9, 10, 11] which maintains low pH conditions in the upper reaches of the creek. With distance downstream, the ARD is diluted by surface waters, causing the pH to increase toward 4 and Fe to become increasingly insoluble. Thus, most of the Fe has precipitated from solution and there is no longer a constant supply of H^+ generated from the precipitation of Fe minerals to keep the pH low. With further dilution from surface waters, the pH increases toward pH 4.4, and Al starts to become insoluble.

Al-hydrolysis reactions

The pH generally rose from 4.4 – 4.9 with increasing distance into the lower reaches of the creek (Table 3) due to dilution from surface waters, H^+ consumption from the dissolution of carbonate basement rocks [eq. 12], and H^+ production from Al-hydrolysis reactions .

Dilution most likely played a role in increasing the pH at the 100 and 120 m locations in the lower reaches, as increased concentrations of Ca that would be associated with carbonate dissolution were not detected at these locations. Further downstream, at the 165 m site, increased concentrations of Ca were observed, suggesting

that carbonate dissolution contributed to the increased pH at this location. Despite the influence of carbonate dissolution, the pH did not increase beyond pH 4.9 in the lower reaches due to the production of H^+ from Al-hydrolysis reactions. Although Al-hydrolysis usually occurs around pH 5.0 (Bigham and Nordstrom, 2000), it has been observed to occur in ARD/AMD waters at pH as low as 4.5 (Sanchez-Espana et al., 2005), which was observed at the XY-ARD stream. The precipitation of Al-hydroxysulfates was prolific in these waters, and can be represented by the hydrolysis of Al to form jurbanite [eq. 13], hydrobasaluminite [eq. 14], and amorphous gibbsite [eq. 15].

$$CaCO_3 + 2H^+ \leftrightarrow Ca^{2+} + H_2CO_3 \quad [12]$$

$$Al^{3+} + SO_4^{2-} + H_2O \leftrightarrow Al(OH)SO_4 + H^+ \quad [13]$$

$$4\,Al^{3+} + SO_4^{2-} + 14\,H_2O \leftrightarrow Al_4(SO_4)(OH)_{10}\text{-}4H_2O + 10\,H^+ \quad [14]$$

$$Al^{3+} + H_2O \leftrightarrow Al(OH)_3 + 3\,H^+ \quad [15]$$

Redox reactions

Given the large pool of ferrous iron in these waters (Table 5), microbial Fe(II)-oxidation was likely occurring. Under acidic conditions (pH < 4), the oxidation of ferrous iron by oxygen is negligible (Singer and Stumm, 1970) and microbial Fe(II)-oxidation [eq. 5] is the dominant mechanism generating ferric iron (Johnson and Hallberg, 2003). Although microbial Fe(II)-oxidation consumes protons, this is counterbalanced by proton generation from the precipitation of Fe(III)-minerals (schwertmannite, jarosite) and thus the pH does not increase.

The precipitation of Fe(III)-minerals in the stream suggests that microbial oxidation was important, yet the proportion of Fe(II) comprising the total Fe pool remains fairly constant and high (60 – 75 % Fe(II)) with distance downstream (Table 5), despite the fact

that the pH increased above 4 (Table 5). Theoretically, as the pH exceeds 4, Fe(II)-oxidation by oxygen should be prevalent (Singer and Stumm, 1970), so it was unclear why such high levels of Fe(II) persist into the lower reaches. Thermodynamic modeling of these waters indicates that Fe(II) should be present at near-zero concentrations in the lower reaches (Figure 5), suggesting that slow reaction kinetics may be responsible for the high levels of Fe(II) that were measured. Photoreduction of ferric iron has been observed to maintain high levels of Fe(II) in ARD/AMD waters (McKnight et al., 2001), although the incident light energy must exceed 7 W/m^2 for this process to occur (Karlsson et al., 1995). At our site, the incident light energy measured at the creek seldom exceeded 7 W/m^2 even on sunny days, suggesting that photoreduction probably did not play a major role in the maintenance of Fe(II) concentrations in the stream. It is most probable that the high concentrations of Fe(II) present in all of the waters sampled were due to a constant influx of Fe(II)-rich groundwaters to the stream.

Sulphide was not detected at any of the sampling locations which precludes the influence of sulphur-based redox reactions on the geochemistry of these waters. Given that intermediate sulfoxyanions such as sulphite (SO_3^{2-}), thiosulfate (S_2O_3) and polythionates ($S_nO_6^{2-}$) are rapidly oxidized by ferric iron or sulphur-oxidizing microbes (Bigham and Nordstrom, 2000), the absence of sulphide in these waters was not unexpected.

5.1.3. Temporal geochemical evolution

The pH at the 0 m groundwater seep was the only location where the pH was observed to increase over the course of the sampling season, from pH 3.1 in July to pH 3.3 in August (Table 7), and elemental concentrations showed a general decrease over

the course of July – August (Table 7 and 8). The decreased concentrations are probably due to increased pH and consequently decreased ability for rock dissolution. The concentrations of some elements decreased more relative to others (Table 7 and 8), as the solubility of some elements (e.g. Pb, Fe) under acidic conditions are more sensitive to changes in pH relative to others (e.g. K, Si, Na). Concentrations of all dissolved constituents fluctuated with rainfall (Figure 8), suggesting that the aquifer feeding these waters was recharged by meteoric precipitation or that dilution from surface runoff had occurred..

The pH at the 10 m groundwater seep was fairly constant from July – August (Table 7) and concentrations of almost all elements increased substantially over time (Table 7 and 8), despite repeated episodes of meteoric precipitation (Figure 8). This suggested that these groundwaters were recharged by the initial spring snowmelt, and toward the end of the summer deep groundwater may have constituted a greater proportion of these waters.

Over the course of the summer, the pH decreased at each sampling site, but still progressively increased with distance downstream (Table 7). The decrease in pH at each site was driven by increased concentrations of Fe and Al over time (Table 7 and 8) due to waning recharge waters, and thus increased H^+ production from increasingly prolific Fe and Al hydrolysis in the upper and lower reaches, respectively. This decrease in pH was associated with changes in speciation (Figures 10 - 15) and mineralogy at some locations, particularly in the lower reaches of the creek. Metal and sulphate concentrations measured in the upper and lower reaches often continued to increase over time despite rainfall, although very heavy rainfall was associated with decreased concentrations for up to a week in some cases (Figure 8), suggesting that the creek hydrology is a mix of ARD

effluent and surface water discharge. Some episodes of rainfall caused metal and sulphate concentrations to increase, likely due to the resuspension of mineral precipitates in the streambed or the dissolution of soluble minerals that precipitated in the subsurface (Ergas et al., 2006; Sarmiento et al., 2009; Butler et al., 2008; Stillings et al., 2008).

5.2. Mineral precipitates

5.2.1. Terraced iron formations

Terraced iron formations (TIFs) have been documented at many locations including the Tintillo River in the Iberian Pyrite Belt (IPB) (Sanchez-Espana et al., 2007), Carnoules Pb-Zn mine, France (Leblanc et al., 1996), Green Valley coal mine, Indiana, U.S.A (Brake et al., 2001a, 2004), and various other locations around the world (Kawano and Tomita, 2001; Murad and Rojik, 2005). Interestingly, TIF-like formations have been frequently documented in ARD in northern climates (Graham and Kelley, 2009; Lawrence et al., 1998; Kumpulainen et al., 2007), and were observed at the XY-deposit.

Appearance and morphology

Terraced iron formations are morphologically similar to calcareous travertine that forms in hot springs or karst environments, in that they are composed of alternating pools and curved ridges that form perpendicular to the flow of water (Leblanc et al., 1996) (Figure 17). Millimetre to metre scale TIFs have been reported, and their morphology is not considered to be size-dependent (Sanchez-Espana et al., 2007). Macroscopically and microscopically, TIFs are composed of thin, hard wavy laminae alternating with soft, thick laminae (Sanchez-Espana et al., 2007; Kumpulainen et al., 2007; Brake et al., 2001a, 2004). These laminations are thought to arise from various processes, although these vary depending on the specific system in which TIFs are observed.

The TIFs at the XY-deposit likely result from seasonal changes in water temperature and flow conditions. The thin and hard laminae may have been produced when the ARD waters were more diluted (i.e. during the freshet) and at a lower temperature (which would enhance Fe solubility), and consequently less mineral precipitation would occur. The thicker laminae were observed to precipitate as freshet-recharge waters waned toward the end of the summer, when metal and sulphate concentrations were higher and water temperatures were warmer. Increased water temperature is known to decrease the solubility of Fe-hydroxysulphate minerals (Butler and Seitz, 2006), which suggests that increased water temperature and increased metal and sulphate concentrations would result in more prolific mineral precipitation.

Terraced iron formations have also been observed to form because of seasonal variations in the resident microbial populations, with changes in geochemical conditions causing the successive growth of algae followed by diatoms (Brake et al., 2004). It has also been suggested that these laminae may reflect a succession of biologically-derived and inorganically-derived structures (Sanchez-Espana et al., 2007), although influence of microbes on TIF formation is not clear in all situations where terraces have been observed.

Formation: organic factors

Abundant populations of green algae (*Euglena mutabilus, Ulothrix* algae), white filamentous bacterial streamers (unidentified), Fe-oxidizing bacteria (*A. ferrooxidans* and *L. ferrooxidans*) and diatoms (*Nitzschia tubicola*) have been observed to be in some way associated with TIFs at numerous locations (Sanchez-Espana et al., 2007; Brake et al., 2001a,b, 2004; Lawrence et al., 1998). Fungal hyphae are often observed in TIFs, and

form a close association with Fe-oxidizing bacteria (Sanchez-Espana et al., 2007). Algae are known to serve as a site for mineral nucleation, provide a carbon source to other microbial communities, and oxygenate the water column which can promote mineral precipitation (Brake et al., 2001a,b, 2004; Lawrence et al., 1998). While seasonally-alternating populations of microbes have been observed to result in the formation of laminated precipitates in TIFs (Brake et al., 2004), in many cases microbes only serve as a site of mineral nucleation and consequently are considered a passive component in TIF formation (Sanchez-Espana et al., 2007). Although TIFs often contain an abundance of organically-derived structures (Sanchez-Espana et al., 2007), whether microbes are actively working to build these structures at any location where they are observed, including the XY-deposit, remains unclear.

A few bacteria-like microbes encrusted with mineral precipitates were observed in some of the TIF and mineral precipitate samples from the XY-deposit (Figure 56), but they were not extremely abundant when compared to other studies that have observed thick, dense accumulations of microbes in TIFs (Leblanc et al., 1996; Brake et al., 2004; Sanchez-Espana et al., 2007). In the aluminous terrace-like precipitates collected at the XY-deposit, fungal hyphae (Figure 67) and eukaryotic cells (Figure 60) were occasionally observed, although bacteria were not (the microbes were not subject to more refined identification). It is known that microbes in ARD environments often go undetected by microscopy as they become completed encrusted in mineral precipitates (Webster et al. 1998), which may explain their low abundance in these mineral precipitates. However, organic carbon was not detected in these precipitates (Appendix 7), which may suggest that microbes did not play a role in the formation of these minerals (Eneroth and Koch,

2004). The REE distribution patterns provide evidence that microbially-mediated precipitation did occur, however it was limited to the aluminous terrace-like precipitates (Figure 42 E,F), as the TIFs found in the upper reaches of the creek showed a REE distribution characteristic of inorganically-mediated precipitation (Figure 42 A - D).

Although cells were microscopically observed in the TIFs and aluminous terrace-like precipitates from the XY-deposit, there was little field evidence suggesting the presence of microbial life. Occasionally patches of orange thin films and sheeny-microbial exudates (commonly associated with Fe-oxidizing bacteria (D.Fortin, personal comm.)) were observed in areas with low-flowing or stagnant water (Figure 23). Similar thin orange films have been identified at other locations with TIFs(Sanchez Espana et al., 2006, 2007; Kawano and Tomita, 2001) and were thought to have formed due to Fe precipitation around neustonic microbes or because of evaporatively-induced oversaturation at the water surface (Sanchez-Espana et al., 2007). The presence of microbial exudates at our site may suggest that these films were of microbial origin, however, it was likely that a combination of evaporative-induced saturation and microbial processes were responsible for the formation of these films. These schwertmannite films may also contribute to the formation of TIFs, as they have been observed to thicken and eventually sink to the bottom of the water column (Sanchez-Espana et al., 2007). Further evidence for microbial involvement in TIF formation includes the formation of biogenic gas blisters on the precipitates (Figure 25), which were observed in the upper reaches of the creek at the XY-deposit and elsewhere (Fernandez-Remolar et al., 2005).

It was at one time thought that the cold temperatures encountered in northern climates impacted by ARD/AMD would preclude microbial Fe(II)-oxidation. Since then,

numerous strains of psychrotolerant Fe(II)-oxidizing bacteria (*A. ferrooxidans*) have been reported from such environments (Ferroni et al., 1986; Ahonen et al., 1989; Ahonen et al., 1990, Ahonen et al., 1992; Berthelot et al., 1993; Leduc et al., 1993, 1994; Langdahl and Inversen, 1997; Elberling et al., 2000, Johnson et al., 2001; Dopson et al., 2007; Kupka et al., 2007). The rates at which they oxidize Fe(II) are much slower than what is encountered under warmer conditions, which may explain the apparent paucity of microbial life that was observed in the ARD from the XY-deposit. However, given that Fe(II)-oxidizing bacteria have been reported at numerous ARD streams in cold climates, and that algae such as *E. mutabilis*, have been observed to be growing in TIFs at temperatures as low as 0 °C under thin layers of ice at other locations (Brake et al., 2001a), temperature may not be the primary factor limiting the presence of microbes in this system. Alternatively, since the TIFs encountered here are largely of inorganic origin abundant microbial populations are not required for their formation and hence they are not prevalent in this system. Furthermore, it is well known that microbes do not control mineralization from AMD/ARD waters, as mineralization occurs despite physiological conditions between cells (Ferris et al., 1989) and instead is likely controlled by geochemical parameters such as pH, sulphate concentrations and alkalinity (Bigham et al., 1996a; Bigham and Nordstrom, 2000).

Formation: inorganic factors

Given the REE distribution patterns for the TIFs in the upper reaches of the creek and the relatively limited extent microbial life observed in the field and microscopically in mineral precipitate samples, it is likely that these TIFs were formed inorganically. The few microbes that were observed may simply be passive components, having no direct

involvement in TIF formation. For example, calcareous travertine is known to form largely due to inorganic processes, and although cyanobacteria may be present in these formations, they have been attributed to only 10 % of the total formation of these structures (Goulbic, 1973).

If TIFs are formed inorganically, their formation may be a result of a coupling between precipitation rate and the hydrodynamics of the water course (Sanchez-Espana et al., 2007). Furthermore, growth patterns similar to those observed in TIFs have been modeled based upon diffusion-limited aggregation and sedimentation of precipitated minerals and microbial mats (Grotzinger and Rothman 1996; Grotzinger and Knoll, 1999). The presence of sticks, leaves and pepples cemented within TIFs is not uncommon (Kumpulainen et al., 2007; Leblanc et al., 1996; Fernandez-Remolar et al., 2005) and was observed at the XY-deposit. Frequently, small mounds of precipitate were observed to coalesce around pieces of talus or organic detritus in the stream bed, and given the extremely high saturation of these waters with respect to Fe-minerals (Figure 49), it is likely that any obstacle within the stream can act as a site of mineral nucleation (Sanchez-Espana et al., 2007). Furthermore, TIFs composed of different minerals have been documented; rozenite ($Fe(II)SO_4$-$4H_2O$) TIF-like precipitates have been observed to be evaporatively-precipitating from extremely acidic waters (pH < 0.5) at the San Telmo mine in the IPB (Sanchez-Espana, 2005), and Al-rich TIF-like precipitates have been reported from the Green Valley coal mine, Indiana, U.S.A. (Brake et al., 2001a). Similar aluminum-rich precipitates with a terrace-like morphology were observed to form in the ARD creek at the XY-deposit under low flow conditions. The fact that these formations are

morphologically identical to TIFs yet bear different mineralogy suggests that microbial-mediation is not a prerequisite for TIF formation.

5.2.2. Mineralogy

Groundwater seeps and upper reaches

A mixture of jarosite, goethite, schwertmannite and barite (Figure 43) was found to be precipitating at the 10 m groundwater seep in the form of a maroon-coloured hardpan, while the TIFs collected downstream (18 m) were a mixture of schwertmannite, goethite, and occasionally jarosite (Figure 44). Schwertmannite and jarosite were likely the initial secondary minerals formed, as goethite is produced in AMD/ARD waters by the recrystallization of schwertmannite and jarosite (Scroth and Parnell, 2005). The mineralogy of the precipitates at the 0 m groundwater seep was not investigated as the acidic pH of these waters (pH 3.3) resulted in minimal precipitation. However, given the similar geochemical conditions at both groundwater seeps (Table 3), a mixture of schwertmannite, jarosite, and goethite likely comprised the mineral precipitates at 0 m. The occasional presence of barite was not surprising since thermodynamic modeling showed barite to be either oversaturated or at equilibrium with these waters (Appendix 9).

The thin laminations in the TIFs from the XY-deposit are composed of schwertmannite and goethite, while the thicker laminations are composed of a mixture of goethite, schwertmannite, and sometimes jarosite, which is typical of TIFs observed elsewhere (Sanchez-Espana et al., 2007; Kumpulainen et al., 2007; Graham and Kelley, 2009; Fernandez-Remolar et al., 2005). However, the thin laminae in TIFs are almost always exclusively schwertmannite, although both goethite and schwertmannite were detected in the thin laminae of the TIFs from the XY-deposit (Figure 44), owing to the

aging/recrystallization of our samples prior to their analysis. Samples were analyzed for their mineralogy approximately one year after their collection due to logistical problems, and thus partial recrystallization of schwertmannite to goethite would be expected (BIgham et al., 1996; Schwertmann and Carlson, 2005). Although the thin laminae did not show crystal morphology similar to schwertmannite (Figure 51 and 53) it has been reported that this morphology is often not apparent in crusts of schwertmannite (Bigham and Nordstrom, 2000). The mineralogical similarity of the laminae in the TIFs suggests that there were no major seasonal changes in TIF mineralogy, which is in line with what has been reported from other studies (Sanchez-Espana et al., 2007; Kumpulainen et al., 2007; Graham and Kelley, 2009; Fernandez-Remolar et al., 2005) Aluminum hydroxysulphates do not precipitate under acidic conditions since Al is conservative at low pH (Bigham and Nordstrom, 2000), and thus they were not detected at the groundwater seeps or in the upper reaches of the creek (pH 3.5).

Lower reaches

As the pH increased toward 4.4 with distance downstream (100 m), the precipitates took on a more amorphous character and were determined to be a mixture of schwertmannite (minor amounts of goethite) (Figure 46) and an unidentified Al-hydroxysulphate phase (Table 10). This unidentified Al-hydroxysulphate phase may have been jurbanite, as it had a low Al:S molar ratio (Table 10 and 11). Jurbanite was also determined to be oversaturated in these waters (Figure 50). However, jurbanite was not detected by XRD (Figure 46), which suggests that the unidentified Al-phase may have been an X-ray amorphous Al-sulphate precipitate (with a low Al:S molar ratio), instead of jurbanite.

Further into the lower reaches (pH 4.7, 120 m) jurbanite was detected by XRD (Figure 47), although the Al:S molar ratios of these precipitates was very high (Table 10) and did not correspond to jurbanite (Table 11). This suggested that a mineral(s) with a higher Al:S molar ratio (hydrobasaluminite or gibbsite) was also present, which is in line with the mineralogy that has been reported for some ARD/AMD precipitates (Pu et al., 2010). If jurbanite was present (which XRD suggested), it may have only been present in small quantities, but was detected by XRD since it was the most crystalline phase in the sample. Although jurbanite has often been reported to form in moderately acidic Al-rich AMD/ARD waters (Lee et al., 2002; Pu et al., 2010; Karathanasis et al., 1988; Sullivan et al., 1988; van Breeman, 1973), it is very rare, and there are only two confirmed occurrences of jurbanite worldwide (Anthony and McLean, 1976; Sabelli, 1984). Furthermore, its formation in ARD/AMD environments has been contested since it is very soluble (Bigham and Nordstrom, 2000). Although the Al:S molar ratio of these precipitates (120 m) suggested that gibbsite may have been present (Table 10 and 11), it has been suggested that the formation of gibbsite does not occur in AMD/ARD due to high concentrations of sulphate (Bigham and Nordstrom, 2000). Furthermore, gibbsite precipitation in AMD/ARD environments has been noted to occur only under neutral pH conditions (Sanchez-Espana et al., 2005). Thus, it was unclear why such high Al:S molar ratios (suggesting the presence of gibbsite) were detected. Hydrobasaluminite is known to equilibrate with gibbsite over time (Nordstrom and Ball, 1986; Nordstrom, 1982), which may explain the high Al:S molar ratios that are observed, although this reaction is very slow at low temperatures (Nordstrom, 1982). Concurrently, the high Al:S molar ratio may

arise from the rapid rate of Al-precipitation that has been shown to occur at pH > 4.6 (Nordstrom and Ball, 1986; Munk et al., 2002).

Overall, these white-coloured precipitates displayed a striking similarity to mineralized cells (Figure 60), which is in line with the REE distribution for these precipitates (Figure 42) and may suggest that microbially-mediated precipitation had occurred. It is known that Al precipitation is enhanced by the presence of microbes (Urrutia and Beveridge, 1995) which probably contributed to the formation of these precipitates (Nordstrom and Bigham, 2000). The freezing and thawing of cells, which would be seasonally encountered here, may enhance their ability to adsorb Al (Hard et al., 1999) due to cell lysis, and may also be contributing to the high levels of Al that were observed in these precipitates.

The mineralogy at pH 4.9 (165 m) was very similar to that at pH 4.4 (100 m); although the pH at 165 m was too high for the formation of jurbanite (Nordsdtrom, 1982) it was detected by XRD (Figure 48). This suggests that an amorphous Al-sulphate (with an XRD spectrum similar to jurbanite) was the dominant phase forming here. EDS spot-analyses of the precipitates in the lower reaches showed the presence of Si, Ca and Mg (Figure 69). Calcium and Mg probably result from the precipitation of gypsum ($CaSO_4$-$2H_2O$) and dolomite ($Ca,Mg(CO_3)$), which have been observed to be mineralogical components of Al-hydroxysulphates forming in similar settings (Kim et al., 2002; Lu et al., 2010). However, thermodynamic modeling showed them to be undersaturated in these waters (Appendix 9), so if they were present they were likely minor constituents of these precipitates. Aluminum-hydroxysulphates are known to have a very high affinity for Si (Bigham and Nordstrom, 2000), explaining why Si was detected in these samples.

Given the non-laminated and incohesive nature of the precipitates forming at pH 4.4 and pH 4.9, they are likely seasonally transient and are removed from the stream bed during the spring when flow rates are high. Furthermore, white precipitates were not found in the lower reaches of the creek (165 m) in June (Figure 22), providing evidence toward their transient nature.

Alternating white and red-coloured laminae were observed at the waterfall at 120 m (pH 4.7), with white-coloured precipitates at the surface, underlain by successive red, orange, and white-coloured laminae (Figure 21). Although similar structures have been observed at other locations, they were not subject to intensive investigation (Hammarstrom et al., 2003). The white, orange, and red-coloured laminations did not appear to be preserved elsewhere in the lower reaches of the creek, as the waterfall likely protected them from erosion during periods of high flow. The presence of these laminae indicated that at some point the geochemical and hydrological conditions of the creek were different from the conditions encountered during the summer, when the white-coloured precipitates were collected. It is possible that the orange and red-coloured precipitates formed during the spring, winter or fall (i.e. under different flow conditions)since we know the white-coloured precipitates formed in the summer. Alternatively, this waterfall has formed directly over a fault that lies above shallow subsurface Zn-Pb mineralization (Figure 4), and it is possible that waters that have interacted with this area of mineralization emanate as a spring at this waterfall. If this spring were the dominant, although discrete, source of water to this area of the creek during a certain time of the year (fall, winter or spring), it could explain the laminated nature of these precipitates.

Since the time and geochemical conditions under which these precipitates formed were unknown, the interpretation of their mineralogy was difficult as the results could not be verified by thermodynamic modeling. The orange-coloured laminae appeared to be a mixture of hydrobasaluminite and either jurbanite or another Al-suphate phase with a low Al:S molar ratio (Table 10), but their mineralogy could not be confirmed by XRD since only a small quantity of sample was collected. Although orange-coloured precipitates are known to form during the spring in the lower reaches of the creek, they do not have the same mineralogy as the orange-coloured laminae collected here. The red-coloured laminations were composed of schwertmannite (Figure 47), which has been observed elsewhere (Hammarstrom et al., 2003), although their bulk geochemistry suggested that they may have also contained ferrihydrite (Table 10). Ferrihydrite was not detected by XRD (Figure 47), although it is poorly ordered and could have been masked by the schwertmannite spectrum. Ferrihydrite and schwertmannite are often mutually exclusive since they are favoured to precipitate under near-neutral and acidic pH conditions (Bigham et al., 1996a,b), respectively, so their co-occurrence here could be debatable. However, TIF-like crusts of schwertmannite have been observed to form under near-neutral pH (Kumpulainen et al., 2007), conditions that could also be conducive to the formation of ferrihydrite. Further evidence for the formation of this precipitate under near-neutral pH conditions is the presence of Al-hydroxysulphate phases in these laminae, which require at least pH 4.5 conditions to form (Sanchez-Espana et al., 2005; Bigham and Nordstrom, 2000). Additionally, these samples contained anomalous concentrations of Zn, Cd, Cu and Ni (Figures 33, 35, 37), which may indicate that extensive adsorption occurred during the precipitation of these laminae. It is known that the adsorption of these elements occurs at

near-neutral pH (Dzombak and Morel, 1990), and thus this could provide more evidence for the pH conditions under which these laminae formed.

The orange-coloured precipitates that formed during the spring in the lower reaches of the creek were identified as a mixture of goethite, barite, jarosite and schwertmannite (Figure 48), although these results could not be confirmed geochemically (molar ratios) or thermodynamically because only a small quantity of sample could be collected. X-ray diffraction shows relatively few peaks for schwertmannite in this sample; however, it is possible that they are "masked" by the presence of highly crystalline minerals such as barite and jarosite, which has been observed elsewhere (Bigham and Nordstrom, 2000). Furthermore, microscopic examination showed these precipitates to be highly amorphous (Figure 67), and if jarosite and barite were present as major mineral phases the precipitatewould likely not have appeared to be so amorphous. Therefore, it is likely that jarosite and barite represented only minor components of this sample.

5.2.3. Trace element geochemistry

Groundwater seeps and upper reaches

The mineral precipitate samples collected at the groundwater seeps and in the upper reaches of the creek showed a sequence of K_d values where Pb > U > Cu > Zn > Cd > Ni, although the order for Zn and Cd was occasionally switched (Appendix 10). This is in general agreement with the accepted K_d values for ferric-oxyhydroxides (Dzombak and Morel, 1990), although, the accepted sequence does not include values for U. Where K_d values for U have been reported, they generally occur between Cu and Zn (Sanchez-Espana et al., 2006), although we observed U to have a stronger tendency to partition to the solid phase relative to Cu at all of the sites sampled (Appendix 10). Cadmium has

been shown to have a similar K_d to Zn (Lee et al., 2002), which is in line with what we observed for our samples (Appendix 10).

A high degree of Pb partitioning between the solid and aqueous phase in TIFs has been documented (Sanchez-Espana et al., 2007; Lawrence et al., 1998), and was in line with what we observed in the TIFs at the XY-deposit (Figure 28). Lead may have been accumulating in our samples due to its precipitation as plumbojarosite (Hochella et al., 1999); although this mineral was determined to be oversaturated in these waters (Figure 49), it was not detected by XRD (Figure 44), therefore its presence was likely minor. Goethite is known to adsorb substantial quantities of sulphate under low pH conditions (Brady et al., 1986), and Pb-SO_4 ternary complexes have been observed to form at the goethite surface under acidic conditions (Weesner and Bleam, 1998) which could also account for the presence of Pb in these precipitates. Lead speciation in the upper reaches was comprised by mostly $PbSO_4$ and Pb^{2+}, with decreasing amounts of $Pb(SO_4)_2^{2-}$ with decreasing sulphate concentrations (Figure 14). The adsorption of $Pb(SO_4)_2^{2-}$ to Fe-hydroxysulphates has been observed under low pH conditions (Sanchez-Espana et al., 2006) and thus may also have contributed to the accumulation of Pb in these precipitates. The high degree of U partitioning (relative to what is often observed) may have been due to the formation of U(VI)-surface complexes with schwertmannite and goethite, which has been observed elsewhere (Walter et al., 2003). However, the overall content of U in these precipitates was relatively low so this process was probably not extensive.

These precipitates did not show a strong tendency to accumulate Zn (Figure 27), Cd (Figure 30), Ni (Figure 29), Cu (Figure 29) and U (Figure 31) relative to the precipitates that formed in the lower reaches of the creek, which was not unexpected since these

elements do not show extensive adsorption at low pH (Dzombak and Morel, 1990).. However, EDS spot-analyses indicated that some of the schwertmannite crystals in our samples were rich in Zn and Cu (Figure 52) which has been observed to occur when schwertmannite formation is biotically-mediated (Webster et al., 1998), although REE distributions suggested that mineral precipitation was not microbially-mediated (Figure 42), so the reason for high levels of Zn and Cu was not clear. These anomalies were not detected in bulk-geochemical analysis (Appendix 5), reflecting the heterogeneous nature of ARD precipitates.

Overall, there were few variations in the geochemistry of the different laminae of the TIFs, which is consistent with observations made for TIFs at other locations (Leblanc et al., 1996; Kumpulainen et al., 2007).

Lower reaches

The precipitates that formed in the lower reaches showed a similar K_d distribution to the precipitates in the upper reaches (Pb > U > Cu > Zn > Cd > Ni), although the K_d for U exceeded that for Pb at 120 m (pH 4.7) (Appendix 10). Similar to the upper reaches, the K_d for Zn and Cd were often switched for the precipitates in the lower reaches (Appendix 10). The K_d sequence reported for our Al-hydroxysulphate precipitates generally coincided with what has been reported elsewhere (Munk et al., 2002; Lee et al., 2002; Kinniburgh et al., 1976; Sanchez-Espana et al., 2006).

In these waters, Zn was present mostly as $ZnSO_4$ and Zn^{2+}, with only minor contributions from $Zn(SO_4)_2^{2-}$ (Figure 12). Cadmium showed a similar distribution; however, a greater proportion of the Cd was present as $Cd(SO_4)_2^{2-}$ (Figure 12). Nickel and Cu were present as their free divalent ions and uncharged sulphate complexes (Figure

13), while U was mainly present as UO_2SO_4, with lesser amounts of UO_2^{2+} and $UO_2(SO_4)_2^{2-}$ (Figure 15). Thermodynamic modeling showed minerals containing Zn, Cd, Ni, Cu and U to be well below saturation in these waters (Appendix 9), which suggested that their accumulation in these precipitates was likely a result of adsorptive processes.

The K_d values for Zn, Ni, Cu and Cd were anomalously high at pH 4.7 when compared to pH 4.9 (Figures 27, 29, 30), and given that increased adsorption for Zn, Cu, Ni and Cd should occur with increasing pH (5 – 6.5) (Kinniburgh and Jackson, 1981; Lee et al., 2002), it was expected that the precipitates forming at pH 4.9 would have higher K_d values than those forming at pH 4.7. The high level of partitioning observed at this location (pH 4.7) can be explained by an increased adsorption affinity due to an increased rate of adsorbent formation (Dzombak and Morel, 1990) as the formation of Al-hydroxysulphates has been shown to be very rapid at pH > 4.6 (Nordstrom and Ball, 1986; Munk et al., 2002), or, due to adsorption onto microbes, as the formation of these precipitates was determined to be microbially-mediated.

Uranium also showed a very high K_d value at pH 4.7 relative to pH 4.4 and 4.9 (Figure 31), and the adsorption of U to Al-oxyhydroxides has been shown to be very extensive around pH 4.5 (Luo et al., 2009), probably due to the formation of a surface complex with UO_2^{2+} and the Al-mineral (Gu et al., 2003). Given the speciation of U in these waters (Figure 15), it is possible that adsorption had occurred by this mechanism.

The concentration of Si in the precipitates increased with increasing pH (Figure 40), and was likely a reflection of the high affinity of Al and SO_4 for Si (Bigham and Nordstrom, 2000). Interestingly, the K_d values for Pb were highest in the precipitates forming at pH 4.9 (Figure 28), which was unexpected since Pb adsorption is known to occur at lower pH

(Dzombak and Morel, 1990; Munk et al., 2002) and thus most of the Pb would have been removed from the water column upstream from this location. The high K_d value for Pb in these precipitates may have been observed due to an addition of Pb to these waters somewhere between the 120 (pH 4.7) and 165 m (pH 4.9) sites. Waters draining into the creek in this area do not show high concentrations of Pb (Appendix 1), suggesting that an influx of groundwater through the hyporeic zone may have been the source of Pb to these precipitates. Given the sparingly soluble nature of Pb under moderately acidic pH conditions, Pb would have partitioned to the solid phase almost immediately once it entered the stream, resulting in the greater K_d values observed at pH 4.9 relative to pH 4.7.

Red and orange-coloured laminations in Al-rich terraces

It was clear that the red-coloured laminae from the waterfall at 120 m (pH 4.7) contained anomalous concentrations of Zn, Ni, Cu and Cd relative to the other laminae in this sample, and all of the other mineral precipitates in the creek (Figures 33, 35, 37). EDS spot-analysis revealed the presence of Zn in these samples (Figure 64), although EDS-detectable levels of Cd, Ni and Cu were not observed. The orange laminations showed a lower total concentration of Zn, Ni, Cu and Cd relative to both the red and white-coloured laminations (Figures 33, 35, 37), but overall the orange laminations contain higher concentrations of Zn, Cd, Ni and Cu when compared to mineral precipitates collected at other locations along the creek (Figures 33, 35, 37). The reason for the anomalous concentrations in the red (and orange)-coloured laminae can only be speculative given the paucity of geochemical data for the waters from which these precipitates were derived. If these precipitates had formed under near-neutral conditions (which their mineralogy may

suggest) it is possible that the accumulation of Zn, Cd, Ni and Cu is due to the precipitation of amorphous Zn, Cd, Ni and Cu oxides (Sanchez-Espana et al., 2005). Concurrently, these elements become less conservative with increasing pH (Acero et al., 2006), and consequently near-neutral pH conditions would be conducive to extensive adsorptive processes (Dzombak and Morel, 1990). Copper and Zn are known to form ternary complexes with the schwertmannite and ferrihydrite surfaces (Swedlund and Webster, 2001), which could explain the high concentrations of Cu and Zn in these precipitates. Moreover, the red-coloured laminae were composed of a mixture of Fe and Al-minerals, which when present together have been shown to enhance the adsorption of Zn (Anderson and Benjamin, 1990). Furthermore, if aqueous concentrations were anomalously high at the time when these precipitates formed, adsorption edges would be shifted to lower pH (Webster et al., 1998), and thus near-neutral pH conditions may not have been necessary to facilitate the accumulation of such large quantities of Zn, Cd, Ni and Cu observed in these precipitates.

5.2.4. Mineralogical control on the accumulation of trace elements

Nickel, Cu, U and Si generally showed a strong negative correlation with the Fe:S molar ratio, while Cd had a weak negative correlation, suggesting that with increased Fe:S molar ratios there are lower concentrations of Ni, Cu, Cd, U and Si in the precipitates (Figures 35, 37, 39, 40). The only exception to this trend was the red-coloured laminae from 120 m which contained anomalous concentrations of Ni, Cu and Cd (Figure 35 and 37). The strong negative correlation between Ni, Cu and Zn and the Fe:S molar ratio was in line with other studies, as schwertmannite (Fe:S = 4 – 8) has been observed to be a more effective adsorbent than goethite (Fe:S = very high) for these elements at low pH

(Sidenko and Sherrif, 2005), despite the fact that both can sequester these trace elements. Cadmium may have shown a weaker correlation as it is known to form ternary complexes with the goethite surface (Penilla et al., 2005; Webster et al., 1998), resulting in higher concentrations of Cd found at higher Fe:S molar ratios. Alternatively, these negative correlations may have resulted from the fact that in general, the precipitates with the highest Fe:S molar ratios were found under the lowest pH conditions (Table 10), where adsorption and precipitation would be minimal due to the low pH and consequent conservative speciation of Ni, Cu, U, Si and Cd (Acero et al., 2006). Thus, the observed correlation may actually have been a function of pH and not mineralogy. Similarly, other studies documenting the geochemistry and mineralogy of TIFs have concluded that variations in pH and geochemistry controlled the accumulation of trace elements in these precipitates rather than their mineralogy (Kumpulainen et al., 2007).

Nickel, Cu, U, Si and Cd all showed strong positive correlations with the Al:S molar ratios, while Zn showed only a weak positive correlation with Al:S molar ratios, suggesting that with increased Al:S molar ratios, there was an increased accumulation of Ni, Cu, Cd, U and Si within the mineral precipitates (Figures 36, 37, 39, 40). The correlations for U and Si were expected, as U is known to partition very strongly to Al-hydroxysulphates (Luo et al., 2009) and Si has a very high affinity for Al and SO_4 (Bigham and Nordstrom, 2000). Although elevated levels of Ni, Cu and Cd have been observed in these and other Al-rich precipitates (Lee et al., 2002; Sanchez-Espana, 2006; Munk et al., 2002), the adsorption mechanisms governing their accumulation in Al-hydroxysulphates is poorly documented in the literature.

The observed correlations may be somewhat spurious as Al:S molar ratios

increased with increasing pH, and Ni, Cu, Cd and U also become less conservative and are more prone to adsorption and precipitation with increasing pH (Dzombak and Morel, 1990; Lee et al., 2002). Furthermore, a high degree of adsorption of Ni, Cu, and Cd was observed to occur in the precipitates forming at pH 4.7 (Table 29 and 30), probably due to the rapid precipitation of Al-hydroxysulphates under these conditions and consequently enhanced adsorption of these elements. These precipitates had the highest Al:S molar ratio (Table 10), which may explain the good correlation between Ni, Cu, and Cd and the Al:S molar ratio of the precipitates. Thus, the correlation between these elements and Al:S may have actually been a function of pH and not the mineralogy of these precipitates.

Lead and Ba variability could not be explained by the Fe:S or Al:S molar ratios, while Zn variability could not be explained by the Fe:S molar ratios. This suggested that the mineralogy of the Fe-rich precipitates did not control the accumulation of Zn, Ba or Pb within the mineral precipitates, while the mineralogy of the Al-rich precipitates did not govern the accumulation of Ba and Pb. Given that Pb adsorption is known to be most extensive at low pH (Dzomback and Morel, 1990; Lee et al., 2002), the insignificant correlation between Pb and Fe:S was surprising. It probably resulted from the high Pb concentration in the Al-hydroxysulphate precipitates forming at pH 4.9 (Figure 28), due to an addition of Pb to the stream waters. Adsorption studies do not add additional Pb to a solution once it has already been adsorbed, resulting in the preferred adsorption of Pb at low pH being observed. Barium solubility is controlled by sulphate concentrations, as barite is known to be sparingly soluble and precipitate in AMD/ARD waters (Canovas et al., 2007). Additionally, thermodynamic modeling showed that barite was at equilibrium with these waters (Appendix 9) and it was often detected by XRD in precipitates that

formed under a range of pH conditions (Figures 43 and 44, Appendix 8). Similarly, Pb is highly insoluble and can precipitate as anglesite (Canovas et al., 2007), although this mineral was determined to be undersaturated in all of the water sampled (Appendix 9) suggesting that it did not govern Pb solubility. Thus, it appears that a factor other than mineralogy, like concentration or pH, governed the accumulation of Pb and Ba in the mineral precipitates.

5.3. Mineral exploration applications

5.3.1. Geochemical signatures of the ore body

Waters

It is known that waters interacting with mineral deposits can retain geochemical signatures of the ore body (Seal et al., 2002; Hammarstrom and Seal, 2003; Desbarats and Dirom, 2007). In general, the Cd/Zn ratios found in the Active Member (Cd/Zn = 3.0E-03) (Goodfellow et al., 1983a) were preserved in the surface waters of the ARD stream (Table 12). The 0 and 10 m groundwater sites, however, show respectively lower and higher Cd/Zn ratios when compared to those found in the Active Member (Table 12). The variations in the Cd/Zn ratio may have resulted from either an addition of Zn to these waters, possibly through weathering of the regolith, which is known to be rich in Zn (Goodfellow et al., 1983a). Concurrently, if the subsurface dissolution of sphalerite was incongruent, the Cd/Zn molar ratio of the ore deposit would be modified, which could explain the variations in the ratios observed here. The Cd/Zn molar ratios in the waters in the upper and lower reaches of the creek mirror those of the ore body (Table 12), suggesting that the primary source of Zn and Cd to the creek may have been the Active Member. Although Cd showed a slightly greater tendency when compared to Zn to be

adsorbed to the solid phase (Appendix 10), the Cd/Zn ratio in these waters remained fairly constant with distance (Table 12), likely due to the conservative nature of these elements at low pH.

The Pb/(Pb+Zn) ratios of these waters (ranging from 10^{-5} to 10^{-6}) (Table 12) were much lower than those found in the Active Member (0.2 to 0.8) (Goodfellow et al., 1983a), which reflects the sparingly soluble nature of Pb in the surface environment.

Mineral precipitates

The Cd/Zn ratios in the mineral precipitates were highly variable (Table 13), although generally the mineral precipitates with a Cd/Zn ratio closest to that for the Active Member are those that precipitated at low pH (Table 13). The Cd/Zn ratio of the mineral precipitates will vary depending on the tendency of Cd and Zn to adsorb to the precipitates, which we observed to vary with pH (Figures 27 and 30). Although the adsorption of Cd and Zn to mineral precipitates is known to be highly sensitive to pH (Dzombak and Morel, 1990; Lee et al., 2002), there was no significant relationship between the Cd/Zn molar ratio and the pH at which the mineral precipitates formed.

The Pb/(Pb+Zn) ratio of the Active Member were preserved most in the precipitates forming at low pH (Table 13), as Pb becomes increasingly insoluble with increasing pH. The precipitates at 120 m showed a Pb/(Pb+Zn) ratio in line with that for the Active Member (Table 13), probably due to the enhanced adsorption of trace elements that was observed and the low solubility of Pb at under these pH conditions, combined with the proximity of a fault that may be draining waters from shallow subsurface Zn-Pb mineralization (Figure 4). With increased pH, the Pb/(Pb+Zn) ratio of the mineral precipitates deviated from that of the Active Member (Table 13), since Zn is conservative

over a wider range of pH relative to Pb, resulting in generally lower Pb/(Pb+Zn) ratios with increased pH. However, a significant relationship between pH and the Pb/(Pb+Zn) ratios in the mineral precipitates was not observed.

5.3.2. XY-ARD vs. shale ARD

Cd/Zn and Pb/(Pb+Zn) molar ratios

Acid rock drainage was observed to be emanating across the valley where there is no known Zn-Pb mineralization, although shales are common (Figure 2). The Cd/Zn molar ratios from the waters and mineral precipitates collected in the stream likely draining the shales (Table 14) were a few orders of magnitude higher in relation to those in the waters from the XY-drainage (Table 12 and 13) since Cd is largely concentrated in the Active Member (Goodfellow et al., 1983a). The Cd/Zn molar ratios for the waters were found to be significantly different between the two streams, although significant differences were not detected in these ratios in the mineral precipitates, since Cd and Zn behave conservatively at low pH. The Pb/(Pb+Zn) molar ratios for the waters that are likely draining the XY-deposit were significantly lower (Table 12) than those in the shale drainage (Table 14), since the waters from the XY-deposit mineralization contained much more Zn relative to these waters (Appendix 1). Although the Pb/(Pb+Zn) molar ratios in the mineral precipitates from the shale drainage did not coincide with those of the Active Member (Table 14), they were not significantly different compared to the Pb/(Pb+Zn) ratios in the mineral precipitates forming in the waters draining the XY-deposit, due to the sparingly soluble nature of Pb in surface environments.

Major and trace element geochemistry

The waters draining the XY-deposit showed significantly greater concentrations of Na, K, Ca, Zn, Rb, Sr, Cd and Tl, while the shale drainage had significantly greater concentrations of Cr and Ag (Table 16). The higher concentrations of Na, K, Ca, Rb and Sr probably resulted from extensive weathering of carbonate and silicate laminations that are found within the Active Member. Zinc and Cd concentrations were much higher in the waters from the XY-deposit (Table 16) due to the presence of sphalerite in the Active Member, which shows extensive Cd substitution for Zn (Morganti, 1979). Shales are commonly enriched in Cr and Ag (Vine and Tourtelot, 1970), which may explain the elevated concentrations observed in the waters draining the shales when compared to the XY-drainage.

The mineral precipitates forming in the waters draining the XY-deposit showed significantly greater concentrations of Al, Si, Ca, Cr, Zn, Sr, Y, Cd, Ba, Pb, and all of the REEs, while the mineral precipitates from the shale drainage showed significantly higher concentrations in P, Ga, As, Mo, Ag, Sb and Th (Table 17). The greater concentrations of Al, Si, Ca, Zn, Sr, Cd, Ba and Pb in the mineral precipitates at the XY-drainage reflect the presence of the Active Member and the enhanced weathering of silicates and carbonates present in the regolith. Given the higher concentrations of these elements in the XY-drainage, it was not surprising that their concentrations were higher in the mineral precipitates forming in this stream. The zonation of Y and the REEs has not been documented for the XY-deposit, so it was difficult to attribute the concentrations observed here to water-rock interactions with certain strata.

Significantly elevated concentrations of Ba and Pb were noted for the mineral

precipitates at the XY-drainage relative to the shale drainage (Table 17), although significant differences in aqueous concentrations were not detected between the two streams (Table 16). This was due to the low solubility of Ba and Pb, which buffers their aqueous concentrations around the same level in both streams.

The shale drainage has mineral precipitates that are significantly enriched in As, Mo, Sb, Ag, P, Ga and Th relative to the mineral precipitates forming in the waters draining the XY-deposit (Table 17). The higher concentration of Ag is not surprising, as this element was also elevated in these waters relative to those from the XY-drainage (Table 16). The shales are known to be rich in As, Mo, and Sb (Goodfellow et al., 1983a), which could explain the greater concentrations observed in the mineral precipitates. The elevated concentrations of As, Mo and Sb can be explained by the presence of a mono-minerallic schwertmannite mineral precipitate in this stream (Appendix 5), relative to the schwertmannite-goethite mixtures in the XY-drainage. Arsenic, Mo and Sb commonly form oxyanions at low pH (Stumm and Morgan, 1996) and schwertmannite is known to strongly adsorb oxyanions under these conditions (Regenspurg and Peiffer, 2005). Thus, elevated concentrations of As, Mo and Sb in the precipitates (but not the waters) from the shale drainage may have been a function of mineral precipitate mineralogy and not water-rock interactions. However, we have shown that trace element concentrations in the mineral precipitates were generally a function of the prevailing geochemical conditions and pH, rather than mineral precipitate mineralogy, so this may have been an exception to this general rule. Chromium is also known to strongly adsorb (as CrO_4^{2-}) to schwertmannite at low pH (Regenspurg and Peiffer, 2005), although concentrations of Cr were higher in the precipitates at the XY-drainage (Table 17) probably due to the higher concentrations

observed in those waters (Table 16). The higher concentration of P could have been due to weathering of the phosphatic chert unit (hanging wall) or due to the greater density of vegetation observed in the vicinity of these waters relative to the Zn-Pb drainage. Reasons for the elevated concentrations of Ga and Th in these precipitates were unclear, as the zonation of these elements about the XY-deposit has not been documented. Interestingly, there were no significant differences in the Ni and Cu content of both the waters and the mineral precipitates from either stream. This can be explained by the fact that the majority of the Ni and Cu does not reside in the Active Member, but instead in the footwall and hanging wall units (Goodfellow et al., 1983a).

6. Conclusions

This study has shown that this ARD creek draining the XY-deposit experienced a strong seasonal geochemical evolution, with increased concentrations of sulphate and metals and decreased pH over the course of the summer, likely due to waning recharge waters. The seasonal evolution of the mineral precipitate mineralogy was determined to be due to inorganic factors, including changes in flow rates, temperature, pH and aqueous geochemistry, although microbially-mediated precipitation likely occurred at some of the sampling sites. The attenuation of trace elements in the creek was achieved through dilution, hydrolysis, and neutralization reactions; however, microbially-mediated adsorption reactions may have been important for trace metal attenuation at some locations along the stream. Trace metal attenuation was not highly influenced by the mineralogy of the mineral precipitates, and was instead governed by the pH and prevailing geochemical conditions of these waters. Although we determined that microbes were likely to be playing a role in mineral precipitate formation and trace metal attenuation, further work is required to understand their involvement in this ARD system.

7. Applications for mineral exploration

Given the strong seasonality observed in the water chemistry of this ARD stream, it would be advisable to suggest that seasonal sampling campaigns be conducted if ARD streams were used for mineral exploration purposes. For example, if sampling was completed during the freshet, melt waters could sufficiently dilute the signals from the ore body and anomalous concentrations of pathfinder elements could go undetected. Since the mineralogy of the mineral precipitates did not control their accumulation of trace elements, we cannot suggest whether sampling a certain lamination in a mineral precipitate would be most conducive to observing anomalous concentrations of trace elements. Generally, all of the precipitates forming in ARD contain anomalous concentrations of trace elements relative to stream sediment, and consequently it would be difficult for these elements to go undetected. Furthermore, it would be difficult to refine the location of mineralization relative to the ARD stream based on trace element concentrations, as the concentration of trace elements in the precipitates is highly influenced by the unique geochemical dynamics of a particular location in the stream. For example, the extreme concentrations of Zn and Cd in the red laminae at 120 m clearly indicate that the waters from which these precipitates formed were in close proximity to the ore body. However, in order for the signal of the ore body to be preserved, the local hydrological conditions must be conducive to the precipitation or adsorption of these elements. Thus, a systems-approach to understanding how the geochemistry of the ARD stream is influenced by the local hydrology and hydrogeology is strongly suggested.

There was no significant relationship between the pH of the waters and the Cd/Zn and Pb/(Pb+Zn) molar ratios in the waters or the mineral precipitates, suggesting that pH

is not a good indicator for sampling locations where these ratios may be found to be coincident with the Active Member. Furthermore, given the sparingly soluble nature of Pb in the surface environment, using Pb/(Pb+Zn) molar ratios from ARD streams is not suggested for exploration purposes. Perhaps examination of a wider pH range for waters in the Selwyn Basin would indicate a significant relationship between pH and Cd/Zn and Pb/(Pb+Zn) molar ratios, as the pH range in this study was fairly limited (pH 3.1 – 5.0). Lead concentration, instead of Pb/(Pb+Zn) molar ratios in the mineral precipitates may be a more useful indicator of Zn-Pb mineralization, as Pb concentrations were significantly different for the precipitates that formed in the ARD stream draining the XY-deposit and those from the ARD stream draining shales. Despite this, the use of Pb concentrations in mineral precipitates for mineral exploration purposes cannot be validated without sampling a wider range of acidic streams in the Selwyn Basin. Additionally, the results of this study suggest that examining the Cd/Zn molar ratios in the waters would easily indicate their association with the Zn-Pb mineralization, while the Cd/Zn ratios in the mineral precipitates would not delineate acidic waters originating from Zn-Pb mineralization from those originating from shales. Thus, the Cd/Zn ratios in ARD waters may be most practical for vectoring toward areas of undefined Zn-Pb mineralization.

The major and trace element geochemistry of the waters and mineral precipitates in the XY-ARD and the ARD from the shales showed significant differences for certain elements that are known to be concentrated in the Active Member vs. those that are concentrated in the shales. However, interpretation of these results would be difficult without knowledge of the geochemistry of the mineralization and the regolith.

Overall, these results suggest that an intimate understanding of the geology and

geochemistry of the regolith and mineralization are required if ARD waters are to be used as a mineral exploration tool. Otherwise, the characteristically anomalous geochemistry of ARD streams could suggest the presence of an ore body, when in fact the effluent resulted from water-rock interactions with the metal-rich regolith. Thus, ARD stream geochemistry would be most useful as a secondary mineral exploration tool, that is, to be used after the geochemistry of the orebody and regolith have been established. To this end, ARD stream geochemistry could be sampled in the Selwyn Basin and compared to the stream geochemistry of waters that are likely draining the Active Member. Anomalies coincident with those detected in the waters and mineral precipitates forming in the ARD from the Active Member could suggest the presence of additional Zn-Pb mineralization. To further refine the usefulness of ARD for mineral exploration, we suggest that a basin-wide scale study be conducted to characterize other ARD streams in the Selwyn Basin.

8. Acknowledgements

First and foremost my appreciation goes to my wonderful supervisors, Dr. Danielle Fortin and Dr. Paul Gammon, without whom this project would not have been possible. I am indebted to my field assistant, Andre Pellerin (Ph.D. candidate), who provided excellent help and insight with sample collection and was an amazing field companion and fire starter. I would also like to thank Selwyn Resources for their help with site access and logistics. In particular, I am grateful to Justin Himmelright, Jason Dunning (P.Geo), J.J. O'Donnell (P.Geo) and Breanne Patterson. I would also like to thank my "man family" at Don Camp, including Adam MacDonald, Littlefoot, Jason Wright, Pete, Matt and Hunter, all of whom made life in isolation enjoyable. Additional thanks goes to Judy Vaive and Pierre Pelchat at the GSC's Inorganic Geochemical Research Facility for their help with all of the geochemical analyses, Pat Hunt at the GSC's Mineralogical Research Facility for her help with E-SEM, John Stirling at the GSC's Mineralogy Research Facility for his help with the XRD analyses, and to Dianne Moyles at the University of Guelph for her help with the TEM. I would also like to thank Dr. Andrew Gault, my family, Bella, Tilly and Milo for tolerating me over the duration of my thesis writing, and for providing many constructive comments about this manuscript. Special thanks go to my thesis committee for reading such a long thesis. This project was funded through the GSC's Deep Search Program, as part of the Targeted Geoscience Initiatve III.

9. References

Acero, P., Ayora, C., Torrento, C. & Nieto, J.M. (2006). Behaviour of trace metals during schwertmannite precipitation and subsequent transformation into goethite and jarosite. *Geochimica Cosmocimica Acta, 70*: 4130 – 4139.

Ahonen, L. & Tuovinen, O.H. (1989). Effect of temperature on the microbial leaching of sulfide ore material in percolators containing chalcopyrite, pentlandite, sphalerite, pyrrhotite as main minerals. *Biotechnology Letters, 11*: 331 – 336.

Ahonen, L. & Tuovinen, O.H. (1989). Microbial oxidation of ferrous iron at low temperatures. *Applied Environmental Microbiology, 55*: 312 – 316.

Ahonen, L. & Tuovinen, O.H. (1990). Kinetics of sulfur oxidation at suboptimal temperatures. *Applied Environmental Microbiology, 56*: 560 – 562.

Ahonen, L. & Tuovinen, O.H. (1992). Bacterial oxidation of sulfide minerals in column leaching experiments at suboptimal temperatures. *Applied Environmental Microbiology, 58*: 600 – 606.

Anthony, J.W. & McLean, W.J. (1976). Jurbanite, a new post-mine aluminum sulphate mineral from San Manuel, Arizona. *American Mineralogist, 61*: 1 – 4.

Anderson, P.R. & Benjamin, M.M. (1990). Surface and bulk characteristics of binary oxide suspensions. *Environmental Science and Technology, 24*: 692 – 698.

Bambic, D. G., Alpers, C. N., Green, P. G., Fanelli, E., & Silk, W. K. (2006). Seasonal and spatial patterns of metals at a restored copper mine site. I. stream copper and zinc. *Environmental Pollution, 144*(3), 774-782.

Barham, R.J. (1997). Schwertmannite: a unique mineral, contains a replacement ligand, transforms to jarosites, hematites, and/or basic iron sulfate. *Journal of Material Research, 12*: 2751 – 2758.

Berthelot, D., Leduc, L.G. & Ferroni, G.D. (1993). Temperature studies of iron-oxidizing autotrophs and acidophilic heterotrophs isolated from uranium mines. *Canadian Journal of Microbiology, 39*: 384 – 388.

Bigham, J.M., Schwertmann, U., Carlson, L. & Murad, E. (1990). A poorly crystalline oxyhydroxysulfate of iron formed by bacterial oxidation of Fe(II) in acid-mine waters. *Geochimica Cosmochimica Acta, 54*: 2743 – 2758.

Bigham, J.M., Carlson, L. & Murad, E. (1994). Schwertmannite, a new iron oxyhydroxysulfate mineral from Pyhasalmi, Finland, and other localities. *Mineralogical Magazine, 58*: 641 – 648.

Bigham, J.M., Schwertmann, U., Traina, S.J., Winland, R.L. & Wolf, M. (1996a). Influence of pH on mineral speciation in a bioreactor simulating acid mine drainage. *Applied Geochemistry, 60*: 2111-2121.

Bigham, J. M., Schwertmann, U., Traina, S. J., Winland, R. L., & Wolf, M. (1996b). Schwertmannite and the chemical modeling of iron in acid sulfate waters. *Geochimica Cosmochimica Acta, 60*(12), 2111-2121.

Bigham, J.M. & Nordstrom, D.K. (2000). Iron and aluminum hydroxysulphates from acid sulphate waters. Reviews in Mineralogy and Geochemistry vol. 40. Mineralogical Society of America, p. 351−403.

Blowes, D.W & Pacek, C.J. (1994). Acid-neutralization mechanisms in inactive mine tailings, *In*: Jambor, J.L. & Blowes, D.W. (Eds.), Environmental geochemistry of sulphide mine wastes. Mineralogical Association of Canada, Waterloo, Ontario, Short Course Handbook 22, pp. 271 – 292.

Braddock, J.F.. Luong, H.V. & Brown, E.J. (1984). Growth kinetics of *Thiobacillus ferrooxidans* isolated from arsenic mine drainage. *Applied Environmental Microbiology, 48*: 48 – 55.

Brady, K.S., Bigham, J.M., Jaynes, W.F. & Logan, T.J. (1986). Influence of sulphate on Fe-oxide formation: Comparisons with a stream receiving acid mine drainage. *Clays and Clay Minerals, 34*: 266 – 274.

Brake, S.S., Dannelly, H.K. & Connors, K.A. (2001a). Controls on the nature and distribution of an alga in coal-mine waste environments and its potential impact on water quality. *Environmental Geology, 40*: 458 – 469.

Brake, S.S., Dannelly, H.K., Connors, K.A. & Hasiotis, S.T. (2001b). Influence of water chemistry on the distribution of an acidophilic protozoan in an acid mine drainage system at the abandoned Green Valley coal mine, Indiana, USA. *Applied Geochemistry, 16*: 1641 – 1652.

Brake, S.S., Hasiotis, S.T. & Dannelly, H.K. (2004). Diatoms in acid mine drainage and their role in the formation of iron-rich stromatolites. *Geomicrobiology Journal, 21*: 331 – 340.

Butler, T. W., & Seitz, J. C. (2006). Apparent seasonal variations in iron photoreduction in acidic discharge from a former pyrite mine, Oakland, California. *Applied Geochemistry, 21*(7), 1109-1122.

Butler, B. A., Ranville, J. F., & Ross, P. E. (2008). Observed and modeled seasonal trends in dissolved and particulate Cu, Fe, Mn, and Zn in a mining-impacted stream. *Water Research, 42*(12), 3135-3145.

Butler, B. A., Ranville, J. F., & Ross, P. E. (2009). Spatial variations in the fate and transport of metals in a mining-influenced stream, North Fork Clear Creek, Colorado. *Science of the Total Environment, 407*(24), 6223-6234.

Cánovas, C. R., Olías, M., Nieto, J. M., Sarmiento, A. M., & Cerón, J. C. (2007). Hydrogeochemical characteristics of the Tinto and Odiel rivers (SW Spain): Factors controlling metal contents. *Science of the Total Environment, 373*(1), 363-382.

Chapman, B.M., Jones, D.R., & Jung, R.F. (1983). Processes controlling metal ion attenuation in acid drainage streams. *Geochimica Cosmochimica Acta, 47*: 1957 – 1973.

Cravotta, C.A. III (1994). Secondary iron-sulphate minerals as sources of sulphate and acidity: the geochemical evolution of acidic groundwater at a reclaimed surface coal mine in Pennsylvania. *In*: Alpers, C.N. & Blowes, D.W. (Eds.), Environmental geochemistry of sulphide oxidation. American Chemical Society Symposium Series 550, Washington, DC, pp. 345 – 364.

Demirhan, N., & Tuncel Elmali, F. (2003). Spectrophotometric determination of iron(II) with 5- nitro-6-amino-1,10-phenanthroline. *Turkish Journal of Chemistry, 27*(3), 315-321.

Desbarats, A. J., & Dirom, G. C. (2007). Temporal variations in the chemistry of circum-neutral drainage from the 10-level portal, Myra mine, Vancouver island, British Columbia. *Applied Geochemistry, 22*(2), 415-435.

Dopson, M., Halinen, A.K., Rahunen, N., Ozkaya, B., Sahinkaya, E., Kaksonen, A.H., Lindstrom, E.B. & Puhakka, J.A. (2007). Mineral and iron oxidation at low temperatures by pure and mixed cultures of acidophilic microorganisms. *Biotechnology and Bioengineering, 97*: 1205 – 1215.

Dutrizac, J.E. & Jambor, J.L. (2000). Jarosites and their application in hydrometallurgy. *In*: Aplers, C.N., Jambor, J.L. & Nordstrom, D.K. (Eds.), Sulphate Minerals: Crystallography, Geochemistry and Environmental Significance. Reviews in mineralogy and Geochemistry, 40: 405 – 452.

Dzombak, D.A. & Morel, F.M.M. (1990). Surface complexation modeling: Hydrous ferric oxides. John Wiley, New York.

Edwards, K. J., Goebel, B. M., Rodgers, T. M., Schrenk, M. O., Gihring, T. M., Cardona, M. M. (1999). Geomicrobiology of pyrite (FeS_2) dissolution: Case study at Iron Mountain, California. *Geomicrobiology Journal, 16*(2), 155-179.

Elberling, B., Schippers, R. & Sand, W. (2000). Bacterial and chemical oxidation of pyritic mine tailings at low temperatures. *Journal of Contaminant Hydrology, 41*: 225 – 238.

Elzinga, E. J., Peak, D., & Sparks, D. L. (2001). Spectroscopic studies of Pb(II)-sulfate interactions at the goethite-water interface. *Geochimica Cosmochimica Acta, 65*(14), 2219-2230.

Eneroth, E. & Koch, C.B. (2004). Fe-hydroxysulphates from bacterial Fe^{2+} oxidation. *Hyperfine interactions, 156/157*: 423 – 429.

Ergas, S.J., Harrison, J., Bloom, J., Forloney, K., Ahlfeld, D.P., Nusslein, K. & Yuretich, R.F. (2006). Natural attenuation of acid mine drainage by acidophilic and acidotolerant Fe(III)- and sulphate-reducing bacteria. *In*: Remediation of Hazardous Waste in the Subsurface, Ch.7, American Chemical Society, pp. 105 – 127.

Fernández-Remolar, D. C., Morris, R. V., Gruener, J. E., Amils, R., & Knoll, A. H. (2005). The Río Tinto Basin, Spain: Mineralogy, sedimentary geobiology, and implications for interpretation of outcrop rocks at Meridiani Planum, Mars. *Earth and Planetary Science Letters, 240*(1), 149-167.

Ferroni, G.D., Leduc, L.G. & Todd, M. (1986). Isolation and temperature characterization of psychrotrohpic strains of *Thiobacillus ferrooxidans* from the environment of a uranium mine. *Journal of Genetics and Applied Microbiology, 32*: 169 – 175.

Ferris, F.G., Schultze, S., Witten, T.C., Fyfe, W.S. & Beveridge, T.J. (1989). Metal interactions with microbial biofilms in acidic and neutral pH environments. *Applied Environmental microbiology, 55*: 1249 – 1257.

Furrer, G., Phillips, B. L., Ulrich, K., Pöthig, R., & Casey, W. H. (2002). The origin of aluminum flocs in polluted streams. *Science, 297*(5590), 2245-2247.

Goodfellow, W. D., Jonasson, I. R., & Morganti, J. M. (1983a). Zonation of chalcophile elements about the Howard's pass (XY) Zn-Pb deposit, Selwyn Basin, Yukon. *Journal of Geochemical Exploration, 19*(1-3), 503-542.

Goodfellow, W.D. (1983b). Stream sediment and water geochemistry of the Howard's Pass (XY) Zn-Pb deposit and Nor Zn-Pb-Ba occurrence, Selwyn Basin, Yukon and Northwest Territories. GSC open file 845. Geological Survey of Canada, Ottawa.

Gordey, S.P. (1981). Geology of the Nahinni map-area, Yukon Territory and District of Mackenzie. GSC open file 780. Geological Survey of Canada, Ottawa.

Goulbic, S. (1973). The relationship between blue-green algae and carbonate deposits. *In*: Carr, N.G., & White, B.A. (Eds). The Biology of Blue Green Algae: Oxford, U.K., Blackwell Science, pp. 434 – 472.

Graham, G. E., & Kelley, K. D. (2009). The Drenchwater deposit, Alaska: An example of a natural low pH environment resulting from weathering of an undisturbed shale-hosted Zn-Pb-Ag deposit. *Applied Geochemistry, 24*(2), 232-245.

Gramp, J. P., Wang, H., Bigham, J. M., Sandy Jones, F., & Tuovinen, O. H. (2009). Biogenic synthesis and reduction of Fe(III)-hydroxysulfates. *Geomicrobiology Journal, 26*(4), 275-280.

Grotzinger, J.P & Rothman, D.H. (1996). An abiotic model for stromatolite morphogenesis. *Nature, 383*: 423 – 425.

Grotzinger, J.P & Knoll, A.H. (1999). Stromatolites in Precambrian carbonates: Evolutionary mileposts, or environmental dipsticks? *Annual Review of Earth and Planetary Science, 27*: 313 – 358.

Hallmann, R., Friedrich, A., Koops, H.P, Pommereningroser, A., Rohde, K., Zenneck, C. & Sand, W. (1992). Physiological characteristics of *Thiobacillus ferrooxidans* and *Leptospirillium ferrooxidans* and physiological factors influencing microbial metal leaching. *Geomicrobiology Journal, 10*: 193 – 206.

Hammarstrom, J. M., Seal II, R. R., Meier, A. L., & Jackson, J. C. (2003). Weathering of sulfidic shale and copper mine waste: Secondary minerals and metal cycling in Great Smoky Mountains National Park, Tennessee, and North Carolina, USA. *Environmental Geology, 45*(1), 35-57.

Hard, B. C., Walther, C., & Babel, W. (1999). Sorption of aluminum by sulfate-reducing bacteria isolated from uranium mine tailings. *Geomicrobiology Journal, 16*(4), 267-275.

Heiri, O., Lotter, A.F. & Lemcke, G. (2000). Loss on ignition as a method for estimating organic and carbonate content in sediments: reproducibility and comparability of results. *Journal of Paleolimnology, 25*: 101 -110.

Herbert Jr., R. B. (1996). Metal retention by iron oxide precipitation from acidic groundwater in Dalarna, Sweden. *Applied Geochemistry, 11*(1-2), 229-235.

Hochella, M.F., Moore, J.N., Golla, U. & Putnis, A. (1999). A TEM study of samples from acid mine drainage systems: metal-mineral association with implications for transport. *Geochimica Cosmochimica Acta, 63*: 3395 – 3406.

Hofmann, T., & Schuwirth, N. (2008). Zn and Pb release of sphalerite (ZnS)-bearing mine waste tailings. *Journal of Soils and Sediments, 8*(6), 433-441.

Johnson, D.B., Rolfe, S., Hallberg, K.B. & Inversen, E. (2001). Isolation and phylogenetic characterization of acidophilic microorganisms indigenous to acidic drainage waters at an abandoned Norwegian copper mine. *Environmental Microbiology, 3*: 630 – 637.

Johnson, D. B., & Hallberg, K. B. (2003). The microbiology of acidic mine waters. *Research in Microbiology, 154*(7), 466-473.

Jonasson, I.R., Goodfellow, W.D., Walker, D.A. & Jackson, L.E. (1989). Secondary Zn mineralization in post-glacial sediments and talus at Howard's Pass, Yukon Canada – Mineralogy, geochemistry and genesis. *In*: Weathering: its products and deposits, vol 2. Theophrastus Publications, Greece. pp. 523 – 577.

Karathanasis, A.D., Evangelou, V.P. & Tompson, Y.L. (1988). Aluminum and iron equilibria in soil solutions and surface waters of acid mine watersheds. *Journal of Environmental Quality, 17*: 534 – 543.

Karlsson, S., Håkansson, K., Ledin, A., & Allard, B. (1995). Light induced changes of Fe(II) Fe(III) and their implications for colloidal forms of Al, Mn, Cu, Zn and Cd in an acidic lake polluted with mine waste effluents. *Journal of Geochemical Exploration, 52*(1-2), 145-159.

Kawano, M., & Tomita, K. (2001). Geochemical modeling of bacterially induced mineralization of schwertmannite and jarosite in sulfuric acid spring water. *American Mineralogist, 86*(10), 1156-1165.

Keith, D. C., Runnells, D. D., Esposito, K. J., Chermak, J. A., Levy, D. B., & Hannula, S. R. (2001). Geochemical models of the impact of acidic groundwater and evaporative sulfate salts on Boulder Creek at Iron Mountain, California. *Applied Geochemistry, 16*(7-8), 947-961.

Kim, J. J., Kim, S. J., & Tazaki, K. (2002). Mineralogical characterization of microbial ferrihydrite and schwertmannite, and non-biogenic al-sulfate precipitates from acid mine drainage in the Donghae mine area, Korea. *Environmental Geology, 42*(1), 19-31.

Kim, J. J., Kim, S. J., & Choo, C. O. (2003). Seasonal change of mineral precipitates from the coal mine drainage in the Taebaek coal field, South Korea. *Geochemical Journal, 37*(1), 109-121.

Kim, J. J., & Kim, S. J. (2004). Seasonal factors controlling mineral precipitation in the acid mine drainage at Donghae coal mine, Korea. *Science of the Total Environment, 325*(1-3), 181-191.

Kimball, B. E., Rimstidt, J. D., & Brantley, S. L. (2010). Chalcopyrite dissolution rate laws. *Applied Geochemistry, 25*(7), 972-983.

Kinniburgh, D.G., Jackson, M.L. & Syers, J.K. (1976). Adsorption of alkaline earth, transition, and heavy metal cations by hydrous oxide gels of iron and aluminum. *Soil Science Society of America Journal, 40*: 796 – 799.

Kinniburgh, D.G. & Jackson, M.L. (1981). Cation adsorption by hydrous metal oxides and clay, Chapter 3, *In*: Anderson, M.A. & Rubin, A.J. (Eds.), Adsorption of Inorganics at Solid-Liquid Interfaces. Ann Arbor Scientific Publications Inc. Michigan, pp. 91 – 160.

Kumpulainen, S., Carlson, L., & Räisänen, M. (2007). Seasonal variations of ochreous precipitates in mine effluents in Finland. *Applied Geochemistry, 22*(4), 760-777.

Kumpulainen, S., Räisänen, M., Vond Er Kammer, F., & Hofmann, T. (2008). Ageing of synthetic and natural schwertmannites at pH 2-8. *Clay Minerals, 43*(3), 437-448.

Kupka, D., Rzhepishevska, O.I., Dopson, M., Lindstrom, E.B., Karnachuck, O.V. & Tuovinen, H. (2007). Bacterial oxidation of ferrous iron at low temperatures. *Biotechnology and Bioengineering, 97*: 1470 – 1478.

Kwong, Y. T. J., Roots, C. F., Roach, P., & Kettley, W. (1997). Post-mine metal transport and attenuation in the Keno Hill mining district, central Yukon, Canada. *Environmental Geology, 30*(1-2), 98-107.

Kwong, Y. T. J., Whitley, G., & Roach, P. (2009). Natural acid rock drainage associated with black shale in the Yukon Territory, Canada. *Applied Geochemistry, 24*(2), 221-231.

Lacelle, D., Doucet, A., Clark, I. D., & Lauriol, B. (2007). Acid drainage generation and seasonal recycling in disturbed permafrost near Eagle Plains, Northern Yukon Territory, Canada. *Chemical Geology, 243*(1-2), 157-177.

Langdahl, B.R. & Ingvorsen, K. (1997) Temperature characteristics of bacterial iron solubilisation and C-14 assimilation in naturally exposed sulfide ore material at Citronen Fjord, North Greenland (83 degrees N*). FEMS Microbiological Ecology, 23*: 275 – 283.

Lawrence, J. R., Swerhone, G. D. W., & Kwong, Y. T. J. (1998). Natural attenuation of aqueous metal contamination by an algal mat. *Canadian Journal of Microbiology, 44*(9), 825-832.

Leblanc, M., Achard, B., Othman, D. B., Luck, J. M., Bertrand-Sarfati, J., & Personné, J. C. (1996). Accumulation of arsenic from acidic mine waters by ferruginous bacterial accretions (stromatolites). *Applied Geochemistry, 11*(4), 541-554.

Leduc, L.G., Trevors, J.T. & Ferroni, G.D. (1993). Thermal characterization of different isolates of *Thiobacillus ferrooxidans*. *FEMS Microbiology Letters, 108*: 189 – 193.

Leduc, L.G. & Ferroni, G.D. (1994). The chemolithotrophic bacterium *Thiobacillus ferrooxidans*. *FEMS Microbiology Reviews, 14*: 103 – 119.

Lee, G., Bigham, J.M. & Faure, G. (2002). Removal of trace metals by coprecipitation with Fe, Al and Mn from natural waters contaminated with acid mine drainage in the Ducktown Mining District, Tennessee. *Applied Geochemistry, 17*: 569 – 581

Lees, H., Kwok, S. C., & Suzuki, I. (1969). The thermodynamics of iron oxidation by the *Ferrobacilli*. *Canadian Journal of Microbiology, 15*(1), 43-46.

Luo, W., Kelly, S. D., Kemner, K. M., Watson, D., Zhou, J., Jardine, P. M., et al. (2009). Sequestering uranium and technetium through co-precipitation with aluminum in a contaminated acidic environment. *Environmental Science and Technology, 43*(19), 7516-7522.

McKnight, D. M., Kimball, B. A., & Runkel, R. L. (2001). pH dependence of iron photoreduction in a Rocky Mountain stream affected by acid mine drainage. *Hydrological Processes, 15*(10), 1979-1992.

Meldrum, J.L., Jamieson, H.E. & Dyke, L.D. (2001). Oxidation of mine tailings from Rankin Inlet, Nunavut, at subzero temperatures. *Canadian Geotechnical Journal, 38*: 957 – 966.

Morganti, J.M. (1979). The geology and ore deposits of the Howard's Pass area, Yukon. Unpublished Ph.D. Thesis. University of British Columbia, Vancouver, BC. p. 317.

Munk, L., Faure, G., Pride, D. E., & Bigham, J. M. (2002). Sorption of trace metals to an aluminum precipitate in a stream receiving acid rock-drainage; Snake River, Summit County, Colorado. *Applied Geochemistry, 17*(4), 421-430.

Murad, E., & Rojík, P. (2005). Iron mineralogy of mine-drainage precipitates as environmental indicators: Review of current concepts and a case study from the Sokolov Basin, Czech Republic. *Clay Minerals, 40*(4), 427-440.

Ninteman, D.J. (1978). Spontaneous oxidation and combustion of sulphide ores in underground mines, a literature survey. US Bureau of Mines Internal Circular, 8775.

Nordstrom, D.K. (1982). The effect of sulfate on aluminum concentrations in natural waters: some stability relations in the system Al_2O_3-SO_3-H_2O at 298 K. *Geochimica Cosmochimica Acta, 46*: 681 – 692.

Nordstrom, D.K. & Alpers, C.N. (1999). Geochemistry or acid mine waters. In *The Enviornmental Geochemistry of Mineral Deposits. Part a: Processess,Techniques, and Health Issues.* Eds. Plumlee, G.S. and Logsdon, M.J. Littleton, CO, USA: The Society of Economic Geologists, pp. 133 – 160.

Nordstrom, D. K., Alpers, C. N., Ptacek, C. J., & Blowes, D. W. (2000). Negative pH and extremely acidic mine waters from iron mountain, california. *Environmental Science and Technology, 34*(2), 254-258.

Nordstrom, D. K., & Ball, J. W. (1986). The geochemical behavior of aluminum in acidified surface waters. *Science, 232*(4746), 54-56.

Okereke, A. & Stevens, S.E. (1991) Kinetics of Iron Oxidation by Thiobacillus ferrooxidans. Applied Environmental Microbiology, 57*: 1052 – 1056.*

Ostergren, J. D., Brown Jr., G. E., Parks, G. A., & Persson, P. (2000). Inorganic ligand effects on Pb(II) sorption to goethite (α-FeOOH). II. sulfate. *Journal of Colloid and Interface Science, 225*(2), 483-493.

Parker, S. R., Gammons, C. H., Jones, C. A., & Nimick, D. A. (2007). Role of hydrous iron oxide formation in attenuation and diel cycling of dissolved trace metals in a stream affected by acid rock drainage. *Water, Air, and Soil Pollution, 181*(1-4), 247-263.

Penilla, S., Bordas, F. & Bollinger, J.C. (2005). Sequential heavy metals extraction from polluted soils: influence of sulfate overconcentration. *Journal of Colloid Interface Science, 292*: 20 – 28.

Pring, A., Tarantino, S. C., Tenailleau, C., Etschmann, B., Carpenter, M. A., & Zhang, M. (2008). The crystal chemistry of Fe-bearing sphalerites: An infrared spectroscopic study. *American Mineralogist, 93*(4), 591-597.

Pu, X., Vazquez, O., Monnell, J. D., & Neufeld, R. D. (2010). Speciation of aluminum precipitates from acid rock discharges in central Pennsylvania. *Environmental Engineering Science, 27*(2), 169-180.

Regenspurg, S., & Peiffer, S. (2005). Arsenate and chromate incorporation in schwertmannite. *Applied Geochemistry, 20*(6), 1226-1239.

Ritchie, A.I.M. (1994). The waste-rock environment. *In*: , J.L. and Blowes, D.W. (Eds). Short Course Handbook on Environmental Geochemistry of Sulfide Mine Waste. JamborMineralogical Association of Canada, pp. 133 – 161.

Rimstidt, J.D., Chermak, J.A., & Gagen, P.M. (1994). Rates of reaction of galena, sphalerite, chalcopyrite, and arsenopyrite with Fe(III) in acidic solutions. *In:* Alpers, C.N., Blowes, D.W. (Eds.), Environmental Geochemistry of Sulfide Oxidation, American Chemical Society Symposium Series, Vol. 550. American Chemical Society, Washington, D.C. pp. 2 – 13.

Sabelli, C. (1984). On the mineralogy of the Cetine mine of Cotorniano: The sulphate dimorphs jurbanite and rostite. *Per Mineral (Roma),* p. 53 – 65.

Salvarredy-Aranguren, M. M., Probst, A., Roulet, M., & Isaure, M. (2008). Contamination of surface waters by mining wastes in the Milluni Valley (Cordillera Real, Bolivia): Mineralogical and hydrological influences. *Applied Geochemistry, 23*(5), 1299-1324.

Sanchez-España, J., Pamo, E. L., Pastor, E. S., Andrés, J. R., & Rubí, J. A. M. (2005). The natural attenuation of two acidic effluents in Tharsis and La Zarza-Perrunal mines (Iberian Pyrite Belt, Huelva, Spain). *Environmental Geology, 49*(2), 253-266.

Sanchez-España, J., Pamo, E. L., Santofimia, E., Aduvire, O., Reyes, J., & Barettino, D. (2005). Acid mine drainage in the Iberian Pyrite Belt (Odiel River watershed, Huelva, SW Spain): Geochemistry, mineralogy and environmental implications. *Applied Geochemistry, 20*(7), 1320-1356.

Sanchez-España, J., Pamo, E.L., Pastor, E.S., Andres, J.R. & Rubi, J.A.M. (2006). The removal of dissolved metals by hydroxysulfate precipitation during oxidation and neutralization of acid mine waters, Iberian Pyrite Belt. *Aquatic Geochemistry, 12*: 269 – 298.

Sanchez-España, J., Pastor, E.S. and Pamo, E.L. (2007). Iron terraces in acid mine drainage systems: A discussion about the organic and inorganic factors involved in their formation through observations from the Tintillo acidic river (Riotinto min, Huelva, Spain). *Geosphere, 3(3)*: 133 – 151.

Sarmiento, A. M., Nieto, J. M., Olías, M., & Cánovas, C. R. (2009). Hydrochemical characteristics and seasonal influence on the pollution by acid mine drainage in the Odiel River basin (SW Spain). *Applied Geochemistry, 24*(4), 697-714.

Sarradin, P., Le Bris, N., Le Gall, C., & Rodier, P. (2005). Fe analysis by the ferrozine method: Adaptation to FIA towards in situ analysis in hydrothermal environment. *Talanta, 66*(5), 1131-1138.

Schindler, P.W. (1990). Co-adsorption of metal ions and organic ligands: Formation of ternary surface complexes. *In*: Hochella, M.F. & White A.F. (Eds.), Mineral-water Interface Geochemistry, 23. Mineralogical Society of America, p. 281.

Schwertmann, U., Bigham, J. M., & Murad, E. (1995). The first occurrence of schwertmannite in a natural stream environment. *European Journal of Mineralogy, 7*(3), 547-552.

Scroth, A.W. & Parnell, R.A. (2005). Trace metal retention through the schwertmannite to goethite transformation as observed in a field setting Alta Mine, MT. *Applied Geochemistry, 20*: 907 – 917.

Seal, R.R., Hammarstrom, J.M., Foley, N.K. & Alpers, C.N. (2002). Geoenvironmental models for seafloor massive sulphide deposits. *In*: Seal, R.R., Foley, N.K. (Eds.).

Progress on geoenvironmental models for selected deposit types. USGS Open-file Report 02 – 195.

Sidenko, N. V., & Sherriff, B. L. (2005). The attenuation of Ni, Zn and Cu, by secondary Fe phases of different crystallinity from surface and ground water of two sulfide mine tailings in Manitoba, Canada. *Applied Geochemistry, 20*(6), 1180-1194.

Singer, P.C. & Stumm, W. (1970). Acidic mine drainage: rate-determining step. *Science, 167*: 1121

Stillings, L. L., Foster, A. L., Koski, R. A., Munk, L., & Shanks III, W. C. (2008). Temporal variation and the effect of rainfall on metals flux from the historic Beatson mine, Prince William Sound, Alaska, USA. *Applied Geochemistry, 23*(2), 255-278.

Stookey, L.L. (1970). Ferrozine – a new spectrophotometric reagent for iron. *Analytical Chemistry, 42*: 779 – 781.

Stumm, W. & Morgan, J.J. (1995). Aquatic Chemistry – Chemical Equilibria and Rates in Natural Waters, John Wiley & Sons Inc., Third Edition.

Sullivan, P.J., Yelton, J.L., & Reddy K.J. (1988). Solubility relationships of aluminum and iron minerals associated with acid mine drainage. *Environmental Geology and Water Science*, *11*: 238 – 287.

Swedlund, P. J., & Webster, J. G. (2001). Cu and Zn ternary surface complex formation with so_4 on ferrihydrite and schwertmannite. *Applied Geochemistry, 16*(5), 503-511.

Swedlund, P. J., Webster, J. G., & Miskelly, G. M. (2003). The effect of SO_4 on the ferrihydrite adsorption of Co, Pb and Cd: Ternary complexes and site heterogeneity. *Applied Geochemistry, 18*(11), 1671-1689.

Swedlund, P. J., Webster, J. G., & Miskelly, G. M. (2009). Goethite adsorption of Cu(II), Pb(II), Cd(II), and Zn(II) in the presence of sulfate: Properties of the ternary complex. *Geochimica Cosmochimica Acta, 73*(6), 1548-1562.

Takahashi, Y., Hirata, T., Shimizu, H., Ozaki, T., & Fortin, D. (2007). A rare earth element signature of bacteria in natural waters? *Chemical Geology, 244*(3-4), 569-583.

Theobald, P.K., Lakin, H.W., Hawkins, D.B. (1963). The precipitation of Al, Fe and Mn at the junction of Deer Creek with Snake River in Summit Colorado. *Geochimica Cosmochimica Acta, 27*: 121 – 132.

Urrutia, M. M., & Beveridge, T. J. (1995). Formation of short-range ordered aluminosilicates in the presence of a bacterial surface (*Bacillus subtilis*) and organic ligands. *Geoderma, 65*(1-2), 149-165.

Van Breeman, N. (1973). Dissolved Al in acid sulphate soils and in acid mine waters. *Soil Science Society of America Proceedings, 37*: 694 – 697.

Vine, J.D. & Tourtelot, E.B. (1970). Geochemistry of black shale deposits – a summary report. *Economic Geology, 65*: 253 – 272.

Walter, M., Arnold, T., Reich, T., & Bernhard, G. (2003). Sorption of uranium(VI) onto ferric oxides in sulfate-rich acid waters. *Environmental Science and Technology, 37*(13), 2898-2904.

Wang, H., Bigham, J.M. & Tuovinen, O.H. (2006). Formation of schwertmannite and its transformation to jarosite in the presence of acidophilic iron-oxidizing microorganisms. *Materials Science Engineering, 26*: 588 – 592.

Wang, H.M., Bigham, J.M., Jones, F.S. & Tuovinen, O.H. (2007). Synthesis and properties of ammoniojarosites prepared with iron-oxidizing acidophilic microorganisms at 22-65 degrees C. *Geochimica Cosmochimica Acta, 71*: 155 – 164.

Webster, J.G., Nordstrom, D.K., & Smith, K.S. (1994). Transport and natural attenuation of Cu, Zn, As, and Fe in the acid mine drainage of Leviathan and Bryant Creeks. *In:* Alpers C.N. & Blowes, D.W. (Eds). The environmental geochemistry of sulphide oxidation, *American Chemical Society Symposium Series, 550*: 244 – 260.

Webster, J.G., Swedlund, P.J. & Webster, K.S. (1998). Trace metal adsorption onto acid mine drainage Fe(III)oxyhydroxysulfate. *Environmental Science and Technology, 32*: 1361 – 1368.

Weesner, F.J. & Bleam, W.F. (1998). Binding characteristics of Pb^{2+} on anion-modified and pristine hydrous oxide surfaces studied by electrophoretic mobility and X-ray absorption spectroscopy. *Journal of Colloid Interface Science, 205*: 380 – 389.

Yu, J., Heo, B., Choi, I. & Chang, H. (1999). Apparent solubilities of schwertmannite and ferrihydrite in natural stream waters polluted by mine drainage. *Geochimica Cosmochimica Acta, 63*: 3407 – 3416.

Appendix 1: Water chemistry results

ICP-MS (ppb)		Dilution	Li	Be	B	Ti	V	Cr	Co	Cu
D.L.		**1**	0.02	0.005	0.5	0.5	0.1	0.1	0.05	0.1
D.L.		**10**	0.2	0.05	5	5	1	1	0.5	1
Distance (m)	**Date**									
0	20-Jul	10	27.6	3.66	10	< 5	< 1	< 1	2013.8	321
0	28-Jul	10	23.3	2.53	9	< 5	< 1	< 1	1526.8	240
0	03-Aug	10	26.2	2.54	9	< 5	< 1	< 1	1424.7	224
0	06-Aug	10	29.1	2.96	11	< 5	< 1	< 1	1638.6	246
10	19-Jul	10	81.3	9.16	22	< 5	< 1	< 1	1742.2	1045
10	24-Jul	10	84.7	8.79	22	< 5	< 1	< 1	1864.2	1183
10	03-Aug	10	89.0	10.61	22	< 5	< 1	< 1	2141.3	1354
10	06-Aug	10	90.5	9.72	23	< 5	< 1	< 1	2170.2	1386
18	Jul-19	10	27.5	1.73	8	< 5	< 1	< 1	544.8	210
18	Jul-19	10	27.2	1.65	8	< 5	< 1	< 1	541.4	210
18	Jul-20	10	28.7	1.78	7	< 5	< 1	< 1	607.4	220
18	Jul-21	10	28.7	1.86	8	< 5	< 1	< 1	625.8	223
18	Jul-24	10	34.2	2.06	10	< 5	< 1	< 1	793.0	284
18	Jul-28	10	32.6	1.88	10	< 5	< 1	< 1	779.3	267
18	Jul-28	10	32.9	2.08	10	< 5	< 1	< 1	783.6	270
18	Jul-28	10	33.2	1.87	10	< 5	< 1	< 1	804.3	277
18	Jul-30	10	28.2	1.82	8	< 5	< 1	< 1	670.1	224
18	Jul-30	10	28.2	1.77	7	< 5	< 1	< 1	668.0	225
18	Jul-30	10	28.4	1.77	7	< 5	< 1	< 1	671.2	224
18	03-Aug	10	29.5	1.87	10	< 5	< 1	< 1	666.4	232
18	06-Aug	10	35.2	2.07	10	< 5	< 1	< 1	768.0	274
40	Jul-19	10	22.3	1.36	7	< 5	< 1	< 1	424.2	172
40	Jul-19	10	22.4	1.33	7	< 5	< 1	< 1	427.5	175
40	Jul-20	10	23.8	1.54	11	< 5	< 1	< 1	463.7	188
40	Jul-21	10	24.1	1.52	8	< 5	< 1	< 1	512.8	188
40	Jul-24	10	26.1	1.61	8	< 5	< 1	< 1	579.7	204
40	Jul-28	10	26.4	1.67	9	< 5	< 1	< 1	606.4	205
40	Jul-28	10	26.7	1.71	8	< 5	< 1	< 1	599.4	206
40	Jul-28	10	27.3	1.69	7	< 5	< 1	< 1	608.9	210
40	Jul-30	10	25.7	1.57	7	< 5	< 1	< 1	574.1	199

40	Jul-30	10	25.8	1.60	8	< 5	< 1	< 1	567.1	197
40	Jul-30	10	24.1	1.51	8	< 5	< 1	< 1	538.7	183
40	03-Aug	10	27.0	1.67	8	< 5	< 1	< 1	564.2	202
40	03-Aug	10	27.2	1.65	8	< 5	< 1	< 1	565.9	204
40	06-Aug	10	28.0	1.70	9	< 5	< 1	< 1	600.9	209
100	17-Jul	1	17.38	0.556	4.5	0.6	< 0.1	0.2	207.24	116.0
100	17-Jul	1	16.61	0.543	4.5	0.6	< 0.1	0.2	202.26	109.9
100	17-Jul	1	17.23	0.623	4.9	0.7	< 0.1	0.2	208.84	117.8
100	18-Jul	1	16.99	0.653	5.1	0.7	< 0.1	0.2	215.38	115.2
100	18-Jul	1	17.18	0.628	5.0	0.7	< 0.1	0.2	215.61	117.3
100	18-Jul	1	17.21	0.669	5.1	0.7	< 0.1	0.2	220.96	114.1
100	21-Jul	1	18.80	0.789	5.4	0.8	< 0.1	0.2	335.23	137.3
100	24-Jul	1	20.61	0.900	5.7	0.8	< 0.1	0.2	392.03	149.3
100	Jul-28	1	20.69	0.896	5.2	0.8	< 0.1	0.2	403.52	146.2
100	Jul-28	1	20.51	0.855	5.2	0.7	< 0.1	0.1	394.33	145.0
100	Jul-28	1	21.21	0.891	5.5	0.8	< 0.1	0.2	403.52	150.1
100	Jul-30	1	20.82	0.862	5.4	0.8	< 0.1	0.1	394.11	145.3
100	Jul-30	1	18.97	0.825	5.4	0.8	< 0.1	0.1	364.90	135.6
100	01-Aug	1	21.28	0.896	5.4	0.8	< 0.1	0.1	391.05	149.7
100	01-Aug	1	21.20	0.866	5.4	0.8	< 0.1	0.1	390.17	148.3
100	03-Aug	1	22.08	0.914	5.6	0.8	< 0.1	0.2	408.99	153.1
100	06-Aug	1	22.44	0.927	5.6	0.8	< 0.1	0.1	421.70	156.9
120	24-Jul	1	15.73	0.515	5.0	0.6	< 0.1	0.1	244.82	92.9
120	Jul-28	1	17.63	0.508	5.1	0.6	< 0.1	< 0.1	275.28	103.6
120	Jul-28	1	17.52	0.528	5.1	0.7	0.1	< 0.1	274.84	104.2
120	Jul-28	1	16.53	0.514	5.0	0.7	0.1	< 0.1	251.16	94.9
120	Jul-30	1	17.49	0.515	5.0	0.7	< 0.1	< 0.1	271.69	102.5
120	Jul-30	1	17.69	0.511	5.1	0.7	< 0.1	< 0.1	275.82	104.4
120	Jul-30	1	17.00	0.507	4.9	0.6	0.1	< 0.1	264.95	97.1
120	03-Aug	1	18.37	0.534	5.4	0.7	0.1	< 0.1	276.69	107.8
120	06-Aug	1	18.66	0.538	5.6	0.7	< 0.1	< 0.1	287.22	107.3
165	21-Jun	1	6.56	0.044	4.2	< 0.5	< 0.1	< 0.1	72.79	36.7
165	17-Jul	1	14.09	0.221	4.3	0.6	< 0.1	< 0.1	152.94	79.9
165	17-Jul	1	14.06	0.221	4.4	0.6	< 0.1	< 0.1	155.79	81.4
165	17-Jul	1	13.21	0.236	4.3	0.6	< 0.1	< 0.1	150.05	76.3
165	17-Jul	1	14.22	0.243	4.4	0.6	< 0.1	< 0.1	165.53	81.3
165	17-Jul	1	13.88	0.244	4.3	0.6	< 0.1	< 0.1	167.11	80.3

165	18-Jul	1	14.63	0.265	4.3	0.6	< 0.1	< 0.1	179.40	85.0
165	21-Jul	1	15.06	0.371	4.6	0.6	< 0.1	< 0.1	216.69	85.1
165	24-Jul	1	14.36	0.320	4.5	0.6	< 0.1	< 0.1	215.16	80.3
165	28-Jul	1	15.31	0.321	4.8	0.7	< 0.1	< 0.1	226.13	82.0
165	Jul-28	1	15.27	0.327	4.7	0.7	< 0.1	< 0.1	227.25	82.0
165	Jul-28	1	15.31	0.346	4.8	0.6	< 0.1	< 0.1	224.67	83.2
165	Jul-30	1	15.35	0.377	4.9	0.6	< 0.1	< 0.1	228.83	89.2
165	Jul-30	1	15.40	0.362	4.7	0.6	< 0.1	< 0.1	230.61	86.2
165	Jul-30	1	14.91	0.335	4.8	0.6	< 0.1	< 0.1	224.97	80.7
165	01-Aug	1	15.44	0.346	4.9	0.7	< 0.1	< 0.1	232.39	85.1
165	01-Aug	1	15.53	0.365	5.0	0.6	< 0.1	< 0.1	228.91	83.4
165	01-Aug	1	15.50	0.380	4.9	0.6	< 0.1	< 0.1	226.80	83.6
165	01-Aug	1	15.29	0.361	5.0	0.7	< 0.1	< 0.1	228.65	83.1
165	03-Aug	1	16.04	0.366	4.9	0.6	< 0.1	< 0.1	241.59	89.8
165	03-Aug	1	15.87	0.365	4.9	0.7	< 0.1	< 0.1	231.65	86.1
165	06-Aug	1	16.00	0.360	5.2	0.7	< 0.1	< 0.1	230.32	84.4
165	06-Aug	1	16.03	0.334	5.0	0.6	0.2	< 0.1	229.57	83.5
165-a	03-Aug	1	1.40	< 0.005	2.7	< 0.5	0.3	0.1	< 0.05	1.6
Control	21-Jul	1	3.91	< 0.005	1.5	< 0.5	0.1	< 0.1	< 0.05	0.5
Control	17-Jul	1	5.13	0.009	1.6	< 0.5	0.1	< 0.1	< 0.05	0.7
Control	17-Jul	1	5.21	< 0.005	1.7	< 0.5	0.1	< 0.1	< 0.05	0.3
Control	17-Jul	1	5.34	< 0.005	1.9	< 0.5	0.1	< 0.1	< 0.05	0.2
Control	17-Jul	1	5.20	< 0.005	1.7	< 0.5	< 0.1	< 0.1	< 0.05	0.7
Control	17-Jul	1	5.40	< 0.005	1.6	< 0.5	< 0.1	< 0.1	< 0.05	0.4
Control	18-Jul	1	5.12	< 0.005	1.5	< 0.5	0.1	< 0.1	< 0.05	0.3
Control	21-Jul	1	5.18	< 0.005	1.6	< 0.5	< 0.1	< 0.1	< 0.05	0.4
Control	28-Jul	1	5.24	< 0.005	1.6	< 0.5	< 0.1	< 0.1	< 0.05	0.2
Control	28-Jul	1	4.91	< 0.005	1.4	< 0.5	< 0.1	< 0.1	< 0.05	0.2
Control	03-Aug	1	5.40	< 0.005	1.8	< 0.5	0.1	< 0.1	< 0.05	0.2
Control	03-Aug	1	5.30	< 0.005	1.5	< 0.5	0.1	< 0.1	< 0.05	0.2
A4-1	20-Jul	1	82.10	17.805	0.6	1.8	0.1	11.5	708.13	775.7
A4-2	23-Jul	10	56.4	29.46	15	7	< 1	167	1099.1	4675
A4-3	23-Jul	1	2.61	0.029	1.4	< 0.5	0.1	0.3	2.84	3.8
A4-5	23-Jul	1	19.35	8.868	5.0	2.2	< 0.1	42.1	311.92	1325.7
A4-6	23-Jul	1	11.65	6.492	4.8	0.6	< 0.1	8.9	174.51	461.5
Control	23-Jul	1	3.51	0.008	0.7	< 0.5	< 0.1	< 0.1	< 0.05	0.3

DIW blank	19-Jul	1	< 0.02	< 0.005	< 0.5	< 0.5	< 0.1	< 0.1	< 0.05	< 0.1
DIW blank	25-Jul	1	< 0.02	< 0.005	< 0.5	< 0.5	< 0.1	< 0.1	< 0.05	< 0.1
DIW blank	02-Aug	1	< 0.02	< 0.005	< 0.5	< 0.5	< 0.1	< 0.1	< 0.05	< 0.1
DIW blank	06-Aug	1	< 0.02	< 0.005	< 0.5	< 0.5	< 0.1	< 0.1	< 0.05	< 0.1
Acid blank	21-Jun	1	< 0.02	< 0.005	< 0.5	< 0.5	< 0.1	< 0.1	< 0.05	< 0.1
Acid blank	19-Jul	1	< 0.02	< 0.005	< 0.5	< 0.5	< 0.1	< 0.1	< 0.05	< 0.1
Acid blank	25-Jul	1	< 0.02	< 0.005	< 0.5	< 0.5	< 0.1	< 0.1	< 0.05	< 0.1
Acid blank	02-Aug	1	< 0.02	< 0.005	< 0.5	< 0.5	< 0.1	< 0.1	< 0.05	< 0.1
Acid blank	06-Aug	1	< 0.02	< 0.005	< 0.5	< 0.5	< 0.1	< 0.1	< 0.05	< 0.1
Travel blank	19-Jul	1	< 0.02	< 0.005	< 0.5	< 0.5	< 0.1	< 0.1	< 0.05	< 0.1
Travel blank	25-Jul	1	< 0.02	< 0.005	< 0.5	< 0.5	< 0.1	< 0.1	< 0.05	< 0.1
Travel blank	02-Aug	1	< 0.02	< 0.005	< 0.5	< 0.5	< 0.1	< 0.1	< 0.05	< 0.1
Travel blank	06-Aug	1	< 0.02	< 0.005	< 0.5	< 0.5	< 0.1	< 0.1	< 0.05	0.1
Repeats										
18	21-Jul	10	28.7	1.86	8	< 5	< 1	< 1	625.8	223
18	21-Jul	10	28.2	1.90	8	< 5	< 1	< 1	628.6	222
100	18-Jul	1	17.21	0.669	5.1	0.7	< 0.1	0.2	220.96	114.1
100	18-Jul	1	17.39	0.673	5.2	0.7	< 0.1	0.2	220.08	111.9
165	21-Jun	1	6.56	0.044	4.2	< 0.5	< 0.1	< 0.1	72.79	36.7
165	21-Jun	1	6.59	0.046	2.5	< 0.5	< 0.1	< 0.1	72.49	36.3
165	17-Jul	1	14.22	0.243	4.4	0.6	< 0.1	< 0.1	165.53	81.3
165	17-Jul	1	14.51	0.245	4.3	0.6	< 0.1	< 0.1	166.53	81.3
165	01-Aug	1	15.50	0.380	4.9	0.6	< 0.1	< 0.1	226.80	83.6
165	01-Aug	1	15.64	0.370	5.0	0.7	< 0.1	< 0.1	228.61	83.2
Control	17-Jul	1	5.20	< 0.005	1.7	< 0.5	< 0.1	< 0.1	< 0.05	0.7
Control	17-Jul	1	5.18	< 0.005	1.7	< 0.5	< 0.1	< 0.1	< 0.05	0.7
Acid blank	06-Aug	1	< 0.02	< 0.005	< 0.5	< 0.5	< 0.1	< 0.1	< 0.05	< 0.1
Acid blank	06-Aug	1	< 0.02	< 0.005	< 0.5	< 0.5	< 0.1	< 0.1	< 0.05	< 0.1

Controls									
BLANK	1	< 0.02	< 0.005	< 0.5	< 0.5	< 0.1	< 0.1	< 0.05	< 0.1
BLANK	1	0.03	< 0.005	< 0.5	< 0.5	< 0.1	< 0.1	< 0.05	< 0.1
BLANK	1	< 0.02	< 0.005	< 0.5	< 0.5	< 0.1	< 0.1	< 0.05	< 0.1
BLANK	1	< 0.02	< 0.005	< 0.5	< 0.5	< 0.1	< 0.1	< 0.05	< 0.1
BLANK	1	< 0.02	< 0.005	< 0.5	< 0.5	< 0.1	< 0.1	< 0.05	< 0.1
BLANK	1	< 0.02	< 0.005	< 0.5	< 0.5	< 0.1	< 0.1	< 0.05	< 0.1
BLANK	1	< 0.02	< 0.005	< 0.5	< 0.5	< 0.1	< 0.1	< 0.05	< 0.1
BLANK	1	< 0.02	< 0.005	< 0.5	< 0.5	< 0.1	< 0.1	< 0.05	< 0.1
SLRS-4	1	0.50	0.007	5.0	1.2	0.3	0.3	< 0.05	1.7
SLRS-4	1	0.48	0.007	5.1	1.4	0.3	0.3	< 0.05	1.7
SLRS-4	1	0.48	0.006	5.2	1.4	0.3	0.3	< 0.05	1.8
CERTIFIED			0.007 ± 0.002			0.32 ± 0.03	0.33 ± 0.02	0.033 ± 0.006	1.81 ± 0.08
TM-28.2	1	3.61	2.613	10.2	4.5	2.6	5.0	3.93	6.9
TM-28.2	1	3.40	2.316	9.2	4.2	2.4	4.8	3.61	6.4
CERTIFIED INFORMATION		3.6 ± 1.0	2.5 ± 0.49			2.5 ± 0.86	4.7 ± 1.5	3.6 ± 0.78	6.3 ± 1.7
TMDA-51.3	1	17.75	9.490	49.8	13.6	48.0	67.5	74.73	94.4
TMDA-51.3	1	17.58	9.479	49.6	13.4	48.3	68.0	73.91	89.4
CERTIFIED INFORMATION		17.6 ± 1.7	9.83 ± 1.09	49.5 ± 8.0		48.4 ± 3.9	67.5 ± 5.1	71.5 ± 5.6	89.2 ± 8.6

ICP-MS (ppb)		**Dilution**	**Ga**	**Ge**	**As**	**Se**	**Rb**	**Sr**	**Zr**	**Nb**
D.L.		**1**	0.01	0.02	0.1	1	0.05	0.5	0.05	0.01
D.L.		**10**	0.1	0.2	1	10	0.5	5	0.5	0.1
Distance (m)	**Date**									
0	20-Jul	10	0.9	0.2	< 1	54	8.9	936	0.5	< 0.1
0	28-Jul	10	0.8	0.2	< 1	35	7.7	822	< 0.5	< 0.1
0	03-Aug	10	0.8	0.3	< 1	38	8.1	877	< 0.5	< 0.1
0	06-Aug	10	0.9	0.2	< 1	41	9.0	964	< 0.5	< 0.1
10	19-Jul	10	0.4	0.3	< 1	41	16.1	1435	< 0.5	< 0.1

10	24-Jul	10	0.4	0.3	< 1	42	17.3	1610	< 0.5	< 0.1
10	03-Aug	10	0.3	0.3	< 1	64	18.1	1617	0.6	< 0.1
10	06-Aug	10	0.4	0.3	< 1	68	18.1	1643	0.7	< 0.1
18	Jul-19	10	0.4	< 0.2	< 1	14	5.5	1108	< 0.5	< 0.1
18	Jul-19	10	0.4	< 0.2	< 1	14	5.5	1110	< 0.5	< 0.1
18	Jul-20	10	0.5	< 0.2	< 1	15	5.7	1147	< 0.5	< 0.1
18	Jul-21	10	0.4	< 0.2	< 1	16	5.7	1133	< 0.5	< 0.1
18	Jul-24	10	0.5	< 0.2	< 1	16	6.7	1289	< 0.5	< 0.1
18	Jul-28	10	0.5	< 0.2	< 1	17	6.6	1257	< 0.5	< 0.1
18	Jul-28	10	0.5	< 0.2	< 1	16	6.6	1271	< 0.5	< 0.1
18	Jul-28	10	0.5	< 0.2	< 1	16	7.1	1302	< 0.5	< 0.1
18	Jul-30	10	0.5	< 0.2	< 1	15	6.1	1115	< 0.5	< 0.1
18	Jul-30	10	0.5	< 0.2	< 1	15	6.2	1123	< 0.5	< 0.1
18	Jul-30	10	0.5	< 0.2	< 1	16	6.1	1119	< 0.5	< 0.1
18	03-Aug	10	0.5	< 0.2	< 1	16	6.4	1201	< 0.5	< 0.1
18	06-Aug	10	0.5	< 0.2	< 1	16	7.0	1307	< 0.5	< 0.1
40	Jul-19	10	0.3	< 0.2	< 1	13	4.8	1023	< 0.5	< 0.1
40	Jul-19	10	0.3	< 0.2	< 1	13	4.8	1026	< 0.5	< 0.1
40	Jul-20	10	0.4	< 0.2	< 1	15	5.1	1081	< 0.5	< 0.1
40	Jul-21	10	0.4	< 0.2	< 1	14	5.1	1091	< 0.5	< 0.1
40	Jul-24	10	0.4	< 0.2	< 1	15	5.6	1164	< 0.5	< 0.1
40	Jul-28	10	0.5	0.2	< 1	16	5.7	1179	< 0.5	< 0.1
40	Jul-28	10	0.4	< 0.2	< 1	16	5.8	1186	< 0.5	< 0.1
40	Jul-28	10	0.4	< 0.2	< 1	14	6.2	1202	< 0.5	< 0.1
40	Jul-30	10	0.4	< 0.2	< 1	14	5.7	1108	< 0.5	< 0.1
40	Jul-30	10	0.4	< 0.2	< 1	14	5.8	1117	< 0.5	< 0.1
40	Jul-30	10	0.4	< 0.2	< 1	13	5.4	1060	< 0.5	< 0.1
40	03-Aug	10	0.4	< 0.2	< 1	15	6.0	1181	< 0.5	< 0.1
40	03-Aug	10	0.4	< 0.2	< 1	14	6.0	1194	< 0.5	< 0.1
40	06-Aug	10	0.4	< 0.2	< 1	15	6.3	1252	< 0.5	< 0.1
100	17-Jul	1	0.02	0.10	< 0.1	12	3.66	736.2	< 0.05	< 0.01
100	17-Jul	1	0.02	0.10	0.1	12	3.44	707.4	< 0.05	< 0.01
100	17-Jul	1	0.04	0.11	0.1	11	3.70	732.5	< 0.05	< 0.01
100	18-Jul	1	0.03	0.10	0.2	11	3.58	743.8	< 0.05	< 0.01
100	18-Jul	1	0.03	0.11	0.2	11	3.59	750.6	< 0.05	< 0.01
100	18-Jul	1	0.03	0.11	0.2	11	3.54	742.1	< 0.05	< 0.01
100	21-Jul	1	< 0.01	0.08	< 0.1	14	3.99	858.4	< 0.05	< 0.01

100	24-Jul	1	< 0.01	0.07	< 0.1	13	4.48	927.5	0.06	< 0.01
100	Jul-28	1	< 0.01	0.05	< 0.1	13	4.42	923.5	0.06	< 0.01
100	Jul-28	1	< 0.01	0.04	< 0.1	14	4.34	917.6	0.06	< 0.01
100	Jul-28	1	< 0.01	0.06	< 0.1	13	4.78	923.4	0.06	< 0.01
100	Jul-30	1	< 0.01	0.05	< 0.1	13	4.61	903.4	0.06	< 0.01
100	Jul-30	1	< 0.01	0.06	< 0.1	12	4.27	852.9	0.06	< 0.01
100	01-Aug	1	< 0.01	0.05	< 0.1	13	4.75	927.6	0.06	< 0.01
100	01-Aug	1	< 0.01	0.06	< 0.1	13	4.80	937.3	0.06	< 0.01
100	03-Aug	1	< 0.01	0.06	< 0.1	14	4.82	960.5	0.06	< 0.01
100	06-Aug	1	< 0.01	0.04	< 0.1	13	5.01	1006.8	0.07	< 0.01
120	24-Jul	1	< 0.01	0.12	< 0.1	10	3.43	807.4	< 0.05	< 0.01
120	Jul-28	1	< 0.01	0.12	0.1	12	3.73	915.8	< 0.05	< 0.01
120	Jul-28	1	< 0.01	0.12	0.1	12	3.81	930.6	< 0.05	< 0.01
120	Jul-28	1	< 0.01	0.11	0.2	10	3.72	840.6	< 0.05	< 0.01
120	Jul-30	1	< 0.01	0.11	0.1	12	3.79	861.5	< 0.05	< 0.01
120	Jul-30	1	< 0.01	0.12	0.1	12	3.77	919.9	< 0.05	< 0.01
120	Jul-30	1	< 0.01	0.11	0.2	11	3.60	843.2	< 0.05	< 0.01
120	03-Aug	1	< 0.01	0.12	0.2	12	4.10	967.8	< 0.05	< 0.01
120	06-Aug	1	< 0.01	0.12	0.2	11	4.16	998.6	< 0.05	< 0.01
165	21-Jun	1	0.01	0.10	0.1	6	1.89	331.1	< 0.05	< 0.01
165	17-Jul	1	0.03	0.13	0.2	11	3.05	672.2	< 0.05	< 0.01
165	17-Jul	1	0.02	0.13	0.1	11	2.98	672.3	< 0.05	< 0.01
165	17-Jul	1	0.02	0.13	0.2	11	2.78	638.8	< 0.05	< 0.01
165	17-Jul	1	0.01	0.13	0.1	11	2.98	690.8	< 0.05	< 0.01
165	17-Jul	1	0.02	0.13	0.1	12	2.95	691.6	< 0.05	< 0.01
165	18-Jul	1	0.01	0.13	0.2	12	3.08	723.6	< 0.05	< 0.01
165	21-Jul	1	0.01	0.14	0.2	10	3.14	762.3	< 0.05	< 0.01
165	24-Jul	1	0.02	0.14	0.2	11	3.16	754.9	< 0.05	< 0.01
165	28-Jul	1	< 0.01	0.14	0.2	11	3.27	807.8	< 0.05	< 0.01
165	Jul-28	1	< 0.01	0.13	0.2	11	3.27	795.5	< 0.05	< 0.01
165	Jul-28	1	< 0.01	0.14	0.2	11	3.42	793.2	< 0.05	< 0.01
165	Jul-30	1	0.01	0.14	0.2	10	3.37	776.0	< 0.05	< 0.01
165	Jul-30	1	< 0.01	0.14	0.3	10	3.47	795.2	< 0.05	< 0.01
165	Jul-30	1	< 0.01	0.14	0.2	11	3.33	782.7	< 0.05	< 0.01
165	01-Aug	1	< 0.01	0.14	0.1	11	3.49	810.5	< 0.05	< 0.01
165	01-Aug	1	< 0.01	0.15	0.3	10	3.44	811.6	< 0.05	< 0.01
165	01-Aug	1	< 0.01	0.15	0.2	11	3.44	797.7	< 0.05	< 0.01

165	01-Aug	1	< 0.01	0.14	0.1	11	3.43	801.7	< 0.05	< 0.01
165	03-Aug	1	< 0.01	0.15	0.2	11	3.67	857.0	< 0.05	< 0.01
165	03-Aug	1	< 0.01	0.14	0.3	11	3.56	824.0	< 0.05	< 0.01
165	06-Aug	1	< 0.01	0.14	0.2	11	3.55	871.3	< 0.05	< 0.01
165	06-Aug	1	< 0.01	0.14	0.2	9	3.58	864.5	< 0.05	< 0.01
165-a	03-Aug	1	< 0.01	0.67	0.3	9	1.18	263.3	0.11	< 0.01
Control	21-Jul	1	< 0.01	< 0.02	0.1	3	0.39	119.0	< 0.05	< 0.01
Control	17-Jul	1	< 0.01	< 0.02	0.2	3	0.40	149.7	< 0.05	< 0.01
Control	17-Jul	1	< 0.01	< 0.02	0.2	3	0.41	149.6	< 0.05	< 0.01
Control	17-Jul	1	< 0.01	< 0.02	0.2	3	0.42	147.6	< 0.05	< 0.01
Control	17-Jul	1	< 0.01	< 0.02	0.2	3	0.40	155.4	< 0.05	< 0.01
Control	17-Jul	1	< 0.01	< 0.02	0.2	3	0.42	159.4	< 0.05	< 0.01
Control	18-Jul	1	< 0.01	< 0.02	0.1	3	0.40	148.1	< 0.05	< 0.01
Control	21-Jul	1	< 0.01	< 0.02	0.2	3	0.40	152.5	< 0.05	< 0.01
Control	28-Jul	1	< 0.01	< 0.02	0.2	3	0.38	158.2	< 0.05	< 0.01
Control	28-Jul	1	< 0.01	< 0.02	0.1	3	0.38	157.6	< 0.05	< 0.01
Control	03-Aug	1	< 0.01	< 0.02	0.2	3	0.43	166.2	< 0.05	< 0.01
Control	03-Aug	1	< 0.01	< 0.02	0.2	3	0.42	166.8	< 0.05	< 0.01
A4-1	20-Jul	1	0.17	< 0.02	< 0.1	7	1.79	807.6	0.24	< 0.01
A4-2	23-Jul	10	5.1	0.3	3	22	4.0	834	< 0.5	< 0.1
A4-3	23-Jul	1	< 0.01	< 0.02	0.2	6	0.17	83.4	< 0.05	< 0.01
A4-5	23-Jul	1	1.41	0.04	1.1	10	1.31	318.2	0.15	< 0.01
A4-6	23-Jul	1	0.23	0.05	0.2	12	0.85	370.0	< 0.05	< 0.01
Control	23-Jul	1	< 0.01	< 0.02	< 0.1	< 1	0.30	70.0	< 0.05	< 0.01
DIW blank	19-Jul	1	< 0.01	< 0.02	< 0.1	< 1	< 0.05	< 0.5	< 0.05	< 0.01
DIW blank	25-Jul	1	< 0.01	< 0.02	< 0.1	< 1	< 0.05	< 0.5	< 0.05	< 0.01
DIW blank	02-Aug	1	< 0.01	< 0.02	< 0.1	< 1	< 0.05	< 0.5	< 0.05	< 0.01
DIW blank	06-Aug	1	< 0.01	< 0.02	< 0.1	< 1	< 0.05	< 0.5	< 0.05	< 0.01
Acid blank	21-Jun	1	< 0.01	< 0.02	< 0.1	< 1	< 0.05	< 0.5	< 0.05	< 0.01
Acid blank	19-Jul	1	< 0.01	< 0.02	< 0.1	< 1	< 0.05	< 0.5	< 0.05	< 0.01
Acid blank	25-Jul	1	< 0.01	< 0.02	< 0.1	< 1	< 0.05	< 0.5	< 0.05	< 0.01
Acid blank	02-Aug	1	< 0.01	< 0.02	< 0.1	< 1	< 0.05	< 0.5	< 0.05	< 0.01
Acid blank	06-Aug	1	< 0.01	< 0.02	< 0.1	< 1	< 0.05	< 0.5	< 0.05	< 0.01
Travel blank	19-Jul	1	< 0.01	< 0.02	< 0.1	< 1	< 0.05	< 0.5	< 0.05	< 0.01
Travel blank	25-Jul	1	< 0.01	< 0.02	< 0.1	< 1	< 0.05	< 0.5	< 0.05	< 0.01

Travel blank	02-Aug	1	< 0.01	< 0.02	< 0.1	< 1	< 0.05	< 0.5	< 0.05	< 0.01
Travel blank	06-Aug	1	< 0.01	< 0.02	< 0.1	< 1	< 0.05	< 0.5	< 0.05	< 0.01
Repeats										
18	21-Jul	10	0.4	< 0.2	< 1	16	5.7	1133	< 0.5	< 0.1
18	21-Jul	10	0.4	< 0.2	< 1	16	5.6	1138	< 0.5	< 0.1
100	18-Jul	1	0.03	0.11	0.2	11	3.54	742.1	< 0.05	< 0.01
100	18-Jul	1	0.03	0.11	0.1	13	3.57	737.6	< 0.05	< 0.01
165	21-Jun	1	0.01	0.10	0.1	6	1.89	331.1	< 0.05	< 0.01
165	21-Jun	1	0.01	0.10	0.2	6	1.86	322.7	< 0.05	< 0.01
165	17-Jul	1	0.01	0.13	0.1	11	2.98	690.8	< 0.05	< 0.01
165	17-Jul	1	0.01	0.13	0.2	9	2.93	700.1	< 0.05	< 0.01
165	01-Aug	1	< 0.01	0.15	0.2	11	3.44	797.7	< 0.05	< 0.01
165	01-Aug	1	< 0.01	0.14	0.2	10	3.41	811.4	< 0.05	< 0.01
Control	17-Jul	1	< 0.01	< 0.02	0.2	3	0.40	155.4	< 0.05	< 0.01
Control	17-Jul	1	< 0.01	< 0.02	0.1	3	0.44	157.5	< 0.05	< 0.01
Acid blank	06-Aug	1	< 0.01	< 0.02	< 0.1	< 1	< 0.05	< 0.5	< 0.05	< 0.01
Acid blank	06-Aug	1	< 0.01	< 0.02	< 0.1	< 1	< 0.05	< 0.5	< 0.05	< 0.01
Controls										
BLANK		1	< 0.01	< 0.02	< 0.1	< 1	< 0.05	< 0.5	< 0.05	< 0.01
BLANK		1	< 0.01	< 0.02	< 0.1	< 1	< 0.05	< 0.5	< 0.05	< 0.01
BLANK		1	< 0.01	< 0.02	< 0.1	< 1	< 0.05	< 0.5	< 0.05	< 0.01
BLANK		1	< 0.01	< 0.02	< 0.1	< 1	< 0.05	< 0.5	< 0.05	< 0.01
BLANK		1	< 0.01	< 0.02	< 0.1	< 1	< 0.05	< 0.5	< 0.05	< 0.01
BLANK		1	< 0.01	< 0.02	< 0.1	< 1	< 0.05	< 0.5	< 0.05	< 0.01
BLANK		1	< 0.01	< 0.02	< 0.1	< 1	< 0.05	< 0.5	< 0.05	< 0.01
BLANK		1	< 0.01	< 0.02	0.2	< 1	< 0.05	< 0.5	< 0.05	< 0.01
SLRS-4		1	< 0.01	< 0.02	0.7	< 1	1.48	26.3	0.09	< 0.01

SLRS-4	1	0.01	< 0.02	0.7	< 1	1.47	25.9	0.10	< 0.01
SLRS-4	1	0.01	< 0.02	0.7	< 1	1.50	26.7	0.09	< 0.01
CERTIFIED				0.68 ± 0.06			26.3 ± 3.2		
TM-28.2	1	0.03	< 0.02	6.0	4	0.24	51.0	< 0.05	< 0.01
TM-28.2	1	0.03	< 0.02	5.6	3	0.23	47.3	< 0.05	< 0.01
CERTIFIED				5.8 ± 1.4	3.9 ± 0.83		50.5 ± 6.62		
INFORMATION									
TMDA-51.3	1	9.10	< 0.02	16.0	12	15.99	116.0	< 0.05	< 0.01
TMDA-51.3	1	8.83	< 0.02	15.9	13	16.29	115.1	< 0.05	< 0.01
CERTIFIED				15.7 ± 2.0	13.2 ± 2.3		119 ± 11		
INFORMATION		9.2				18.0			

ICP-MS		**Dilution**	**Mo**	**Ag**	**Cd**	**In**	**Sn**	**Sb**	**Te**	**Cs**
D.L.		**1**	0.05	0.005	0.02	0.01	0.01	0.01	0.02	0.01
D.L.		**10**	0.5	0.05	0.2	0.1	0.1	0.1	0.2	0.1
Distance (m)	**Date**									
0	20-Jul	10	< 0.5	< 0.05	1745.6	< 0.1	< 0.1	< 0.1	< 0.2	0.5
0	28-Jul	10	< 0.5	< 0.05	1302.3	< 0.1	< 0.1	< 0.1	< 0.2	0.4
0	03-Aug	10	< 0.5	< 0.05	1259.9	< 0.1	< 0.1	< 0.1	< 0.2	0.5
0	06-Aug	10	< 0.5	< 0.05	1450.6	< 0.1	< 0.1	< 0.1	< 0.2	0.9
10	19-Jul	10	< 0.5	< 0.05	2923.9	< 0.1	< 0.1	< 0.1	< 0.2	1.6
10	24-Jul	10	< 0.5	< 0.05	3741.6	< 0.1	< 0.1	< 0.1	< 0.2	1.8
10	03-Aug	10	0.5	< 0.05	4345.4	< 0.1	< 0.1	< 0.1	< 0.2	1.9
10	06-Aug	10	0.6	< 0.05	4560.5	< 0.1	< 0.1	< 0.1	< 0.2	1.8
18	Jul-19	10	< 0.5	< 0.05	571.0	< 0.1	< 0.1	< 0.1	< 0.2	0.3
18	Jul-19	10	< 0.5	< 0.05	570.1	< 0.1	< 0.1	< 0.1	< 0.2	0.3
18	Jul-20	10	< 0.5	< 0.05	605.3	< 0.1	< 0.1	< 0.1	< 0.2	0.4
18	Jul-21	10	< 0.5	< 0.05	618.5	< 0.1	< 0.1	< 0.1	< 0.2	0.4
18	Jul-24	10	< 0.5	< 0.05	717.8	< 0.1	< 0.1	< 0.1	< 0.2	0.4
18	Jul-28	10	< 0.5	< 0.05	717.9	< 0.1	< 0.1	< 0.1	< 0.2	0.4
18	Jul-28	10	< 0.5	< 0.05	720.8	< 0.1	< 0.1	< 0.1	< 0.2	0.4
18	Jul-28	10	< 0.5	< 0.05	719.6	< 0.1	0.2	< 0.1	< 0.2	0.5
18	Jul-30	10	< 0.5	< 0.05	676.0	< 0.1	< 0.1	< 0.1	< 0.2	0.4

18	Jul-30	10	< 0.5	< 0.05	675.9	< 0.1	< 0.1	< 0.1	< 0.2	0.4
18	Jul-30	10	< 0.5	< 0.05	680.8	< 0.1	< 0.1	< 0.1	< 0.2	0.4
18	03-Aug	10	< 0.5	< 0.05	694.4	< 0.1	< 0.1	< 0.1	< 0.2	0.4
18	06-Aug	10	< 0.5	< 0.05	747.4	< 0.1	< 0.1	< 0.1	< 0.2	0.5
40	Jul-19	10	< 0.5	< 0.05	443.0	< 0.1	< 0.1	< 0.1	< 0.2	0.3
40	Jul-19	10	< 0.5	< 0.05	447.4	< 0.1	< 0.1	< 0.1	< 0.2	0.3
40	Jul-20	10	1.1	< 0.05	490.0	< 0.1	0.2	0.2	< 0.2	0.3
40	Jul-21	10	< 0.5	< 0.05	501.6	< 0.1	< 0.1	0.2	< 0.2	0.3
40	Jul-24	10	0.5	< 0.05	567.8	< 0.1	< 0.1	< 0.1	< 0.2	0.3
40	Jul-28	10	0.6	< 0.05	591.9	< 0.1	< 0.1	< 0.1	< 0.2	0.3
40	Jul-28	10	0.6	< 0.05	608.2	< 0.1	< 0.1	< 0.1	< 0.2	0.3
40	Jul-28	10	< 0.5	< 0.05	615.1	< 0.1	< 0.1	< 0.1	< 0.2	0.4
40	Jul-30	10	< 0.5	< 0.05	580.9	< 0.1	< 0.1	< 0.1	< 0.2	0.3
40	Jul-30	10	0.5	< 0.05	579.1	< 0.1	< 0.1	< 0.1	< 0.2	0.3
40	Jul-30	10	< 0.5	< 0.05	547.1	< 0.1	< 0.1	< 0.1	< 0.2	0.3
40	03-Aug	10	< 0.5	< 0.05	594.6	< 0.1	< 0.1	< 0.1	< 0.2	0.4
40	03-Aug	10	0.6	< 0.05	598.3	< 0.1	< 0.1	< 0.1	< 0.2	0.4
40	06-Aug	10	< 0.5	< 0.05	620.2	< 0.1	< 0.1	< 0.1	< 0.2	0.4
100	17-Jul	1	0.29	0.016	240.98	< 0.01	< 0.01	0.13	< 0.02	0.18
100	17-Jul	1	0.28	0.015	234.91	< 0.01	< 0.01	0.13	< 0.02	0.15
100	17-Jul	1	0.35	0.017	247.82	< 0.01	< 0.01	0.14	< 0.02	0.17
100	18-Jul	1	0.31	0.015	253.10	< 0.01	< 0.01	0.13	< 0.02	0.17
100	18-Jul	1	0.33	0.014	257.60	< 0.01	0.02	0.13	< 0.02	0.17
100	18-Jul	1	0.36	0.015	260.72	< 0.01	< 0.01	0.14	< 0.02	0.17
100	21-Jul	1	0.38	0.012	336.59	< 0.01	< 0.01	0.12	< 0.02	0.18
100	24-Jul	1	0.42	0.015	383.63	< 0.01	< 0.01	0.11	< 0.02	0.22
100	Jul-28	1	0.41	0.012	401.74	< 0.01	< 0.01	0.09	< 0.02	0.24
100	Jul-28	1	0.40	0.011	397.03	< 0.01	< 0.01	0.09	< 0.02	0.21
100	Jul-28	1	0.42	0.016	402.68	< 0.01	< 0.01	0.10	< 0.02	0.26
100	Jul-30	1	0.37	0.014	403.44	< 0.01	< 0.01	0.10	< 0.02	0.23
100	Jul-30	1	0.27	0.012	372.27	< 0.01	< 0.01	0.08	< 0.02	0.20
100	01-Aug	1	0.34	0.015	407.34	< 0.01	< 0.01	0.09	< 0.02	0.25
100	01-Aug	1	0.33	0.015	405.29	< 0.01	< 0.01	0.09	< 0.02	0.25
100	03-Aug	1	0.35	0.014	423.98	< 0.01	< 0.01	0.08	< 0.02	0.26
100	06-Aug	1	0.37	0.015	440.36	< 0.01	< 0.01	0.08	< 0.02	0.29
120	24-Jul	1	1.03	0.011	250.42	< 0.01	< 0.01	0.15	< 0.02	0.16
120	Jul-28	1	1.00	0.008	283.33	< 0.01	< 0.01	0.16	< 0.02	0.15

120	Jul-28	1	1.17	0.008	289.21	< 0.01	< 0.01	0.17	< 0.02	0.16
120	Jul-28	1	1.31	0.011	264.19	< 0.01	< 0.01	0.17	< 0.02	0.17
120	Jul-30	1	1.00	0.009	285.60	< 0.01	< 0.01	0.15	< 0.02	0.16
120	Jul-30	1	1.03	0.008	285.95	< 0.01	< 0.01	0.16	< 0.02	0.16
120	Jul-30	1	1.01	0.009	279.99	< 0.01	< 0.01	0.15	< 0.02	0.14
120	03-Aug	1	1.27	0.010	295.09	< 0.01	< 0.01	0.17	< 0.02	0.18
120	06-Aug	1	1.00	0.010	299.19	< 0.01	< 0.01	0.17	< 0.02	0.18
165	21-Jun	1	1.09	0.011	62.85	< 0.01	< 0.01	0.17	< 0.02	0.06
165	17-Jul	1	0.68	0.013	180.98	< 0.01	< 0.01	0.16	< 0.02	0.12
165	17-Jul	1	0.62	0.012	176.94	< 0.01	< 0.01	0.16	< 0.02	0.12
165	17-Jul	1	0.74	0.011	167.02	< 0.01	< 0.01	0.16	< 0.02	0.12
165	17-Jul	1	0.61	0.010	186.69	< 0.01	< 0.01	0.15	< 0.02	0.26
165	17-Jul	1	0.68	0.009	184.41	< 0.01	< 0.01	0.15	< 0.02	0.12
165	18-Jul	1	0.76	0.009	197.70	< 0.01	< 0.01	0.15	< 0.02	0.12
165	21-Jul	1	0.81	0.007	223.86	< 0.01	0.02	0.16	< 0.02	0.13
165	24-Jul	1	0.95	0.009	219.16	< 0.01	< 0.01	0.16	< 0.02	0.13
165	28-Jul	1	0.97	0.007	244.23	< 0.01	< 0.01	0.16	< 0.02	0.15
165	Jul-28	1	1.00	0.006	240.61	< 0.01	< 0.01	0.15	< 0.02	0.15
165	Jul-28	1	1.14	0.010	232.56	< 0.01	< 0.01	0.17	< 0.02	0.15
165	Jul-30	1	0.92	0.008	243.87	< 0.01	< 0.01	0.16	< 0.02	0.15
165	Jul-30	1	0.87	0.007	245.49	< 0.01	< 0.01	0.16	< 0.02	0.18
165	Jul-30	1	1.08	0.007	242.13	< 0.01	< 0.01	0.15	< 0.02	0.12
165	01-Aug	1	1.07	0.007	243.99	< 0.01	< 0.01	0.16	< 0.02	0.15
165	01-Aug	1	1.07	0.008	248.42	< 0.01	< 0.01	0.16	< 0.02	0.15
165	01-Aug	1	1.19	0.008	251.23	< 0.01	< 0.01	0.16	< 0.02	0.14
165	01-Aug	1	1.04	0.007	247.41	< 0.01	< 0.01	0.16	< 0.02	0.14
165	03-Aug	1	1.07	0.009	247.90	< 0.01	< 0.01	0.17	< 0.02	0.18
165	03-Aug	1	1.13	0.009	246.32	< 0.01	< 0.01	0.17	< 0.02	0.16
165	06-Aug	1	0.99	0.007	259.28	< 0.01	< 0.01	0.16	< 0.02	0.16
165	06-Aug	1	0.91	0.008	258.14	< 0.01	< 0.01	0.15	< 0.02	0.15
165-a	03-Aug	1	21.12	< 0.005	7.91	< 0.01	< 0.01	0.81	< 0.02	< 0.01
Control	21-Jul	1	1.18	< 0.005	0.63	< 0.01	< 0.01	0.12	< 0.02	< 0.01
Control	17-Jul	1	1.42	< 0.005	1.02	< 0.01	< 0.01	0.13	< 0.02	< 0.01
Control	17-Jul	1	1.43	< 0.005	0.98	< 0.01	< 0.01	0.13	< 0.02	< 0.01
Control	17-Jul	1	1.41	< 0.005	1.01	< 0.01	< 0.01	0.16	< 0.02	< 0.01
Control	17-Jul	1	1.51	< 0.005	1.08	< 0.01	< 0.01	0.13	< 0.02	< 0.01
Control	17-Jul	1	1.47	< 0.005	1.06	< 0.01	< 0.01	0.13	< 0.02	< 0.01

Control	18-Jul	1	1.37	< 0.005	1.05	< 0.01	< 0.01	0.13	< 0.02	< 0.01
Control	21-Jul	1	1.40	< 0.005	0.99	< 0.01	< 0.01	0.12	< 0.02	< 0.01
Control	28-Jul	1	1.41	< 0.005	1.05	< 0.01	< 0.01	0.12	< 0.02	< 0.01
Control	28-Jul	1	1.41	< 0.005	1.03	< 0.01	< 0.01	0.12	< 0.02	< 0.01
Control	03-Aug	1	1.47	< 0.005	1.14	< 0.01	< 0.01	0.13	< 0.02	< 0.01
Control	03-Aug	1	1.44	< 0.005	1.13	< 0.01	< 0.01	0.13	< 0.02	< 0.01
A4-1	20-Jul	1	0.31	0.291	60.37	0.05	0.01	0.07	< 0.02	0.03
A4-2	23-Jul	10	1.2	0.43	213.7	1.0	< 0.1	< 0.1	< 0.2	0.6
A4-3	23-Jul	1	5.90	< 0.005	12.76	< 0.01	< 0.01	0.61	< 0.02	< 0.01
A4-5	23-Jul	1	4.02	0.121	73.62	0.30	< 0.01	0.38	< 0.02	0.14
A4-6	23-Jul	1	0.10	0.098	126.53	0.04	0.01	0.23	< 0.02	0.03
Control	23-Jul	1	0.09	< 0.005	0.10	< 0.01	< 0.01	0.10	< 0.02	< 0.01
DIW blank	19-Jul	1	< 0.05	< 0.005	< 0.02	< 0.01	0.01	< 0.01	< 0.02	< 0.01
DIW blank	25-Jul	1	< 0.05	< 0.005	< 0.02	< 0.01	< 0.01	< 0.01	< 0.02	< 0.01
DIW blank	02-Aug	1	0.09	< 0.005	< 0.02	< 0.01	< 0.01	< 0.01	< 0.02	< 0.01
DIW blank	06-Aug	1	< 0.05	< 0.005	< 0.02	< 0.01	< 0.01	< 0.01	< 0.02	< 0.01
Acid blank	21-Jun	1	< 0.05	< 0.005	< 0.02	< 0.01	< 0.01	< 0.01	< 0.02	< 0.01
Acid blank	19-Jul	1	< 0.05	< 0.005	< 0.02	< 0.01	< 0.01	< 0.01	< 0.02	< 0.01
Acid blank	25-Jul	1	< 0.05	< 0.005	< 0.02	< 0.01	< 0.01	< 0.01	< 0.02	< 0.01
Acid blank	02-Aug	1	< 0.05	< 0.005	< 0.02	< 0.01	< 0.01	< 0.01	< 0.02	< 0.01
Acid blank	06-Aug	1	< 0.05	< 0.005	< 0.02	< 0.01	< 0.01	< 0.01	< 0.02	< 0.01
Travel blank	19-Jul	1	< 0.05	< 0.005	< 0.02	< 0.01	0.01	< 0.01	< 0.02	< 0.01
Travel blank	25-Jul	1	< 0.05	< 0.005	< 0.02	< 0.01	< 0.01	< 0.01	< 0.02	< 0.01
Travel blank	02-Aug	1	< 0.05	< 0.005	< 0.02	< 0.01	< 0.01	< 0.01	< 0.02	< 0.01
Travel blank	06-Aug	1	< 0.05	< 0.005	< 0.02	< 0.01	< 0.01	< 0.01	< 0.02	< 0.01
Repeats										
18	21-Jul	10	< 0.5	< 0.05	618.5	< 0.1	< 0.1	< 0.1	< 0.2	0.4
18	21-Jul	10	< 0.5	< 0.05	615.1	< 0.1	< 0.1	< 0.1	< 0.2	0.4
100	18-Jul	1	0.36	0.015	260.72	< 0.01	< 0.01	0.14	< 0.02	0.17
100	18-Jul	1	0.36	0.014	261.14	< 0.01	< 0.01	0.14	< 0.02	0.16
165	21-Jun	1	1.09	0.011	62.85	< 0.01	< 0.01	0.17	< 0.02	0.06
165	21-Jun	1	1.09	0.012	62.19	< 0.01	< 0.01	0.17	< 0.02	0.06

165	17-Jul	1	0.61	0.010	186.69	< 0.01	< 0.01	0.15	< 0.02	0.26
165	17-Jul	1	0.59	0.010	187.47	< 0.01	< 0.01	0.14	< 0.02	0.12
165	01-Aug	1	1.19	0.008	251.23	< 0.01	< 0.01	0.16	< 0.02	0.14
165	01-Aug	1	1.18	0.008	246.99	< 0.01	< 0.01	0.16	< 0.02	0.15
Control	17-Jul	1	1.51	< 0.005	1.08	< 0.01	< 0.01	0.13	< 0.02	< 0.01
Control	17-Jul	1	1.35	< 0.005	1.08	< 0.01	< 0.01	0.13	< 0.02	< 0.01
Acid blank	06-Aug	1	< 0.05	< 0.005	< 0.02	< 0.01	< 0.01	< 0.01	< 0.02	< 0.01
Acid blank	06-Aug	1	< 0.05	< 0.005	< 0.02	< 0.01	< 0.01	< 0.01	< 0.02	< 0.01
Controls										
BLANK		1	< 0.05	< 0.005	< 0.02	< 0.01	< 0.01	< 0.01	< 0.02	< 0.01
BLANK		1	< 0.05	< 0.005	< 0.02	< 0.01	< 0.01	< 0.01	< 0.02	< 0.01
BLANK		1	< 0.05	< 0.005	< 0.02	< 0.01	< 0.01	< 0.01	< 0.02	< 0.01
BLANK		1	< 0.05	< 0.005	< 0.02	< 0.01	< 0.01	< 0.01	< 0.02	< 0.01
BLANK		1	< 0.05	< 0.005	< 0.02	< 0.01	< 0.01	< 0.01	< 0.02	< 0.01
BLANK		1	< 0.05	< 0.005	< 0.02	< 0.01	< 0.01	< 0.01	< 0.02	< 0.01
BLANK		1	< 0.05	< 0.005	< 0.02	< 0.01	< 0.01	< 0.01	< 0.02	< 0.01
BLANK		1	< 0.05	< 0.005	0.03	< 0.01	< 0.01	< 0.01	< 0.02	< 0.01
SLRS-4		1	0.20	< 0.005	< 0.02	< 0.01	< 0.01	0.25	< 0.02	< 0.01
SLRS-4		1	0.20	< 0.005	< 0.02	< 0.01	< 0.01	0.25	< 0.02	< 0.01
SLRS-4		1	0.20	< 0.005	< 0.02	< 0.01	< 0.01	0.26	< 0.02	0.01
CERTIFIED			0.21 ± 0.02		0.012 ± 0.002			0.23 ± 0.04		
TM-28.2		1	4.35	2.700	1.42	< 0.01	4.27	3.28	< 0.02	< 0.01
TM-28.2		1	4.09	2.735	1.36	< 0.01	4.04	3.13	< 0.02	< 0.01
CERTIFIED			4.1 ± 1.4		1.3 ± 0.44			3.1 ± 0.74		
INFORMATION				3.30						
TMDA-51.3		1	57.36	12.746	26.11	< 0.01	17.66	14.33	< 0.02	< 0.01
TMDA-51.3		1	57.61	13.208	26.50	< 0.01	17.38	14.38	< 0.02	< 0.01
CERTIFIED			58.4 ± 5.5	13.2 ± 1.4	25.8 ± 2.5		18.4 ± 2.0	13.8 ± 3.1		
INFORMATION										

ICP-MS (ppb)		Dilution	La	Ce	Pr	Nd	Sm	Eu	Tb	Gd
D.L.		**1**	0.01	0.01	0.005	0.005	0.005	0.005	0.005	0.005
D.L.		**10**	0.1	0.1	0.05	0.05	0.05	0.05	0.05	0.05
Distance (m)	**Date**									
0	20-Jul	10	56.1	250.8	61.65	413.24	177.25	56.96	51.89	333.95
0	28-Jul	10	39.6	175.8	43.28	289.02	127.18	41.58	37.84	246.49
0	03-Aug	10	40.1	178.0	43.13	286.67	125.65	40.79	37.29	246.27
0	06-Aug	10	45.8	203.4	49.21	333.85	145.82	47.01	42.45	276.53
10	19-Jul	10	40.6	150.3	40.64	273.39	124.70	40.25	36.67	237.46
10	24-Jul	10	43.4	155.9	43.26	290.03	132.30	43.19	39.97	255.77
10	03-Aug	10	49.0	178.9	50.39	342.41	155.89	51.58	47.72	305.82
10	06-Aug	10	50.8	183.3	51.54	352.17	159.07	52.97	49.50	313.79
18	Jul-19	10	13.3	54.9	12.92	83.50	35.23	11.34	9.94	65.24
18	Jul-19	10	13.4	54.8	12.76	83.47	34.96	11.23	9.92	65.18
18	Jul-20	10	14.5	60.9	14.27	92.22	39.11	12.53	11.19	73.36
18	Jul-21	10	14.9	63.3	14.89	96.26	40.42	13.02	11.65	76.07
18	Jul-24	10	17.6	75.1	17.87	116.26	49.29	15.75	14.00	93.80
18	Jul-28	10	17.5	74.7	17.91	114.71	49.51	15.99	14.23	94.03
18	Jul-28	10	17.4	74.9	17.89	115.92	49.00	15.99	14.23	92.87
18	Jul-28	10	17.9	76.0	18.22	118.03	49.77	16.44	14.46	95.13
18	Jul-30	10	15.9	70.2	16.65	108.03	46.03	14.86	13.14	86.54
18	Jul-30	10	15.9	70.7	16.65	108.81	46.43	14.97	13.39	87.73
18	Jul-30	10	16.0	70.6	16.81	109.23	46.63	15.03	13.46	87.47
18	03-Aug	10	16.0	69.2	16.22	106.17	44.99	14.51	12.96	84.84
18	06-Aug	10	17.4	73.9	17.43	112.99	48.55	15.69	14.09	92.96
40	Jul-19	10	10.5	42.0	9.70	62.87	26.38	8.48	7.42	49.10
40	Jul-19	10	10.6	42.0	9.71	63.31	26.55	8.51	7.46	49.40
40	Jul-20	10	11.8	48.0	11.13	72.62	30.79	9.83	8.61	57.72
40	Jul-21	10	12.0	49.6	11.59	75.85	32.18	10.38	9.18	60.15
40	Jul-24	10	13.8	57.9	13.56	88.18	37.33	12.04	10.73	70.12
40	Jul-28	10	14.0	59.6	13.90	91.75	38.74	12.50	11.23	73.35
40	Jul-28	10	14.4	60.5	14.21	93.29	39.93	12.72	11.36	73.50
40	Jul-28	10	14.6	62.5	14.66	96.46	40.83	13.11	11.61	75.84
40	Jul-30	10	13.9	59.0	13.92	90.83	38.45	12.39	10.97	71.66

40	Jul-30	10	13.9	58.9	13.73	90.93	38.29	12.34	10.97	71.95
40	Jul-30	10	12.9	54.8	12.73	84.27	36.03	11.63	10.33	67.93
40	03-Aug	10	13.8	58.0	13.52	88.95	37.67	12.09	10.75	70.86
40	03-Aug	10	13.9	57.9	13.61	89.27	37.89	12.11	10.90	70.80
40	06-Aug	10	14.2	59.6	14.07	91.66	38.55	12.51	11.11	72.73
100	17-Jul	1	5.57	22.47	4.280	27.021	11.044	3.563	3.071	20.593
100	17-Jul	1	5.37	19.67	4.401	27.802	11.353	3.636	3.120	21.074
100	17-Jul	1	5.73	21.45	4.756	30.279	12.373	3.977	3.384	22.727
100	18-Jul	1	6.03	22.33	5.053	32.318	13.231	4.258	3.642	24.470
100	18-Jul	1	5.97	22.38	5.101	32.346	13.194	4.253	3.636	24.383
100	18-Jul	1	6.16	23.70	5.421	34.648	14.209	4.539	3.919	26.118
100	21-Jul	1	8.46	33.79	7.793	50.849	20.354	6.688	5.744	38.307
100	24-Jul	1	9.54	39.61	8.768	58.944	24.078	7.871	6.758	45.284
100	Jul-28	1	9.63	40.25	9.144	59.665	24.671	7.988	6.866	45.653
100	Jul-28	1	9.53	40.03	8.767	58.117	24.119	7.851	6.713	44.763
100	Jul-28	1	9.85	41.20	8.974	60.386	25.027	8.094	6.981	46.575
100	Jul-30	1	9.82	40.87	7.918	61.502	25.239	8.221	7.073	47.286
100	Jul-30	1	9.13	38.01	8.766	58.264	23.870	7.802	6.714	44.774
100	01-Aug	1	9.70	40.03	8.646	58.453	24.073	7.828	6.719	44.834
100	01-Aug	1	9.76	40.37	8.953	58.678	24.268	7.923	6.770	45.134
100	03-Aug	1	9.98	41.03	9.195	61.152	25.345	8.215	7.094	47.109
100	06-Aug	1	10.35	41.88	9.520	62.477	25.830	8.361	7.158	47.529
120	24-Jul	1	6.06	24.97	5.804	38.309	15.657	5.080	4.483	29.977
120	Jul-28	1	6.84	28.29	6.422	41.948	17.149	5.581	4.927	32.889
120	Jul-28	1	6.97	28.42	6.433	41.624	17.175	5.576	4.888	32.668
120	Jul-28	1	6.42	26.52	6.242	40.954	16.786	5.414	4.778	31.881
120	Jul-30	1	6.73	27.85	6.394	42.308	17.275	5.612	4.950	33.033
120	Jul-30	1	6.90	28.55	6.311	41.244	16.916	5.509	4.858	32.392
120	Jul-30	1	6.58	27.48	6.277	41.377	16.763	5.470	4.832	32.222
120	03-Aug	1	7.00	28.22	6.375	41.823	17.007	5.558	4.892	32.707
120	06-Aug	1	7.08	28.74	6.533	42.515	17.584	5.673	5.042	33.679
165	21-Jun	1	1.62	5.13	1.043	6.457	2.128	0.670	0.631	4.448
165	17-Jul	1	4.07	14.69	3.202	20.521	8.423	2.667	2.350	15.721
165	17-Jul	1	4.01	14.95	3.300	20.994	8.658	2.709	2.397	16.138
165	17-Jul	1	3.83	14.43	3.205	20.427	8.311	2.629	2.307	15.520
165	17-Jul	1	4.24	15.94	3.490	22.256	9.170	2.913	2.583	17.183
165	17-Jul	1	4.21	15.98	3.504	22.353	9.148	2.913	2.549	17.136

165	18-Jul	1	4.55	16.78	3.678	23.464	9.669	3.068	2.733	18.291
165	21-Jul	1	5.41	21.17	4.887	31.759	13.159	4.250	3.822	25.332
165	24-Jul	1	5.29	20.65	4.781	31.335	12.960	4.169	3.752	24.983
165	28-Jul	1	5.64	22.80	5.286	35.020	14.417	4.623	4.164	27.757
165	Jul-28	1	5.55	22.39	5.229	34.276	14.144	4.553	4.063	27.263
165	Jul-28	1	5.51	21.75	5.058	33.235	13.739	4.410	3.935	26.373
165	Jul-30	1	5.80	23.48	5.526	36.261	14.974	4.800	4.320	29.042
165	Jul-30	1	5.78	22.65	5.254	34.607	14.399	4.670	4.198	28.205
165	Jul-30	1	5.58	22.37	5.230	34.228	14.114	4.564	4.094	27.441
165	01-Aug	1	5.73	22.34	5.153	33.941	14.006	4.538	4.103	27.264
165	01-Aug	1	5.71	23.27	5.457	35.642	14.638	4.726	4.258	28.551
165	01-Aug	1	5.70	23.05	5.397	35.352	14.606	4.730	4.223	28.310
165	01-Aug	1	5.64	22.76	5.290	34.809	14.422	4.651	4.171	27.849
165	03-Aug	1	5.87	22.70	5.322	34.532	14.266	4.594	4.123	27.790
165	03-Aug	1	5.70	22.63	5.296	34.634	14.297	4.585	4.086	27.640
165	06-Aug	1	5.90	23.56	5.492	35.767	14.740	4.761	4.247	28.531
165	06-Aug	1	5.84	23.25	5.382	35.326	14.483	4.691	4.185	28.026
165-a	03-Aug	1	< 0.01	< 0.01	< 0.005	0.014	< 0.005	< 0.005	< 0.005	0.006
Control	21-Jul	1	0.01	0.02	< 0.005	0.017	0.006	< 0.005	< 0.005	0.008
Control	17-Jul	1	< 0.01	< 0.01	< 0.005	0.007	< 0.005	< 0.005	< 0.005	< 0.005
Control	17-Jul	1	< 0.01	< 0.01	< 0.005	0.008	< 0.005	< 0.005	< 0.005	< 0.005
Control	17-Jul	1	< 0.01	< 0.01	< 0.005	0.007	< 0.005	< 0.005	< 0.005	< 0.005
Control	17-Jul	1	< 0.01	< 0.01	< 0.005	0.007	< 0.005	< 0.005	< 0.005	< 0.005
Control	17-Jul	1	< 0.01	< 0.01	< 0.005	0.007	< 0.005	< 0.005	< 0.005	< 0.005
Control	18-Jul	1	< 0.01	< 0.01	< 0.005	0.007	< 0.005	< 0.005	< 0.005	< 0.005
Control	21-Jul	1	< 0.01	< 0.01	< 0.005	0.007	< 0.005	< 0.005	< 0.005	< 0.005
Control	28-Jul	1	< 0.01	< 0.01	< 0.005	0.007	< 0.005	< 0.005	< 0.005	< 0.005
Control	28-Jul	1	< 0.01	< 0.01	< 0.005	0.008	< 0.005	< 0.005	< 0.005	< 0.005
Control	03-Aug	1	< 0.01	< 0.01	< 0.005	0.008	< 0.005	< 0.005	< 0.005	< 0.005
Control	03-Aug	1	< 0.01	< 0.01	< 0.005	0.008	< 0.005	< 0.005	< 0.005	< 0.005
A4-1	20-Jul	1	53.69	135.02	25.274	143.160	57.757	16.598	11.993	89.389
A4-2	23-Jul	10	67.2	161.0	31.07	172.46	76.81	22.57	16.38	117.79
A4-3	23-Jul	1	0.05	0.05	0.008	0.042	0.011	< 0.005	< 0.005	0.020
A4-5	23-Jul	1	21.19	50.72	8.531	54.859	23.783	6.933	4.939	35.789
A4-6	23-Jul	1	18.11	22.43	5.032	26.365	9.302	2.758	2.255	16.447
Control	23-Jul	1	< 0.01	< 0.01	< 0.005	0.009	< 0.005	< 0.005	< 0.005	< 0.005

DIW blank	19-Jul	1	< 0.01	< 0.01	< 0.005	< 0.005	< 0.005	< 0.005	< 0.005	< 0.005
DIW blank	25-Jul	1	< 0.01	< 0.01	< 0.005	< 0.005	< 0.005	< 0.005	< 0.005	< 0.005
DIW blank	02-Aug	1	< 0.01	< 0.01	< 0.005	< 0.005	< 0.005	< 0.005	< 0.005	< 0.005
DIW blank	06-Aug	1	< 0.01	< 0.01	< 0.005	< 0.005	< 0.005	< 0.005	< 0.005	< 0.005
Acid blank	21-Jun	1	< 0.01	< 0.01	< 0.005	< 0.005	< 0.005	< 0.005	< 0.005	< 0.005
Acid blank	19-Jul	1	< 0.01	< 0.01	< 0.005	< 0.005	< 0.005	< 0.005	< 0.005	< 0.005
Acid blank	25-Jul	1	< 0.01	< 0.01	< 0.005	< 0.005	< 0.005	< 0.005	< 0.005	< 0.005
Acid blank	02-Aug	1	< 0.01	< 0.01	< 0.005	< 0.005	< 0.005	< 0.005	< 0.005	< 0.005
Acid blank	06-Aug	1	< 0.01	< 0.01	< 0.005	< 0.005	< 0.005	< 0.005	< 0.005	< 0.005
Travel blank	19-Jul	1	< 0.01	< 0.01	< 0.005	< 0.005	< 0.005	< 0.005	< 0.005	< 0.005
Travel blank	25-Jul	1	< 0.01	< 0.01	< 0.005	< 0.005	< 0.005	< 0.005	< 0.005	< 0.005
Travel blank	02-Aug	1	< 0.01	< 0.01	< 0.005	< 0.005	< 0.005	< 0.005	< 0.005	< 0.005
Travel blank	06-Aug	1	< 0.01	< 0.01	< 0.005	< 0.005	< 0.005	< 0.005	< 0.005	< 0.005
Repeats										
18	21-Jul	10	14.9	63.3	14.89	96.26	40.42	13.02	11.65	76.07
18	21-Jul	10	14.9	63.5	14.90	96.92	40.82	13.08	11.68	76.38
100	18-Jul	1	6.16	23.70	5.421	34.648	14.209	4.539	3.919	26.118
100	18-Jul	1	6.31	23.78	5.449	34.746	14.245	4.573	3.904	26.313
165	21-Jun	1	1.62	5.13	1.043	6.457	2.128	0.670	0.631	4.448
165	21-Jun	1	1.59	5.16	1.059	6.525	2.132	0.668	0.623	4.434
165	17-Jul	1	4.24	15.94	3.490	22.256	9.170	2.913	2.583	17.183
165	17-Jul	1	4.29	15.66	3.444	21.998	9.029	2.868	2.528	16.998
165	01-Aug	1	5.70	23.05	5.397	35.352	14.606	4.730	4.223	28.310
165	01-Aug	1	5.78	23.21	5.403	35.402	14.669	4.712	4.224	28.439
Control	17-Jul	1	< 0.01	< 0.01	< 0.005	0.007	< 0.005	< 0.005	< 0.005	< 0.005
Control	17-Jul	1	< 0.01	< 0.01	< 0.005	0.007	< 0.005	< 0.005	< 0.005	< 0.005
Acid blank	06-Aug	1	< 0.01	< 0.01	< 0.005	< 0.005	< 0.005	< 0.005	< 0.005	< 0.005
Acid blank	06-Aug	1	< 0.01	< 0.01	< 0.005	< 0.005	< 0.005	< 0.005	< 0.005	< 0.005

Controls									
BLANK	1	< 0.01	< 0.01	< 0.005	< 0.005	< 0.005	< 0.005	< 0.005	< 0.005
BLANK	1	< 0.01	< 0.01	< 0.005	< 0.005	< 0.005	< 0.005	< 0.005	< 0.005
BLANK	1	< 0.01	< 0.01	< 0.005	< 0.005	< 0.005	< 0.005	< 0.005	< 0.005
BLANK	1	< 0.01	< 0.01	< 0.005	< 0.005	< 0.005	< 0.005	< 0.005	< 0.005
BLANK	1	< 0.01	< 0.01	< 0.005	< 0.005	< 0.005	< 0.005	< 0.005	< 0.005
BLANK	1	< 0.01	< 0.01	< 0.005	< 0.005	< 0.005	< 0.005	< 0.005	< 0.005
BLANK	1	< 0.01	< 0.01	< 0.005	< 0.005	< 0.005	< 0.005	< 0.005	< 0.005
BLANK	1	< 0.01	< 0.01	< 0.005	0.005	< 0.005	< 0.005	< 0.005	< 0.005
SLRS-4	1	0.28	0.36	0.069	0.272	0.057	0.008	< 0.005	0.034
SLRS-4	1	0.28	0.36	0.069	0.268	0.060	0.008	< 0.005	0.035
SLRS-4	1	0.29	0.36	0.070	0.268	0.057	0.008	< 0.005	0.035
CERTIFIED									
TM-28.2	1	< 0.01	< 0.01	< 0.005	< 0.005	< 0.005	< 0.005	< 0.005	< 0.005
TM-28.2	1	< 0.01	< 0.01	< 0.005	< 0.005	< 0.005	< 0.005	< 0.005	< 0.005
CERTIFIED INFORMATION									
TMDA-51.3	1	< 0.01	< 0.01	< 0.005	< 0.005	< 0.005	< 0.005	< 0.005	< 0.005
TMDA-51.3	1	< 0.01	< 0.01	< 0.005	< 0.005	< 0.005	< 0.005	< 0.005	< 0.005
CERTIFIED INFORMATION									

ICP-MS (ppb)		**Dilution**	**Dy**	**Ho**	**Er**	**Tm**	**Yb**	**Lu**	**Hf**	**Ta**
D.L.		**1**	0.005	0.005	0.005	0.005	0.005	0.005	0.01	0.01
D.L.		**10**	0.05	0.05	0.05	0.05	0.05	0.05	0.1	0.1
Distance (m)	**Date**									
0	20-Jul	10	308.67	61.49	164.21	21.39	123.32	18.62	< 0.1	< 0.1
0	28-Jul	10	226.03	44.89	119.40	15.44	90.30	13.54	< 0.1	< 0.1
0	03-Aug	10	222.70	44.65	116.39	15.03	88.89	13.14	< 0.1	< 0.1
0	06-Aug	10	250.11	50.31	132.59	16.95	99.93	15.07	< 0.1	< 0.1
10	19-Jul	10	219.95	44.77	122.26	16.76	104.50	16.58	< 0.1	< 0.1

10	24-Jul	10	238.29	48.86	134.35	18.39	113.46	18.26	< 0.1	< 0.1
10	03-Aug	10	292.31	59.33	162.88	22.71	141.13	22.74	< 0.1	< 0.1
10	06-Aug	10	300.86	62.31	171.92	23.49	147.40	23.78	< 0.1	< 0.1
18	Jul-19	10	58.55	11.66	31.34	4.09	24.98	3.85	< 0.1	< 0.1
18	Jul-19	10	59.28	11.70	31.04	4.13	24.91	3.85	< 0.1	< 0.1
18	Jul-20	10	66.73	13.18	35.12	4.62	28.27	4.36	< 0.1	< 0.1
18	Jul-21	10	69.17	13.74	37.08	4.88	29.56	4.61	< 0.1	< 0.1
18	Jul-24	10	84.26	16.94	45.06	5.97	36.54	5.61	< 0.1	< 0.1
18	Jul-28	10	83.45	16.74	44.68	5.90	36.08	5.44	< 0.1	< 0.1
18	Jul-28	10	84.18	16.62	45.10	6.04	36.59	5.58	< 0.1	< 0.1
18	Jul-28	10	85.03	17.00	45.94	5.94	36.54	5.65	< 0.1	< 0.1
18	Jul-30	10	78.94	15.62	41.85	5.46	33.59	5.20	< 0.1	< 0.1
18	Jul-30	10	80.11	15.79	42.32	5.49	33.69	5.17	< 0.1	< 0.1
18	Jul-30	10	79.64	15.87	42.39	5.59	33.92	5.21	< 0.1	< 0.1
18	03-Aug	10	77.66	15.41	41.34	5.43	33.39	5.15	< 0.1	< 0.1
18	06-Aug	10	82.97	16.57	44.62	5.75	35.13	5.44	< 0.1	< 0.1
40	Jul-19	10	43.78	8.75	23.20	3.14	18.96	2.91	< 0.1	< 0.1
40	Jul-19	10	44.40	8.86	23.60	3.12	19.08	2.90	< 0.1	< 0.1
40	Jul-20	10	51.57	10.28	28.03	3.62	22.04	3.35	< 0.1	< 0.1
40	Jul-21	10	54.37	10.76	28.92	3.78	23.11	3.51	< 0.1	< 0.1
40	Jul-24	10	63.90	12.74	34.19	4.47	27.10	4.14	< 0.1	< 0.1
40	Jul-28	10	66.31	13.15	35.11	4.62	27.93	4.32	< 0.1	< 0.1
40	Jul-28	10	67.84	13.26	35.77	4.68	28.11	4.42	< 0.1	< 0.1
40	Jul-28	10	69.82	13.65	36.42	4.79	29.10	4.49	< 0.1	< 0.1
40	Jul-30	10	65.49	13.10	35.11	4.55	27.72	4.26	< 0.1	< 0.1
40	Jul-30	10	65.41	12.92	34.60	4.56	27.54	4.21	< 0.1	< 0.1
40	Jul-30	10	61.55	12.17	32.62	4.30	26.07	3.97	< 0.1	< 0.1
40	03-Aug	10	64.42	12.68	34.19	4.47	27.32	4.22	< 0.1	< 0.1
40	03-Aug	10	65.23	12.80	34.38	4.48	27.51	4.27	< 0.1	< 0.1
40	06-Aug	10	66.46	13.14	34.94	4.61	28.40	4.35	< 0.1	< 0.1
100	17-Jul	1	18.024	3.599	9.588	1.229	7.470	1.142	< 0.01	< 0.01
100	17-Jul	1	18.463	3.677	9.765	1.262	7.707	1.179	< 0.01	< 0.01
100	17-Jul	1	19.842	3.951	10.517	1.355	8.290	1.266	< 0.01	< 0.01
100	18-Jul	1	21.483	4.259	11.367	1.461	8.905	1.360	< 0.01	< 0.01
100	18-Jul	1	21.434	4.255	11.365	1.468	8.901	1.352	< 0.01	< 0.01
100	18-Jul	1	22.913	4.564	12.150	1.566	9.536	1.453	< 0.01	< 0.01
100	21-Jul	1	34.608	6.753	18.041	2.311	14.196	2.146	< 0.01	< 0.01

100	24-Jul	1	40.482	7.943	21.192	2.710	16.695	2.494	< 0.01	< 0.01
100	Jul-28	1	40.763	8.066	21.548	2.742	17.030	2.548	< 0.01	< 0.01
100	Jul-28	1	39.816	7.910	21.085	2.694	16.649	2.478	< 0.01	< 0.01
100	Jul-28	1	41.529	8.234	21.954	2.804	17.366	2.604	< 0.01	< 0.01
100	Jul-30	1	42.172	8.361	22.176	2.829	17.441	2.604	< 0.01	< 0.01
100	Jul-30	1	40.071	7.898	21.006	2.683	16.424	2.461	< 0.01	< 0.01
100	01-Aug	1	39.974	7.919	21.042	2.680	16.586	2.483	< 0.01	< 0.01
100	01-Aug	1	40.143	7.950	21.133	2.696	16.644	2.497	< 0.01	< 0.01
100	03-Aug	1	41.943	8.291	22.143	2.824	17.529	2.630	< 0.01	< 0.01
100	06-Aug	1	42.565	8.374	22.429	2.869	17.764	2.686	< 0.01	< 0.01
120	24-Jul	1	26.806	5.299	14.161	1.827	11.051	1.688	< 0.01	< 0.01
120	Jul-28	1	29.613	5.841	15.555	2.004	12.122	1.839	< 0.01	< 0.01
120	Jul-28	1	29.370	5.796	15.446	1.989	12.056	1.841	< 0.01	< 0.01
120	Jul-28	1	28.800	5.682	15.093	1.943	11.814	1.799	< 0.01	< 0.01
120	Jul-30	1	29.791	5.868	15.641	2.017	12.153	1.853	< 0.01	< 0.01
120	Jul-30	1	29.390	5.800	15.499	1.987	12.079	1.853	< 0.01	< 0.01
120	Jul-30	1	29.155	5.733	15.364	1.967	11.926	1.814	< 0.01	< 0.01
120	03-Aug	1	29.391	5.779	15.426	2.003	12.072	1.853	< 0.01	< 0.01
120	06-Aug	1	30.150	5.981	15.921	2.048	12.537	1.922	< 0.01	< 0.01
165	21-Jun	1	3.567	0.750	1.922	0.224	1.141	0.188	< 0.01	< 0.01
165	17-Jul	1	13.655	2.749	7.267	0.938	5.595	0.869	< 0.01	< 0.01
165	17-Jul	1	14.036	2.806	7.428	0.957	5.750	0.890	< 0.01	< 0.01
165	17-Jul	1	13.485	2.698	7.156	0.921	5.518	0.853	< 0.01	< 0.01
165	17-Jul	1	15.124	3.026	8.046	1.033	6.238	0.962	< 0.01	< 0.01
165	17-Jul	1	15.176	3.018	8.062	1.041	6.194	0.968	< 0.01	< 0.01
165	18-Jul	1	16.130	3.238	8.563	1.100	6.561	1.018	< 0.01	< 0.01
165	21-Jul	1	22.486	4.494	11.947	1.532	9.228	1.419	< 0.01	< 0.01
165	24-Jul	1	22.256	4.468	11.873	1.522	9.135	1.399	< 0.01	< 0.01
165	28-Jul	1	24.763	4.927	13.132	1.682	10.056	1.548	< 0.01	< 0.01
165	Jul-28	1	24.404	4.837	12.945	1.660	9.931	1.534	< 0.01	< 0.01
165	Jul-28	1	23.220	4.643	12.479	1.599	9.616	1.469	< 0.01	< 0.01
165	Jul-30	1	25.836	5.137	13.614	1.740	10.432	1.602	< 0.01	< 0.01
165	Jul-30	1	24.962	5.011	13.271	1.695	10.143	1.559	< 0.01	< 0.01
165	Jul-30	1	24.525	4.878	12.946	1.661	9.948	1.529	< 0.01	< 0.01
165	01-Aug	1	24.523	4.861	13.020	1.678	10.100	1.552	< 0.01	< 0.01
165	01-Aug	1	25.348	5.035	13.520	1.729	10.365	1.592	< 0.01	< 0.01
165	01-Aug	1	25.023	4.998	13.267	1.709	10.270	1.579	< 0.01	< 0.01

165	01-Aug	1	24.903	4.935	13.202	1.701	10.224	1.570	< 0.01	< 0.01
165	03-Aug	1	24.464	4.840	12.895	1.655	10.006	1.537	< 0.01	< 0.01
165	03-Aug	1	24.388	4.848	12.894	1.654	10.046	1.528	< 0.01	< 0.01
165	06-Aug	1	25.459	5.040	13.505	1.744	10.525	1.612	< 0.01	< 0.01
165	06-Aug	1	25.224	4.965	13.290	1.704	10.295	1.590	< 0.01	< 0.01
165-a	03-Aug	1	0.006	< 0.005	0.006	< 0.005	0.008	< 0.005	< 0.01	< 0.01
Control	21-Jul	1	0.008	< 0.005	< 0.005	< 0.005	< 0.005	< 0.005	< 0.01	< 0.01
Control	17-Jul	1	< 0.005	< 0.005	< 0.005	< 0.005	< 0.005	< 0.005	< 0.01	< 0.01
Control	17-Jul	1	< 0.005	< 0.005	< 0.005	< 0.005	< 0.005	< 0.005	< 0.01	< 0.01
Control	17-Jul	1	< 0.005	< 0.005	< 0.005	< 0.005	< 0.005	< 0.005	< 0.01	< 0.01
Control	17-Jul	1	< 0.005	< 0.005	< 0.005	< 0.005	< 0.005	< 0.005	< 0.01	< 0.01
Control	17-Jul	1	< 0.005	< 0.005	< 0.005	< 0.005	< 0.005	< 0.005	< 0.01	< 0.01
Control	18-Jul	1	< 0.005	< 0.005	< 0.005	< 0.005	< 0.005	< 0.005	< 0.01	< 0.01
Control	21-Jul	1	< 0.005	< 0.005	< 0.005	< 0.005	< 0.005	< 0.005	< 0.01	< 0.01
Control	28-Jul	1	< 0.005	< 0.005	< 0.005	< 0.005	< 0.005	< 0.005	< 0.01	< 0.01
Control	28-Jul	1	< 0.005	< 0.005	< 0.005	< 0.005	< 0.005	< 0.005	< 0.01	< 0.01
Control	03-Aug	1	< 0.005	< 0.005	< 0.005	< 0.005	< 0.005	< 0.005	< 0.01	< 0.01
Control	03-Aug	1	< 0.005	< 0.005	< 0.005	< 0.005	< 0.005	< 0.005	< 0.01	< 0.01
A4-1	20-Jul	1	59.541	10.420	24.910	3.123	18.973	2.821	< 0.01	< 0.01
A4-2	23-Jul	10	86.49	15.47	39.28	5.12	32.12	4.76	< 0.1	< 0.1
A4-3	23-Jul	1	0.016	< 0.005	0.011	< 0.005	0.008	< 0.005	< 0.01	< 0.01
A4-5	23-Jul	1	26.289	4.658	11.639	1.489	9.409	1.391	< 0.01	< 0.01
A4-6	23-Jul	1	12.230	2.373	6.072	0.765	4.556	0.712	< 0.01	< 0.01
Control	23-Jul	1	< 0.005	< 0.005	< 0.005	< 0.005	< 0.005	< 0.005	< 0.01	< 0.01
DIW blank	19-Jul	1	< 0.005	< 0.005	< 0.005	< 0.005	< 0.005	< 0.005	< 0.01	< 0.01
DIW blank	25-Jul	1	< 0.005	< 0.005	< 0.005	< 0.005	< 0.005	< 0.005	< 0.01	< 0.01
DIW blank	02-Aug	1	< 0.005	< 0.005	< 0.005	< 0.005	< 0.005	< 0.005	< 0.01	< 0.01
DIW blank	06-Aug	1	< 0.005	< 0.005	< 0.005	< 0.005	< 0.005	< 0.005	< 0.01	< 0.01
Acid blank	21-Jun	1	< 0.005	< 0.005	< 0.005	< 0.005	< 0.005	< 0.005	< 0.01	< 0.01
Acid blank	19-Jul	1	< 0.005	< 0.005	< 0.005	< 0.005	< 0.005	< 0.005	< 0.01	< 0.01
Acid blank	25-Jul	1	< 0.005	< 0.005	< 0.005	< 0.005	< 0.005	< 0.005	< 0.01	< 0.01
Acid blank	02-Aug	1	< 0.005	< 0.005	< 0.005	< 0.005	< 0.005	< 0.005	< 0.01	< 0.01
Acid blank	06-Aug	1	< 0.005	< 0.005	< 0.005	< 0.005	< 0.005	< 0.005	< 0.01	< 0.01
Travel blank	19-Jul	1	< 0.005	< 0.005	< 0.005	< 0.005	< 0.005	< 0.005	< 0.01	< 0.01
Travel blank	25-Jul	1	< 0.005	< 0.005	< 0.005	< 0.005	< 0.005	< 0.005	< 0.01	< 0.01

Travel blank	02-Aug	1	< 0.005	< 0.005	< 0.005	< 0.005	< 0.005	< 0.005	< 0.01	< 0.01
Travel blank	06-Aug	1	< 0.005	< 0.005	< 0.005	< 0.005	< 0.005	< 0.005	< 0.01	< 0.01
Repeats										
18	21-Jul	10	69.17	13.74	37.08	4.88	29.56	4.61	< 0.1	< 0.1
18	21-Jul	10	70.16	13.93	37.08	4.82	29.67	4.60	< 0.1	< 0.1
100	18-Jul	1	22.913	4.564	12.150	1.566	9.536	1.453	< 0.01	< 0.01
100	18-Jul	1	23.011	4.593	12.173	1.567	9.522	1.453	< 0.01	< 0.01
165	21-Jun	1	3.567	0.750	1.922	0.224	1.141	0.188	< 0.01	< 0.01
165	21-Jun	1	3.546	0.751	1.920	0.224	1.146	0.185	< 0.01	< 0.01
165	17-Jul	1	15.124	3.026	8.046	1.033	6.238	0.962	< 0.01	< 0.01
165	17-Jul	1	14.933	2.989	7.961	1.025	6.105	0.953	< 0.01	< 0.01
165	01-Aug	1	25.023	4.998	13.267	1.709	10.270	1.579	< 0.01	< 0.01
165	01-Aug	1	25.202	4.985	13.362	1.713	10.280	1.574	< 0.01	< 0.01
Control	17-Jul	1	< 0.005	< 0.005	< 0.005	< 0.005	< 0.005	< 0.005	< 0.01	< 0.01
Control	17-Jul	1	< 0.005	< 0.005	< 0.005	< 0.005	< 0.005	< 0.005	< 0.01	< 0.01
Acid blank	06-Aug	1	< 0.005	< 0.005	< 0.005	< 0.005	< 0.005	< 0.005	< 0.01	< 0.01
Acid blank	06-Aug	1	< 0.005	< 0.005	< 0.005	< 0.005	< 0.005	< 0.005	< 0.01	< 0.01
Controls										
BLANK		1	< 0.005	< 0.005	< 0.005	< 0.005	< 0.005	< 0.005	< 0.01	< 0.01
BLANK		1	< 0.005	< 0.005	< 0.005	< 0.005	< 0.005	< 0.005	< 0.01	< 0.01
BLANK		1	< 0.005	< 0.005	< 0.005	< 0.005	< 0.005	< 0.005	< 0.01	< 0.01
BLANK		1	< 0.005	< 0.005	< 0.005	< 0.005	< 0.005	< 0.005	< 0.01	< 0.01
BLANK		1	< 0.005	< 0.005	< 0.005	< 0.005	< 0.005	< 0.005	< 0.01	< 0.01
BLANK		1	< 0.005	< 0.005	< 0.005	< 0.005	< 0.005	< 0.005	< 0.01	< 0.01
BLANK		1	< 0.005	< 0.005	< 0.005	< 0.005	< 0.005	< 0.005	< 0.01	< 0.01
BLANK		1	< 0.005	< 0.005	< 0.005	< 0.005	< 0.005	< 0.005	< 0.01	< 0.01
SLRS-4		1	0.024	< 0.005	0.013	< 0.005	0.012	< 0.005	< 0.01	< 0.01

SLRS-4		1	0.024	< 0.005	0.013	< 0.005	0.012	< 0.005	< 0.01	< 0.01
SLRS-4 CERTIFIED		1	0.024	< 0.005	0.014	< 0.005	0.012	< 0.005	< 0.01	< 0.01
TM-28.2		1	< 0.005	< 0.005	< 0.005	< 0.005	< 0.005	< 0.005	< 0.01	< 0.01
TM-28.2 CERTIFIED INFORMATION		1	< 0.005	< 0.005	< 0.005	< 0.005	< 0.005	< 0.005	< 0.01	< 0.01
TMDA-51.3		1	< 0.005	< 0.005	< 0.005	< 0.005	< 0.005	< 0.005	< 0.01	< 0.01
TMDA-51.3 CERTIFIED INFORMATION		1	< 0.005	< 0.005	< 0.005	< 0.005	< 0.005	< 0.005	< 0.01	< 0.01

ICP-MS (ppb)		**Dilution**	**W**	**Re**	**Tl**	**Pb**	**Bi**	**Th**	**U**
D.L.		**1**	0.02	0.005	0.005	0.01	0.02	0.02	0.005
D.L.		**10**	0.2	0.05	0.05	0.1	0.1	0.1	0.05
Distance (m)	**Date**								
0	20-Jul	10	< 0.2	< 0.05	14.91	21.5	< 0.1	1.1	16.56
0	28-Jul	10	< 0.2	< 0.05	11.65	15.5	< 0.1	0.9	11.33
0	03-Aug	10	< 0.2	< 0.05	12.96	13.7	< 0.1	0.6	11.09
0	06-Aug	10	< 0.2	< 0.05	15.15	14.4	< 0.1	0.7	12.46
10	19-Jul	10	< 0.2	< 0.05	26.65	11.5	< 0.1	0.6	495.82
10	24-Jul	10	< 0.2	< 0.05	27.49	10.7	< 0.1	0.5	519.97
10	03-Aug	10	< 0.2	< 0.05	28.36	10.7	< 0.1	0.5	588.47
10	06-Aug	10	< 0.2	< 0.05	29.61	10.7	< 0.1	0.5	605.78
18	Jul-19	10	< 0.2	< 0.05	7.20	6.6	< 0.1	0.4	66.45
18	Jul-19	10	< 0.2	< 0.05	7.19	6.6	< 0.1	0.4	66.38
18	Jul-20	10	< 0.2	< 0.05	7.54	6.8	< 0.1	0.5	71.46
18	Jul-21	10	< 0.2	< 0.05	7.62	6.8	< 0.1	0.4	71.62
18	Jul-24	10	< 0.2	< 0.05	9.20	8.5	< 0.1	0.5	81.30
18	Jul-28	10	< 0.2	< 0.05	9.17	8.3	< 0.1	0.5	80.84
18	Jul-28	10	< 0.2	< 0.05	9.21	8.4	< 0.1	0.5	81.81
18	Jul-28	10	< 0.2	< 0.05	9.50	9.3	< 0.1	0.5	79.47
18	Jul-30	10	< 0.2	< 0.05	8.81	8.1	< 0.1	0.4	73.20

18	Jul-30	10	< 0.2	< 0.05	8.79	8.1	< 0.1	0.4	73.34
18	Jul-30	10	< 0.2	< 0.05	8.84	8.1	< 0.1	0.4	73.56
18	03-Aug	10	< 0.2	< 0.05	9.30	8.0	< 0.1	0.4	81.83
18	06-Aug	10	< 0.2	< 0.05	10.05	8.7	< 0.1	0.5	90.07
40	Jul-19	10	< 0.2	< 0.05	5.56	4.6	< 0.1	0.3	51.86
40	Jul-19	10	< 0.2	< 0.05	5.61	4.7	< 0.1	0.3	51.96
40	Jul-20	10	0.3	< 0.05	5.97	5.3	0.7	0.3	56.74
40	Jul-21	10	< 0.2	< 0.05	6.18	5.1	< 0.1	0.3	57.52
40	Jul-24	10	< 0.2	< 0.05	6.94	6.0	< 0.1	0.4	65.07
40	Jul-28	10	< 0.2	< 0.05	7.24	6.1	< 0.1	0.4	66.39
40	Jul-28	10	< 0.2	< 0.05	7.47	6.3	< 0.1	0.4	68.22
40	Jul-28	10	< 0.2	< 0.05	7.45	7.5	< 0.1	0.4	69.04
40	Jul-30	10	< 0.2	< 0.05	7.36	6.6	< 0.1	0.3	62.77
40	Jul-30	10	< 0.2	< 0.05	7.42	6.7	< 0.1	0.3	62.00
40	Jul-30	10	< 0.2	< 0.05	6.98	8.6	< 0.1	0.3	58.02
40	03-Aug	10	< 0.2	< 0.05	7.84	6.6	< 0.1	0.3	69.03
40	03-Aug	10	< 0.2	< 0.05	7.70	6.6	< 0.1	0.3	69.02
40	06-Aug	10	< 0.2	< 0.05	8.17	7.5	< 0.1	0.4	75.42
100	17-Jul	1	< 0.02	0.015	2.343	1.97	< 0.02	0.04	30.365
100	17-Jul	1	< 0.02	0.016	2.476	2.06	< 0.02	0.04	31.933
100	17-Jul	1	< 0.02	0.015	2.675	2.20	< 0.02	0.06	32.153
100	18-Jul	1	< 0.02	0.015	3.183	1.81	< 0.02	0.05	34.578
100	18-Jul	1	< 0.02	0.016	3.219	1.79	< 0.02	0.06	34.732
100	18-Jul	1	< 0.02	0.015	3.294	1.90	< 0.02	0.06	35.627
100	21-Jul	1	< 0.02	0.016	3.915	2.22	< 0.02	0.09	43.664
100	24-Jul	1	< 0.02	0.016	4.468	3.31	< 0.02	0.12	51.323
100	Jul-28	1	< 0.02	0.015	4.669	2.51	< 0.02	0.11	51.221
100	Jul-28	1	< 0.02	0.015	4.516	2.46	< 0.02	0.10	49.933
100	Jul-28	1	< 0.02	0.015	4.447	4.05	< 0.02	0.13	52.313
100	Jul-30	1	< 0.02	0.015	4.876	3.18	< 0.02	0.11	49.178
100	Jul-30	1	< 0.02	0.014	4.682	2.44	< 0.02	0.09	44.777
100	01-Aug	1	< 0.02	0.015	4.428	3.56	< 0.02	0.11	51.406
100	01-Aug	1	< 0.02	0.015	4.494	3.45	< 0.02	0.11	51.825
100	03-Aug	1	< 0.02	0.016	5.135	3.38	< 0.02	0.12	55.711
100	06-Aug	1	< 0.02	0.015	5.338	3.83	< 0.02	0.14	59.805
120	24-Jul	1	< 0.02	0.034	3.068	1.98	< 0.02	< 0.02	44.203
120	Jul-28	1	< 0.02	0.038	3.379	1.56	< 0.02	< 0.02	48.834

120	Jul-28	1	< 0.02	0.037	3.365	1.52	< 0.02	< 0.02	49.193
120	Jul-28	1	< 0.02	0.037	3.032	2.43	< 0.02	< 0.02	46.084
120	Jul-30	1	< 0.02	0.035	3.458	1.93	< 0.02	< 0.02	48.695
120	Jul-30	1	< 0.02	0.036	3.355	1.54	< 0.02	< 0.02	48.753
120	Jul-30	1	< 0.02	0.034	3.340	1.45	< 0.02	0.02	47.388
120	03-Aug	1	< 0.02	0.039	3.525	2.23	< 0.02	< 0.02	51.930
120	06-Aug	1	< 0.02	0.040	3.846	2.15	< 0.02	< 0.02	54.965
165	21-Jun	1	< 0.02	0.020	1.275	0.33	< 0.02	< 0.02	0.710
165	17-Jul	1	< 0.02	0.029	1.953	1.08	< 0.02	< 0.02	25.290
165	17-Jul	1	< 0.02	0.030	1.999	1.20	< 0.02	< 0.02	26.353
165	17-Jul	1	< 0.02	0.028	1.995	1.12	< 0.02	< 0.02	20.663
165	17-Jul	1	< 0.02	0.030	2.441	1.02	< 0.02	< 0.02	27.968
165	17-Jul	1	< 0.02	0.031	2.436	1.00	< 0.02	< 0.02	27.845
165	18-Jul	1	< 0.02	0.030	2.488	1.04	< 0.02	< 0.02	27.139
165	21-Jul	1	< 0.02	0.035	2.611	1.19	< 0.02	< 0.02	39.127
165	24-Jul	1	< 0.02	0.037	2.622	1.46	< 0.02	< 0.02	39.026
165	28-Jul	1	< 0.02	0.041	2.880	1.17	< 0.02	< 0.02	40.763
165	Jul-28	1	< 0.02	0.041	2.875	1.15	< 0.02	< 0.02	40.259
165	Jul-28	1	< 0.02	0.038	2.588	1.75	< 0.02	< 0.02	40.629
165	Jul-30	1	< 0.02	0.039	3.018	1.55	< 0.02	< 0.02	41.410
165	Jul-30	1	< 0.02	0.038	2.930	1.49	< 0.02	< 0.02	41.863
165	Jul-30	1	< 0.02	0.038	2.903	1.13	< 0.02	< 0.02	37.322
165	01-Aug	1	< 0.02	0.039	3.000	1.44	< 0.02	< 0.02	38.817
165	01-Aug	1	< 0.02	0.040	3.052	1.48	< 0.02	< 0.02	42.466
165	01-Aug	1	< 0.02	0.039	3.030	1.47	< 0.02	< 0.02	41.845
165	01-Aug	1	< 0.02	0.039	2.992	1.48	< 0.02	< 0.02	42.075
165	03-Aug	1	< 0.02	0.040	2.967	1.88	< 0.02	< 0.02	44.509
165	03-Aug	1	0.07	0.041	2.957	1.87	< 0.02	< 0.02	44.146
165	06-Aug	1	< 0.02	0.043	3.267	1.47	< 0.02	< 0.02	47.466
165	06-Aug	1	< 0.02	0.043	3.238	1.41	< 0.02	< 0.02	46.501
165-a	03-Aug	1	< 0.02	0.073	0.178	0.03	< 0.02	< 0.02	33.055
Control	21-Jul	1	< 0.02	0.007	0.009	0.08	< 0.02	< 0.02	4.280
Control	17-Jul	1	< 0.02	0.006	0.011	0.27	< 0.02	< 0.02	6.520
Control	17-Jul	1	< 0.02	0.007	0.011	0.27	< 0.02	< 0.02	6.522
Control	17-Jul	1	< 0.02	0.007	0.012	0.26	< 0.02	< 0.02	6.392
Control	17-Jul	1	< 0.02	0.008	0.011	0.26	< 0.02	< 0.02	6.562
Control	17-Jul	1	0.04	0.007	0.011	0.27	< 0.02	< 0.02	6.458

Control	18-Jul	1	< 0.02	0.007	0.011	0.26	< 0.02	< 0.02	6.515
Control	21-Jul	1	< 0.02	0.007	0.010	0.28	< 0.02	< 0.02	6.531
Control	28-Jul	1	< 0.02	0.007	0.010	0.25	< 0.02	< 0.02	6.882
Control	28-Jul	1	< 0.02	0.007	0.010	0.24	< 0.02	< 0.02	6.970
Control	03-Aug	1	< 0.02	0.008	0.013	0.35	< 0.02	< 0.02	7.687
Control	03-Aug	1	< 0.02	0.008	0.013	0.29	< 0.02	< 0.02	7.596
A4-1	20-Jul	1	< 0.02	< 0.005	0.193	2.22	< 0.02	0.99	81.171
A4-2	23-Jul	10	< 0.2	< 0.05	1.56	6.5	< 0.1	63.2	183.69
A4-3	23-Jul	1	< 0.02	0.013	0.012	< 0.01	< 0.02	< 0.02	5.848
A4-5	23-Jul	1	< 0.02	0.012	0.448	1.75	< 0.02	17.27	65.153
A4-6	23-Jul	1	< 0.02	0.015	0.115	0.89	< 0.02	2.36	46.316
Control	23-Jul	1	< 0.02	< 0.005	< 0.005	< 0.01	< 0.02	< 0.02	0.039
DIW blank	19-Jul	1	< 0.02	< 0.005	< 0.005	< 0.01	< 0.02	< 0.02	< 0.005
DIW blank	25-Jul	1	< 0.02	< 0.005	< 0.005	< 0.01	< 0.02	< 0.02	< 0.005
DIW blank	02-Aug	1	< 0.02	< 0.005	< 0.005	< 0.01	< 0.02	< 0.02	< 0.005
DIW blank	06-Aug	1	< 0.02	< 0.005	< 0.005	< 0.01	< 0.02	< 0.02	< 0.005
Acid blank	21-Jun	1	< 0.02	< 0.005	< 0.005	< 0.01	< 0.02	< 0.02	< 0.005
Acid blank	19-Jul	1	< 0.02	< 0.005	< 0.005	< 0.01	< 0.02	< 0.02	< 0.005
Acid blank	25-Jul	1	< 0.02	< 0.005	< 0.005	< 0.01	< 0.02	< 0.02	< 0.005
Acid blank	02-Aug	1	< 0.02	< 0.005	< 0.005	0.02	< 0.02	< 0.02	< 0.005
Acid blank	06-Aug	1	< 0.02	< 0.005	< 0.005	< 0.01	< 0.02	< 0.02	< 0.005
Travel blank	19-Jul	1	< 0.02	< 0.005	< 0.005	< 0.01	< 0.02	< 0.02	< 0.005
Travel blank	25-Jul	1	< 0.02	< 0.005	< 0.005	< 0.01	< 0.02	< 0.02	< 0.005
Travel blank	02-Aug	1	< 0.02	< 0.005	< 0.005	< 0.01	< 0.02	< 0.02	< 0.005
Travel blank	06-Aug	1	< 0.02	< 0.005	< 0.005	< 0.01	< 0.02	< 0.02	< 0.005
Repeats									
18	21-Jul	10	< 0.2	< 0.05	7.62	6.8	< 0.1	0.4	71.62
18	21-Jul	10	< 0.2	< 0.05	7.61	6.8	< 0.1	0.4	72.28
100	18-Jul	1	< 0.02	0.015	3.294	1.90	< 0.02	0.06	35.627
100	18-Jul	1	< 0.02	0.015	3.299	1.88	< 0.02	0.06	35.331
165	21-Jun	1	< 0.02	0.020	1.275	0.33	< 0.02	< 0.02	0.710
165	21-Jun	1	< 0.02	0.020	1.183	0.29	< 0.02	< 0.02	0.708

165	17-Jul	1	< 0.02	0.030	2.441	1.02	< 0.02	< 0.02	27.968
165	17-Jul	1	< 0.02	0.030	2.421	1.01	< 0.02	< 0.02	30.433
165	01-Aug	1	< 0.02	0.039	3.030	1.47	< 0.02	< 0.02	41.845
165	01-Aug	1	< 0.02	0.040	3.025	1.47	< 0.02	< 0.02	42.624
Control	17-Jul	1	< 0.02	0.008	0.011	0.26	< 0.02	< 0.02	6.562
Control	17-Jul	1	0.04	0.008	0.011	0.23	< 0.02	< 0.02	6.313
Acid blank	06-Aug	1	< 0.02	< 0.005	< 0.005	< 0.01	< 0.02	< 0.02	< 0.005
Acid blank	06-Aug	1	< 0.02	< 0.005	< 0.005	< 0.01	< 0.02	< 0.02	< 0.005
Controls									
BLANK		1	< 0.02	< 0.005	< 0.005	< 0.01	< 0.02	< 0.02	< 0.005
BLANK		1	< 0.02	< 0.005	< 0.005	< 0.01	< 0.02	< 0.02	< 0.005
BLANK		1	< 0.02	< 0.005	< 0.005	< 0.01	< 0.02	< 0.02	< 0.005
BLANK		1	< 0.02	< 0.005	< 0.005	< 0.01	< 0.02	< 0.02	< 0.005
BLANK		1	< 0.02	< 0.005	< 0.005	< 0.01	< 0.02	< 0.02	< 0.005
BLANK		1	< 0.02	< 0.005	< 0.005	< 0.01	< 0.02	< 0.02	< 0.005
BLANK		1	< 0.02	< 0.005	< 0.005	< 0.01	< 0.02	< 0.02	< 0.005
BLANK		1	< 0.02	< 0.005	< 0.005	< 0.01	< 0.02	< 0.02	0.006
SLRS-4		1	< 0.02	0.007	0.007	0.08	< 0.02	< 0.02	0.047
SLRS-4		1	< 0.02	0.007	0.006	0.08	< 0.02	< 0.02	0.047
SLRS-4		1	< 0.02	0.007	0.006	0.08	< 0.02	< 0.02	0.046
CERTIFIED						0.086 ± 0.007			0.050 ± 0.003
TM-28.2		1	< 0.02	< 0.005	3.929	4.26	3.77	< 0.02	5.979
TM-28.2		1	< 0.02	< 0.005	3.909	4.21	3.87	< 0.02	5.900
CERTIFIED					3.7 ± 0.47	4.1 ± 1.0			5.7 ± 0.72
INFORMATION							3.10		
TMDA-51.3		1	18.19	< 0.005	21.754	75.06	15.08	< 0.02	28.662
TMDA-51.3		1	18.67	< 0.005	21.659	74.40	14.84	< 0.02	28.271

CERTIFIED INFORMATION		15.4			21.1 ± 1.9	73.3 ± 5.7	12.9			29.1 ± 4.1

ICP-ES (ppm)		**Dilution**	**Al**	**Br**	**Ca**	**Cl**	**Fe**	**K**	**Mg**	**Mn**
D.L.		**1**	**0.02**	**0.05**	**0.02**	**0.1**	**0.005**	**0.05**	**0.005**	**0.001**
D.L.		**10**	**0.2**	**0.5**	**0.2**	**1**	**0.05**	**0.5**	**0.05**	**0.01**
Distance (m)	**Date**	10	470.4	< 0.5	291.5	< 1	190.16	1.5	469.54	51.66
0	20-Jul	10	322.5	< 0.5	232.7	< 1	118.57	1.5	331.12	38.01
0	28-Jul	10	306.4	< 0.5	251.7	1	131.50	1.5	318.56	36.18
0	03-Aug	10	353.9	< 0.5	285.5	2	158.23	1.6	371.32	41.40
0	06-Aug	10	683.3	< 0.5	368.4	2	200.59	3.7	719.95	45.29
10	19-Jul	10	707.0	< 0.5	390.9	2	210.64	4.1	823.17	50.59
10	24-Jul	10	816.0	< 0.5	386.8	3	289.53	4.2	959.86	58.63
10	03-Aug	10	847.5	< 0.5	387.5	2	303.12	4.3	996.41	60.69
10	06-Aug	10	140.1	< 0.5	225.1	< 1	58.23	1.9	224.48	14.16
18	Jul-19	10	138.2	< 0.5	221.4	< 1	57.28	1.8	221.21	13.95
18	Jul-20	10	157.5	< 0.5	235.8	< 1	64.56	1.9	247.87	15.80
18	Jul-21	10	164.6	< 0.5	236.0	< 1	66.11	1.9	254.43	16.33
18	Jul-24	10	189.7	< 0.5	252.8	< 1	73.55	2.1	296.27	19.15
18	Jul-28	10	187.5	< 0.5	252.7	< 1	76.81	2.1	303.09	19.30
18	Jul-28	10	189.7	< 0.5	255.0	< 1	77.68	2.1	306.15	19.49
18	Jul-28	10	186.2	< 0.5	249.4	< 1	73.01	2.1	299.15	19.19
18	Jul-30	10	171.6	< 0.5	235.4	< 1	68.94	2.0	273.94	17.82
18	Jul-30	10	169.9	< 0.5	232.8	< 1	68.21	1.9	270.67	17.61
18	Jul-30	10	171.9	< 0.5	235.7	< 1	69.20	1.9	273.65	17.84
18	03-Aug	10	174.5	< 0.5	251.4	< 1	76.75	2.1	288.41	17.66
18	06-Aug	10	187.6	< 0.5	264.7	< 1	84.42	2.2	314.45	18.97
40	Jul-19	10	106.2	< 0.5	209.8	< 1	36.70	1.8	178.33	10.79
40	Jul-19	10	107.4	< 0.5	211.6	< 1	37.26	1.8	179.61	10.90
40	Jul-20	10	124.1	< 0.5	223.0	< 1	45.17	1.8	202.14	12.45
40	Jul-21	10	130.3	< 0.5	224.2	< 1	46.32	1.8	208.60	12.98

40	Jul-24	10	147.7	< 0.5	237.9	< 1	50.60	2.0	239.36	15.01
40	Jul-28	10	150.7	< 0.5	244.5	< 1	56.41	2.0	252.37	15.61
40	Jul-28	10	149.5	< 0.5	243.2	< 1	55.98	2.0	250.79	15.53
40	Jul-28	10	150.6	< 0.5	240.7	< 1	50.22	2.1	250.64	15.65
40	Jul-30	10	143.8	< 0.5	231.1	< 1	51.34	1.9	236.88	15.09
40	Jul-30	10	142.8	< 0.5	228.5	< 1	50.88	1.9	234.32	14.94
40	Jul-30	10	132.8	< 0.5	214.4	< 1	48.63	1.8	218.29	14.01
40	03-Aug	10	142.7	< 0.5	240.8	< 1	53.65	2.0	243.96	14.78
40	03-Aug	10	143.4	< 0.5	243.1	< 1	55.08	2.0	245.43	14.86
40	06-Aug	10	148.6	< 0.5	253.8	< 1	55.50	2.1	261.85	15.58
100	17-Jul	1	40.28	< 0.05	160.69	< 0.1	10.895	1.44	96.260	4.914
100	17-Jul	1	39.31	< 0.05	164.25	0.1	10.673	1.44	98.377	4.883
100	17-Jul	1	45.26	< 0.05	164.49	0.2	11.731	1.44	101.195	5.256
100	18-Jul	1	50.29	< 0.05	170.79	0.2	13.679	1.49	107.332	5.618
100	18-Jul	1	50.14	< 0.05	168.81	0.2	13.397	1.48	105.981	5.544
100	18-Jul	1	54.01	< 0.05	175.79	0.3	14.470	1.49	112.997	5.997
100	21-Jul	1	84.72	< 0.05	199.91	0.3	20.653	1.64	150.608	8.705
100	24-Jul	1	95.18	< 0.05	212.65	0.4	20.247	1.75	171.584	10.029
100	Jul-28	1	97.64	< 0.05	213.51	0.4	24.822	1.72	177.550	10.271
100	Jul-28	1	96.22	< 0.05	210.48	0.4	24.578	1.72	175.562	10.115
100	Jul-28	1	96.65	< 0.05	211.29	0.3	20.127	1.83	176.664	10.269
100	Jul-30	1	95.60	< 0.05	206.79	0.2	21.329	1.73	171.059	10.184
100	Jul-30	1	90.81	< 0.05	196.04	0.2	20.665	1.65	162.221	9.666
100	01-Aug	1	94.84	< 0.05	211.89	0.2	21.651	1.77	174.108	9.994
100	01-Aug	1	94.54	< 0.05	210.61	0.2	21.843	1.73	173.064	9.929
100	03-Aug	1	98.69	< 0.05	217.07	0.2	24.335	1.82	182.199	10.246
100	06-Aug	1	103.05	< 0.05	228.78	0.2	25.549	1.87	194.415	10.752
120	24-Jul	1	42.05	< 0.05	220.34	< 0.1	12.136	1.70	155.286	6.601
120	Jul-28	1	47.79	< 0.05	239.79	< 0.1	16.525	1.79	173.680	7.173
120	Jul-28	1	50.82	< 0.05	239.41	0.1	16.521	1.78	172.798	7.167
120	Jul-28	1	44.24	< 0.05	228.80	0.1	12.166	1.76	165.915	6.862
120	Jul-30	1	46.08	< 0.05	225.17	0.2	13.499	1.76	162.257	6.974
120	Jul-30	1	47.41	< 0.05	238.42	0.2	16.583	1.79	173.435	7.105
120	Jul-30	1	49.25	< 0.05	221.25	0.2	13.978	1.72	159.474	6.873
120	03-Aug	1	46.92	< 0.05	240.17	0.2	15.141	1.87	174.039	6.925
120	06-Aug	1	45.78	< 0.05	253.60	0.2	16.939	1.96	186.941	7.233
165	21-Jun	1	0.48	< 0.05	89.41	0.2	3.560	0.85	47.346	1.709

165	17-Jul	1	7.44	< 0.05	181.06	0.2	8.175	1.44	100.336	3.805
165	17-Jul	1	7.30	< 0.05	180.98	0.1	8.194	1.46	100.338	3.778
165	17-Jul	1	7.74	< 0.05	170.53	0.2	7.673	1.39	95.211	3.684
165	17-Jul	1	9.52	< 0.05	183.69	0.2	9.075	1.47	104.362	4.089
165	17-Jul	1	9.73	< 0.05	185.82	0.2	9.139	1.48	105.442	4.120
165	18-Jul	1	11.97	< 0.05	191.62	0.2	9.965	1.50	110.306	4.287
165	21-Jul	1	23.85	< 0.05	212.87	0.2	12.813	1.59	135.647	5.557
165	24-Jul	1	18.93	< 0.05	214.85	0.3	10.297	1.61	139.422	5.552
165	28-Jul	1	20.71	< 0.05	235.96	0.3	13.878	1.71	156.515	6.098
165	Jul-28	1	21.40	< 0.05	235.39	0.3	14.113	1.71	156.264	6.103
165	Jul-28	1	19.72	< 0.05	228.30	0.3	10.664	1.71	150.890	5.898
165	Jul-30	1	24.32	< 0.05	224.93	0.3	11.635	1.71	150.065	6.157
165	Jul-30	1	23.11	< 0.05	222.56	0.3	11.439	1.69	147.683	6.060
165	Jul-30	1	24.04	< 0.05	222.30	0.3	12.090	1.69	146.655	5.962
165	01-Aug	1	23.76	< 0.05	236.20	0.3	13.591	1.72	156.451	6.159
165	01-Aug	1	23.34	< 0.05	236.13	0.3	13.571	1.72	156.559	6.145
165	01-Aug	1	24.35	< 0.05	234.84	0.3	13.415	1.70	157.751	6.039
165	01-Aug	1	23.50	< 0.05	234.78	0.3	13.661	1.73	159.279	6.125
165	03-Aug	1	21.10	< 0.05	238.24	0.3	12.121	1.77	160.884	5.968
165	03-Aug	1	21.47	< 0.05	238.04	0.3	12.137	1.78	161.102	5.976
165	06-Aug	1	22.25	< 0.05	254.81	0.3	14.625	1.82	169.225	6.360
165	06-Aug	1	22.05	< 0.05	254.75	0.4	14.532	1.83	171.565	6.356
165-a	03-Aug	1	< 0.02	< 0.05	174.41	< 0.1	< 0.005	1.04	29.679	< 0.001
Control	21-Jul	1	0.02	< 0.05	81.04	0.3	0.007	0.61	28.442	0.001
Control	17-Jul	1	< 0.02	< 0.05	105.72	0.2	< 0.005	0.62	36.846	< 0.001
Control	17-Jul	1	< 0.02	< 0.05	106.36	0.2	< 0.005	0.62	37.082	< 0.001
Control	17-Jul	1	< 0.02	< 0.05	105.79	0.3	< 0.005	0.65	36.622	< 0.001
Control	17-Jul	1	< 0.02	< 0.05	104.77	0.3	< 0.005	0.63	36.406	< 0.001
Control	17-Jul	1	< 0.02	< 0.05	105.07	0.2	< 0.005	0.63	36.496	< 0.001
Control	18-Jul	1	< 0.02	< 0.05	105.54	0.2	< 0.005	0.61	36.725	< 0.001
Control	21-Jul	1	< 0.02	< 0.05	106.48	0.2	< 0.005	0.61	37.195	< 0.001
Control	28-Jul	1	< 0.02	< 0.05	110.03	0.2	< 0.005	0.61	38.841	< 0.001
Control	28-Jul	1	< 0.02	< 0.05	110.63	0.2	< 0.005	0.61	39.037	< 0.001
Control	03-Aug	1	< 0.02	< 0.05	114.67	0.2	< 0.005	0.65	40.339	< 0.001
Control	03-Aug	1	< 0.02	< 0.05	114.29	0.2	< 0.005	0.65	40.111	< 0.001
A4-1	20-Jul	10	52.8	< 0.5	154.5	< 1	35.55	< 0.5	273.32	33.42

A4-2	23-Jul	10	169.7	< 0.5	187.2	< 1	250.29	< 0.5	347.11	28.04
A4-3	23-Jul	1	0.07	< 0.05	50.59	< 0.1	< 0.005	0.30	23.778	0.093
A4-5	23-Jul	1	54.75	< 0.05	92.04	< 0.1	77.827	0.35	126.643	8.983
A4-6	23-Jul	1	31.06	< 0.05	114.99	< 0.1	9.076	0.53	114.225	5.373
Control	23-Jul	1	< 0.02	< 0.05	8.46	< 0.1	< 0.005	0.30	5.513	< 0.001
DIW blank	19-Jul	1	< 0.02	< 0.05	< 0.02	0.1	< 0.005	< 0.05	< 0.005	< 0.001
DIW blank	25-Jul	1	< 0.02	< 0.05	< 0.02	< 0.1	< 0.005	< 0.05	< 0.005	< 0.001
DIW blank	02-Aug	1	< 0.02	< 0.05	< 0.02	< 0.1	< 0.005	< 0.05	< 0.005	< 0.001
DIW blank	06-Aug	1	< 0.02	< 0.05	< 0.02	< 0.1	< 0.005	< 0.05	< 0.005	< 0.001
Acid blank	21-Jun	1	< 0.02	< 0.05	< 0.02	< 0.1	< 0.005	< 0.05	< 0.005	< 0.001
Acid blank	19-Jul	1	< 0.02	< 0.05	< 0.02	< 0.1	< 0.005	< 0.05	< 0.005	< 0.001
Acid blank	25-Jul	1	< 0.02	< 0.05	< 0.02	< 0.1	< 0.005	< 0.05	< 0.005	< 0.001
Acid blank	02-Aug	1	< 0.02	< 0.05	< 0.02	< 0.1	< 0.005	< 0.05	< 0.005	< 0.001
Acid blank	06-Aug	1	< 0.02	< 0.05	< 0.02	< 0.1	< 0.005	< 0.05	< 0.005	< 0.001
Travel blank	19-Jul	1	< 0.02	< 0.05	< 0.02	< 0.1	< 0.005	< 0.05	< 0.005	< 0.001
Travel blank	25-Jul	1	< 0.02	< 0.05	< 0.02	< 0.1	< 0.005	< 0.05	< 0.005	< 0.001
Travel blank	02-Aug	1	< 0.02	< 0.05	< 0.02	< 0.1	< 0.005	< 0.05	< 0.005	< 0.001
Travel blank	06-Aug	1	< 0.02	< 0.05	< 0.02	< 0.1	< 0.005	< 0.05	< 0.005	< 0.001
Repeats										
40	19-Jul	10	107.4	< 0.5	211.6	< 1	37.26	1.8	179.61	10.90
40	19-Jul	10	106.2	< 0.5	209.4	< 1	36.80	1.7	177.58	10.81
100	03-Aug	1	98.69	< 0.05	217.07	0.2	24.335	1.82	182.199	10.246
100	03-Aug	1	97.63	< 0.05	215.98	0.3	24.255	1.82	180.543	10.150
165	18-Jul	1	11.97	< 0.05	191.62	0.2	9.965	1.50	110.306	4.287
165	18-Jul	1	12.15	< 0.05	189.01	0.2	10.065	1.50	109.229	4.343
Control	21-Jul	1	< 0.02	< 0.05	106.48	0.2	< 0.005	0.61	37.195	< 0.001
Control	21-Jul	1	< 0.02	< 0.05	107.34	0.2	< 0.005	0.61	37.522	< 0.001
DIW blank	06-Aug	1	< 0.02	< 0.05	< 0.02	< 0.1	< 0.005	< 0.05	< 0.005	< 0.001
DIW blank	06-Aug	1	< 0.02	< 0.05	< 0.02	< 0.1	< 0.005	< 0.05	< 0.005	< 0.001

CONTROLS									
BLANK		1	< 0.02	< 0.05	< 0.02	< 0.1	< 0.005	< 0.05	< 0.005	< 0.001
BLANK		1	< 0.02	< 0.05	< 0.02	< 0.1	< 0.005	< 0.05	< 0.005	< 0.001
BLANK		1	< 0.02	< 0.05	< 0.02	< 0.1	< 0.005	< 0.05	< 0.005	< 0.001
BLANK		1	< 0.02	< 0.05	< 0.02	< 0.1	< 0.005	< 0.05	< 0.005	< 0.001
ION-96.3		1	< 0.02	< 0.05	89.90	92.0	< 0.005	4.13	26.039	< 0.001
CERTIFIED (ppm)					90.6 ± 8.5	93 ± 5.9		4 ± 0.45	25.7 ± 1.8	
INFORMATION (ppm)										
SLRS-4		1	0.06	0.08	5.90	2.1	0.103	0.69	1.611	0.003
CERTIFIED (ppm)					6.2 ± 0.2			0.68 ± 0.02	1.6 ± 0.1	
CERTIFIED (ppb)			54 ± 4				103 ± 5			3.37 ± 0.18
TMDA-51.3		1	0.10	< 0.05	14.03	10.3	0.107	0.65	3.475	0.087
TMDA-51.3		1	0.10	< 0.05	14.44	10.5	0.109	0.67	3.528	0.087
CERTIFIED (ppb)			96.8 ± 9.4				109 ± 12.8			84.9 ± 7.1

ICP-ES (ppm)		**Na**	**Ni**	**P**	**S**	**Sc**	**Si**	**Y**	**Zn**
D.L.		**0.05**	**0.002**	**0.05**	**0.05**	**0.001**	**0.02**	**0.001**	**0.005**
D.L.		**0.5**	**0.02**	**0.5**	**0.5**	**0.01**	**0.2**	**0.01**	**0.05**
Distance (m)	**Date**	1.1	9.09	< 0.5	2122.8	0.04	14.2	2.10	513.84
0	20-Jul	1.1	6.17	< 0.5	1496.5	0.02	12.2	1.53	373.30
0	28-Jul	1.1	6.00	< 0.5	1465.7	0.02	12.5	1.46	349.71
0	03-Aug	1.3	6.87	< 0.5	1691.7	0.03	13.2	1.66	411.56
0	06-Aug	1.6	11.60	< 0.5	2762.1	0.05	29.0	1.54	337.93
10	19-Jul	1.6	13.18	< 0.5	2959.0	0.05	28.5	1.73	401.35
10	24-Jul	1.8	14.98	< 0.5	3407.6	0.06	29.4	2.09	454.76
10	03-Aug	1.9	15.25	< 0.5	3503.7	0.06	29.1	2.16	475.32
10	06-Aug	1.2	3.35	< 0.5	825.0	0.01	11.5	0.41	103.20
18	Jul-19	1.1	3.35	< 0.5	810.4	0.01	11.4	0.41	102.49
18	Jul-20	1.1	3.65	< 0.5	902.7	0.01	11.6	0.46	115.11

18	Jul-21	1.2	3.75	< 0.5	926.4	0.02	11.7	0.49	117.73
18	Jul-24	1.3	4.32	< 0.5	1057.4	0.02	12.4	0.57	138.24
18	Jul-28	1.3	4.38	< 0.5	1063.4	0.02	12.6	0.59	142.03
18	Jul-28	1.3	4.37	< 0.5	1076.0	0.02	12.6	0.59	142.36
18	Jul-28	1.3	4.28	< 0.5	1052.5	0.02	12.5	0.58	141.05
18	Jul-30	1.6	3.96	< 0.5	972.6	0.02	12.3	0.55	135.09
18	Jul-30	1.2	3.90	< 0.5	961.4	0.02	12.1	0.54	134.06
18	Jul-30	1.2	3.96	< 0.5	975.2	0.02	12.2	0.55	135.15
18	03-Aug	1.4	4.08	< 0.5	1014.6	0.02	12.5	0.53	128.13
18	06-Aug	1.4	4.38	< 0.5	1092.9	0.02	13.1	0.57	134.43
40	Jul-19	0.9	2.66	< 0.5	660.7	< 0.01	10.1	0.31	79.67
40	Jul-19	0.9	2.66	< 0.5	667.2	< 0.01	10.2	0.31	78.96
40	Jul-20	1.0	2.98	< 0.5	746.5	0.01	10.5	0.36	90.50
40	Jul-21	1.0	3.07	< 0.5	772.0	0.01	10.5	0.38	95.06
40	Jul-24	1.1	3.47	< 0.5	866.9	0.01	11.0	0.44	109.27
40	Jul-28	1.2	3.60	< 0.5	903.9	0.01	11.3	0.46	114.64
40	Jul-28	1.1	3.58	< 0.5	899.6	0.01	11.2	0.46	114.90
40	Jul-28	1.1	3.62	< 0.5	900.3	0.02	11.6	0.47	116.99
40	Jul-30	1.1	3.41	< 0.5	861.4	0.01	11.3	0.46	114.63
40	Jul-30	1.1	3.40	< 0.5	852.4	0.01	11.3	0.46	114.16
40	Jul-30	1.1	3.16	< 0.5	801.1	0.01	10.5	0.42	105.91
40	03-Aug	1.2	3.43	< 0.5	881.3	0.01	11.5	0.44	108.20
40	03-Aug	1.2	3.48	< 0.5	886.7	0.01	11.6	0.44	108.52
40	06-Aug	1.2	3.68	< 0.5	930.9	0.01	11.9	0.46	109.85
100	17-Jul	0.68	1.339	< 0.05	344.62	0.003	7.75	0.135	37.737
100	17-Jul	0.68	1.322	< 0.05	347.80	0.003	7.70	0.133	38.437
100	17-Jul	0.71	1.381	< 0.05	360.36	0.004	8.01	0.144	40.179
100	18-Jul	0.72	1.482	< 0.05	381.36	0.004	8.29	0.157	43.019
100	18-Jul	0.71	1.455	< 0.05	376.70	0.004	8.11	0.153	42.507
100	18-Jul	0.73	1.524	< 0.05	401.14	0.004	8.14	0.163	45.636
100	21-Jul	0.84	2.056	< 0.05	537.98	0.007	8.59	0.244	63.074
100	24-Jul	0.90	2.262	< 0.05	597.01	0.008	8.99	0.282	73.332
100	Jul-28	0.93	2.306	< 0.05	615.70	0.008	9.07	0.292	75.731
100	Jul-28	0.93	2.315	< 0.05	607.13	0.008	9.12	0.293	75.905
100	Jul-28	0.96	2.321	< 0.05	611.05	0.009	9.55	0.300	76.244
100	Jul-30	0.93	2.243	< 0.05	600.06	0.008	9.28	0.297	77.192
100	Jul-30	0.90	2.160	< 0.05	572.09	0.008	8.80	0.284	74.111

100	01-Aug	0.95	2.253	< 0.05	608.22	0.008	9.49	0.291	74.307
100	01-Aug	0.95	2.266	< 0.05	605.77	0.008	9.31	0.286	73.463
100	03-Aug	0.99	2.344	< 0.05	633.79	0.009	9.57	0.296	75.447
100	06-Aug	1.02	2.454	< 0.05	667.48	0.009	9.65	0.302	76.809
120	24-Jul	0.81	1.724	< 0.05	479.36	0.003	6.75	0.184	51.853
120	Jul-28	0.90	1.872	< 0.05	529.64	0.003	7.33	0.205	56.766
120	Jul-28	0.90	1.887	< 0.05	530.11	0.004	7.34	0.204	56.967
120	Jul-28	0.87	1.776	< 0.05	501.49	0.004	7.15	0.197	54.885
120	Jul-30	0.88	1.786	< 0.05	497.57	0.004	7.30	0.206	56.627
120	Jul-30	0.90	1.884	< 0.05	524.23	0.003	7.27	0.203	56.412
120	Jul-30	0.86	1.768	< 0.05	491.02	0.004	7.13	0.199	56.001
120	03-Aug	0.94	1.895	< 0.05	523.51	0.004	7.53	0.204	54.875
120	06-Aug	1.00	1.992	< 0.05	551.15	0.004	7.58	0.209	56.389
165	21-Jun	0.30	0.499	< 0.05	138.36	< 0.001	3.72	0.032	13.460
165	17-Jul	0.64	1.111	< 0.05	306.81	< 0.001	6.27	0.100	30.344
165	17-Jul	0.64	1.116	< 0.05	306.82	< 0.001	6.24	0.102	30.433
165	17-Jul	0.62	1.085	< 0.05	291.46	< 0.001	5.87	0.099	28.945
165	17-Jul	0.66	1.187	< 0.05	317.88	< 0.001	6.28	0.110	31.971
165	17-Jul	0.66	1.187	< 0.05	321.68	< 0.001	6.31	0.110	32.346
165	18-Jul	0.69	1.240	< 0.05	333.41	< 0.001	6.38	0.114	34.133
165	21-Jul	0.74	1.516	< 0.05	411.36	0.001	6.36	0.156	44.051
165	24-Jul	0.73	1.505	< 0.05	411.07	0.001	5.87	0.154	44.381
165	28-Jul	0.81	1.679	< 0.05	456.55	0.001	6.31	0.170	49.557
165	Jul-28	0.82	1.699	< 0.05	455.20	0.001	6.42	0.172	49.517
165	Jul-28	0.80	1.593	< 0.05	439.45	0.001	6.29	0.166	48.029
165	Jul-30	0.80	1.612	< 0.05	445.87	0.002	6.42	0.177	51.142
165	Jul-30	0.79	1.603	< 0.05	438.65	0.002	6.34	0.175	50.372
165	Jul-30	0.80	1.614	< 0.05	434.79	0.001	6.44	0.172	49.693
165	01-Aug	0.84	1.654	< 0.05	461.38	0.001	6.62	0.175	50.459
165	01-Aug	0.83	1.657	< 0.05	459.99	0.001	6.59	0.174	50.422
165	01-Aug	0.82	1.643	< 0.05	466.70	0.001	6.53	0.173	50.817
165	01-Aug	0.83	1.662	< 0.05	457.29	0.001	6.66	0.176	50.177
165	03-Aug	0.84	1.662	< 0.05	457.45	0.001	6.52	0.169	48.155
165	03-Aug	0.84	1.641	< 0.05	458.86	0.001	6.54	0.170	48.226
165	06-Aug	0.89	1.760	< 0.05	503.90	0.001	6.54	0.175	50.552
165	06-Aug	0.89	1.760	< 0.05	504.78	0.001	6.55	0.175	50.550
165-a	03-Aug	0.30	0.108	< 0.05	47.02	< 0.001	2.80	< 0.001	1.583

Control	21-Jul	0.53	0.004	< 0.05	61.38	< 0.001	2.41	< 0.001	0.154
Control	17-Jul	0.59	0.007	< 0.05	83.03	< 0.001	2.43	< 0.001	0.289
Control	17-Jul	0.59	0.006	< 0.05	83.80	< 0.001	2.44	< 0.001	0.290
Control	17-Jul	0.64	0.006	< 0.05	82.71	< 0.001	2.47	< 0.001	0.295
Control	17-Jul	0.59	0.007	< 0.05	82.03	< 0.001	2.50	< 0.001	0.318
Control	17-Jul	0.59	0.007	< 0.05	82.12	< 0.001	2.47	< 0.001	0.314
Control	18-Jul	0.60	0.007	< 0.05	82.65	< 0.001	2.45	< 0.001	0.304
Control	21-Jul	0.60	0.006	< 0.05	84.14	< 0.001	2.45	< 0.001	0.292
Control	28-Jul	0.61	0.006	< 0.05	88.07	< 0.001	2.61	< 0.001	0.301
Control	28-Jul	0.61	0.006	< 0.05	88.61	< 0.001	2.60	< 0.001	0.300
Control	03-Aug	0.63	0.006	< 0.05	93.01	< 0.001	2.66	< 0.001	0.307
Control	03-Aug	0.62	0.006	< 0.05	92.61	< 0.001	2.65	< 0.001	0.305
A4-1	20-Jul	< 0.5	2.61	< 0.5	651.7	0.01	9.4	0.31	5.02
A4-2	23-Jul	0.9	4.11	4.1	1158.7	0.15	10.4	0.44	18.28
A4-3	23-Jul	0.29	0.116	< 0.05	50.27	< 0.001	1.57	< 0.001	1.077
A4-5	23-Jul	0.48	1.355	1.30	404.46	0.048	4.29	0.137	6.375
A4-6	23-Jul	0.66	1.328	0.11	318.20	0.007	5.04	0.096	9.606
Control	23-Jul	0.50	0.005	< 0.05	12.11	< 0.001	2.14	< 0.001	0.008
DIW blank	19-Jul	< 0.05	< 0.002	< 0.05	< 0.05	< 0.001	< 0.02	< 0.001	< 0.005
DIW blank	25-Jul	< 0.05	< 0.002	< 0.05	< 0.05	< 0.001	< 0.02	< 0.001	< 0.005
DIW blank	02-Aug	< 0.05	< 0.002	< 0.05	< 0.05	< 0.001	< 0.02	< 0.001	< 0.005
DIW blank	06-Aug	0.05	< 0.002	< 0.05	< 0.05	< 0.001	< 0.02	< 0.001	< 0.005
Acid blank	21-Jun	< 0.05	< 0.002	< 0.05	< 0.05	< 0.001	< 0.02	< 0.001	< 0.005
Acid blank	19-Jul	< 0.05	< 0.002	< 0.05	< 0.05	< 0.001	< 0.02	< 0.001	< 0.005
Acid blank	25-Jul	< 0.05	< 0.002	< 0.05	< 0.05	< 0.001	< 0.02	< 0.001	< 0.005
Acid blank	02-Aug	< 0.05	< 0.002	< 0.05	< 0.05	< 0.001	< 0.02	< 0.001	< 0.005
Acid blank	06-Aug	< 0.05	< 0.002	< 0.05	< 0.05	< 0.001	< 0.02	< 0.001	< 0.005
Travel blank	19-Jul	< 0.05	< 0.002	< 0.05	< 0.05	< 0.001	< 0.02	< 0.001	< 0.005
Travel blank	25-Jul	< 0.05	< 0.002	< 0.05	< 0.05	< 0.001	< 0.02	< 0.001	< 0.005
Travel blank	02-Aug	< 0.05	< 0.002	< 0.05	< 0.05	< 0.001	< 0.02	< 0.001	< 0.005
Travel blank	06-Aug	< 0.05	< 0.002	< 0.05	< 0.05	< 0.001	< 0.02	< 0.001	< 0.005
Repeats									
40	19-Jul	0.9	2.66	< 0.5	667.2	< 0.01	10.2	0.31	78.96

40	19-Jul	0.9	2.62	< 0.5	668.2	< 0.01	10.1	0.31	78.93
100	03-Aug	0.99	2.344	< 0.05	633.79	0.009	9.57	0.296	75.447
100	03-Aug	0.99	2.366	< 0.05	629.11	0.009	9.56	0.297	75.392
165	18-Jul	0.69	1.240	< 0.05	333.41	< 0.001	6.38	0.114	34.133
165	18-Jul	0.69	1.237	< 0.05	336.85	< 0.001	6.47	0.115	33.793
Control	21-Jul	0.60	0.006	< 0.05	84.14	< 0.001	2.45	< 0.001	0.292
Control	21-Jul	0.60	0.007	< 0.05	84.83	< 0.001	2.45	< 0.001	0.295
DIW blank	06-Aug	0.05	< 0.002	< 0.05	< 0.05	< 0.001	< 0.02	< 0.001	< 0.005
DIW blank	06-Aug	0.05	< 0.002	< 0.05	< 0.05	< 0.001	< 0.02	< 0.001	< 0.005
CONTROLS									
BLANK		< 0.05	< 0.002	< 0.05	< 0.05	< 0.001	< 0.02	< 0.001	< 0.005
BLANK		< 0.05	< 0.002	< 0.05	< 0.05	< 0.001	< 0.02	< 0.001	< 0.005
BLANK		< 0.05	< 0.002	< 0.05	< 0.05	< 0.001	< 0.02	< 0.001	< 0.005
BLANK		< 0.05	< 0.002	< 0.05	< 0.05	< 0.001	< 0.02	< 0.001	< 0.005
ION-96.3		49.08	< 0.002	< 0.05	36.86	< 0.001	1.18	< 0.001	< 0.005
CERTIFIED (ppm)		48.6 ± 5			36.6 ± 2.8		1.16 ± 0.17		
INFORMATION (ppm)									
SLRS-4		2.20	< 0.002	< 0.05	2.35	< 0.001	1.99	< 0.001	< 0.005
CERTIFIED (ppm)		2.4 ± 0.2							
CERTIFIED (ppb)			0.67 ± 0.08						0.93 ± 0.1
TMDA-51.3		5.04	0.070	< 0.05	4.09	< 0.001	0.24	< 0.001	0.135
TMDA-51.3		5.06	0.069	< 0.05	4.03	< 0.001	0.25	< 0.001	0.132
CERTIFIED (ppb)			68.3 ± 5.1						137 ± 14

IC (ppm)	**Dilution**	**F**	**Cl**	**SO_4**	**Br**	**NO_3**	**PO_4**
D.L.	**1**	**0.01**	**0.02**	**0.02**	**0.02**	**0.02**	**0.02**

		10	0.1	0.2	0.2	0.2	0.2	0.2
		20	0.2	0.4	0.4	0.4	0.4	0.4
		100	1	2	2	2	2	2
Distance (m)	**Date**							
0	20-Jul	100	< 1	< 2	5392	< 2	< 2	< 2
0	28-Jul	100	11	< 2	5944	< 2	< 2	< 2
0	21-Jul	100	< 1	< 2	4484	< 2	3	< 2
0	03-Aug	100	< 1	< 2	4403	< 2	< 2	< 2
0	06-Aug	100	< 1	< 2	5047	< 2	< 2	< 2
10	19-Jul	100	23	3	8120	< 2	< 2	< 2
10	24-Jul	100	25	3	7787	< 2	< 2	< 2
10	03-Aug	100	37	3	9256	< 2	< 2	< 2
10	06-Aug	100	39	3	10187	< 2	< 2	< 2
18	Jul-19	100	< 1	< 2	2487	< 2	3	< 2
18	Jul-20	100	< 1	< 2	2661	< 2	< 2	< 2
18	Jul-21	100	< 1	< 2	2808	< 2	< 2	< 2
18	Jul-24	100	< 1	< 2	3238	< 2	< 2	< 2
18	Jul-28	100	< 1	2	3245	< 2	< 2	< 2
18	Jul-28	100	< 1	2	3251	< 2	< 2	< 2
18	Jul-28	100	< 1	< 2	3213	< 2	< 2	< 2
18	Jul-30	100	< 1	< 2	2970	< 2	< 2	< 2
18	Jul-30	100	< 1	< 2	3011	< 2	< 2	< 2
18	Jul-30	100	< 1	< 2	2951	< 2	< 2	< 2
18	03-Aug	100	< 1	< 2	3047	< 2	< 2	< 2
18	06-Aug	100	< 1	< 2	3301	< 2	< 2	< 2
40	Jul-19	20	< 0.2	< 0.4	2021	< 0.4	0.7	< 0.4
40	Jul-19	100	< 1	< 2	1996	< 2	4	< 2
40	Jul-20	100	< 1	< 2	2278	< 2	9	< 2
40	Jul-21	100	< 1	< 2	2346	< 2	< 2	< 2
40	Jul-24	100	< 1	< 2	2609	< 2	< 2	< 2
40	Jul-28	100	< 1	< 2	2647	< 2	< 2	< 2
40	Jul-28	100	< 1	< 2	2724	< 2	< 2	< 2
40	Jul-28	100	< 1	< 2	2806	< 2	< 2	< 2
40	Jul-30	100	< 1	< 2	2579	< 2	< 2	< 2
40	Jul-30	100	< 1	< 2	2580	< 2	6	< 2
40	Jul-30	100	< 1	< 2	2412	< 2	3	< 2
40	03-Aug	100	< 1	< 2	2672	< 2	< 2	< 2

40	03-Aug	100	< 1	< 2	2674	< 2	2	< 2
40	06-Aug	100	< 1	< 2	2678	< 2	< 2	< 2
100	17-Jul	10	< 0.1	0.4	1104	< 0.2	0.8	< 0.2
100	17-Jul	20	< 0.2	< 0.4	1070	< 0.4	0.9	< 0.4
100	17-Jul	20	< 0.2	< 0.4	1125	< 0.4	0.6	< 0.4
100	18-Jul	20	< 0.2	0.6	1179	< 0.4	0.7	< 0.4
100	18-Jul	20	< 0.2	0.5	1181	< 0.4	0.7	< 0.4
100	18-Jul	20	< 0.2	< 0.4	1227	< 0.4	0.8	< 0.4
100	21-Jul	20	< 0.2	< 0.4	1660	< 0.4	0.6	< 0.4
100	Jul-24	20	< 0.2	< 0.4	1860	< 0.4	0.5	< 0.4
100	Jul-28	20	< 0.2	0.5	1897	< 0.4	0.5	< 0.4
100	Jul-28	20	< 0.2	0.4	1893	< 0.4	0.4	< 0.4
100	Jul-28	20	< 0.2	0.4	1898	< 0.4	0.4	< 0.4
100	Jul-30	20	< 0.2	< 0.4	1878	< 0.4	0.4	< 0.4
100	Jul-30	20	< 0.2	< 0.4	1760	< 0.4	0.5	< 0.4
100	01-Aug	20	< 0.2	0.4	1879	< 0.4	< 0.4	< 0.4
100	01-Aug	20	< 0.2	< 0.4	1869	< 0.4	0.7	< 0.4
100	03-Aug	20	< 0.2	< 0.4	1937	< 0.4	0.6	< 0.4
100	06-Aug	100	< 1	5	2062	< 2	4	< 2
120	24-Jul	20	< 0.2	< 0.4	1468	< 0.4	0.5	< 0.4
120	Jul-28	20	< 0.2	< 0.4	1549	< 0.4	0.5	< 0.4
120	Jul-30	20	< 0.2	< 0.4	1530	< 0.4	0.5	< 0.4
120	Jul-30	20	< 0.2	< 0.4	1626	< 0.4	1.0	< 0.4
120	Jul-30	20	< 0.2	< 0.4	1530	< 0.4	1.0	< 0.4
120	03-Aug	20	< 0.2	< 0.4	1630	< 0.4	0.5	< 0.4
120	06-Aug	20	< 0.2	< 0.4	1730	< 0.4	0.4	< 0.4
120	21-Jun	10	0.4	< 0.2	435.5	< 0.2	0.5	< 0.2
120	17-Jul	10	< 0.1	< 0.2	945.5	< 0.2	0.6	< 0.2
165	17-Jul	10	< 0.1	< 0.2	948.4	< 0.2	0.6	< 0.2
165	17-Jul	10	< 0.1	< 0.2	885.4	< 0.2	0.6	< 0.2
165	17-Jul	10	< 0.1	< 0.2	981.5	< 0.2	0.6	< 0.2
165	17-Jul	10	< 0.1	0.3	953.0	< 0.2	0.6	< 0.2
165	18-Jul	10	< 0.1	0.5	1052	< 0.2	0.6	< 0.2
165	21-Jul	20	< 0.2	< 0.4	1280	< 0.4	< 0.4	< 0.4
165	24-Jul	20	< 0.2	< 0.4	1273	< 0.4	0.9	< 0.4
165	28-Jul	20	< 0.2	< 0.4	1419	< 0.4	0.4	< 0.4
165	Jul-28	20	< 0.2	< 0.4	1414	< 0.4	0.5	< 0.4

165	Jul-28	20	< 0.2	< 0.4	1356	< 0.4	0.6	< 0.4
165	Jul-30	20	< 0.2	0.4	1362	< 0.4	< 0.4	< 0.4
165	Jul-30	20	< 0.2	< 0.4	1364	< 0.4	0.7	< 0.4
165	Jul-30	20	< 0.2	0.4	1356	< 0.4	0.6	< 0.4
165	01-Aug	20	< 0.2	< 0.4	1423	< 0.4	0.6	< 0.4
165	01-Aug	20	< 0.2	< 0.4	1394	< 0.4	< 0.4	< 0.4
165	03-Aug	20	< 0.2	< 0.4	1427	< 0.4	0.6	< 0.4
165	03-Aug	20	< 0.2	0.5	1430	< 0.4	0.5	< 0.4
165	06-Aug	20	< 0.2	< 0.4	1532	< 0.4	0.5	< 0.4
165	06-Aug	20	< 0.2	0.4	1504	< 0.4	0.6	< 0.4
Control	21-Jul	1	0.12	0.27	183.7	< 0.02	< 0.02	0.03
Control	17-Jul	10	0.1	0.4	248.6	< 0.2	< 0.2	< 0.2
Control	17-Jul	10	0.1	0.3	247.9	< 0.2	< 0.2	< 0.2
Control	17-Jul	10	0.1	0.4	251.9	< 0.2	0.9	< 0.2
Control	17-Jul	10	0.1	0.3	252.0	< 0.2	< 0.2	< 0.2
Control	17-Jul	10	0.1	0.5	251.6	< 0.2	< 0.2	< 0.2
Control	18-Jul	10	0.1	0.3	251.4	< 0.2	0.4	< 0.2
Control	21-Jul	10	0.1	0.5	256.7	< 0.2	< 0.2	< 0.2
Control	28-Jul	10	0.1	0.3	267.2	< 0.2	< 0.2	< 0.2
Control	28-Jul	10	0.1	0.3	268.2	< 0.2	< 0.2	< 0.2
Control	03-Aug	10	0.1	< 0.2	282.9	< 0.2	< 0.2	< 0.2
Control	03-Aug	10	0.1	0.4	281.5	< 0.2	< 0.2	< 0.2
A4-1	20-Jul	20	< 0.2	< 0.4	1943	< 0.4	< 0.4	< 0.4
A4-2	23-Jul	100	< 1	< 2	3537	< 2	3	< 2
A4-3	23-Jul	1	0.11	0.07	152.4	< 0.02	0.27	< 0.02
A4-5	23-Jul	20	< 0.2	< 0.4	1227	< 0.4	0.9	< 0.4
A4-6	23-Jul	10	< 0.1	0.3	968.5	< 0.2	1.3	< 0.2
Control	23-Jul	1	0.05	0.06	37.18	< 0.02	< 0.02	< 0.02
REPEATS								
40	28-Jul	**100**	**< 1**	**< 2**	**2806**	**< 2**	**< 2**	**< 2**
40	28-Jul	**100**	**< 1**	**< 2**	**2804**	**< 2**	**< 2**	**< 2**
100	17-Jul	**20**	**< 0.2**	**< 0.4**	**1125**	**< 0.4**	**0.6**	**< 0.4**
100	17-Jul	**20**	**< 0.2**	**< 0.4**	**1125**	**< 0.4**	**0.6**	**< 0.4**

100	21-Jul	**20**	**< 0.2**	**< 0.4**	**1660**	**< 0.4**	**0.6**	**< 0.4**
100	21-Jul	**20**	**< 0.2**	**< 0.4**	**1660**	**< 0.4**	**0.6**	**< 0.4**
165	17-Jul	**10**	**< 0.1**	**0.3**	**953.0**	**< 0.2**	**0.6**	**< 0.2**
165	17-Jul	**10**	**< 0.1**	**0.3**	**953.2**	**< 0.2**	**0.7**	**< 0.2**
165	21-Jul	**20**	**< 0.2**	**< 0.4**	**1280**	**< 0.4**	**< 0.4**	**< 0.4**
165	21-Jul	**20**	**< 0.2**	**< 0.4**	**1282**	**< 0.4**	**< 0.4**	**< 0.4**
CONTROLS								
BLANK		**1**	**< 0.01**	**0.04**	**< 0.02**	**< 0.02**	**< 0.02**	**< 0.02**
BLANK		**1**	**< 0.01**	**< 0.02**	**< 0.02**	**< 0.02**	**< 0.02**	**< 0.02**
BLANK		**1**	**< 0.01**	**< 0.02**	**< 0.02**	**< 0.02**	**< 0.02**	**< 0.02**
BLANK		**1**	**< 0.01**	**0.03**	**0.06**	**< 0.02**	**< 0.02**	**< 0.02**
BLANK		**1**	**< 0.01**	**0.04**	**0.05**	**< 0.02**	**< 0.02**	**< 0.02**
HAMILTON-20		**1**	**0.42**	**64.16**	**45.56**	**0.06**	**9.54**	**< 0.02**
HAMILTON-20		**1**	**0.42**	**63.81**	**45.44**	**0.05**	**9.51**	**< 0.02**
HAMILTON-20		**1**	**0.42**	**64.22**	**45.60**	**< 0.02**	**9.51**	**< 0.02**
HAMILTON-20		**1**	**0.42**	**64.14**	**45.57**	**< 0.02**	**9.49**	**< 0.02**
CERTIFIED			**0.42 ± 0.08**	**64.7 ± 4.5**	**45.8 ± 3.2**		**10.85 ± 0.93**	
ION 96.2		**1**	**0.17**	**77.34**	**106.1**	**< 0.02**	**14.25**	**< 0.02**
ION 96.2		**1**	**0.17**	**76.74**	**105.3**	**< 0.02**	**14.14**	**< 0.02**
ION 96.2		**1**	**0.17**	**77.51**	**106.8**	**< 0.02**	**14.21**	**< 0.02**
ION 96.2		**1**	**0.16**	**77.46**	**106.7**	**< 0.02**	**14.20**	**< 0.02**
CERTIFIED			**0.18 ± 0.058**	**78.2 ± 6.66**	**106. ± 9.24**		**15.6 ± 1.156**	

Appendix 2: Ferrozine results

Sample	Abs (562 nm)			Fe2+ by ferrozine		Total Fe by ICP
	1	2	Average	Measured conc (mg/L)	Corrected conc (mg/L)	Conc (mg/L)
acid blank	0	0.001	0.001	2.1	0.0	-
control	0.000	0.000	0.000	2.0	0.0	< 0.005
10	2.482	2.429	2.4555	219.3	217.3	289.53
10 (rep)	2.48	2.429	2.4545	219.3	217.2	
18	0.559	0.559	0.559	51.5	49.4	76.75
18 (rep)	0.585	0.578	0.5815	53.5	51.4	
40	0.413	0.396	0.4045	37.8	35.8	53.65
100	0.212	0.182	0.197	19.5	17.4	24.34
120	0.128	0.131	0.1295	13.5	11.4	15.14
165	0.101	0.103	0.102	11.1	9.0	12.12

"Control" was de-ionized water. Corrected concentrations were derived by subtracting the acid blank concentration from the measured concentrations for each sample.

Appendix 3: pe derivations and temperature correction

Distance (m)	Date	Measured ORP (mV)	Adjusted for SHE	Temp (°C)	pe (T adjusted)
18	18-07	490	689	3.6	12.569
	06-08	440	639	9.2	11.425
40	18-07	470	669	4.0	12.186
	06-08	417	616	13.2	10.860
100	18-07	426	625	8.9	11.187
	06-08	376	575	11.3	10.205
120	24-07	370	569	7.2	10.199
	03-08	355	554	8.8	10.167
165	18-07	384	583	5.8	10.551
	06-08	355	554	9.5	9.8948

SHE = 199 mV

Equation for pe temperature adjustment using the Nernst equation:

pe = ORP x (96 484 / (2.3 x 8.314 x T)),

where T is in Kelvin and ORP is in V and corrected for SHE.

Appendix 4: Aqua Regia Digestion Method

Reagents

12 M HCl **16 M HNO_3**

Procedure:

1. Weight out 1.0 g of each sample into labelled 50 mL polypropylene centrifuge tubes.

2. Add 6 mL of 12 M HCl and 2 mL of 16 M HNO_3 to residues.

3. Cap tightly and vortex the sample to suspend.

4. Loosen caps and leave the samples in the fumehood over night.

5. Loosen caps and heat samples in a water bath (approximately 3 hours). Start the water at approximately 35^{o}C and allow the samples to heat with the bath to 90^{o}C. Vortex samples every 30 minutes with the caps on tight. Loosen caps before replacing samples in water bath.

6. Continue heating for 1 hour at 90^{o}C, remove from waterbath.

7. Add 20 mL reverse osmosis – deionized (RO-DI) H_2O and vortex to suspend the sample. Centrifuge for 10 minutes @ 2800 rpm.

8. Decant the supernatant into a labelled 50 mL polypropylene centrifuge tube.

9. Rinse the residues with 10 mL of RO-DI H_2O, cap, vortex to suspend and centrifuge for 10 minutes @ 2800 rpm. Decant rinse into centrifuge tube from step 9.

10. Repeat step 9 once more.

11. Adjust the final volume of tubes to 50 mL with RO-DI H_2O, cap and shake thoroughly to mix.

Appendix 5: Elemental analyses for mineral precipitates

ICP-MS (ppm)		Li	Be	Mn	Co	Ni	Cu	Zn	Ga
D.L.		0.04	0.01	0.2	0.1	0.4	0.2	1	0.02
Distance (m)	Date								
18	19-Jul	3.04	0.28	34.8	3.1	26.4	49.6	610	0.93
10	19-Jul	0.19	0.07	41.1	3.4	19.7	28.9	429	0.52
10	19-Jul	0.30	0.13	46.6	2.7	22.4	38.4	516	0.45
A4	23-Jul	0.14	0.09	25.0	0.9	5.5	37.0	34	4.75
18	21-Jul	0.07	0.05	29.9	1.8	17.0	25.9	1016	0.34
40	20-Jul	0.16	0.04	36.1	1.1	6.4	36.8	364	0.28
40	20-Jul	0.12	0.04	45.4	2.5	17.1	37.7	541	0.55
40	28-Jul	0.08	0.06	39.7	1.4	7.8	24.3	348	0.20
40	28-Jul	0.06	0.04	36.3	1.0	5.7	22.5	287	0.22
165	01-Aug	0.29	1.60	28.2	1.3	12.2	18.4	346	0.09
165	01-Aug	1.18	1.29	78.7	4.4	29.9	41.9	411	0.26
120	28-Jul	0.06	1.95	10.9	1.3	86.1	128.0	8890	0.05
165	02-Aug	1.02	2.05	34.6	1.6	38.2	86.4	2275	0.42
165	02-Aug	2.44	0.75	250.0	13.5	74.6	138.4	1584	1.33
18	28-Jul	0.07	0.10	30.4	1.4	8.8	30.6	458	0.33
18	28-Jul	0.04	0.07	24.0	1.0	6.0	26.7	392	0.35
120	28-Jul	0.07	2.12	32.3	2.7	62.0	85.8	5192	0.03
120	28-Jul	< 0.04	1.92	20.8	1.9	56.0	73.4	3875	0.04
18	21-Jul	0.06	0.04	30.2	1.8	18.3	23.3	871	0.28
18	21-Jul	< 0.04	0.03	24.0	1.2	12.3	18.5	598	0.32
100	28-Jul	0.09	1.28	35.1	2.6	47.5	83.6	1012	0.08
100	28-Jul	0.07	1.33	14.1	1.7	46.9	108.9	1253	0.09
120	28-Jul	< 0.04	1.11	66.9	12.9	297.6	523.8	15001	0.24
40	21-Jul	0.05	0.03	40.2	1.4	7.6	24.5	344	0.26
40	21-Jul	< 0.04	0.03	36.8	1.0	5.0	28.2	304	0.26
100	28-Jul	0.09	1.13	22.6	1.2	9.0	35.9	339	0.11
100	28-Jul	0.05	1.08	15.8	0.9	9.2	47.1	324	0.12

REPEATS

A4	23-Jul	0.14	0.09	25.0	0.9	5.5	37.0	34	4.75
A4	23-Jul	0.16	0.11	54.3	2.2	10.3	41.6	74	4.48
18	28-Jul	0.04	0.07	24.0	1.0	6.0	26.7	392	0.35
18	28-Jul	< 0.04	0.06	24.1	1.0	6.2	22.2	330	0.35
CONTROLS									
BLANK		< 0.04	< 0.01	< 0.2	< 0.1	< 0.4	< 0.2	< 1	< 0.02
Fe2O3		< 0.04	< 0.01	2.5	2.0	0.9	0.3	1	0.05
GXR-1		4.49	0.81	926.8	8.0	39.2	1211.8	814	4.45
GXR-3		130.23	22.85	23722.9	44.1	50.5	12.0	196	5.88
Till-2		32.56	1.50	613.0	12.8	30.3	143.0	110	7.09

ICP-MS (ppm)		**Ge**	**As**	**Se**	**Rb**	**Sr**	**Y**	**Zr**	**Nb**
D.L.		0.04	0.2	2	0.1	1	0.02	0.1	0.02
Distance (m)	Date								
18	19-Jul	0.04	10.3	< 2	1.8	9	8.41	3.8	< 0.02
10	19-Jul	0.07	10.5	3	1.7	38	5.94	3.9	< 0.02
10	19-Jul	0.12	16.7	3	1.5	35	9.94	3.2	0.03
A4	23-Jul	0.09	11.9	3	0.3	1	1.05	0.8	0.02
18	21-Jul	0.12	8.0	< 2	0.3	16	6.06	0.9	0.02
40	20-Jul	0.18	3.0	< 2	0.2	5	5.77	1.0	< 0.02
40	20-Jul	0.13	9.2	4	0.6	8	4.53	2.6	0.03
40	28-Jul	0.11	1.5	< 2	0.1	5	6.25	0.7	< 0.02
40	28-Jul	0.15	2.4	< 2	0.1	5	4.94	0.7	0.03
165	01-Aug	< 0.04	1.0	< 2	0.4	6	6.78	0.7	< 0.02
165	01-Aug	< 0.04	6.9	< 2	1.6	16	11.60	2.0	< 0.02
120	28-Jul	0.05	< 0.2	< 2	< 0.1	184	144.42	0.5	< 0.02
165	02-Aug	0.09	7.3	< 2	1.7	21	113.97	3.5	< 0.02

165	02-Aug	0.08	27.1	5	4.8	22	65.65	7.5	0.07
18	28-Jul	0.11	6.8	< 2	0.3	7	9.29	1.2	0.03
18	28-Jul	0.14	6.6	< 2	0.2	5	7.88	0.9	0.02
120	28-Jul	< 0.04	1.3	< 2	< 0.1	76	95.63	0.4	< 0.02
120	28-Jul	< 0.04	< 0.2	< 2	< 0.1	47	83.99	0.3	< 0.02
18	21-Jul	0.12	7.4	< 2	0.2	15	5.10	0.7	0.02
18	21-Jul	0.12	6.2	< 2	0.2	12	5.87	0.6	< 0.02
100	28-Jul	0.08	< 0.2	< 2	< 0.1	4	33.97	0.3	< 0.02
100	28-Jul	0.14	1.0	< 2	< 0.1	3	56.10	0.5	< 0.02
120	28-Jul	0.67	0.4	2	< 0.1	68	542.01	0.7	< 0.02
40	21-Jul	0.18	1.9	< 2	< 0.1	5	4.12	0.4	< 0.02
40	21-Jul	0.21	1.8	< 2	< 0.1	4	3.08	0.5	0.02
100	28-Jul	0.05	1.3	< 2	0.2	5	5.42	0.6	< 0.02
100	28-Jul	0.09	1.1	< 2	0.1	3	6.67	0.7	< 0.02
REPEATS									
A4	23-Jul	0.09	11.9	3	0.3	1	1.05	0.8	0.02
A4	23-Jul	0.11	23.9	< 2	0.4	1	1.23	0.7	< 0.02
18	28-Jul	0.14	6.6	< 2	0.2	5	7.88	0.9	0.02
18	28-Jul	0.13	7.1	< 2	0.2	5	8.03	0.8	0.02
CONTROLS									
BLANK		< 0.04	< 0.2	< 2	< 0.1	< 1	< 0.02	< 0.1	< 0.02
Fe2O3		0.62	< 0.2	< 2	< 0.1	< 1	< 0.02	< 0.1	0.02
GXR-1		0.42	422.2	16	2.1	144	26.55	7.7	0.10
GXR-3		6.15	4069.2	< 2	94.6	925	10.80	44.3	0.67
Till-2		0.04	22.9	< 2	36.3	11	10.87	3.0	2.86
ICP-MS (ppm)		Mo	Ag	Cd	In	Sn	Sb	Te	Cs

D.L.		0.1	0.01	0.04	0.02	0.02	0.02	0.04	0.02
Distance (m)	Date								
18	19-Jul	11.8	0.22	0.99	0.03	0.14	2.35	< 0.04	0.45
10	19-Jul	3.3	0.41	3.35	< 0.02	0.04	3.51	< 0.04	0.14
10	19-Jul	7.9	0.42	3.85	< 0.02	0.05	3.75	< 0.04	0.14
A4	23-Jul	60.8	0.56	0.22	0.27	0.02	6.21	< 0.04	0.07
18	21-Jul	9.7	0.11	3.07	0.02	0.03	0.55	< 0.04	0.07
40	20-Jul	13.3	0.13	0.90	< 0.02	< 0.02	3.02	< 0.04	0.05
40	20-Jul	13.0	0.24	0.76	0.03	0.31	3.93	< 0.04	0.14
40	28-Jul	7.4	0.07	1.23	< 0.02	< 0.02	1.67	< 0.04	0.15
40	28-Jul	7.6	0.10	0.81	< 0.02	< 0.02	2.02	< 0.04	0.03
165	01-Aug	15.8	0.06	1.40	< 0.02	< 0.02	1.04	< 0.04	0.10
165	01-Aug	23.6	0.22	1.70	< 0.02	0.08	2.53	< 0.04	0.41
120	28-Jul	16.6	0.05	39.11	< 0.02	< 0.02	0.73	< 0.04	< 0.02
165	02-Aug	12.6	0.50	6.49	0.02	0.09	2.12	< 0.04	0.43
165	02-Aug	22.1	0.61	7.70	0.03	0.32	6.74	0.06	0.84
18	28-Jul	7.3	0.08	1.23	0.02	0.03	0.47	< 0.04	0.05
18	28-Jul	8.6	0.09	0.86	0.02	< 0.02	0.43	< 0.04	0.04
120	28-Jul	7.5	0.05	24.29	< 0.02	< 0.02	0.55	< 0.04	< 0.02
120	28-Jul	5.5	0.03	17.60	< 0.02	< 0.02	0.46	< 0.04	< 0.02
18	21-Jul	8.2	0.08	3.14	< 0.02	0.05	0.39	< 0.04	0.11
18	21-Jul	9.4	0.10	2.12	0.02	< 0.02	0.39	< 0.04	0.13
100	28-Jul	9.7	0.19	4.33	< 0.02	< 0.02	1.24	< 0.04	0.04
100	28-Jul	13.6	0.19	5.16	< 0.02	< 0.02	1.84	< 0.04	0.02
120	28-Jul	51.7	0.19	213.75	< 0.02	< 0.02	3.71	< 0.04	< 0.02
40	21-Jul	8.2	0.11	1.10	< 0.02	< 0.02	2.07	< 0.04	0.03
40	21-Jul	10.2	0.12	0.68	< 0.02	< 0.02	2.28	< 0.04	< 0.02
100	28-Jul	11.7	0.09	1.11	0.02	< 0.02	1.27	< 0.04	0.04
100	28-Jul	13.7	0.08	0.94	0.02	< 0.02	1.55	< 0.04	0.20
REPEATS									
A4	23-Jul	60.8	0.56	0.22	0.27	0.02	6.21	< 0.04	0.07
A4	23-Jul	60.2	0.52	0.62	0.26	0.02	6.28	< 0.04	0.15

18	28-Jul	8.6	0.09	0.86	0.02	< 0.02	0.43	< 0.04	0.04
18	28-Jul	8.7	0.09	0.86	0.02	< 0.02	0.43	< 0.04	0.03
CONTROLS									
BLANK		< 0.1	< 0.01	< 0.04	< 0.02	< 0.02	< 0.02	< 0.04	< 0.02
Fe2O3		< 0.1	0.03	< 0.04	< 0.02	< 0.02	< 0.02	< 0.04	< 0.02
GXR-1		17.8	31.23	2.38	0.72	23.06	93.63	13.38	2.82
GXR-3		6.0	0.09	0.32	< 0.02	0.61	41.16	0.09	191.53
Till-2		12.1	0.26	0.29	0.06	1.94	0.69	< 0.04	6.55

ICP-MS (ppm)		**Ba**	**La**	**Ce**	**Pr**	**Nd**	**Sm**	**Eu**	**Tb**
D.L.		0.4	0.02	0.02	0.01	0.01	0.01	0.01	0.01
Distance (m)	Date								
18	19-Jul	63.0	1.29	4.57	0.96	5.93	2.36	0.65	0.38
10	19-Jul	50.4	0.57	2.10	0.56	3.83	1.55	0.41	0.24
10	19-Jul	36.1	0.54	2.38	0.75	5.74	2.60	0.71	0.43
A4	23-Jul	2.8	0.34	1.10	0.24	1.48	0.63	0.15	0.07
18	21-Jul	67.5	0.58	2.15	0.49	3.31	1.25	0.34	0.21
40	20-Jul	38.7	0.37	1.68	0.44	2.94	1.20	0.33	0.23
40	20-Jul	53.7	0.38	1.56	0.38	2.53	0.99	0.27	0.18
40	28-Jul	72.6	0.39	2.13	0.61	4.38	1.72	0.44	0.28
40	28-Jul	51.6	0.36	2.00	0.57	4.09	1.61	0.41	0.24
165	01-Aug	157.5	0.31	1.29	0.34	2.24	1.15	0.35	0.26
165	01-Aug	847.2	1.47	4.17	0.91	5.46	2.51	0.69	0.48
120	28-Jul	45.8	5.34	21.44	5.05	32.31	13.82	4.40	3.72
165	02-Aug	125.3	5.06	19.11	4.37	27.62	12.98	4.12	3.43
165	02-Aug	117.8	5.35	18.11	3.73	21.97	8.59	2.53	1.95
18	28-Jul	48.6	0.73	3.01	0.76	5.23	2.10	0.59	0.37
18	28-Jul	42.8	0.62	2.96	0.81	5.60	2.23	0.59	0.35

120	28-Jul	41.9	3.58	12.80	2.93	18.50	8.02	2.57	2.26
120	28-Jul	16.2	3.54	11.37	2.46	15.48	6.50	2.06	1.83
18	21-Jul	44.7	0.50	1.76	0.40	2.64	1.01	0.27	0.17
18	21-Jul	48.8	0.52	2.05	0.49	3.46	1.30	0.34	0.21
100	28-Jul	114.4	3.10	10.35	2.05	12.14	4.13	1.22	0.92
100	28-Jul	26.4	5.44	17.86	3.64	21.47	7.00	1.98	1.49
120	28-Jul	19.7	37.37	92.91	17.07	98.44	29.78	9.38	9.07
40	21-Jul	79.4	0.28	1.59	0.46	3.27	1.30	0.32	0.19
40	21-Jul	44.9	0.24	1.41	0.42	3.04	1.18	0.29	0.16
100	28-Jul	65.5	0.35	1.67	0.44	2.95	1.30	0.36	0.23
100	28-Jul	35.5	0.41	2.33	0.65	4.34	1.94	0.52	0.32
REPEATS									
A4	23-Jul	2.8	0.34	1.10	0.24	1.48	0.63	0.15	0.07
A4	23-Jul	4.3	0.40	1.23	0.26	1.55	0.66	0.16	0.08
18	28-Jul	42.8	0.62	2.96	0.81	5.60	2.23	0.59	0.35
18	28-Jul	30.1	0.64	3.00	0.81	5.63	2.27	0.60	0.35
CONTROLS									
BLANK		< 0.4	< 0.02	< 0.02	< 0.01	< 0.01	< 0.01	< 0.01	< 0.01
Fe2O3		< 0.4	< 0.02	< 0.02	< 0.01	< 0.01	< 0.01	< 0.01	< 0.01
GXR-1		467.3	4.53	8.96	1.19	5.53	2.10	0.47	0.63
GXR-3		2297.4	6.00	12.94	1.53	5.99	1.39	0.34	0.22
Till-2		88.8	29.06	68.34	6.82	25.81	4.97	0.73	0.56
ICP-MS (ppm)		Gd	Dy	Ho	Er	Tm	Yb	Lu	Hf
D.L.		0.01	0.01	0.01	0.01	0.01	0.01	0.01	0.02
Distance (m)	Date								

18	19-Jul	2.68	2.12	0.40	1.09	0.16	1.09	0.16	0.09
10	19-Jul	1.79	1.35	0.27	0.77	0.12	0.75	0.12	0.12
10	19-Jul	3.09	2.37	0.47	1.30	0.20	1.26	0.19	0.08
A4	23-Jul	0.58	0.31	0.05	0.13	0.02	0.12	0.02	0.02
18	21-Jul	1.50	1.16	0.23	0.65	0.09	0.59	0.09	0.03
40	20-Jul	1.57	1.26	0.25	0.69	0.10	0.61	0.09	0.03
40	20-Jul	1.24	1.00	0.20	0.53	0.08	0.48	0.07	0.06
40	28-Jul	1.94	1.58	0.31	0.87	0.13	0.84	0.12	0.02
40	28-Jul	1.72	1.33	0.27	0.75	0.11	0.72	0.11	< 0.02
165	01-Aug	1.50	1.75	0.34	1.06	0.18	1.56	0.23	< 0.02
165	01-Aug	3.03	3.02	0.55	1.61	0.27	2.04	0.30	0.05
120	28-Jul	24.18	21.99	4.35	11.97	1.65	10.65	1.65	< 0.02
165	02-Aug	21.05	21.15	4.11	11.92	1.78	12.31	1.90	0.09
165	02-Aug	13.27	11.30	2.16	5.78	0.78	4.91	0.74	0.17
18	28-Jul	2.63	2.09	0.42	1.16	0.16	1.00	0.16	0.03
18	28-Jul	2.58	1.96	0.40	1.09	0.16	0.97	0.15	0.03
120	28-Jul	14.24	13.69	2.74	7.71	1.07	7.12	1.11	< 0.02
120	28-Jul	11.87	11.06	2.26	6.38	0.88	5.66	0.89	< 0.02
18	21-Jul	1.23	0.92	0.19	0.50	0.07	0.45	0.07	< 0.02
18	21-Jul	1.55	1.15	0.23	0.64	0.09	0.58	0.09	< 0.02
100	28-Jul	6.53	5.23	1.06	2.90	0.40	2.48	0.40	< 0.02
100	28-Jul	10.94	8.34	1.71	4.57	0.60	3.57	0.56	< 0.02
120	28-Jul	64.95	52.37	11.55	30.72	3.75	20.33	3.33	0.03
40	21-Jul	1.38	1.05	0.21	0.62	0.09	0.58	0.09	0.03
40	21-Jul	1.13	0.87	0.17	0.51	0.08	0.49	0.07	0.02
100	28-Jul	1.57	1.40	0.27	0.79	0.13	0.91	0.14	< 0.02
100	28-Jul	2.21	1.83	0.34	1.01	0.16	1.13	0.17	0.02
REPEATS									
A4	23-Jul	0.58	0.31	0.05	0.13	0.02	0.12	0.02	0.02
A4	23-Jul	0.61	0.35	0.06	0.15	0.02	0.14	0.02	< 0.02
18	28-Jul	2.58	1.96	0.40	1.09	0.16	0.97	0.15	0.03
18	28-Jul	2.59	1.96	0.39	1.10	0.16	0.98	0.15	0.02

CONTROLS									
BLANK		< 0.01	< 0.01	< 0.01	< 0.01	< 0.01	< 0.01	< 0.01	< 0.02
Fe2O3		< 0.01	< 0.01	< 0.01	< 0.01	< 0.01	< 0.01	< 0.01	< 0.02
GXR-1		3.26	4.23	0.86	2.44	0.33	2.03	0.27	0.18
GXR-3		1.54	1.34	0.28	0.83	0.12	0.78	0.12	1.00
Till-2		3.90	2.71	0.45	1.13	0.15	0.90	0.12	0.05

ICP-MS (ppm)		**Ta**	**W**	**Re**	**Tl**	**Pb**	**Bi**	**Th**	**U**
D.L.		0.02	0.02	0.01	0.01	0.02	0.04	0.04	0.01
Distance (m)	Date								
18	19-Jul	< 0.02	0.10	0.01	1.61	69.05	0.12	2.55	27.77
10	19-Jul	< 0.02	0.14	0.01	1.22	50.54	0.07	0.38	4.42
10	19-Jul	< 0.02	0.11	0.01	1.31	63.00	< 0.04	0.33	4.69
A4	23-Jul	< 0.02	0.04	0.02	0.07	1.82	< 0.04	16.55	2.64
18	21-Jul	< 0.02	0.02	0.02	0.59	21.70	< 0.04	1.34	8.86
40	20-Jul	< 0.02	0.02	0.02	0.25	11.52	< 0.04	0.81	1.35
40	20-Jul	< 0.02	0.08	0.02	0.37	30.83	0.05	1.04	1.39
40	28-Jul	< 0.02	0.03	0.02	0.32	8.63	< 0.04	0.57	1.62
40	28-Jul	< 0.02	0.08	0.01	0.31	11.82	< 0.04	0.73	1.19
165	01-Aug	< 0.02	0.03	0.04	0.25	7.60	< 0.04	0.66	22.73
165	01-Aug	< 0.02	0.31	0.11	0.67	25.93	< 0.04	1.22	30.67
120	28-Jul	< 0.02	< 0.02	0.02	0.07	3.63	< 0.04	0.34	521.94
165	02-Aug	< 0.02	0.09	0.03	0.89	43.15	< 0.04	1.57	94.95
165	02-Aug	< 0.02	0.27	0.02	1.74	117.13	0.14	2.65	40.44
18	28-Jul	< 0.02	< 0.02	0.02	0.71	19.00	< 0.04	0.98	2.56
18	28-Jul	< 0.02	< 0.02	0.02	0.75	16.75	< 0.04	1.35	1.87
120	28-Jul	< 0.02	< 0.02	0.03	0.11	2.50	< 0.04	0.30	149.37
120	28-Jul	< 0.02	< 0.02	0.03	0.08	1.99	< 0.04	0.23	77.61
18	21-Jul	< 0.02	< 0.02	0.02	0.51	16.32	< 0.04	1.06	8.13

18	21-Jul	< 0.02	< 0.02	0.02	0.56	17.53	< 0.04	1.25	7.18
100	28-Jul	< 0.02	< 0.02	0.05	0.15	11.44	< 0.04	0.53	38.31
100	28-Jul	< 0.02	0.03	0.02	0.15	17.15	< 0.04	0.85	45.61
120	28-Jul	< 0.02	0.05	0.03	1.27	8.52	< 0.04	< 0.04	149.75
40	21-Jul	< 0.02	< 0.02	0.04	0.46	12.27	< 0.04	0.77	0.85
40	21-Jul	< 0.02	< 0.02	0.03	0.40	14.51	< 0.04	0.99	0.54
100	28-Jul	< 0.02	< 0.02	< 0.01	0.25	11.54	< 0.04	1.21	12.71
100	28-Jul	< 0.02	< 0.02	< 0.01	0.20	14.78	< 0.04	1.38	15.47
REPEATS									
A4	23-Jul	< 0.02	0.04	0.02	0.07	1.82	< 0.04	16.55	2.64
A4	23-Jul	< 0.02	< 0.02	< 0.01	0.07	2.87	< 0.04	15.68	2.68
18	28-Jul	< 0.02	< 0.02	0.02	0.75	16.75	< 0.04	1.35	1.87
18	28-Jul	< 0.02	< 0.02	< 0.01	0.75	16.06	< 0.04	1.32	1.85
CONTROLS									
BLANK		< 0.02	< 0.02	< 0.01	< 0.01	< 0.02	< 0.04	< 0.04	< 0.01
Fe2O3		< 0.02	< 0.02	0.05	< 0.01	0.02	< 0.04	< 0.04	< 0.01
GXR-1		< 0.02	174.73	< 0.01	0.35	674.35	1440.28	1.21	31.47
GXR-3		0.03	884.35	0.01	3.08	13.57	0.76	2.08	2.59
Till-2		< 0.02	7.88	< 0.01	0.33	22.16	4.85	9.76	3.00

ICP-MS (ppm)		**Al**	**B**	**Ca**	**Cr**	**Fe**	**K**	**Mg**	**Na**
D.L.		10	3	10	0.5	3	25	3	25
Distance (m)	Date								
18	19-Jul	31952	< 3	218	5.7	180933	408	712	< 25

10	19-Jul	6817	< 3	448	3.5	276771	724	414	< 25
10	19-Jul	10630	< 3	434	4.3	279573	529	510	< 25
A4	23-Jul	2264	< 3	146	82.6	378085	41	177	< 25
18	21-Jul	5122	< 3	545	4.3	437217	66	248	< 25
40	20-Jul	6695	< 3	381	5.7	425916	46	279	< 25
40	20-Jul	5210	< 3	258	6.6	348028	167	199	< 25
40	28-Jul	6050	< 3	479	4.2	409630	< 25	407	< 25
40	28-Jul	5997	< 3	337	4.9	418783	32	276	< 25
165	01-Aug	177882	3	1105	3.4	30523	52	716	< 25
165	01-Aug	141674	12	971	6.0	41913	224	814	< 25
120	28-Jul	202956	< 3	13621	3.5	19537	< 25	389	< 25
165	02-Aug	173144	< 3	2190	8.4	57353	267	1000	< 25
165	02-Aug	44468	< 3	1376	14.9	87073	1137	884	47
18	28-Jul	4963	< 3	407	3.5	398647	66	319	< 25
18	28-Jul	4610	< 3	312	4.3	429069	39	228	< 25
120	28-Jul	204217	< 3	4467	3.7	13097	< 25	397	< 25
120	28-Jul	183466	< 3	2611	3.2	13139	< 25	251	29
18	21-Jul	4484	< 3	589	3.6	412279	59	275	< 25
18	21-Jul	4441	< 3	411	3.4	420532	36	170	< 25
100	28-Jul	143754	< 3	445	3.3	118548	< 25	277	< 25
100	28-Jul	126005	< 3	299	4.9	157912	< 25	156	< 25
120	28-Jul	68934	< 3	4712	5.0	331721	< 25	209	< 25
40	21-Jul	5390	< 3	499	5.6	441594	< 25	392	< 25
40	21-Jul	5320	< 3	316	5.7	454619	< 25	239	< 25
100	28-Jul	137541	< 3	463	6.4	116630	43	326	< 25
100	28-Jul	120370	< 3	290	5.8	169772	< 25	199	< 25

REPEATS

A4	23-Jul	2264	< 3	146	82.6	378085	41	177	< 25
A4	23-Jul	2275	< 3	147	78.5	384136	60	170	< 25
18	28-Jul	4610	< 3	312	4.3	429069	39	228	< 25
18	28-Jul	4409	< 3	320	4.4	434354	43	232	< 25

CONTROLS								
BLANK	< 10	< 3	< 10	< 0.5	< 3	< 25	< 3	< 25
Fe2O3	< 10	< 3	< 10	1.4	567757	< 25	3	< 25
GXR-1	3120	12	8229	7.5	244560	315	1344	355
GXR-3	22955	182	127779	13.9	181724	7167	6942	7311
Till-2	24915	4	1335	34.9	32870	2965	6624	231

ICP-MS (ppm)		**P**	**S**	**Sc**	**Si**	**Ti**	**V**
D.L.		25	25	0.5	10	1	1
Distance (m)	Date						
18	19-Jul	245	27950	6.2	1367	17	11
10	19-Jul	216	36015	2.4	852	3	6
10	19-Jul	314	39992	2.8	1372	11	10
A4	23-Jul	8379	47866	4.5	265	2	16
18	21-Jul	299	43502	1.3	780	3	5
40	20-Jul	112	46126	1.4	631	2	5
40	20-Jul	222	37395	1.7	522	6	13
40	28-Jul	54	47008	1.7	645	1	3
40	28-Jul	61	46782	1.4	609	2	4
165	01-Aug	38	75415	18.5	2546	1	7
165	01-Aug	196	60080	17.4	2090	13	26
120	28-Jul	< 25	24990	15.1	1952	< 1	3
165	02-Aug	263	48828	15.3	4587	10	24
165	02-Aug	666	14338	7.0	1246	83	75
18	28-Jul	290	42561	1.7	648	4	5
18	28-Jul	291	47440	1.4	728	2	5
120	28-Jul	< 25	49901	15.1	4243	< 1	2
120	28-Jul	< 25	50352	13.6	3150	< 1	1
18	21-Jul	266	42233	1.2	715	2	4
18	21-Jul	259	44628	1.1	723	1	5

100	28-Jul	< 25	60435	9.5	5336	< 1	< 1
100	28-Jul	< 25	56876	10.6	572	< 1	1
120	28-Jul	< 25	22432	4.4	282	< 1	17
40	21-Jul	78	47925	2.1	729	< 1	2
40	21-Jul	72	47620	1.5	714	< 1	1
100	28-Jul	41	66767	14.2	3059	1	2
100	28-Jul	30	61917	14.8	2464	1	2
REPEATS							
A4	23-Jul	8379	47866	4.5	265	2	16
A4	23-Jul	7962	45394	4.7	241	2	17
18	28-Jul	291	47440	1.4	728	2	5
18	28-Jul	298	47796	1.4	698	3	6
CONTROLS							
BLANK		< 25	< 25	< 0.5	< 10	< 1	< 1
Fe2O3		< 25	< 25	0.5	13	< 1	< 1
GXR-1		372	2294	1.9	820	60	77
GXR-3		944	1589	16.3	13324	361	33
Till-2		522	322	4.6	207	1043	41

Appendix 6: Water temperatures

Table A6-1: Water temperatures measured at each sampling site for successive dates over the course of the sampling season.

Date	Distance (m)						
	0	**10**	**18**	**40**	**100**	**120**	**165**
18-Jul	2.6	6.4	3.6	4.0	8.3	-	6.3
20-Jul	3.6	7.5	3.9	4.5	3.6	-	7.2
21-Jul	1.8	6.0	1.9	2.6	4.3	-	3.8
28-Jul	3.0	8.0	2.6	2.1	1.5	1.7	1.6
30-Jul	12.2	7.5	8.8	12.5	12.2	9.8	9.3
03-Aug	4.0	8.5	5.3	6.5	7.3	7.3	8.6
06-Aug	11.6	9.9	6.5	5.2	5.1	4.7	5

Appendix 7: Loss on ignition results for organic carbon content

Table A7-1: Masses of mineral precipitate remaining after heating at successive temperatures for LOI analyses, as described by Heiri et al., 2001.

Distance (m)	Description	Date	Weight (g)				
			crucible + wet sample	wet sample only	after 105 °C	after 550 °C	after 950 °C
18	TIFs	20-Jul	37.13	8.00	32.45	31.96	31.54
18	TIFs (replicate)	20-Jul	40.23	8.05	35.60	35.1	34.64
100	orange precipitate	28-Jul	34.63	8.07	28.80	28.42	28.27
120	white precipitate	28-Jul	38.79	8.03	23.05	22.44	22.06
120	white precipitate (replicate)	28-Jul	34.23	8.05	28.40	28.04	27.87

Table A7-2: Percent organic (LOI 550) and inorganic (LOI 950) carbon in mineral precipitate samples. The error associated with this analysis is ±5 % (Heiri et al., 2001).

Distance (m)	Description	Date	Organic C LOI 550	Carbonate C LOI 950
18	TIFs	20-Jul	1.51%	1.29%
18	TIFs (replicate)	20-Jul	1.40%	1.29%
100	orange precipitate	28-Jul	1.32%	0.52%
120	white precipitate	28-Jul	2.65%	1.65%
120	white precipitate (replicate)	28-Jul	1.27%	0.60%

Appendix 8: **XRD spectra (not used in results)**

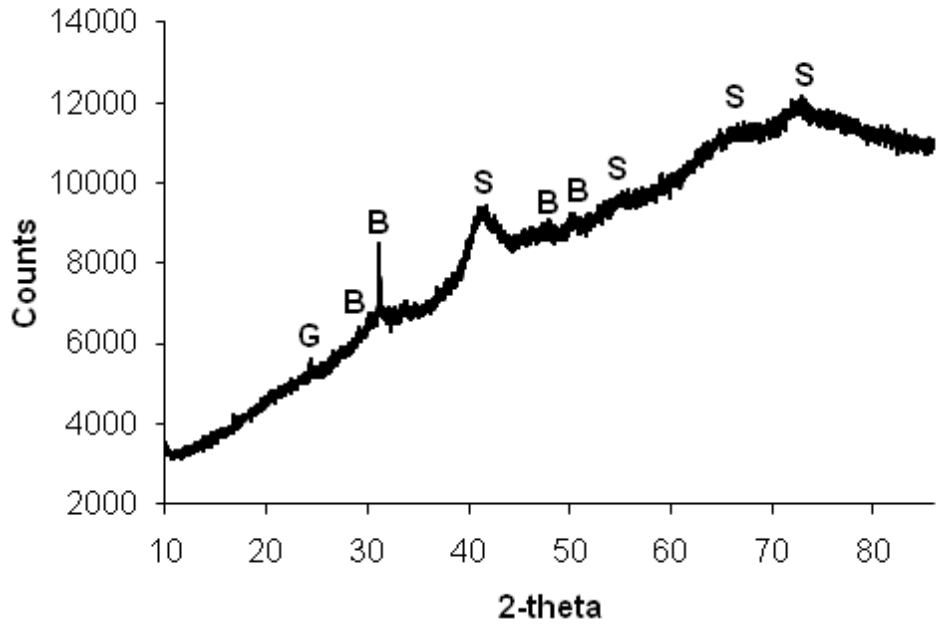

Figure A8-1: XRD spectrum for red-coloured TIF laminae collected at 18 m (July 20, 2008). G=goethite, B=barite, S=schwertmannite

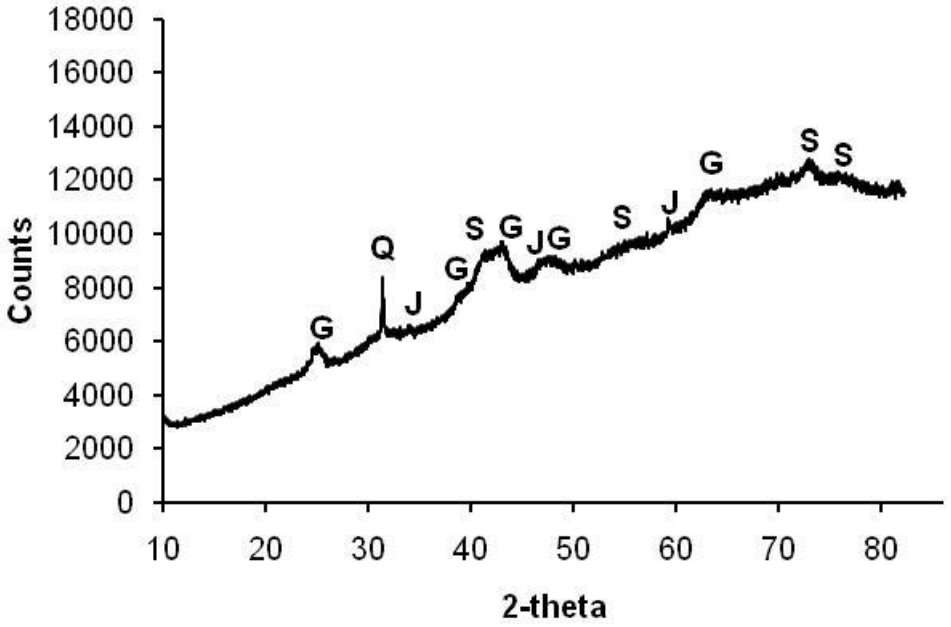

Figure A8-2: XRD spectrum for non-laminated light orange-coloured precipitates from 100 m (July 21, 2008). G = goethite, S = schwertmannite, J = jarosite, Q = quartz

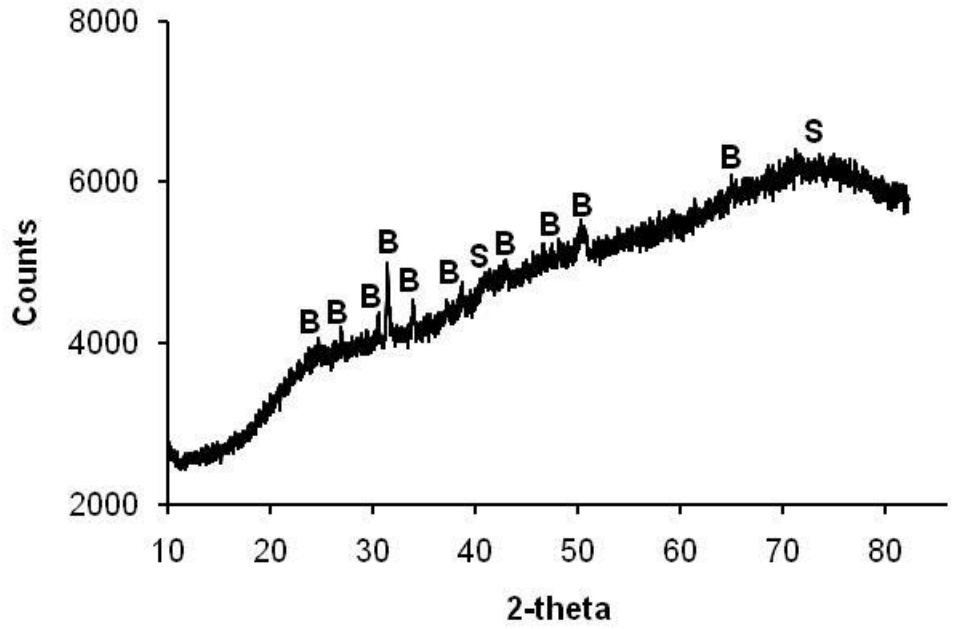

Figure A8-3: XRD spectra for light orange-coloured mineral precipitates collected at 100 m (July 21, 2008). B = barite, S =schwertmannite.

Table A8-1: Mineral spectra used for fitting XRD scans. ICDD = International Centre for Diffraction Data.

Mineral name	ICDD code
Goethite	00-029-0713
Barite	01-083-2053
Schwertmannite	00-047-1775
Jarosite	01-076-0629
Quartz	01-089-8950
Jurbanite	01-078-0593

Appendix 9: Saturation indices for minerals derived from thermodynamic modeling

Table A9-1: Saturation indices for Al-minerals derived from thermodynamic modeling (Phreeqc-i). Basaluminite = $Al_4(SO_4)(OH)_{10}$; Jurbanite = $Al(OH)SO_4$; Alunite = $KAl_3(SO_4)_2(OH)_6$; Halloysite = $Al_2Si_2O_5(OH)_4$; K-Aluminite = $KAl(SO_4)_2$-$12H_2O$; Boehmite = AlOOH; Gibsite = $Al(OH)_3$

			July 17				
Distance (m)	**Basaluminite**	**Jurbanite**	**Alunite**	**Halloysite**	**K-Alum**	**Boehmite**	**Gibbsite**
0	-7.89	0.81	-2.14	-7.23	-6.45	-4.51	-3.91
10	-3.85	1.29	1.32	-4.42	-5.98	-3.02	-2.47
18	-4.24	0.81	-0.16	-5.54	-7.06	-3.21	-2.62
40	-1.54	1.00	1.41	-3.92	-7.23	-2.34	-1.76
100	5.07	1.31	5.54	0.63	-8.08	0.14	0.65
165	8.02	1.14	6.41	2.15	-8.79	0.94	1.49
			Aug-06				
0	-6.70	0.77	-0.31	-5.39	-6.88	-3.39	-2.92
10	-2.80	1.43	2.55	-3.38	-5.92	-2.44	-1.95
18	-5.31	0.75	0.13	-5.42	-7.00	-3.11	-2.60
40	-5.80	0.59	0.24	-5.17	-7.29	-2.91	-2.47
100	1.99	1.27	4.47	-0.91	-7.5	-0.69	-0.21
165	5.53	1.22	5.93	0.93	-8.16	0.37	0.87

Table A9-2: Saturation indices for Fe-minerals, derived from thermodynamic modeling (Phreeqc-i). Ferrihydrite = $Fe(OH)_3$; Goethite = (FeOOH); H-Jarosite = $(H_3O)Fe_3(SO_4)_2(OH)_6$; K-Jarosite = $KFe_3(SO_4)_2(OH)_6$; Na-Jarosite = $NaFe_3(SO_4)_2(OH)_6$; Pb-Jarosite = $PbFe_6(SO_4)_4(OH)_{12}$; Schwertmannite = $Fe_8O_8(SO_4)(OH)_6$

				Jul-17			
Distance (m)	**Ferrihydrite**	**Goethite**	**H-Jarosite**	**K-Jarosite**	**Na-Jarosite**	**Pb-Jarosite**	**Schwertman-nite**
0	0.31	3.20	6.14	8.80	5.01	11.17	10.36
10	1.01	3.86	6.85	10.03	6.06	11.83	15.06
18	0.85	3.72	5.32	8.53	4.67	9.92	13.37
40	1.03	3.90	4.57	8.06	4.12	8.78	14.18
100	1.59	4.42	2.70	6.59	2.69	4.91	16.62
165	1.92	4.77	1.25	5.95	1.98	3.88	18.19
				Aug-06			
0	0.68	3.48	6.38	8.69	5.05	9.17	12.39
10	1.38	4.20	7.63	10.75	6.84	12.43	17.67
18	0.74	3.57	5.57	8.39	4.62	8.56	12.53
40	0.68	3.47	5.33	7.87	4.12	6.86	11.82
100	1.48	4.29	4.34	7.76	3.95	6.82	16.61
165	1.83	4.65	2.87	7.01	3.13	5.25	18.22

Table A9-3: Mineral saturation indices for Zn-minerals determined by thermodynamic modeling (Phreeqc-i). Bianchite = $ZnSO_4$-6H_2O; Goslarite = $ZnSO_4$-7H_2O; Zincosite = $ZnSO_4$.

				Jul-17			
Distance	**Bianchite**	**Goslarite**	**Zincosite**	**$Zn_2(OH)_2SO_4$**	**$Zn_3O(SO_4)_2$**	**$Zn_3(OH)_6SO_4$**	**$ZnSO_4$-H_2O**
0	-3.08	-2.63	-9.94	-9.01	-28.93	-23.26	-4.83
10	-3.29	-2.87	-9.93	-8.71	-28.17	-21.95	-4.92
18	-3.79	-3.35	-10.60	-9.22	-29.68	-22.46	-5.51
40	-3.92	-3.48	-10.70	-8.82	-29.33	-21.00	-5.62
100	-4.32	-3.93	-10.84	-7.84	-27.92	-17.27	-5.88
165	-4.42	-3.99	-11.10	-6.82	-27.52	-14.02	-6.07
				Aug-06			
0	-3.19	-2.82	-9.55	-8.77	-27.25	-22.32	-4.67
10	-3.18	-2.79	-9.63	-8.32	-27.08	-21.01	-4.70
18	-3.67	-3.28	-10.17	-9.25	-28.62	-22.79	-5.22
40	-3.77	-3.42	-10.06	-9.41	-28.22	-23.07	-5.21
100	-3.95	-3.58	-10.34	-8.07	-27.37	-18.70	-5.44
165	-4.14	-3.75	-10.62	-7.21	-27.01	-15.74	-5.69

Table A9-4: Mineral saturation indices for other sulphate minerals, calculated by thermodynamic modeling (Phreeqc-i). Anglesite = $PbSO_4$; Barite = $BaSO_4$; Gypsum = $CaSO_4$-$2H_2O$.

Jul-17			
Distance (m)	**Anglesite**	**Barite**	**Gypsum**
0	-1.98	0.35	-0.15
10	-2.29	0.58	-0.04
18	-2.49	0.29	-0.35
40	-2.66	0.63	-0.40
100	-3.11	0.49	-0.61
165	-3.38	0.68	-0.55
	Aug-06		
0	-2.22	0.32	-0.21
10	-2.39	0.55	-0.01
18	-2.41	0.25	-0.26
40	-2.51	0.25	-0.31
100	-2.81	0.39	-0.39
165	-3.21	0.66	-0.35

Table A9-5: Saturation indices for Cd phases calculated by thermodynamic modeling (Phreeqc-i).

			Jul-17			
Distance (m)	**$Cd(OH)_2$**	**$Cd_3(OH)_2(SO_4)_2$**	**$Cd_3(OH)_4SO_4$**	**$CdSO_4$**	**$CdSO_4$-H_2O**	**$CdSO_4$-$3H_2O$**
0	-14.42	-21.32	-29.01	-8.16	-6.31	-5.98
10	-13.29	-20.07	-27.05	-7.84	-6.05	-5.75
18	-13.43	-21.52	-27.99	-8.50	-6.71	-6.40
40	-12.85	-26.67	-27.77	-8.70	-6.87	-6.54
100	-11.84	-20.61	-24.85	-9.06	-7.22	-6.88
165	-12.85	-21.03	-26.67	-8.70	-6.87	-6.54
			Aug-06			
0	-13.50	-21.11	-28.35	-7.93	-6.21	-5.95
10	-12.77	-19.50	-26.31	-7.59	-5.84	-5.57
18	-13.42	-21.44	-28.18	-8.28	-6.53	-6.25
40	-13.25	-21.68	-28.28	-8.24	-6.54	-6.50
100	-11.84	-20.28	-25.48	-8.48	-6.75	-6.49
165	-10.72	-19.74	-23.30	-8.77	-7.02	-6.74

Table A9-6: Saturation indices for Cu minerals/phases calculated by thermodynamic modeling (Phreeqc-i). Chalcanthite = $CuSO_4$-$5H_2O$.

Jul-17				
Distance (m)	**Chalcanthite**	**$Cu(OH)_2$**	**Cu_2SO_4**	**$CuSO_4$**
0	-5.20	-9.24	-33.43	-11.90
10	-4.69	-7.86	-29.75	-11.18
18	-5.49	-8.15	-31.03	-11.99
40	-5.58	-7.51	-30.92	-12.20
100	-5.83	-6.40	-30.03	-12.51
165	-5.58	-7.51	-30.92	-12.20
		Aug-06		
0	-5.40	-8.61	-30.09	-11.62
10	-4.58	-7.43	-29.07	-10.89
18	-5.37	-8.81	-30.41	-11.27
40	-5.53	-8.14	-29.97	-11.67
100	-5.67	-6.68	-28.84	-11.93
165	-5.95	-5.58	-28.60	-12.29

Table A9-7: Saturation indices for Ni minerals/phases calculated by thermodynamic modeling (Phreeqc-i). Retgersite = $NiSO_4$-$6H_2O$.

Jul-17			
Distance (m)	**$Ni(OH)_2$**	**$Ni_4(OH)_6SO_4$**	**Retgersite**
0	-12.43	-33.24	-4.33
10	-11.35	-30.62	-4.22
18	-11.49	-31.69	-4.87
40	-10.93	-29.64	-4.97
100	-9.99	-27.03	-5.36
165	-10.93	-29.64	-4.97
	Aug-06		
0	-11.56	-32.50	-4.51
10	-10.83	-29.60	-4.10
18	-11.44	-31.92	-4.73
40	-11.24	-32.18	-4.73
100	-9.89	-27.93	-5.04
165	-8.71	-24.27	-5.20

Table A9-8: Saturation indices for U phases calculated by thermodynamic modeling (Phreeqc-i).

Jul-17			
Distance (m)	**$UO_{2(amorphous)}$**	**$UO_2(OH)_2$**	**UO_3**
0	-25.96	-8.55	-10.98
10	-22.14	-6.31	-8.68
18	-22.59	-6.59	-8.96
40	-22.28	-5.94	-8.35
100	-21.06	-4.82	-7.25
165	-22.28	-5.94	-8.35
	Aug-06		
0	-22.93	-7.98	-10.27
10	-21.89	-6.04	-8.35
18	-22.27	-6.66	-8.99
40	-21.84	-6.59	-8.85
100	-20.37	-5.05	-7.35
165	-19.59	-3.76	-6.08

Appendix 10: K_d values for Fe, Al, Zn, Ni, Cu, Cd, Ba, Pb and U

Table A10-1: K_d values for various elements at each location in the creek

Distance (m)	pH	Fe	Al	Zn	Ni	Cu	Cd	Ba	Pb	U
10	3.6	4.3E-02	9.3E-05	6.0E-05	6.2E-05	1.3E-03	1.6E-04	1.2	2.1	5.2E-03
18	3.5	9.7E-02	1.7E-03	2.5E-04	2.7E-04	9.5E-03	2.2E-04	2.5	4.5	0.2
18	3.5	2.0E-01	2.1E-04	3.0E-04	1.5E-04	4.1E-03	5.7E-04	2.4	1.2	6.4E-02
18	3.5	1.7E-01	1.9E-04	1.3E-04	5.8E-05	4.2E-03	1.8E-04	1.9	0.8	1.6E-02
40	3.9	2.9E-01	3.4E-04	1.7E-04	9.6E-05	6.2E-03	2.4E-04	1.7	1.2	1.2E-02
100	4.4	1.8E-01	9.8E-03	4.1E-04	4.2E-04	1.9E-02	9.1E-04	1.3	2.3	0.3
120	4.7	3.7E-02	2.9E-02	6.7E-03	1.6E-03	5.0E-02	1.7E-02	0.6	1.0	6.0
165	4.9	1.0E-01	4.9E-02	8.5E-04	5.6E-04	2.4E-02	1.6E-03	4.4	7.5	0.7